Primary minerals of the Jáchymov ore district

Primární minerály jáchymovského rudního revíru

(237 figs, 160 tabs)

PETR ONDRUŠ[1] – FRANTIŠEK VESELOVSKÝ[1] – ANANDA GABAŠOVÁ[1] – JAN HLOUŠEK[2] – VLADIMÍR ŠREIN[3] – IVAN VAVŘÍN[1] – ROMAN SKÁLA[1] – JIŘÍ SEJKORA[4] – MILAN DRÁBEK[1]

[1] *Czech Geological Survey, Klárov 3, CZ-118 21 Prague 1*
[2] *U Roháčových kasáren 24, CZ-100 00 Prague 10*
[3] *Institute of Rock Structure and Mechanics, V Holešovičkách 41, CZ-182 09, Prague 8*
[4] *National Museum, Václavské náměstí 68, CZ-115 79, Prague 1*

One hundred and seventeen primary mineral species are described and/or referenced. Approximately seventy primary minerals were known from the district before the present study. All known reliable data on the individual minerals from Jáchymov are presented. New and more complete X-ray powder diffraction data for argentopyrite, sternbergite, and an unusual (Co,Fe)-rammelsbergite are presented. The following chapters describe some unknown minerals, erroneously quoted minerals and imperfectly identified minerals.
The present work increases the number of all identified, described and/or referenced minerals in the Jáchymov ore district to 384.

Key words: primary minerals, XRD, microprobe, unit-cell parameters, Jáchymov.

History of mineralogical research of the Jáchymov ore district

A systematic study of Jáchymov minerals commenced early after World War II, during the period of 1947–1950. This work was aimed at supporting uranium exploitation. However, due to the general political situation and the existence of the "Iron curtain", the deposit became a *Terra prohibita*. Only shortly before the closure of uranium mining, in the period of 1956–1960, a research of non-uranium ores was conducted in the mines, including a wider mineralogical study [351]. Following this period, only several isolated studies were undertaken, including some students' diploma works. Studies of Jáchymov minerals realized that specimens accompanied by a detailed location are of particular value for genetic and interpretative work. The non-accessibility of such samples at present was significantly offset by the opportunity to study samples collected during the late fifties and deposited in the permanent documentation of the Czech Geological Survey, Prague. A valuable listing of samples with details of location was secured from records of the late F. Mrňa. Significant quantities of material were obtained from several museums, from private collectors, and through new collecting.

Approximately seventy primary minerals were known from the district before the present study. This research added another forty-four primary minerals, thus the number of described and/or referenced minerals from the Jáchymov deposit has increased to 384. A list of primary minerals is included in the Appendix.

Analytical part – methods

All mentioned minerals in the following encyclopaedia are identified unambiguously by X-ray diffraction and/or chemical analysis.

Chemical analyses

Polished sections were first studied under the microscope for the identification of minerals and definition of their relations. Suitable sections were selected for electron microprobe (EMP) study and analyses, and interesting domains were marked. With EMP, marked places were first examined, and where necessary, the remaining parts of section were examined, too. Chemical composition was examined in a qualitative mode, and quantitative analyses were made on selected objects. Both types of analyses were performed with ED system, but in cases of line coincidence of the analysed elements (Pb–Bi–S, Hg–S), WD system was used, or a special software, allowing separation of coinciding lines. Correction programs ZAF4, Phi(rhoZ) and Quadrilateral were used for conversion of the measured values to weight percentages. The following natural minerals and synthetic phases were used as standards for analysis of individual elements: *pyrite*, *galena*, *stibnite*, *arsenopyrite*, *bismuthinite*, *löllingite*, *sphalerite*, *cinnabar*, *cassiterite, scheelite*, *quartz*, *wollastonite*, *hyalophane*, *albite*, *orthoclase*, PbTe, Cu_2Se, PbSe, SnS_2, TiO, Al_2O_3, $FeSiO_4$, $MnSiO_4$, metallic Cu, Ni, Co, Ag.

Analytical conditions: CamScan 4 with ISIS – eLink energy dispersion analyser, 15 kV, 3 nA for silicate analyses, 25 kV, 2.5 nA for other analyses, WD Microspec analyser.

Results of quantitative analyses are presented, with the descriptions of the individual minerals, in tables consisting of two parts. The first part gives analyses in wt.%, and analyses are arranged in the sequence of sample numbers. In the second part, calculated numbers of atoms per formula unit (apfu) are given, data are ascendently sorted according to values in the highlighted column. Reference to data from literature is by citation number in square brackets.

Analysis of proustite-pyrargyrite phases

A routine spot analysis resulted in the destruction of mineral phases accompanied by a considerable increase in a relative proportion of Ag. To eliminate phase destruction due to thermal instability, the minerals were not analysed in spots but by scanning mode from small areas, approximately 80×50 μm in size, with homogeneity controlled with BSE image. This situation set limits to the size of the analysed objects, excluding thin lamellae and minute inclusions.

Electron microscopy

TESLA BS 340 scanning electron microscope with 75 to 3000 magnification was used. Samples were coated by Au–Pd, C or Al.

Crystal structure analysis

X-ray powder diffraction analysis was done with Philips X'pert System diffractometer using the following conditions: Cu K_α radiation, 40 kV/40 mA, secondary graphite monochromator, step 0.02° 2θ, time 4–10 s, samples placed on Si wafer. The recorded data were processed using the ZDS-WX Search/Match X-ray diffraction software [478]. Qualitative phase analysis was made with the same software with the support of the ZDS-WX Search/Match X-ray diffraction database [478]. Data were calibrated with an internal standard (*quartz*, Si), or using a calibration procedure, correcting for sample eccentricity (correction factor $\cos(\theta).\mathrm{cotg}(\theta)/\lambda^2$). Refined unit-cell parameters were calculated with the FullProf program [462].

PRIMARY MINERALS – ENCYCLOPAEDIC PART

Acanthite Ag_2S

Acanthite was described by Kenngott [221] in two samples collected at Jáchymov in the 18th century and deposited in the Emperor's mineral collection in Vienna. The mineral name is derived from the Greek *acanthi* for a thorn or an arrow, reminiscent of the shape of its crystals. Individual, seemingly orthorhombic *acanthite* crystals are deposited on drusy gangue. The crystals are up to 5 mm long, terminated by a steep pyramid. They are black in colour, with metallic lustre, and the mineral is malleable.

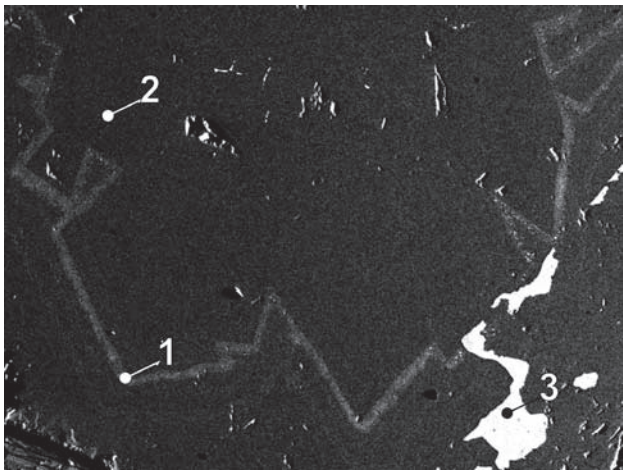

Fig. 1. J114P/C. Grow zone in sphalerite contains fine grains of acanthite. 1 – acanthite + sphalerite, 2 – sphalerite, 3 – rammelsbegite. Svornost shaft, 8th level, Geschieber vein. BSE image. Magnification 160×.

Polished sections show some isotropic domains besides dominant anisotropic parts. Microhardness values and optical properties are similar to those of *argentite*. This material corresponds to *acanthite* sections orientated at random, since *argentite* is unstable below 176 °C.

The study of polished sections of *acanthite* pseudomorphs after *argentite* shows obvious photosensitivity in a light beam of microscope. In the course of observation of freshly polished samples, the surface is coated by minute silver particles, which diffuse light in a similar manner as dust on the surface of a polished section. The phenomenon is best observed under crossed polarizers. The effect appears in several seconds and the number of particles increases with time. Subsequent checking with lower magnification shows the limits of affected area. Similar effects were not observed in *proustite* or *pyrargyrite*. No reference to the above effect was found in ore microscopy textbooks.

Table 1. Chemical analyses of acanthite.

sample	pt.	Ag	Cu	Fe	Co	Ni	S	As	Sb	Total
						weight %				
J-702	9	86.15	0.12	0.05	0.07	0.19	12.61	0.55	0.61	100.35
J-702	10	87.92	0.08	0.08	0.07	0.07	12.44		0.05	100.71
J-702	11	85.16	0.06	0.05	0.04	0.06	12.72	0.07		98.16
J-702	12	87.16	0.09	0.05	0.09	0.08	12.82	0.40		100.69

Table 2. Calculated unit-cell parameters of acanthite from Jáchymov for the space group $P2_1/c$.

sample	*a*	*b*	*c*	β
		(Å)		(°)
J-824	4.2399(6)	6.9224(9)	9.549(1)	125.607(8)

Aikinite $PbCuBiS_3$

It forms anhedral grains up to 50 μm in size, enclosed in *chalcopyrite*, along fractures in *chalcopyrite* and along *arsenopyrite-chalcopyrite* interface. It is often accompanied by *stannite*, in part in mutual intergrowth. *Aikinite* crystallized probably in a similar interval as *stannite*. The studied sample comes from the Giftkies adit.

Aikinite and *matildite*, usually in a mixture, replace several grains of *bismuth* enclosed in *uraninite*, which is surrounded by *rammelsbergite*. The sample comes from the Eliáš mine.

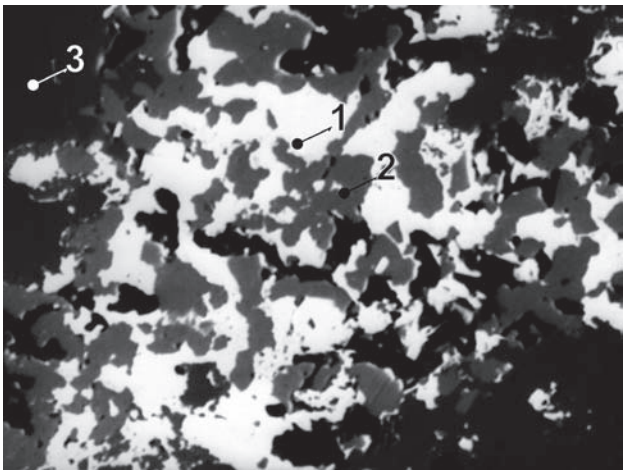

Fig. 2. J061P. 1 – aikinite, 2 – stannite, 3 – chalcopyrite. Giftkies adit. BSE image. Magnification 330×.

Albite $NaAlSi_3O_8$

Albite is a widespread mineral in *albite-muscovite* mica schists occurring in the eastern part of the Jáchymov ore district. Common are *albite* porphyroblasts with a zoning structure indicated by inclusions of *quartz*, mica and *rutile*. Chemical composition varies to An_{10} with rims containing more than 10 mol. % *anorthite*. *Albite* is accompanied by numerous minerals including *pyrite*, *graphite* and rare *arsenopyrite*.

Albite forms minor grains in *quartz* gangue carrying *chalcopyrite*, *hyalophane*, *Ba-orthoclase*, chlorite and *galena* from the Eliáš mine.

Table 3. Chemical analyses of aikinite.

sample	pt.	Cu	Ag	Fe	Zn	Co	Ni	Pb	Bi	Sb	S	Total
						weight %						
J061P	4	8.81	1.46	0.23	0.25			35.56	35.54		15.66	97.51
J061P	5	10.70	0.68	0.30	0.39			36.15	35.76		16.92	100.90
J061P	6	10.11	0.60	0.46	0.18			35.74	35.75		16.53	99.37
J061P	7	10.73	0.23	0.28	0.43			35.82	35.68		16.56	99.73
J061P	6	10.37	0.74	0.14		0.04	0.01	35.78	36.03	0.59	16.60	100.30
J061P	7	10.42	0.60	0.12		0.06	0.04	35.85	35.77	0.31	16.78	99.95
J061P	8	10.39	0.55	0.11		0.01	0.03	35.55	35.87	0.55	16.56	99.62
J061P	9	10.65	0.19	0.19				35.73	35.67	0.47	16.47	99.37
J061P	10	10.29	0.87	0.21		0.09	0.05	35.67	35.99	0.43	16.68	100.28
J061P	11	11.02	0.71	0.09		0.11	0.03	35.64	35.76	0.52	16.97	100.85
J061P	12	10.49	0.59	0.15		0.10	0.01	35.73	35.71	0.57	16.87	100.22
MP27	B2	9.71	0.40					32.37	38.47		17.43	98.38

sample	pt.	Cu	Ag	Fe	Zn	subtotal	Pb	Bi	Sb	subtotal	S	Total
						number of atoms						
J061P	4	0.84	0.08	0.03	0.02	0.97	1.04	1.03		1.03	2.96	6
J061P	5	0.95	0.04	0.03	0.03	1.05	0.99	0.97		0.97	2.99	6
J061P	6	0.92	0.03	0.05	0.02	1.02	1.00	0.99		0.99	2.99	6
J061P	7	0.97	0.01	0.03	0.04	1.05	1.00	0.98		0.98	2.97	6
J061P	6	0.94	0.04	0.01		1.00	1.00	0.99	0.03	1.02	2.98	6
J061P	7	0.94	0.03	0.01		1.00	1.00	0.98	0.02	1.00	3.01	6
J061P	8	0.95	0.03	0.01		0.99	0.99	1.00	0.03	1.02	2.99	6
J061P	9	0.97	0.01	0.02		1.00	1.00	0.99	0.02	1.01	2.98	6
J061P	10	0.93	0.05	0.02		1.01	0.99	0.99	0.02	1.01	2.99	6
J061P	11	0.98	0.04	0.01		1.04	0.97	0.97	0.02	0.99	2.99	6
J061P	12	0.94	0.03	0.02		1.00	0.99			0.98	2.99	6
MP27	B2	0.88				0.88	0.90			1.07	2.99	6

Table 4. Chemical analysis of albite.

sample	pt.	Na_2O	K_2O	FeO	MnO	MgO	CaO	BaO	Al_2O_3	SiO_2	Total
						weight %					
J112P	11	11.40	0.09	0.15	0.13	0.19	0.11	0.06	19.63	68.19	99.95

sample	pt.	Na	K	Fe	Mg	Ca	subtotal	Al	Si	O
						number of atoms				
J112P	11	0.97		0.01	0.01	0.01	0.99	1.01	2.98	8

Alloclasite (Co,Fe)AsS

The mineral forms a thin rim on botryoidal *rammelsbergite* in the direction toward the surrounding *quartz* (Fig. 3).

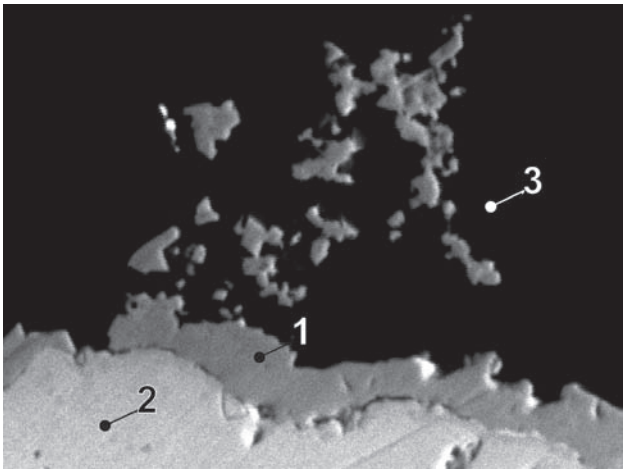

Fig. 3. MP27/A-3. 1 – alloclasite, 2 – rammelsbergite, 3 – quartz. Eliáš mine. BSE image. Magnification 400×.

In reflected light, *alloclasite* is not notably different from *rammelsbergite* but shows only a weak anisotropy under crossed polarizers. The rim represents the last growth zone of *rammelsbergite* showing concentric zoning.

Rammelsbergite encloses *nickeline* and dendritic *silver,* which is in part enclosed in *nickeline*. *Silver* is accompanied by *mercurian silver*, *imiterite* and *cinnabar*, which occur in free spaces of *silver* dendrite or in *quartz* vugs.

Alloclasite is a very rare mineral. The studied sample comes from the Eliáš mine.

Anilite Cu_7S_4

Anilite occurs in aggregates up to 5 mm long with *chalcocite*, *djurleite* and *bornite*, usually as a minor component. *Anilite* predominance in such aggregates is exceptional. The mineral is tied to copper mineralization. It was identified in milky white *quartz* from the Svornost shaft, Daniel level, Trojická vein, or in red hornfelsic *quartz* from the Svornost shaft, 5th level, near the Prokop vein.

Ankerite $CaFe(CO_3)_2$

It is usually brownish yellow and contains also low amounts of Mn. *Ankerite* is probably a quite old gangue carbonate, as it forms centres of *siderite* crystals which are not common, but are overgrown by other carbonates. *Ankerite* is a fairly common mineral in carbonate veins but is not as widespread as *dolomite*.

Table 5. Chemical analyses of alloclasite.

sample	pt.	S	Fe	Co	Ni	Cu	As	Sb	Total
					weight %				
MP27	A1	17.88	1.58	21.86	11.58	0.05	46.24	0.33	99.52
MP27	A2	18.03	2.26	23.50	9.60	0.12	46.45		99.96
MP27	A2a	18.47	2.26	24.03	9.39	0.06	47.05		101.27
MP27	A4	20.97	7.85	24.79	3.99	0.04	42.15	0.10	99.90

sample	pt.	Fe	Co	Ni	subtotal	As	S	Total
				number of atoms				
MP27	A1	0.05	0.63	0.33	1.01	1.04	0.94	3
MP27	A2	0.07	0.67	0.27	1.01	1.04	0.94	3
MP27	A2a	0.07	0.67	0.26	1.01	1.04	0.95	3
MP27	A4	0.23	0.68	0.11	1.02	0.91	1.06	3

Table 6. Chemical analyses of anilite.

sample	pt.	Cu	Ag	Fe	Ni	Zn	S	Sb	As	Total
						weight %				
J041P	a6	76.95	0.23	0.76	0.19	0.20	21.84	0.32	0.24	100.73
J041P	a7	76.27	0.67	0.28	0.14	0.21	22.83	0.19	0.13	100.72
J041P	a9	76.26	0.11	0.45	0.17	0.06	22.37	0.19	0.19	99.80
J010P	ad	76.94	0.88	0.33			21.75		0.58	100.48
J019P	6b	76.84	0.87	0.29			20.64		0.48	99.12

sample	pt.	Cu	Ag	Fe	Ni	Zn	subtotal	S	Sb	As	subtotal	Total
							number of atoms					
J041P	a6	6.94	0.01	0.08	0.02	0.02	7.07	3.90	0.02	0.02	3.94	11
J041P	a7	6.83	0.04	0.03	0.01	0.02	6.93	4.05	0.01	0.01	4.07	11
J041P	a9	6.89	0.01	0.05	0.02	0.01	6.97	4.01	0.01	0.02	4.03	11
J010P	ad	6.97	0.05	0.03			7.05	3.91	0.04		3.95	11
J019P	6b	7.10	0.05	0.03			7.18	3.78	0.04		3.82	11

Table 7. Calculated unit-cell parameters of anilite from Jáchymov for the space group *Pnma*.

sample	*a*	*b*	*c*
		(Å)	
J041P	7.932(2)	7.826(1)	11.008(2)

Table 8. Homogenization temperature Th of fluid inclusions in ankerite.

sample	mineral	Th	salinity	mineralization stage
		°C	wt.%	
J006I 1	ankerite	118–142	22–23	*arsenide*

Table 9. Calculated unit-cell parameters of ankerite for the space group $R\bar{3}$.

sample	*a*	*c*
	(Å)	
J051P	4.819(2)	16.123(3)
MP511C (J-922)	4.8356(6)	16.094(3)

Annite $KFe_3AlSi_3O_{10}(OH,F)_2$

Annite forms flakes in greisen, 1 cm long, green black in colour. It contains abundant *hematite* located along cleavage planes. It is associated with *ferberite*, *topaz*, *apatite*, *scheelite* and *molybdenite*. The sample comes from the Rovnost I shaft, probably from 8th level.

Table 10. Chemical analyses of annite.

sample	pt.	Na_2O	K_2O	FeO	MnO	MgO	TiO_2	Al_2O_3	SiO_2	Total
						weight %				
J142P	1	0.60	9.25	23.20	0.30	0.69	0.44	21.51	37.19	93.18
J142P	2	0.56	9.40	22.44	0.26	0.76	0.64	21.69	37.15	92.90
J142P	3	0.38	10.13	21.57	0.34	0.57	0.67	22.21	38.37	94.26
J142P	4	0.57	9.72	23.23	0.44	0.69	0.60	21.58	36.77	93.60

sample	pt.	K	Na	subtotal	Fe	Mn	Mg	Al	subtotal	Al	Si	Ti	subtotal	O
							number of atoms							
J142P	1	0.93	0.09	1.02	1.52	0.02	0.06	0.94	2.55	1.05	2.92	0.03	4.00	11
J142P	2	0.94	0.08	1.03	1.47	0.02	0.07	0.96	2.53	1.04	2.92	0.04	4.00	11
J142P	3	1.00	0.06	1.05	1.39	0.02	0.05	1.01	2.47	1.01	2.95	0.04	4.00	11
J142P	4	0.97	0.09	1.06	1.53	0.03	0.06	0.92	2.54	1.07	2.89	0.04	4.00	11

Antimony Sb

Antimony was reported from Jáchymov by Schneiderhöhn and Ramdohr [466] but only in a listing of localities from which they studied *antimony* samples, without any other information. However, as they did not mention *miargyrite* from this locality, it is possible that the locality information may be incorrect.

Table 11. Chemical analysis of antimony.

sample	pt.	S	Cu	As	Ag	Sb	Total
				weight %			
J105P	D1	0.76	0.07	0.28	1.22	96.38	98.70

sample	pt.	Ag	Sb	S	Total
		number of atoms			
J105P	D1	0.01	0.95	0.03	0.98

Antimony was identified as small round grains up to 3 μm in size, enclosed in *miargyrite* in *dolomite* gangue. It is a very rare mineral. Our study suggests that the two minerals crystallized at the same time, as indicated for the *miargyrite–antimony* pair by the equilibrium relations in the Ag–Sb–S system [427], [444]. *Stibnite*, *pyrite*, *sphalerite*, *pyrargyrite*, *arsenic*, *dyscrasite*, *stibarsen*, and *robinsonite* are associated in a broader assemblage. The studied sample comes from the Svornost shaft, Adit level, Hildebrand vein.

Argentite Ag_2S

In the present state of knowledge, correct naming of this mineral is somewhat difficult. *Argentite* is a cubic polymorph of Ag_2S, unstable below 176 °C, undergoing spontaneous inversion to the monoclinic polymorph – *acanthite*. The name *argentite* can be applied perhaps only to those specimens of Ag_2S, which show euhedral/subhedral cubic crystal morphology or individual samples for which the primary crystallization as the cubic phase is proved by other methods. Even so, such crystals are in fact pseudomorphs of *acanthite* after *argentite* (Fig. 4).

Mrňa a Pavlů [351] presented updated information on *argentite* from Jáchymov. They found that it is the main mineral of Ag in the ores of *arsenide* stage. It fills cavities after *silver* dendrites and especially vugs in arsenide ores.

In ores of the *arsenic-sulphide* stage, it occupies a similar position as *proustite* but is subordinate. *Argentite* forms minute (1–2 mm) anhedral to subhedral grains in arsenic or euhedral crystals max. 5 mm in size, dominated by rhombic dodecahedron. They occur jointly with other silver minerals in vein cavities [351].

Argentite occurs mainly in upper parts of Jáchymov veins, where it forms veinlets together with other silver minerals and *pyrite* aggregates in carbonate gangue. Polished sections show rare sections of crystals with combination of (100) and (111) faces, deposited on arsenides, mainly *nickeline*. The colour is silver white turning into grey after some time.

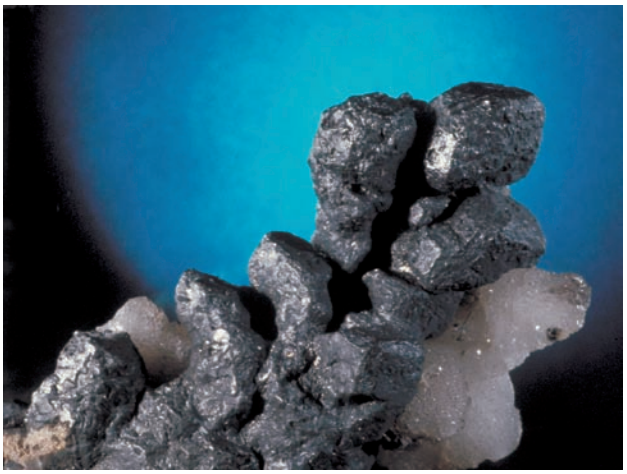

Fig. 4. Group of argentite crystals on carbonate gangue (width of figure 5 cm). Photo J. & E. Sejkora.

Polished sections show mainly anisotropic domains corresponding to randomly orientated sections of *acanthite* next to relics of isotropic material. It is photosensitive – see acanthite above. Its grains are rimmed by *pyrite* aggregates, *arsenides,* and rare *chalcopyrite* in *dolomite* or *calcite*.

Argentopyrite $AgFe_2S_3$

Argentopyrite was decribed from Jáchymov by Sartorius in 1866 [438]. Tschermak [469] considered the

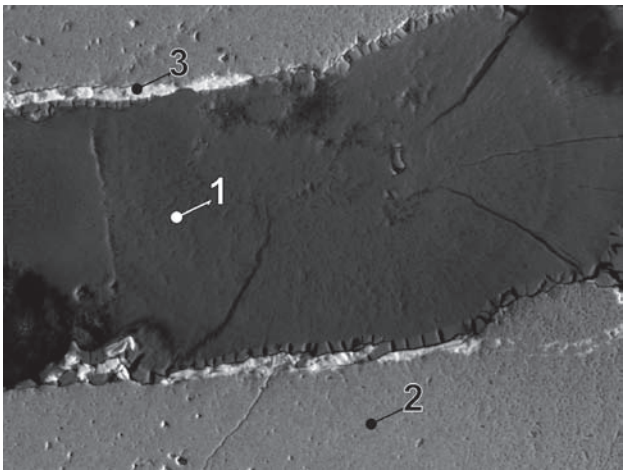

Fig. 5. J116P/D-2. 1 – annabergite, 2 – pyrite, 3 – Ag-Fe-sulphides. Svornost shaft, 8th level, Geschieber vein. BSE image. Magnification 270×.

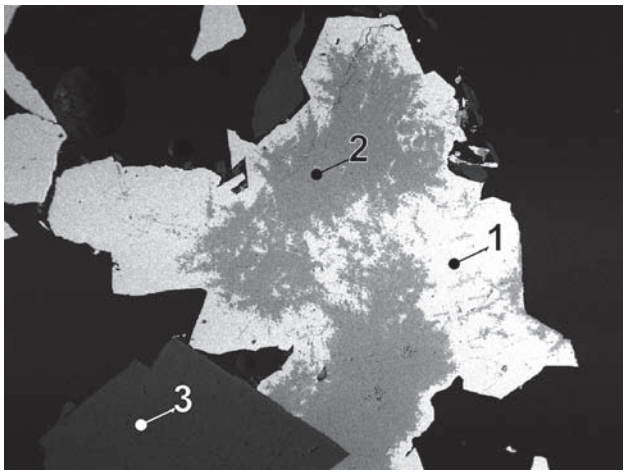

Fig. 6. J166P (NM9527). 1 – argentopyrite, 2 – Ag-pyrite, 3 – ankerite. Svornost shaft, 8th level, Geschieber vein. BSE image. Magnification 20×.

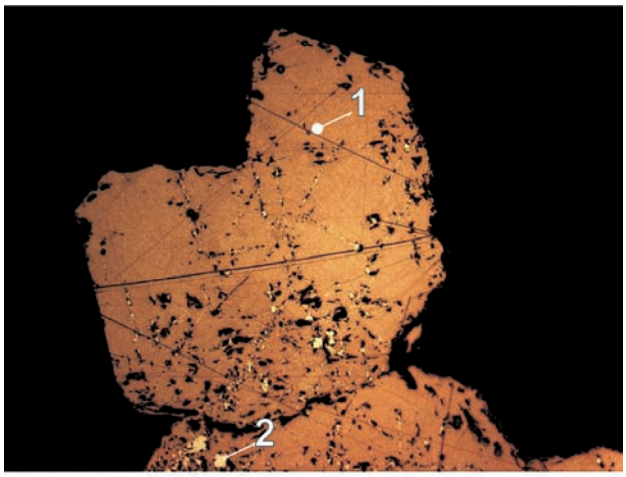

a

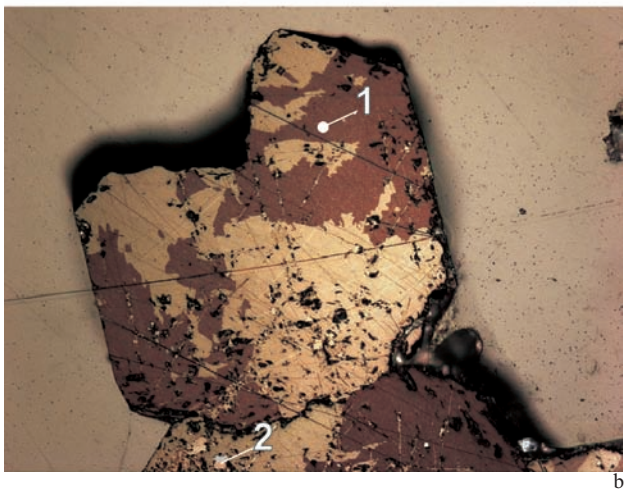

b

Fig. 7a, b. NM4810. Cross-section of prismatic argentopyrite crystals as seen with single polarizer and crossed polarizers. Strong anisotropy indicates intergrowth of crystals in different orientation. Minor marcasite indicates beginning decomposition of argentopyrite. 1 – argentopyrite, 2 – marcasite. Magnification 50×.

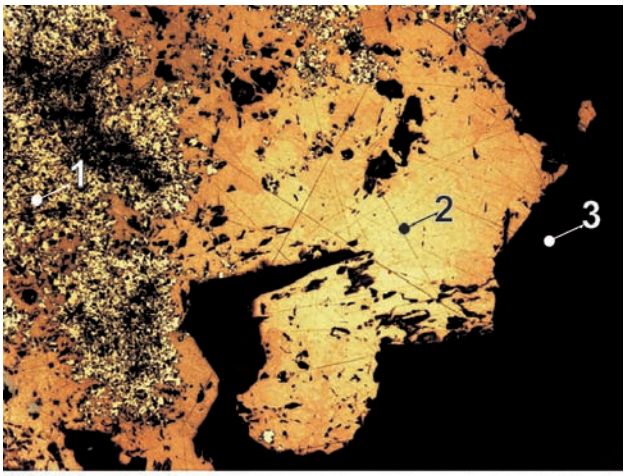

a

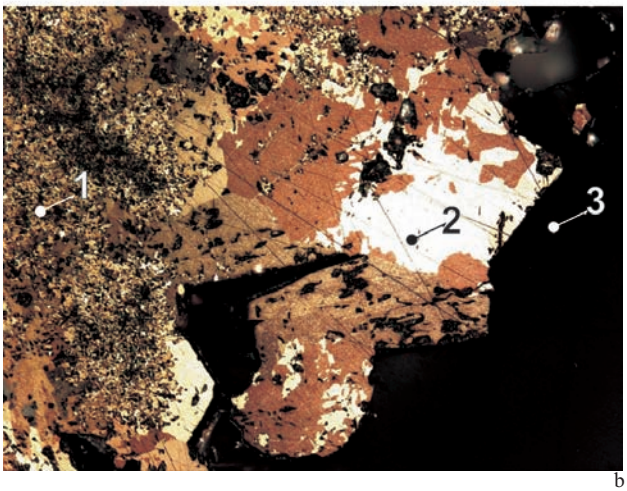

b

Fig. 8a, b. NM9527A. Anisotropic aggregate of argentopyrite as seen with single polarizer and crossed polarizers. Indication of cleavage at argentopyrite margin. Argentopyrite is extensively decomposed to acanthite+marcasite aggregate. 1 – acanthite+marcasite after argentopyrite, 2 – argentopyrite, 3 – carbonate. Svornost shaft, 8th level, Geschieber vein. Magnification 50×.

Fig. 10. Argentopyrite crystals on proustite (width of figure 9.5 mm). Photo J. & E. Sejkora.

Fig. 11. Group of argentopyrite crystals (width of figure 1.1 cm). Photo J. & E. Sejkora.

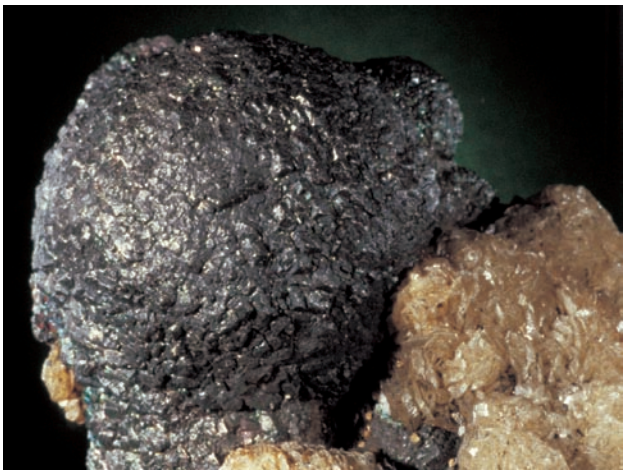

Fig. 9. Hemispherical aggregate with argentopyrite crystals (width of figure 5 cm). Photo J. & E. Sejkora.

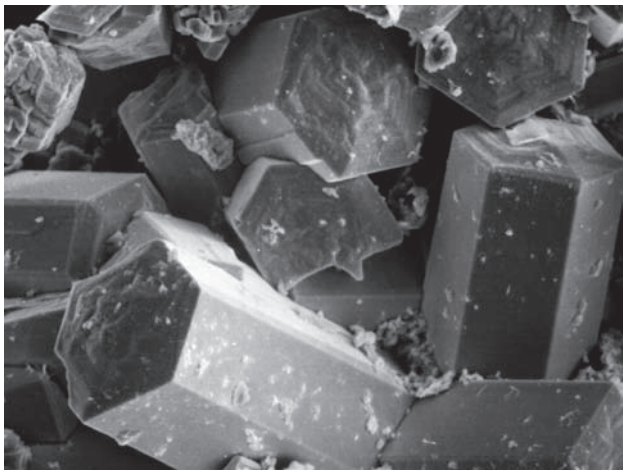

Fig. 12. J-853. Columnar crystals of argentopyrite on arsenic. Svornost shaft. SE image. Magnification 330×. Photo A. Gabašová.

crystals as pseudomorphs due to their inhomogeneity. Schrauf (1871) [339] measured the morphology of several *argentopyrite* crystals from private collections. He concluded that the material forms twinned orthorhombic crystals with twin plane (110) and he rejected a contention that these are pseudomorphs, as the crystals were homogeneous yellow grey on fracture surface. The density measured on 25 mg of material was 5.53 g/cm^3.

The present study indicates that all the descriptions of previous authors were correct. Differences relate to the fact that *argentopyrite* tends to be subject to alteration, which differs in various samples and results in variable composition of crystals.

Argentopyrite is most common in prismatic crystals striated parallel to elongation, which are yellow brown, grey yellow or bronze-red in colour (Figs 9–12). The striated crystals are triplets but crystals with smooth faces are also present, grading to tabular crystals. The main mass or larger crystals of *argentopyrite* are usually deposited on diarsenides or triarsenides. *Argentopyrite* is particularly abundant in vugs after leached silver in association with *acanthite*, *proustite* and *galena*. Some samples carry a younger generation of *argentopyrite* in lustrous crystals together with *proustite* resting on older crystals of *argentopyrite*. Some crystals are enclosed in proustite (Figs 7 and 8).

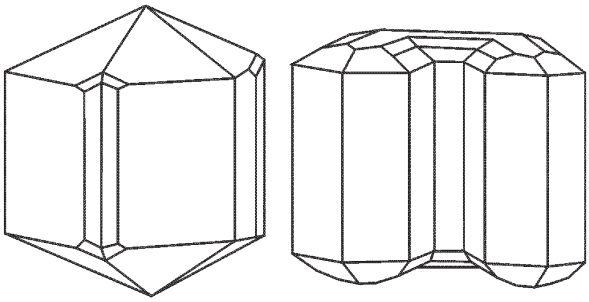

Fig. 13. Argentopyrite according to Schrauf in [492].

Chemical study of this mineral faces problems related to the variable degree of its alteration. Very fine lamel-

Table 12. Chemical analyses of argentopyrite.

sample	pt.	Ag	Fe	Cu	Pb	Bi	Sb	S	As	Sb	Total
						weight %					
SR001	3	33.89	35.69	0.23				30.38	0.04	0.05	100.28
SR001	4	33.80	35.34	0.29				30.46	0.12	0.08	100.09
SR001	5	34.10	35.32	0.11				30.32	0.13	0.04	100.02
SR001	6	34.35	35.61	0.10				30.46	0.04	0.05	100.61
SR001	7	33.97	35.24	0.21				30.24	0.06	0.05	99.77
SR001	8	34.02	35.28	0.26				30.22	0.18	0.04	100.00
NM4810	1	35.24	34.68					30.13	0.01		100.07
NM4810	2	34.70	34.54					29.74			98.98
NM4810	3	34.96	34.58					29.79			99.33
NM4810	4	35.43	35.41					30.37			101.22
NM4810	5	35.15	34.99					30.63	0.29		101.06
NM4810	6	34.47	34.84	0.13				30.08	0.04		99.55
NM9527	1	34.89	35.37					30.13			100.39
NM9527	2	34.82	35.52					29.96			100.30
NM9527	3	34.79	35.62					30.15			100.56
NM9527	4	34.64	35.31					29.95			99.90
NM9527	5	34.45	35.60					30.15			100.20
NM9527	6	34.39	35.58					30.18			100.15
NM-4809	1	33.63	35.95	0.07	0.08			30.82			100.55
NM-4809	2	34.17	36.11	0.14	0.20			31.31			101.93
NM-4809	3	33.72	35.95	0.13	0.18	0.45		30.85			101.28
NM-4809	4	33.77	35.87	0.11	0.15	0.22		30.82			100.94
NM-4809	5	33.85	36.11	0.16	0.23	0.23		31.06			101.64
NM-4809	6	33.28	35.94	0.17	0.14	0.20		30.75			100.48
NM-4809	7	32.30	35.07	0.17				30.02			97.56
NM-4809	8	33.02	35.30	0.09	0.09	0.07		30.31	0.07		98.95
NM-4809	9	32.59	35.08	0.11				30.83			98.61
NM-4809	10	32.66	35.10	0.14	0.28	0.19		30.75			99.12
NM-4809	11	33.01	34.82	0.13	0.07	0.07		30.04			98.14
NM-9526	1	33.84	35.95					30.26			100.05
NM-9523	1	33.36	35.93	0.28		0.22		30.82			100.61
NM-9523	2	33.30	35.91	0.37	0.18		0.36	30.91			101.03
NM-9523	3	33.62	36.01	0.41				30.81			100.85
NM-9523	4	33.40	35.37	0.41	0.11	0.21	0.74	30.90			101.14
NM-9523	5	33.33	35.81	0.41		0.26		30.55			100.36

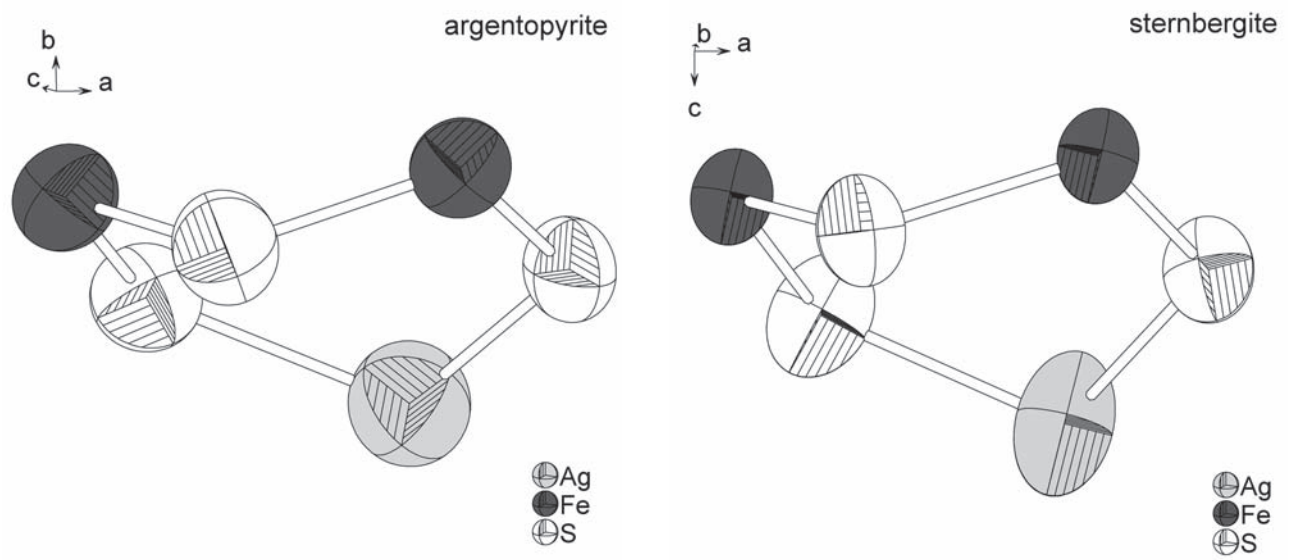

Fig. 14. Comparison of distorted six-member rings S–Fe–S–Fe–S–Ag in the structure of argentopyrite (top) and sternbergite [430] (bottom). Two Fe atoms are positioned above the triangle defined by S atoms and Ag atom is on the opposite side of the triangle.

Table 12. *(continued)*

sample	pt.	Ag	Cu	Fe	S	As	Total
				number of atoms			
SR001	3	0.98		1.96	3.05		6
SR001	4	0.99	0.01	2.01	2.98		6
SR001	5	0.99	0.01	2.00	3.00	0.01	6
SR001	6	1.00	0.01	2.00	2.99	0.01	6
SR001	7	1.00	0.01	2.00	2.99		6
SR001	8	1.00	0.01	2.00	2.99		6
NM4810	1	1.04		1.97	2.99		6
NM4810	2	1.03		1.99	2.98		6
NM4810	3	1.04		1.98	2.98		6
NM4810	4	1.03		1.99	2.98		6
NM4810	5	1.02		1.97	3.00	0.01	6
NM4810	6	1.02		1.99	2.99		6
NM9527	1	1.02		2.00	2.97		6
NM9527	2	1.02		2.02	2.96		6
NM9527	3	1.02		2.01	2.97		6
NM9527	4	1.02		2.01	2.97		6
NM9527	5	1.01		2.02	2.97		6
NM9527	6	1.01		2.01	2.98		6
NM-4809	1	0.98		2.01	3.01		6
NM-4809	2	0.98	0.01	2.00	3.02		6
NM-4809	3	0.98	0.01	2.01	3.00		6
NM-4809	4	0.98	0.01	2.01	3.00		6
NM-4809	5	0.97	0.01	2.01	3.01		6
NM-4809	6	0.97	0.01	2.02	3.00		6
NM-4809	7	0.96	0.01	2.02	3.01		6
NM-4809	8	0.97		2.01	3.01		6
NM-4809	9	0.96	0.01	1.99	3.05		6
NM-4809	10	0.96	0.01	1.99	3.04		6
NM-4809	11	0.98	0.01	2.00	3.01		6
NM-9526	1	0.99		2.03	2.98		6
NM-9523	1	0.97	0.01	2.01	3.00		6
NM-9523	2	0.96	0.02	2.00	3.00		6
NM-9523	3	0.97	0.02	2.01	3.00		6
NM-9523	4	0.97	0.02	1.98	3.01		6
NM-9523	5	0.97	0.02	2.01	2.99		6

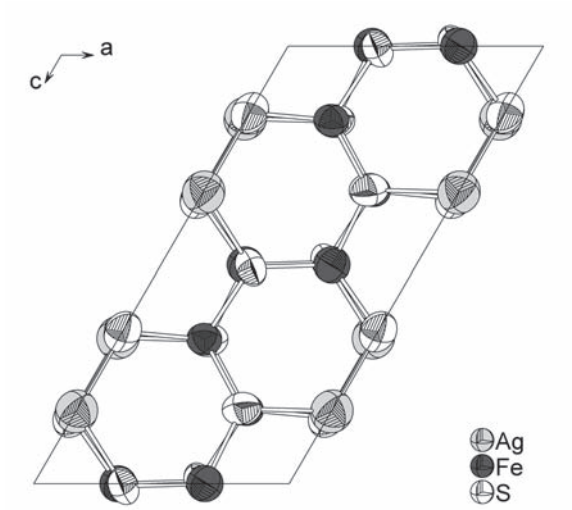

Fig. 15. Pseudo-hexagonal motifs of 6 – member circles of S–Fe–S–Fe–S–Ag dominate in a projection of crystal structure of argentopyrite into a plane (010).

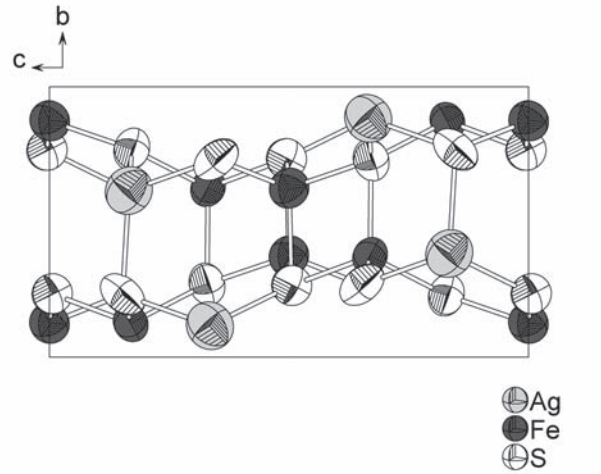

Fig. 16. A projection of crystal structure of argentopyrite into a plane (100) shows deformation of 6 – member circles of S–Fe–S–Fe–S–Ag and their ordering in layers parallel with (010).

Table 13. Calculated unit-cell parameters of argentopyrite from Jáchymov for the space group $P2_1/c$.

sample	*a*	*b*	*b*	β
		(Å)		(°)
NM9527 [485]	6.688(2)	6.477(1)	13.268(4)	120.03(3)

lar intergrowth of *argentopyrite* and its alteration products constitute irregular zones. Alteration proceeds from the centre of the crystal to the rims, and some marginal parts contain unaltered material.

Sartorius [438] described the mineral as forming hexagonal prisms up to 2 mm long with pyramidal faces. The mineral was of light lead colour with yellow tint, black streak. Very brittle, hardness 3.5–4, density on 18 mg sample 6.47 g/cm^3 at 12 °C. Chemical analysis yielded 39.3 wt.% Fe, 26.5 wt.% Ag, and 34.2 wt.% S calculated from the loss. Crystallographic measurement indicated that the crystals are monoclinic, twinned on (250) plane. A small amount of As was interpreted as derived from *proustite*. The chemical composition is thus close to *sternbergite* [438].

Tschermak [469] reported that *argentopyrite* can be overgrown by *pyrargyrite*, and two of 11 specimens con-

Table 14. X-ray powder diffraction data for argentopyrite indexed in the space group $P2_1/c$.

h	*k*	*l*	d_{obs}	d_{calc}	I_{rel}	*h*	*k*	*l*	d_{obs}	d_{calc}	I_{rel}
1	0	0	5.797	5.784	23.3	0	3	2		2.016	
1	0	–2		5.771		2	2	1	1.9913	1.9867	4.4
0	0	2	5.742	5.729	6.5	1	3	1	1.9307	1.9305	46.3
0	1	1	5.638	5.627	14.3	1	3	–3		1.9295	
1	–1	–1	4.652	4.647	12.1	3	0	0		1.9281	
1	1	–2	4.297	4.304	8.5	3	0	–6	1.9220	1.9237	46.3
1	1	1	3.614	3.612	74.7	0	0	6	1.9109	1.9095	44.8
1	1	–3		3.606		0	2	5	1.8694	1.8689	9.8
2	0	–2	3.346	3.345	60.5	2	3	–2	1.8103	1.8107	46.6
1	0	2	3.315	3.321	100.0	2	1	–7		1.8123	
1	0	–4		3.313		1	3	2	1.8056	1.8067	56.9
0	1	3	3.284	3.288	16.9	1	3	–4		1.8055	
0	2	0	3.232	3.230	38.0	2	3	–1	1.7880	1.7889	5.8
0	2	1	3.110	3.109	73.1	2	3	–3		1.7881	
2	–1	–2	2.972	2.971	6.4	3	2	–1	1.7473	1.7489	14.0
2	1	–2		2.971		3	2	–5		1.7467	
1	1	2	2.952	2.953	19.5	4	0	–4	1.6724	1.6727	10.3
1	1	–4		2.948		1	3	3		1.6676	
1	2	–1	2.906	2.909	34.2	1	3	–5		1.6663	
2	0	0	2.878	2.892	29.8	2	0	4	1.6645	1.6602	14.9
2	0	–4		2.886		2	0	–8	1.6554	1.6565	19.3
2	1	–1		2.877		3	2	0		1.6556	
2	1	–3		2.874		3	2	–6		1.6528	
1	2	0	2.824	2.820	2.8	0	2	6	1.6439	1.6438	5.6
1	2	–2	2.824	2.819		0	4	0	1.6147	1.6151	14.8
2	1	–4	2.632	2.635	9.5	4	1	–4		1.6192	
0	1	4	2.618	2.618	7.5	4	1	–3	1.6031	1.6039	9.0
1	2	1	2.593	2.595	25.3	4	1	–5		1.6028	
1	2	–3	2.593	2.592		1	2	5	1.5957	1.5971	7.3
1	1	3	2.437	2.440	43.1	1	2	–7		1.5955	
1	1	–5	2.437	2.436		1	4	0	1.5542	1.5556	4.8
2	1	1	2.343	2.347	5.9	3	2	1	1.5479	1.5468	5.0
2	1	–5	2.343	2.342		3	2	–7	1.5439	1.5438	9.9
1	2	2	2.316	2.315	14.8	0	2	7	1.4599	1.4600	3.1
1	2	–4	2.316	2.313		1	4	2	1.4525	1.4524	3.4
2	2	–1	2.278	2.278	13.5	1	4	–4		1.4517	
2	2	–3	2.278	2.277		4	3	–4	1.3209	1.3210	7.8
2	0	–6	2.168	2.173	11.9	4	1	–9		1.3208	
1	0	4		2.170		2	0	6	1.3186	1.3178	2.2
1	0	–6		2.166		2	3	4	1.3156	1.3148	6.4
0	3	1	2.114	2.116	12.5	2	3	–8	1.3121	1.3130	10.8
3	1	–3	2.114	2.108		4	3	–5		1.3120	
1	2	3	2.041	2.042	4.1	3	4	0	1.2380	1.2381	5.3
1	2	–5		2.040		3	4	–6	1.2380	1.2369	
1	3	–2	2.015	2.018	5.3	5	2	–5	1.2361	1.2362	4.8
						0	4	6		1.2331	

tained a younger generation of *argentopyrite* resting on *pyrargyrite*. Broken *argentopyrite* crystals show mat yellow grey core surrounded by strongly lustrous white yellow crust which defined the crystal surface. In individual samples, the crust was of equal width on various crystals, so small crystals were nearly free of the grey core. One 5 mm long crystal carried *pyrargyrite* in the grey core. These observations led Tschermak to the conclusion that *argentopyrite* is not an independent mineral but a pseudomorph of several minerals after an unknown mineral. Morphological measurements supported monoclinic symmetry. Separate analyses of the core and rims of the crystals resulted in a conclusion that the rims may also show compositional differences. The density of the core was determined at 4.88 g/cm^3. Tschermak concluded that the cores are composed of a mixture of *marcasite* and *pyrrhotite*, while the rims contain also *acanthite*. He considered the former descriptions of *pyrrhotite* crystals incorrect and related to the studied pseudomorphs [469].

According to this study, *argentopyrite* is monoclinic with space group $P2_1/c$ [485]. The unit-cell parameters are presented in Table 13. Table 14 presents powder diffraction data of the studied *argentopyrite* indexed in agreement with the refined crystal structure [485].

The *argentopyrite* structure [485] is strongly pseudohexagonal (Figs 14a and 15). The projection on (100) plane (Fig. 16) documents a "layered" character of the structure. The hexagonal S–Fe–S–Fe–S–Ag rings are not strictly planar, as shown in Fig. 14a, b. The same motif is observed in the structure of *sternbergite* [430].

Argentotennantite $(Ag,Cu)_6[(Cu,Ag)_4\ (Fe,Zn)_2]\ (As,Sb)_4\ S_{13}$

It was identified as several isolated grains up to 25 μm in size, enclosed in *quartz* gangue. *Rammelsbergite*, spheroidal *pyrite*, and rare *freibergite* occur in the associated paragenesis. *Argentotennantite* was also found as an inclusion in *chalcopyrite* associated with *pyrite* and *galena*. The studied sample comes from an adit above the Unruhe adit.

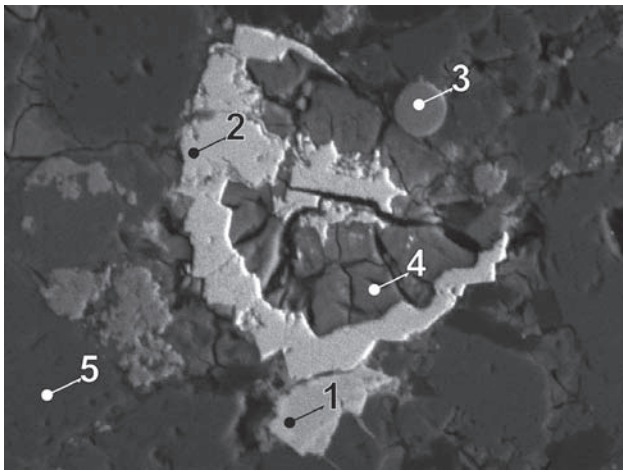

Fig. 17. J160P/A. 1 – argentotennantite, 2 – rammelsbergite, 3 – pyrite, 4 – annabergite, 5 – quartz. Adit above Unruhe adit. BSE image. Magnification 800×.

Arsenic As

Zepharovich (1875) [470] described *arsenic* crystals as short fine needles 1.5×0.5 mm in size, in sheaf-like aggregates in vugs of fine-grained *arsenic*. The sample was collected in 1872 in the Geschieber vein.

Vrba [362] described a specimen of *arsenic* covered with equant crystals of *chalcocite*. The full sequence in this paragenesis is as follows: *arsenic* aggregate is covered by spongy spheroidal *silver*, followed by a crust of *löllingite* crystals, covered in turn by scattered *calcite* in low rhombohedral crystals and by *chalcocite* crystals.

Table 15. Chemical analyses of argentotennantite.

sample	pt.	Cu	Ag	Fe	Zn	Co	Ni	As	Sb	S	Total
						weight %					
J160P	1	24.70	21.32	5.59	1.57	0.05	0.43	16.20	5.52	24.31	99.70
J160P	E1	24.59	21.10	5.99	1.41			17.13	5.50	24.36	100.09
J160P	E2	25.04	21.07	5.45	1.70			16.73	5.88	24.41	100.27
J160P	E3	20.01	24.84	5.87	1.82			9.41	14.77	22.35	99.08
J160P	E4	19.98	26.92	5.97	0.80			10.18	13.59	22.95	100.39
J160P	5	20.40	24.61	4.92	2.35			10.47	13.64	23.07	99.45
J160P	6	23.56	22.79	5.48	1.62			14.66	7.87	24.05	100.03

sample	pt.	Cu	Ag	Fe	Zn	Ni	subtotal	As	Sb	S	subtotal	Total
						number of atoms						
J160P	1	6.49	3.30	1.67	0.40	0.12	11.98	3.61	0.76	12.65	17.020	29
J160P	E1	6.43	3.25	1.78	0.36		11.82	3.80	0.75	12.63	17.176	29
J160P	E2	6.55	3.24	1.62	0.43		11.84	3.71	0.80	12.65	17.156	29
J160P	E3	5.63	4.12	1.88	0.50		12.12	2.24	2.17	12.46	16.875	29
J160P	E4	5.54	4.40	1.88	0.21		12.03	2.39	1.97	12.61	16.968	29
J160P	5	5.66	4.02	1.55	0.63		11.87	2.47	1.98	12.69	17.130	29
J160P	6	6.27	3.57	1.66	0.42		11.92	3.31	1.09	12.68	17.083	29

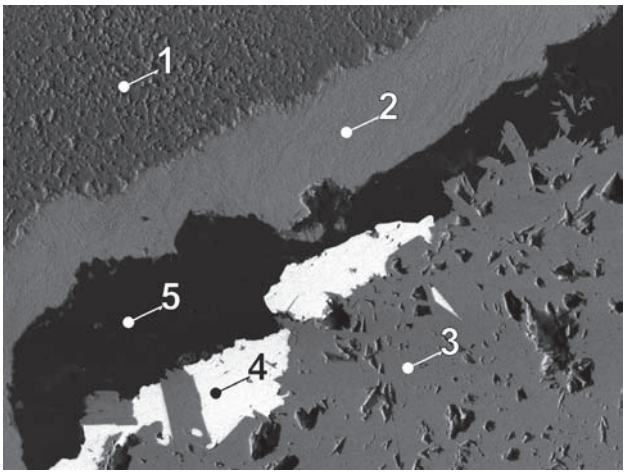

Fig. 18. MP420A/D-3. 1 – fine-grained arsenic, 2 – coarse-grained arsenic, 3 – löllingite, 4 – galena, 5 – calcite. Barbora shaft. BSE image. Magnification 130×.

Fig. 20. Aggregate of arsenic (width of figure 8 cm). Photo J. & E. Sejkora.

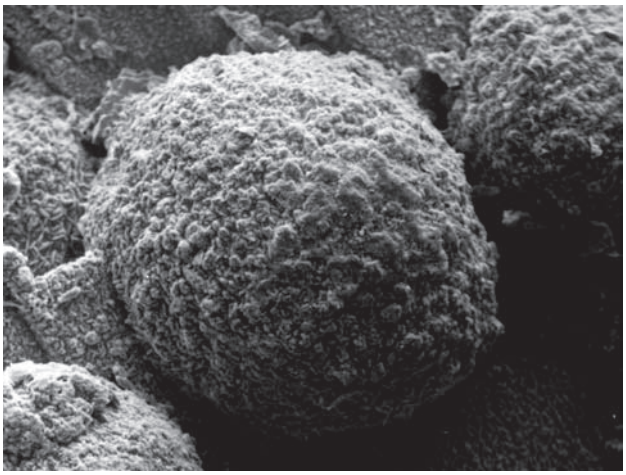

Fig. 19. VS4231. Botryoidal aggregates of arsenic on dolomitic carbonate. SE image. Magnification 100×. Photo A. Gabašová.

Fig. 21. Thin-bedded aggregate of arsenic (width of figure 8 cm). Photo J. & E. Sejkora.

Table 16. Chemical analyses of arsenic.

sample	pt.	As	S	Sb	Bi	Fe	Co	Ni	Ag	Cu	Total
						weight %					
J024P	a8	98.59	0.27	0.67		0.19	0.07	0.11		0.13	100.03
J024P	a9	98.31	0.26	0.87		0.33	0.16	0.07		0.32	100.32
J105P	A1a	68.61	0.27	14.76	5.06	0.04			0.90		89.64
J105P	E1	92.86	0.09	7.18					0.19	0.05	100.36
J105P	E2	93.40	0.06	6.82					0.15	0.07	100.51
J105P	A1	91.99	0.02	7.82		0.07			0.11	0.07	100.07

sample	pt.	As	S	Sb	Bi	Total
			number of atoms			
J024P	a8	0.98	0.01			1
J024P	a9	0.98	0.01	0.01		1
J105P	A1a	0.85		0.11	0.02	1
J105P	E1	0.95		0.05		1
J105P	E2	0.95		0.04		1
J105P	A1	0.95		0.05		1

A recent study of Jáchymov *arsenic* was published by Mrňa and Pavlů (1967) [351]. They characterized *arsenic* as the most abundant mineral of the *arsenic–sulphide* mineralization stage. Major occurrences were reported from the Geschieber vein, Svornost shaft, where the mineral was present along the whole exposed length of the vein, except for borehole HG-1, reaching below the lowermost level of the shaft. The most extensive *arsenic* bodies in the Geschieber vein (Svornost shaft) were found at the 5th and 10th level, reaching from several metres up to 10 m. Smaller quantities of *arsenic* are deposited on arsenide ores of the Ag paragenesis.

Nearly monomineralic *arsenic* masses form spheroidal aggregates up to 15 cm in diameter, showing a shell-like internal structure. In some parts of the veins, it formed spongy aggregates with numerous small vugs covered with minute crystals of other ore minerals of this stage.

Oxidation of polished sections exposed to air reveals structural heterogeneity of seemingly compact aggregates.

Arsenic is most frequently associated with silver minerals, which either fill vugs or overgrow *arsenic* aggregates. They sometimes enclose small globular *silver* aggregates, dendritic *silver* is less common here. Silver minerals and native *silver* do not show structures of replacement by *arsenic*.

A rim of tiny *löllingite* crystals often marks the boundary between *arsenic* and gangue. The main gangue mineral is *dolomite*, sometimes slightly replacing *arsenic*. Among trace elements in *arsenic*, an admixture of Bi and Sb is notable [351].

The present study confirmed the published observations and brought some new data. However, inclusions in *arsenic*, considered as *stibarsen*, were not found during an examination of the same polished sections.

Arsenic is medium-grained, slightly porous, with a macroscopic concentric structure. The aggregates show botryoidal surface when developed in vugs. Freshly exposed *arsenic* has a light bluish grey colour (Figs 20 and 21). After some 15 minutes, it turns bluish and then darker brownish. Later on, it is covered by a brown-black layer of alteration products, which mimic the internal structure of the aggregates, consisting of radiating columnar grains with serrated boundaries. Only stable minerals such as diarsenides, *bismuth*, *bismuthinite*, a.o., remain unaltered in this stage.

Observations in polished sections show that fine-grained central aggregates get altered more readily than the outer parts. During oxidation, arsenic gets covered by tiny octahedra of *arsenolite.*

The vugs in *arsenic* were often produced by leaching of enclosed skeletal *silver*, which remained preserved only exceptionally. Walls of the vugs are free of younger arsenides or other minerals. Vugs in arsenic frequently carry *proustite* or rare *xanthoconite*. *Arsenic* may enclose grains of *bismuth* with narrow rims of *bismuthinite*. Lower parts of botryoidal *arsenic* may enclose *skutterudite* with increased Ni and Fe content. *Arsenic* crystals sometimes present in vugs in *arsenic* or gangue are tabular with orthorhombic shape.

Unusual *arsenic* compositions were found in a paragenesis with antimony minerals from the Hildebrand vein (Svornost shaft, Adit level). The older, more compact *arsenic* enclosing *nickel-skutterudite* is fairly pure (0.5 wt.% Sb) but younger grains contain an admixture of Sb increasing up to 7 wt.% Sb in the outer zone 30–40 μm wide. The marginal zone encloses *dyscrasite*. A vug in older *arsenic* contains *stibarsen*, *calcite*, and an intermetallic Bi-Sb phase with element ratio 1:1, and an arsenic alloy containing 15 wt.% Sb.

Arsenolamprite As

According to Hintze [418], who first described the mineral (1904 from Marienberg [418]), *arsenolamprite* was present in the Geyer, Geschieber and Hofmann veins at Jáchymov. It forms thin platy and malleable tables up to 5 mm, similar in appearance to dark *molybdenite*. It is enclosed in botryoidal *arsenic* in dolomite gangue. Later on, an *arsenolamprite* specimen was collected on a dump of the Rovnost I shaft in 1946 by J. H. Bernard (personal communication) and identified by Z. Johan (personal communication). The mineral was not observed in the present study.

Arsenopyrite FeAsS

Mrňa and Pavlů [351] studied a*rsenopyrite* from Jáchymov. They noted that the mineral was quite rare in the veins. *Arsenopyrite* forms small strongly fractured lenticular masses associated with *pyrite* in *quartz* gangue or fine-grained impregnations of star-shaped crystals at margins of minerals of the *sulphidic* stage. Larger crystals

Table 17. Calculated unit-cell parameters of arsenopyrite from Jáchymov for the space group $P\bar{1}$.

sample	*a*	*b*	*c*	α	β	γ
		(Å)			(°)	
J-855	5.746(2)	5.703(2)	5.790(1)	90	112.61(2)	90

Table 18. Chemical analyses of arsenopyrite.

sample	pt.	Fe	Co	Ni	Ag	Cu	As	Sb	S	Total
					weight %					
J061P	1	32.15	0.82	1.05		0.43	46.07	0.39	19.89	100.80
MP427	2	33.17					48.83		18.17	100.17
MP427	2	33.04					46.49		18.74	98.27
J034P	23	33.70	0.45	0.38	0.20	0.32	45.18	0.41	19.22	99.86
J034P	24	34.33	0.33	0.49		0.38	45.18	0.39	19.81	100.91
J034P	25	33.45	0.41	0.60	0.61	0.44	44.27	0.59	19.92	100.29

sample	pt.	Fe	Ni	Co	subtotal	As	S	Total
					number of atoms			
J061P	1	0.93	0.03	0.02	0.98	1.00	1.01	3
MP427	2	0.98			0.98	1.08	0.94	3
MP427	2	0.99			0.99	1.04	0.98	3
J034P	23	0.99	0.01		1.00	0.99	0.98	3
J034P	24	0.99	0.01		1.01	0.97	1.00	3
J034P	25	0.97	0.02		0.99	0.96	1.01	3

in *quartz* gangue are usually crushed but undeformed aggregates show an arborescent structure [351].

These observations were confirmed by the present study. It is concluded that majority of *arsenopyrite* crystallized early – in the *Sn–W sulpharsenide* stage. *Arsenopyrite* forms anhedral or euhedral crystals up to 1 cm in size, disseminated in altered wall–rock composed of fine muscovite with *anatase* or in *quartz* veins, where it is accompanied by *pyrite* and *chalcopyrite* with exsolutions of *stannite*. *Arsenopyrite* may enclose *cassiterite*, *monazite-(Ce)* and *ilmenite*. *Muscovite* mica schists carrying *arsenopyrite* contain also *topaz* and zoned *tungstenian rutile*. This type of *arsenopyrite* comes from the Giftkies adit, and Nikolaj shaft, 1st level, crosscut adit to Rovnost I shaft.

Another wall-rock sample composed of dark chlorite with corroded *pyrite* rimmed by *hematite* is mineralized by tiny *arsenopyrite* in grains max. 0.2 mm in size, intergrown with *löllingite*. Both the *arsenopyrite* and *löllingite* enclose minor *bismuth*, *gold, clausthalite*, *bismuth* + Bi-telluride mixture and *bismuth* + *aurostibite* mixture. This type of mineralization probably pre-dates the oldest type of mineralization at Jáchymov. The sample studied comes from the Barbora shaft, below 7th level, probably near vein 1S.

Anhedral grains of *arsenopyrite* accompanied by *chalcopyrite* in carbonate gangue are very rare.

Arsenpolybasite $(Ag,Cu)_{16}(As,Sb)_2S_{11}$

The mineral occurred in the central part of the Jáchymov deposit. Its colour is steel grey with a greenish tint. Fracture is uneven, imperfect cleavage along the basal face for hexagonal orientation. Thin fragments are dark red in transmitted light. Granular aggregates up to 2 mm are enclosed in *quartz*-carbonate gangue. It also occurs in hexagonal tabular crystals or rare prisms.

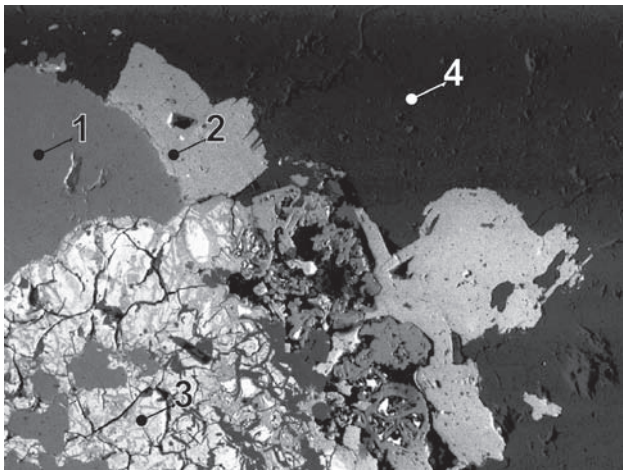

Fig. 23. MP271B/B-3. 1 – rammelsbergite, 2 – arsenpolybasite, 3 – uraninite, 4 – calcite. Barbora shaft, 4th/5th level, No. 32 vein. BSE image. Magnification 270×.

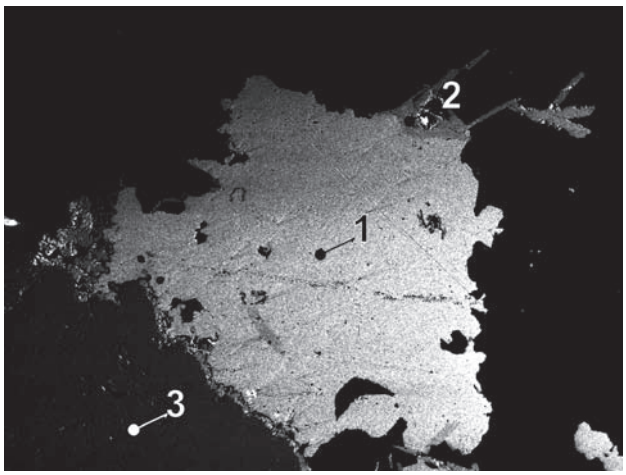

Fig. 24. MP271B/A-9. 1 – acanthite, 2 – arsenpolybasite, 3 – rammelsbergite. Barbora shaft, 4th/5th level, No. 32 vein. BSE image. Magnification 400×.

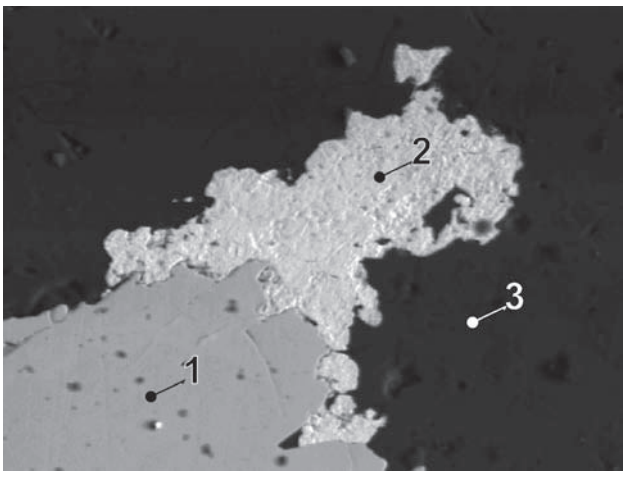

Fig. 22. MP271B. 1 – arsenpolybasite, 2 – Hg-silver, 3 – calcite. Barbora shaft, 4th/5th level, No. 32 vein. BSE image. Magnification 800×.

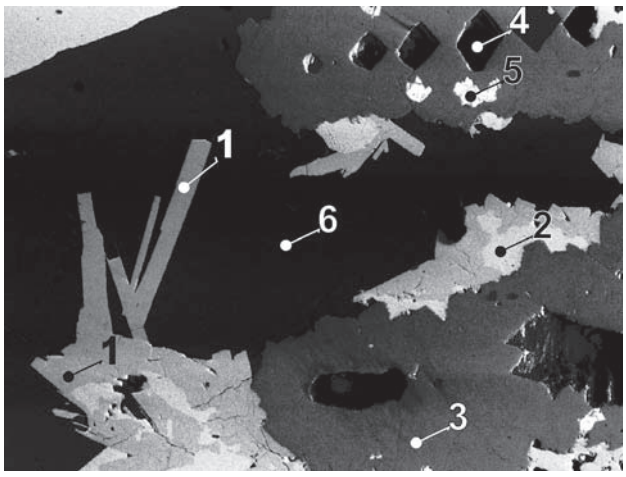

Fig. 25. MP271E/B. 1 – arsenpolybasite, 2 – acanthite, 3 – rammelsbergite, 4 – perimorphs of rammelsbergite after silver, 5 – uraninite, 6 – calcite. Barbora shaft, 4th/5th level, No. 32 vein. BSE image. Magnification 50×.

Arsenpolybasite is deposited on *rammelsbergite* and *argentite* in anhedral grains or thin tabular crystals. It is overgrown with *chalcopyrite* or other sulphides. It is enclosed in *calcite* or exceptionally *dolomite*. It shows characteristic dark red internal reflections along cleavage in a polished section (Fig. 26).

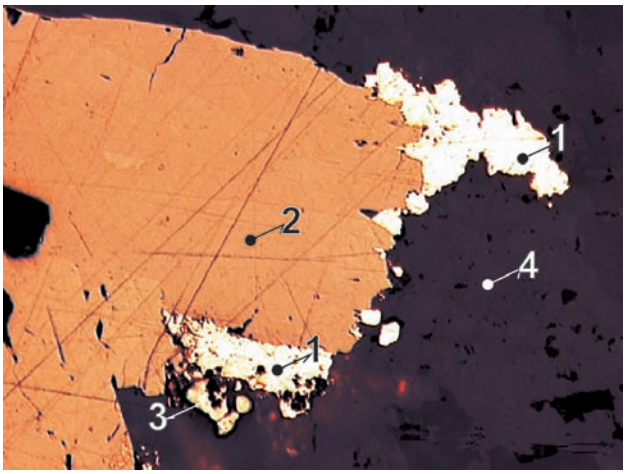

Fig. 26. MP271B/B-2. Tabular crystals of arsenpolybasite contain at margins mercurian silver accompanied by minor chalcopyrite. 1 – Hg-silver, 2 – arsenpolybasite, 3 – chalcopyrite, 4 – calcite. Barbora shaft, 4th/5th level, No. 32 vein. Reflected light, single polarizer. Magnification 260×.

Table 19. Calculated unit-cell parameters of arsenpolybasite from Jáchymov for the space group *C*2/*m*.

sample	*a*	*b*	*c*	β
		(Å)		(°)
J-868	26.008(1)	15.238(2)	23.969(2)	90

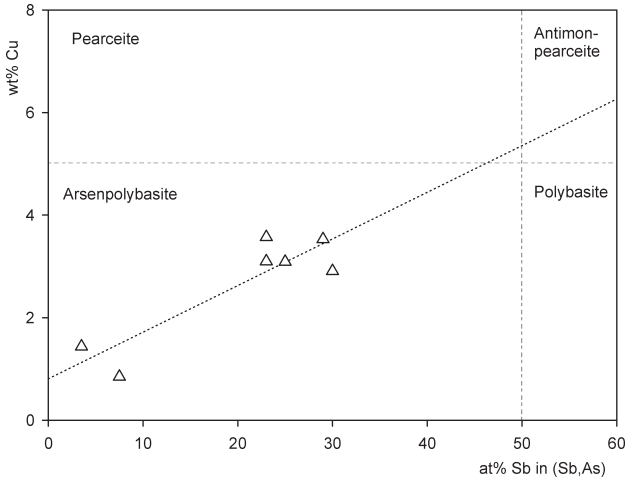

Fig. 27. Composition of arsenpolybasite from Jáchymov compared with the solid solution in a synthetic system [441].

As/Sb and Cu/Ag ratios in the Jáchymov minerals of the *arsenpolybasite–polybasite* [441] series vary to such extent that the samples show a nearly continuous series (see chemical analyses of *polybasite*). Samples come from the Barbora shaft, 5th level, vein No. 32 and from the Eliáš mine. *Arsenpolybasite* was also identified as a small inclusion in central part of *stephanite* from the Svornost shaft, 12th level, Geschieber vein.

Ashanite $(Nb,Ta,U,Fe,Mn)_4\ O_8$

This mineral was identified as a single elongated grain 80×10 μm in size. It contains major W and Nb, significant Fe and low Ti, Mn, Ta, and Sn. The crystal is enclosed in *annite* with *hematite* positioned along cleavage. The sample comes from the Rovnost I shaft, probably 8th level.

Table 20. Chemical analyses of arsenpolybasite.

sample	pt.	Ag	Cu	Fe	Co	Ni	Zn	As	Sb	S	Total
							weight %				
SR2712	1	73.16	3.10	0.21			0.32	5.18	2.57	16.25	100.79
SR2712	3	73.98	3.57	0.26			0.31	4.89	2.63	16.43	102.07
SR2712	3a	73.95	3.53	0.25			0.32	4.84	3.29	16.30	102.48
SR2712	4	73.29	3.09	0.42			0.13	4.81	2.82	16.41	100.97
SR2712	15	72.95	2.91	0.49			0.13	5.42	3.38	16.33	101.61
J031P	a2	76.35	0.85	0.14	0.05	0.10		6.21	0.81	15.86	100.37
J031P	a3	74.98	1.44	0.45	0.05	0.06		6.60	0.37	16.02	99.97

sample	pt.	Ag	Cu	Fe	Co	Ni	Zn	subtotal	As	Sb	S	subtotal	Total
							number of atoms						
SR2712	1	14.76	1.06	0.08			0.11	16.01	1.50	0.46	11.03	12.99	29
SR2712	3	14.73	1.21	0.10			0.10	16.13	1.40	0.46	11.00	12.87	29
SR2712	3a	14.72	1.19	0.10			0.11	16.12	1.39	0.58	10.92	12.88	29
SR2712	4	14.74	1.06	0.16			0.04	16.00	1.39	0.50	11.10	13.00	29
SR2712	15	14.61	0.99	0.19			0.04	15.83	1.56	0.60	11.00	13.17	29
J031P	a2	15.66	0.30	0.06	0.02	0.04		16.07	1.83	0.15	10.95	12.93	29
J031P	a3	15.29	0.50	0.18	0.02	0.02		16.01	1.94	0.07	10.99	13.00	29

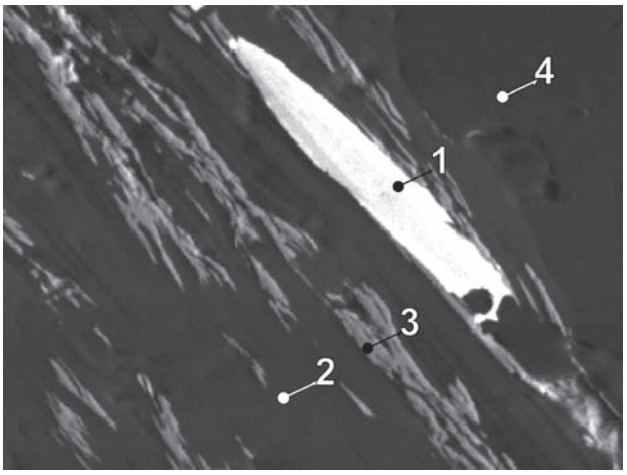

Fig. 28. J145P. 1 – ashanite, 2 – annite, 3 – hematite, 4 – quartz. Rovnost shaft, ore dump. BSE image. Magnification 530×.

Aurostibite $AuSb_2$

Aurostibite occurs in rounded grains of several microns in size. Pure *aurostibite* is exceptional – it usually forms a mixture with *bismuth* in a variable ratio. A small Au surplus may indicate the presence of minor free *gold*. The mineral is always enclosed in *arsenopyrite* or *löllingite*. *Aurostibite* was identified in a single sample in association with *gold*, *bismuth*, unidentified Bi-telluride and *clausthalite*. The sample comes from the Barbora shaft, between 7th and 8th level, probably near vein 1S.

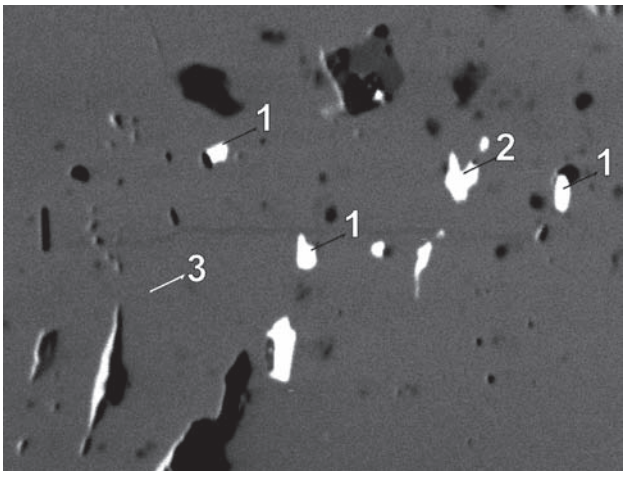

Fig. 29. 1 – bismuth, 2 – aurostibite, 3 – löllingite. Barbora shaft, 7th/8th level, probably No. 1S vein. BSE image. Magnification 530×.

Table 21. Chemical analysis of aurostibite.

sample	pt.	Au	Sb	Total	Au	Sb	Total
		weight %			number of atoms		
MP427	18	50.70	49.30	100.00	1.17	1.83	3

Barite $BaSO_4$

Barite occurs in small crystals on *siderite* in vugs of the Sen Boží vein [358]. It also forms tabular crystals up to 1 cm in a carbonate cavity. The specimen contains conchoidal *arsenic* with *argentopyrite* along fractures and *proustite*. This specimen comes from the Svornost shaft.

The second sample (from the Mineralogical collection of the Chemical Technology University, Prague) is a *polybasite* crystal 2 cm long covered with tabular *barite* crystals. Both the *barite* samples do not show increased Sr or Ca contents. Mrňa and Pavlů [419] recorded barite from the Reichsgeschieb adit.

Barite is a rare mineral in the district.

Bismuth Bi

Mrňa and Pavlů (1967) [351] classified *bismuth* occurrences into several groups according to the shape of grains, which correlates with different modes of formation:

a) Perfect skeletal, coarse to quill-like crystals up to 10 cm long, rimmed by diarsenide crust; this is the oldest *bismuth*, which – analogously to *silver* – belongs to the oldest ore minerals in Jáchymov veins. This type of *bismuth* is the most abundant (Figs 36, 37).

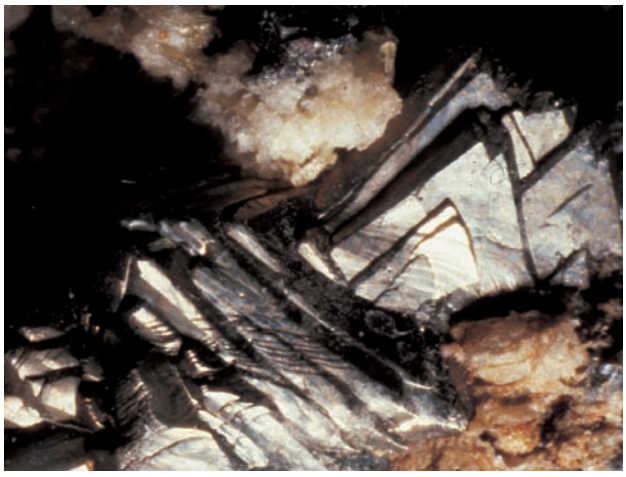

Fig. 30. Bismuth crystals in the gangue cavities (width of figure 1.3 cm). Photo J. & E. Sejkora.

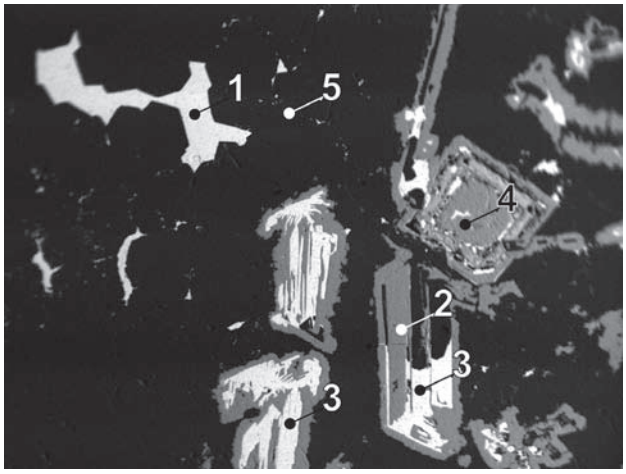

Fig. 31. J144P/B. 1 – bismuth (younger), 2 – rammelsbergite, 3 – bismuth (older), 4 – nickel-skutterudite, 5 – quartz. Eliáš mine, dump. BSE image. Magnification 38×.

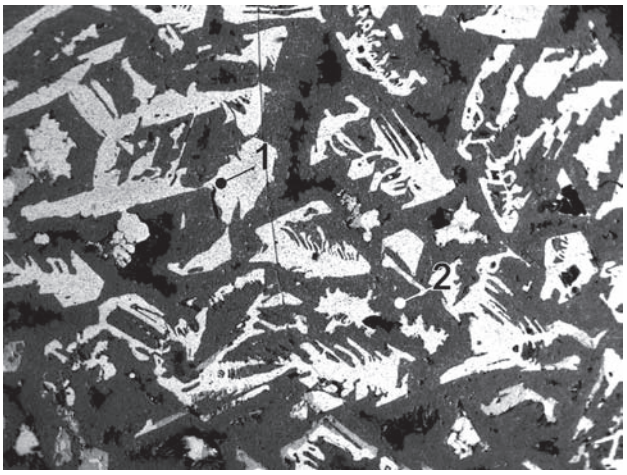

Fig. 32. MP94. 1 – bismuth, 2 – rammelsbergite. Eliáš mine, 1st level, 2A vein. BSE image. Magnification 38×.

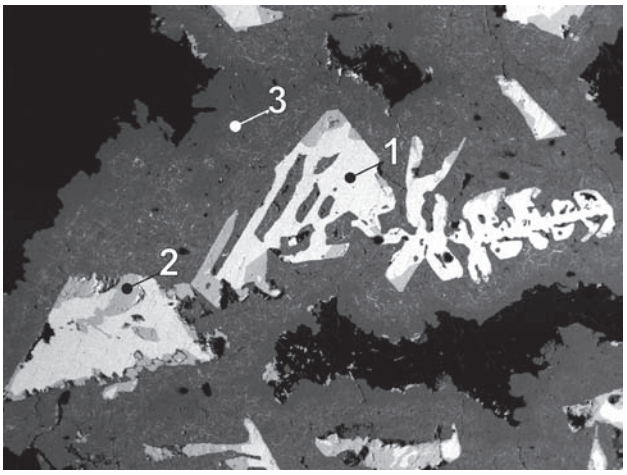

Fig. 33. MP97/A. 1 – bismuth, 2 – bismuthinite, 3 – rammelsbergite. Eliáš mine, A vein. BSE image. Magnification 30×.

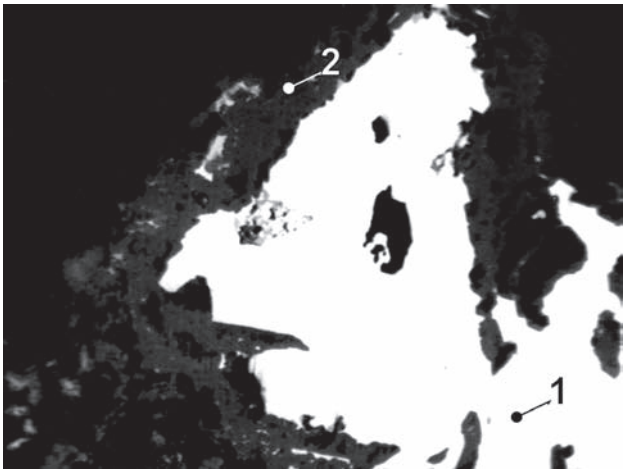

Fig. 34. MP129. 1 – bismuth, 2 – löllingite. Rovnost I shaft, 10th level, Bergkittler vein. BSE image. Magnification 33×.

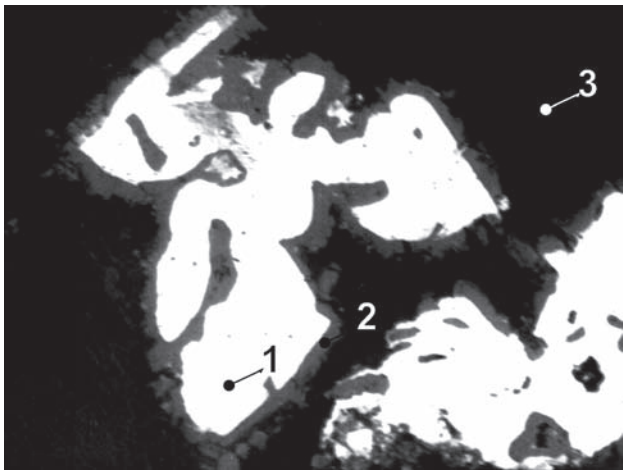

Fig. 35. MP329C. 1 – bismuth, 2 – safflorite, 3 – quartz. Bratrství shaft, Adit level, Zdař Bůh vein. BSE image. Magnification 80×.

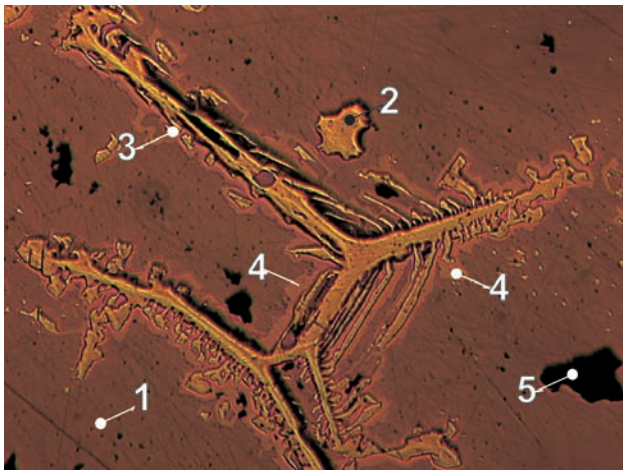

Fig. 36. J024P. Skeletal aggregate of native bismuth is partly replaced by bismuthinite. Boundary between native bismuth and native arsenic is formed by a thin zone of rammelsbergite. Black areas are carbonate. 1 – arsenic, 2 – bismuth, 3 – bismuthinite, 4 – rammelsbergite, 5 – carbonate. Svornost shaft, 5th level. Reflected light, single polarizer. Magnification 130×.

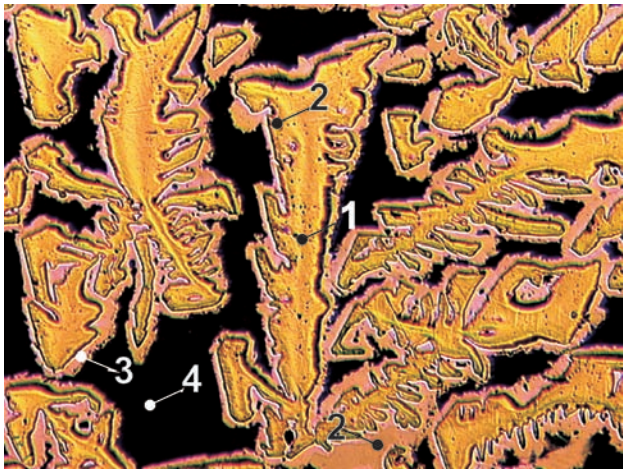

Fig. 37. J026P. Skeletal crystal aggregate of native bismuth is partly replaced by bismuthinite. A rim of skutterudite protected bismuth against complete replacement. All ore minerals are enclosed in carbonate. 1 – bismuth, 2 – bismuthinite, 3 – skutterudite, 4 – carbonate. Svornost shaft, 5th level. Reflected light, single polarizer. Magnification 130×.

Table 22. Calculated unit-cell parameters of bismuth from Jáchymov for the space group $R\bar{3}m$.

sample	*a*	*c*
	(Å)	
J-695	4.569(2)	11.88(1)
J-719	4.5445(3)	11.861(1)
J-720	4.563(1)	11.923(3)
J-772	4.5466(2)	11.860(1)
J-842	4.5508(3)	11.792(2)
VS4231	4.552(1)	11.875(2)
VS4238	4.515(1)	11.929(4)
VS20291	4.5459(2)	11.889(2)
J101P (J-917)	4.5530(3)	11.883(2)
J124P (J-918)	4.5472(3)	11.859(4)
J152P (J-919)	4.5581(3)	11.855(3)
J148P (J-920)	4.5448(4)	11.856(1)

Table 23. Chemical analyses of bismuth. Source data in wt.%.

sample	pt.	Bi	Ag	Pb	Zn	Cu	As	S	Total
					weight %				
J024P	1	98.77	0.38	0.35	0.05	0.24	0.11	0.10	100.00
J024P	2	98.61	0.63	0.31	0.10	0.20	0.08	0.07	100.00
J024P	3	98.60	0.85	0.20	0.04	0.12	0.06	0.13	100.00
J026P	a4	98.29	0.24	0.64	0.13	0.05	0.22	0.43	100.00
J026P	a5	98.08	0.10	0.84	0.10	0.37	0.35	0.16	100.00
J026P	a6	98.10	1.13	0.20	0.05	0.06	0.38	0.08	100.00

b) Regenerated *bismuth* in anhedral and lobate grains in integranular cavities of *quartz*. *Bismuth* of the first and second type may be closely associated at sites only few millimetres apart. Regenerated *bismuth* fills some leached zones in *nickel-skutterudite,* fractures in ore minerals or constitutes perimorphs after dendritic *silver*. The younger *bismuth* was derived by redeposition of older *bismuth*. This type is common.

c) Fine-grained *bismuth*. Some authors introduced this description for a metal constituting minute rod-shaped particles intergrown with triarsenides. Outer shape of these intergrowth aggregates is irregular or corresponds to crystal shapes of arsenides. This type of *bismuth* formed by exsolution of Bi from the host mineral during cooling. This type is exceptional (Figs 115–117).

d) Acicular crystals up to 1 cm long, with striation of crystal faces parallel to elongation. This type is enclosed in *quartz* and forms free crystals in vugs [351]. This type is very rare.

This study shows that *bismuth* is white-silver to light bronze in colour and has a strong metallic lustre. The surface soon turns mat and corroded (Fig. 30).

The early skeletal *bismuth* is usually enclosed in *quartz*, less frequently in *dolomite*. It is typically rimmed by *rammelsbergite*, rarely by *safflorite* and sometimes by *nickel-skutterudite*.

In rare cases, the diarsenide rim is absent and *bismuth* is enclosed only in triarsenides – *skutterudite* or *nickel-skutterudite*.

The rims around *bismuth* are often described as *safflorite* in the older literature, and *rammelsbergite* is not mentioned. Zückert [423] and Mrňa and Pavlů [383] specified that due to the difficulties with optical discrimination of *safflorite* from *rammelsbergite*, they took the convention to describe the mineral as *safflorite*. This explains why *safflorite* has been frequently reported from Jáchymov, although it is in fact rather rare compared to *rammelsbergite*.

In some cases, skeletal *bismuth* was leached after deposition of arsenide rims. The resulting cavities were sometimes filled with *quartz*, which may also surround *bismuth*. Zückert [423] listed numerous minerals interpreted to replace skeletal *bismuth*: *nickel-skutterudite*, *skutterudite*, *quartz*, *calcite*, *arsenic*, *bismuthinite*, *silver*, *chalcopyrite*, *chalcocite*, *proustite* and *enargite*.

The b) type of regenerated *bismuth* forms minute anhedral inclusions in dark red *realgar* in samples of ore breccia. *Bismuth* in perimorphs after dendritic *silver* indicates transport of mobilized Bi for a notable distance, as no joint occurrence of dendritic *silver* and primary *bismuth* has been documented.

The c) type of fine-grained *bismuth* was found only in *nickel-skutterudite* crystals with some zones formed by myrmekitic intergrowths of *bismuth* and *rammelsbergite*.

Another form of younger *bismuth* includes short, twisted wires striated parallel to elongation, deposited in cavities.

In addition to the discussed Bi migration by hydrothermal re-mobilization, some Bi migration took place in the thermal regime of younger dyke intrusions (e.g., basalt). The transport of Bi for distances of 5–10 m from the original site and its deposition in fine veinlets and drops was suggested [383]. If the process took place at temperatures above the melting point of Bi, the metal should occur in spheroidal drops.

Additional modes of *bismuth* occurrence differ from the above four types. Minor native *bismuth* was identified in greisen as grains and thin lamellae in *molybdenite*. The sample comes from the Rovnost I shaft, probably 8th level, and from a *quartz* vein in the Klement shaft. Minor *bismuth* in lamellae along cleavages in *actinolite* associates with *pyrite*, *chalcopyrite*, *arsenopyrite* and *löllingite* in skarn from dumps at the Eliáš mine and Vladimír shaft.

Bismuthinite is the most common mineral replacing *bismuth*. Replacement of *bismuth* by *bismutite* is less common. Replacement of *bismuth* by *zavaritskite*, proceeding in a concentric pattern from margins, has been recorded in one example.

Bismuthinite Bi_2S_3

The most common mode of *bismuthinite* occurrence are rims around *bismuth*, formed by replacement of *bismuth*, particularly of its skeletal crystals. The increase in volume accompanying this replacement often results in fracturing of the enclosing *quartz*. Another form of *bismuthinite*, thin acicular crystals, occurs enclosed in *quartz* as individual crystals or radiating aggregates (Fig. 40). *Bismuthinite* is a common mineral in the district.

Table 24. Calculated unit-cell parameters of bismuthinite from Jáchymov for the space group *Pbnm*.

sample	*a*	*b*	*c*
		(Å)	
J042P	11.110(2)	11.386(2)	4.004(1)
J042P	11.178(1)	11.342(3)	4.000(1)
J043P	11.116(2)	11.412(1)	3.999(1)
J045P	11.1473(6)	11.3018(5)	3.9804(2)
J101P (J-917)	11.1700(5)	11.3219(7)	3.9992(2)
J148P (J-920)	11.1546(8)	11.3869(9)	4.0092(3)
J-695	11.171(2)	11.348(2)	3.986(1)
J-720	11.161(2)	11.327(2)	3.9968(6)
J-772	11.172(2)	11.340(4)	4.000(1)
VS20291	11.149(1)	11.373(1)	4.0081(5)
VS4231	11.160(2)	11.391(2)	3.999(1)
VS4238	11.1436(5)	11.2992(3)	3.9864(3)

Chemical composition is typically simple. Only one sample contained significant Sb. It was *quartz* gangue with skeletal *bismuth* rimmed by a narrow zone of *rammelsbergite*, which was covered by *Sb-bismuthinite*, confined to concave rims of *rammelsbergite*. Antimony content varied, with the maximum at Bi/Sb = 2 : 1. The specimen comes from the Svornost shaft, 2nd level, Geschieber vein.

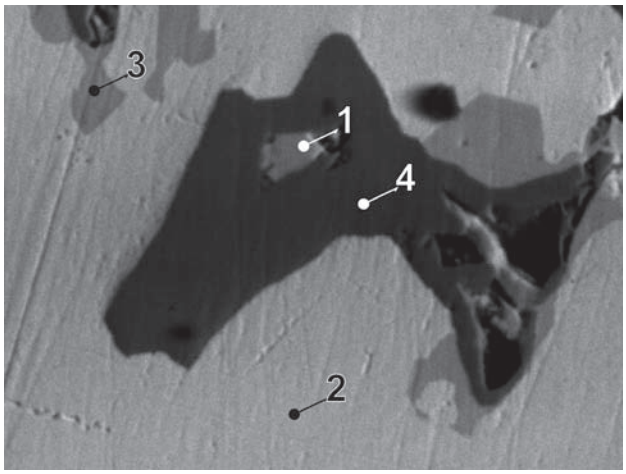

Fig. 38. J121P. 1 – Sb-bismuthinite, 2 – bismuth, 3 – bismuthinite, 4 – rammelsbergite. Svornost shaft, 2nd level, Geschieber vein. BSE image. Magnification 1150×.

Table 25. Chemical analyses of bismuthinite.

sample	pt.	Bi	Sb	Pb	Ag	Zn	Cu	S	As	Total
						weight %				
J024P	4	80.37		0.67	0.09	0.06	0.21	18.55	0.12	100.07
J024P	5	80.37		0.49	0.13	0.05	0.27	18.54	0.16	100.01
J024P	7	80.15		0.72	0.11	0.06	0.23	18.63	0.10	100.00
J024P	8	80.43		0.14	0.13	0.06	0.26	18.85	0.13	100.00
J024P	9	80.19		0.37	0.08	0.09	0.20	18.89	0.18	100.00
J026P	a4	80.24		0.65	0.10	0.07	0.19	18.56	0.11	99.92
J026P	a5	80.70		0.47	0.09	0.10	0.24	18.44	0.20	100.24
J026P	a1	80.53		0.26	0.21	0.06	0.27	18.60	0.07	100.00
J026P	a2	80.25		0.45	0.26	0.05	0.26	18.50	0.23	100.00
J026P	a3	80.23		0.56	0.13	0.07	0.31	18.57	0.13	100.00
J121P	1	58.35	19.14					22.17		99.66
J121P	2	59.08	17.74					22.12		98.94

sample	pt.	Bi	Sb	Pb	Zn	Cu	subtotal	S	As	subtotal	Total
						number of atoms					
J024P	4	1.98		0.02	0.01	0.02	2.02	2.97	0.01	2.98	5
J024P	5	1.98		0.01	0.00	0.02	2.01	2.97	0.01	2.98	5
J026P	a4	1.97		0.02	0.01	0.02	2.01	2.98	0.01	2.99	5
J026P	a5	1.99		0.01	0.01	0.02	2.03	2.96	0.01	2.97	5
J024P	7	1.97		0.02	0.01	0.02	2.01	2.98	0.01	2.99	5
J024P	8	1.96			0.01	0.02	1.99	3.00	0.01	3.00	5
J024P	9	1.95			0.01	0.02	1.98	3.00	0.01	3.01	5
J121P	1	1.24	0.70				1.93	3.07		3.07	5
J121P	2	1.26	0.65				1.92	3.08		3.08	5
J026P	a1	1.98			0.01	0.02	2.00	2.98	0.01	2.98	5
J026P	a2	1.97				0.02	2.00	2.96	0.02	2.98	5
J026P	a3	1.97			0.01	0.03	2.00	2.97	0.01	2.98	5

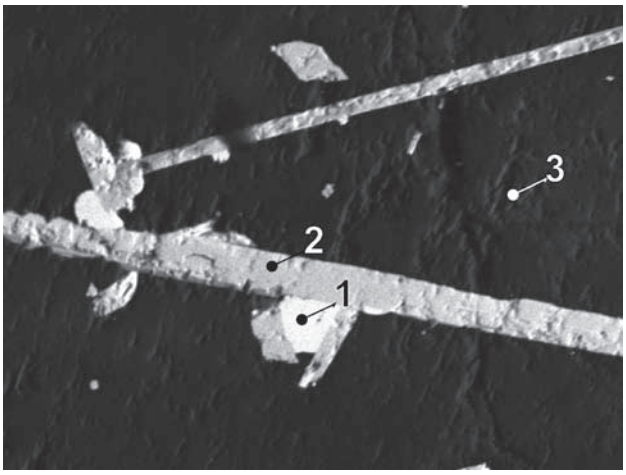

Fig. 39. MP421. 1 – bismuth, 2 – bismuthinite, 3 – calcite. Svornost shaft, 12th level, Bergkittler vein. BSE image. Magnification 6×.

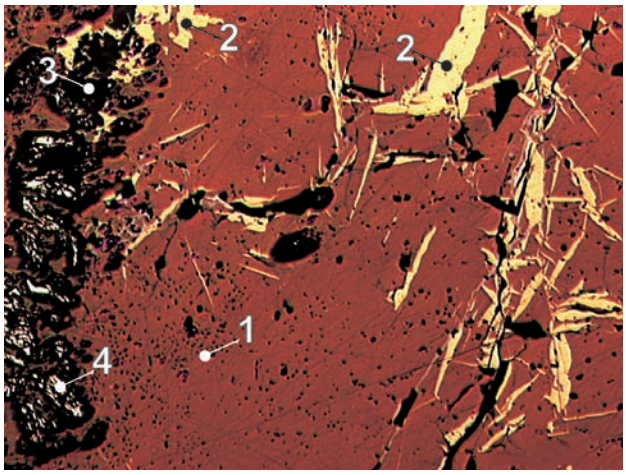

Fig. 41. J014P. 1 – bornite, 2 – chalcopyrite, 3 – tennantite, 4 – pyrite. Svornost shaft, Adit level. Reflected light, single polarizer. Magnification 160×.

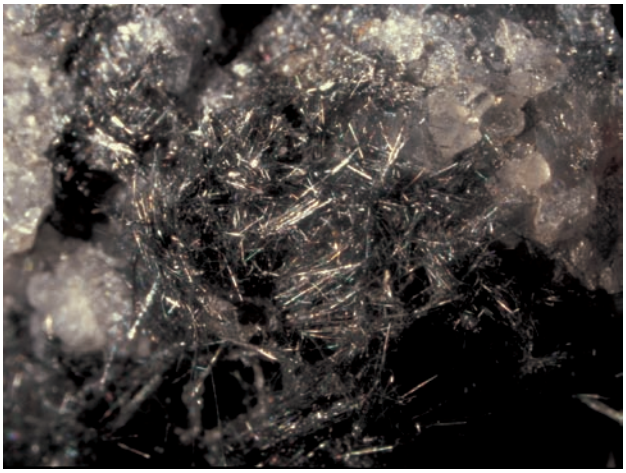

Fig. 40. Hair-like bismuthinite crystals in gangue cavities (width of figure 1.3 cm). Photo J. & E. Sejkora.

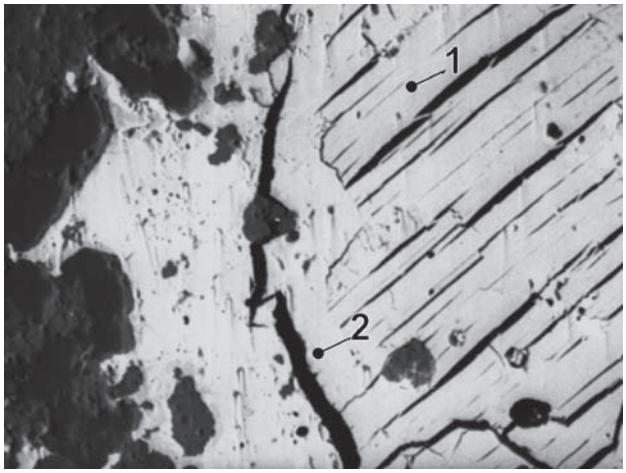

Fig. 42. J063P. Pressure fractures in bornite are filled by chalcopyrite. Zone with pyrite relics (high relief) contains tennantite. 1 – covellite, 2 – bornite. Rovnost I shaft, 3rd level, Geister vein. BSE image. Magnification 230×.

Another sample contains *bismuthinite* with 2 wt.% Se, associated with *chalcopyrite* and *siegenite*. The sample comes from the Svornost shaft, 5th level, Prokop vein.

Bornite Cu_5FeS_4

Mrňa and Pavlů [351] presented new data on *bornite* from Jáchymov. They recorded only isolated occurrences in various parts of the ore district, including Plavno and Rovnost I shafts. *Bornite* forms massive aggregates or small veinlets. It always contains exsolved *chalcopyrite*, and sometimes associates with *chalcocite*. The gangue is formed by *quartz* [351].

The presence of *bornite* is characteristic of the *carbonate–uraninite* stage, with *bornite* and *chalcopyrite* enclosed in spheroidal aggregates or along contraction fractures in coffinitized *uraninite*.

Samples studied within the present project contained *bornite* aggregates up to several cm across. The mineral has a characteristic pink brown colour. It forms intergrowths with other sulphides, mainly *chalcopyrite*, *pyrite*, *chalcocite,* and *tennantite* (Fig. 41). Rather common is lamellar intergrowth with *tennantite*. *Bornite* may locally replace platy *silver*.

Orientated contraction fractures in *bornite* are healed by *chalcopyrite*. The fractures may form intersecting arrays or en-echelon groups. *Bornite* also occurs in a fine-grained mixture with *chalcopyrite*. *Bornite* may replace *chalcocite*; alternatively, it fills fractures in *pyrite*. Rare

Table 26. Calculated unit-cell parameters of bornite from Jáchymov for the space group *Pbca*.

sample	*a*	*b*	*c*
		(Å)	
J014P	11.020(2)	21.96(1)	10.887(3)
J058P	11.050(5)	21.94(1)	10.895(7)
J041P	11.035(2)	21.701(5)	10.964(2)

Table 27. Chemical analyses of bornite.

sample	pt.	Cu	Ag	Fe	Ni	Co	Zn	S	Bi	Sb	As	Total
						weight %						
MP112	4	63.08	0.28	11.04				25.36	0.17	0.34		100.27
MP112	4a	63.11	0.19	11.14				25.33	0.22	0.31		100.30
MP112	4b	62.99	0.34	10.97				25.74	0.31	0.27		100.62
MP112	4c	63.23	0.26	10.83				25.67	0.10	0.39		100.48
J041P	a1	63.26	0.31	10.32	0.34		0.02	25.58		0.44	0.11	100.38
J041P	a5	62.89	0.57	10.24	0.32		0.14	25.62		0.35	0.66	100.79
99528	11	63.49	0.55	10.15	0.12		0.47	25.39		0.35		100.52
99528	13	62.84	0.22	10.94	0.15		0.53	25.27		0.37	0.34	100.66
J058P	1	61.53	0.67	11.03	0.37	0.19		24.76		0.33	1.01	99.89
J058P	2	61.61	1.20	10.73	0.22	0.20		25.02		0.21	0.60	99.79
J068P	D	61.85	0.22	11.29				24.92			2.25	100.55
J021P	5	62.31	1.28	11.26				25.32				100.17
J021P	6	62.67	0.67	11.37				25.41				100.12
J014P	a14	62.23	1.92	10.85				25.51				100.51
J014P	a15	62.47	1.76	11.14				24.99				100.36
J010P	4	61.46	1.75	11.23				25.33				99.77
J010P	5	62.49	1.49	11.57				25.78				101.33

sample	pt.	Cu	Ag	Fe	Ni	Co	Zn	subtotal	S	Sb	As	subtotal	Total
							number of atoms						
MP112	4	4.99	0.01	1.00				6.00	3.98	0.01		3.99	10
MP112	4a	5.00	0.01	1.00				6.01	3.97	0.01		3.99	10
MP112	4b	4.96	0.02	0.98				5.96	4.02	0.01		4.03	10
MP112	4c	4.99	0.01	0.97				5.97	4.01	0.02		4.03	10
J041P	a1	5.00	0.01	0.93	0.03			5.97	4.01	0.02	0.01	4.03	10
J041P	a5	4.96	0.03	0.92	0.03		0.01	5.94	4.00	0.01	0.04	4.06	10
99528	11	5.02	0.03	0.91	0.01		0.04	6.01	3.98	0.01		3.99	10
99528	13	4.96	0.01	0.98	0.01		0.04	6.01	3.95	0.02	0.02	3.99	10
J058P	1	4.92	0.03	1.00	0.03	0.02		6.00	3.92		0.07	3.99	10
J058P	2	4.92	0.06	0.98	0.02	0.02		5.99	3.96		0.04	4.00	10
J068P	D	4.90		1.02				5.92	3.92		0.15	4.07	10
J021P	5	4.94	0.06	1.02				6.02	3.98			3.98	10
J021P	6	4.96	0.03	1.02				6.01	3.99			3.99	10
J014P	a14	4.93	0.09	0.98				6.00	4.00			4.00	10
J014P	a15	4.97	0.08	1.01				6.06	3.94			3.94	10
J010P	4	4.90	0.08	1.02				6.00	4.00			4.00	10
J010P	5	4.90	0.07	1.03				6.00	4.00			4.00	10

examples of myrmekitic exsolved *galena* in *bornite* were observed. It may also form exsolutions in *chalcopyrite*.

Calcite

Mrňa and Pavlů (1967) [351] conducted a detailed study of carbonates from Jáchymov veins. *Calcite* with a low Mn content accompanies ores of the *sulphidic* stage. White or transparent *calcite* accompanies ore minerals in the vein filling showing a bilateral symmetry. Central vugs are often coated by freely grown *calcite* rhombohedra. Minor fractures accompanying the main branch of the Bludná Fault zone often carry abundant light pink Mn-rich *calcite* [351].

Thin tabular *calcite* crystals with hexagonal outline, crystallized in vugs, are known under the historic name "Papierkalzit". This is the youngest carbonate in Jáchymov veins, deposited on low-temperature minerals such as *smythite*, *sternbergite*, *cinnabar*, *imiterite*, and *pyrrhotite*. However, in its total quantity in the veins, *calcite* is far behind *dolomite*.

Crystal structure refinement

The crystal structure was refined by the Rietveld method using powder diffraction pattern of sample J004I (start angle, step, end angle (°2θ Cu$K_{\alpha 1\alpha 2}$): 18.0, 0.02, 120.0) recorded with Philips X'Pert diffractometer in Bragg-Brentano setting for reflection. The FullProf 2k [462] program with the WinPlotr graphic facility [464] was used for refinement. Model crystal structures presented in tables 1, 2, 7 a 8 in Reeder [465] were used. *Calcite* was refined in the trigonal space group $R\bar{3}c$ in hexagonal setting with a single variable fractional co-ordinate ($x_O \sim 0.257$). Temperature parameters (isotropic temperature factors of individual atoms), unit-cell parameters, parameters describing width and shape of diffractions (pseudo-Voigt profile function was used) and parameters

Table 28. Rietveld structure refinement of calcite from Jáchymov. Calculated unit-cell parameters, unit-cell volume, fraction-coordinates of C and O, total temperature factor and parameters of the refinement accordance are included.

sample	*a* (Å)	*c* (Å)	*V* (Å^3)	z_C	x_O	y_O	z_O	R_p (%)	R_{wp} (%)	χ^2
J004I	4.9844(2)	17.0376(8)	366.58(2)	¼	0.2596(6)	0	¼	7.0	9.4	1.05

isotropic temperature factors: B_{Ca} = 2.72(7) Å^{-2}; B_C = 2.7(1) Å^{-2}; B_O = 3.57(9) Å^{-2}.

Table 29. Homogenization temperature Th of fluid inclusions in calcites from Jáchymov.

sample		mineral	*Th	salinity	mineralization stage
			°C	wt.%	
J004I	1	calcite	70–80	3.6–4.0	*sulphide*
J004I	1	calcite	below 100	0.2–0.5	*sulphide*
NM9527	1	Mg-calcite	112–123		*arsenic-sulphide*

* temperature of homogenization (Th)

Table 30. Calculated unit-cell parameters of calcite from Jáchymov for the space group $R\bar{3}c$.

sample	*a*	*c*
	(Å)	
J-854	4.9890(9)	16.951(6)

characterizing X-ray microabsorption due to uneven sample surface were refined in addition to fraction co-ordinates. The results of refinement are given in Table 28.

Cassiterite SnO_2

According to Mrňa and Pavlů, *cassiterite* is a common component in apical parts of younger granite, e.g., in the Rovnost I and Bratrství shafts. It forms grains up to 5 mm in size. Sometimes it penetrates the rocks of metamorphic exocontact in the form of thin and irregular *quartz* veinlets. It is accompanied by *arsenopyrite*, less frequently *wolframite* in tabular crystals, and minor *chalcopyrite*. *Cassiterite* does not occur in veins

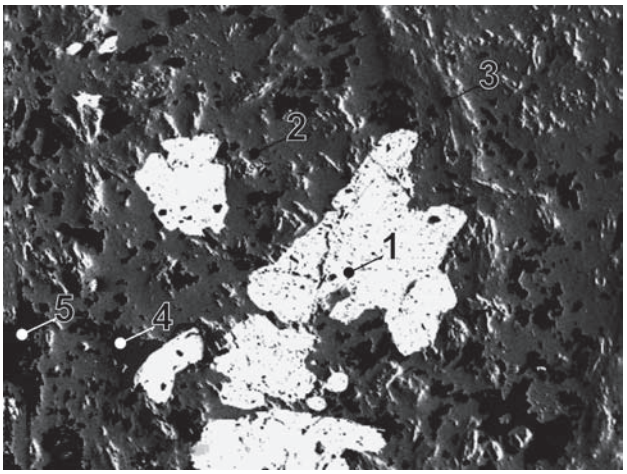

Fig. 43. SR99137/b. Irregular cassiterite grains enclosed by magnetite and flaky hematite. Cassiterite is in places replaced by sphalerite. In the matrix is also chlorite and quartz. 1 – cassiterite, 2 – magnetite, 3 – hematite, 4 – sphalerite, 5 – quartz. Skarn. Plavno. BSE image. Magnification 58×.

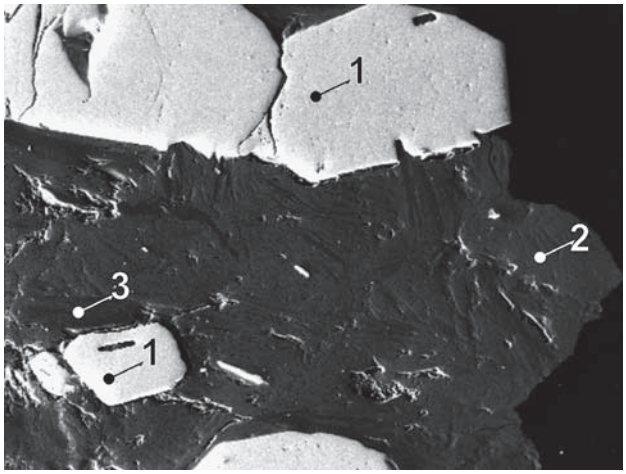

Fig. 44. SR99139/a. Euhedral cassiterite enclosed in biotite mass in various stages of chloritization. 1 – cassiterite, 2 – biotite, 3 – chlorite. Skarn. Plavno. BSE image. Magnification 56×.

with the *five-element* mineralization (Mrňa, MS, written communication).

The present work found *cassiterite* in small round grains enclosed in ores. It is usually enclosed in sulphides – mainly *arsenopyrite* or *pyrite* and sometimes in *quartz*. *Cassiterite* is commonly associated with *stannite*. It thus represents a mineral of the older, higher-temperature stage of mineralization. Its occurrences concentrate in the northeastern part of the ore district, but rare finds were recorded in other parts. Small *cassiterite* grains were identified in *actinolite* skarn in the Eliáš mine, and large grains occurred in skarn in the Plavno shaft. *Cassiterite* was also found in the Geister vein, which indicates that the structures along which the *five-element* mineralization was deposited existed long before the *five-element* mineralization.

Chalcocite Cu_2S

Massive disseminated *chalcocite* in the Červená, Fiedler and Geister veins was described by Vogl [59]. *Arsenic* samples with *chalcocite* crystals from the Hildebrand vein, collected in 1885 by F. Babánek, were studied by

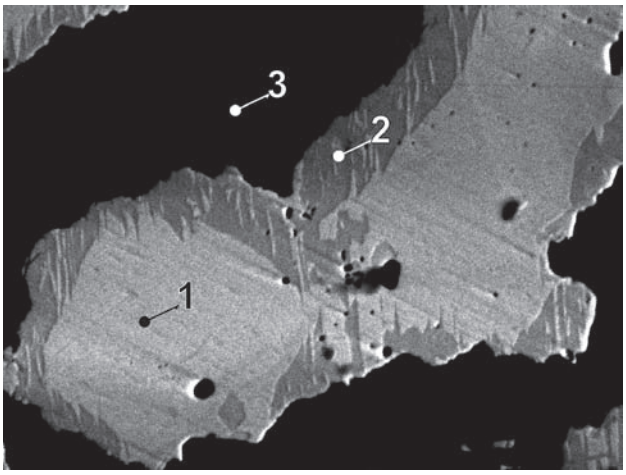

Fig. 45. J089P/F. 1 – chalcocite, 2 – bornite, 3 – quartz. Giftkies adit. BSE image. Magnification 400×.

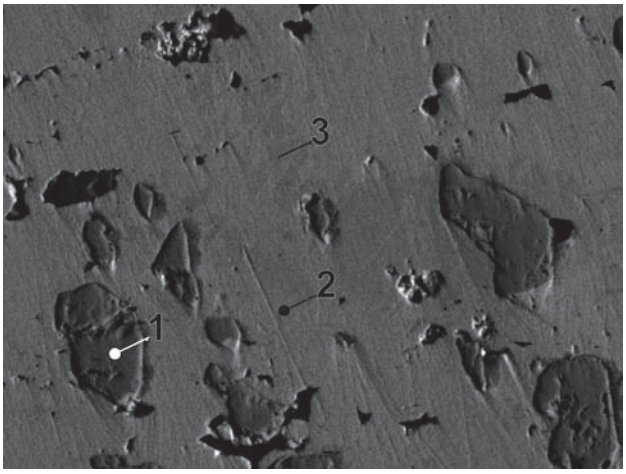

Fig. 46. MP 380. 1 – pyrite, 2 – chalcocite, 3 – bornite. Panorama mine, Zuzana vein. BSE image. Magnification 530×.

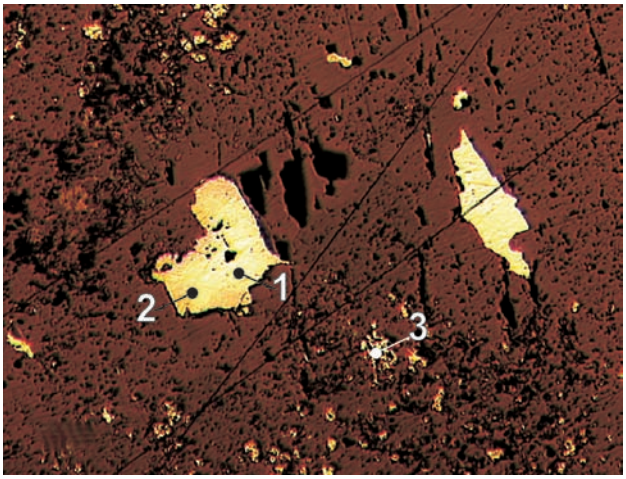

Fig. 47. MP112*. Zoned chalcocite grains with up to 5 wt.% Fe in rims. Aggregate intergrowth of bismuth and bismuthinite in surroundings of chalcocite. 1 – chalcocite, 2 – Fe-chalcocite, 3 – bismuth and bismuthinite. Rovnost I shaft. Reflected light, single polarizer. Magnification 60×.

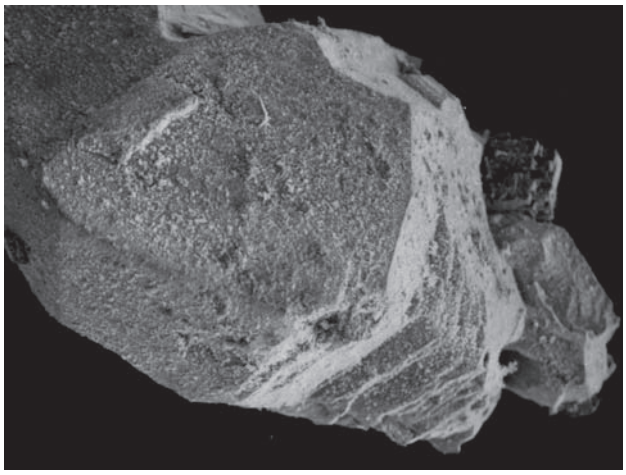

Fig. 48. NM9087. Equant chalcocite crystal grown on native arsenic. SE image. Magnification 50×. Photo A. Gabašová.

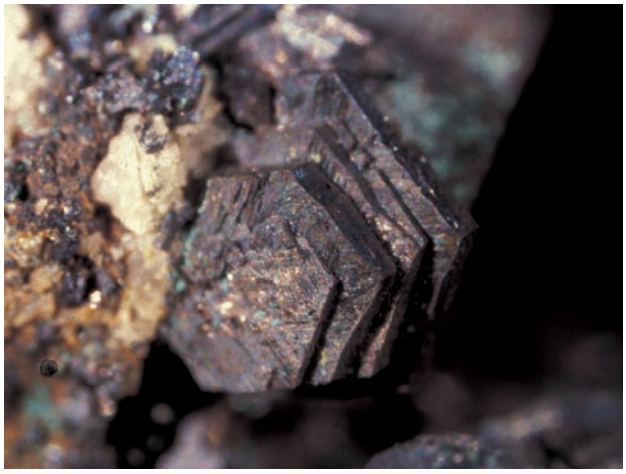

Fig. 49. Group of tabular crystals of chalcocite up to 2 mm (width of figure 5 mm). Photo J. & E. Sejkora.

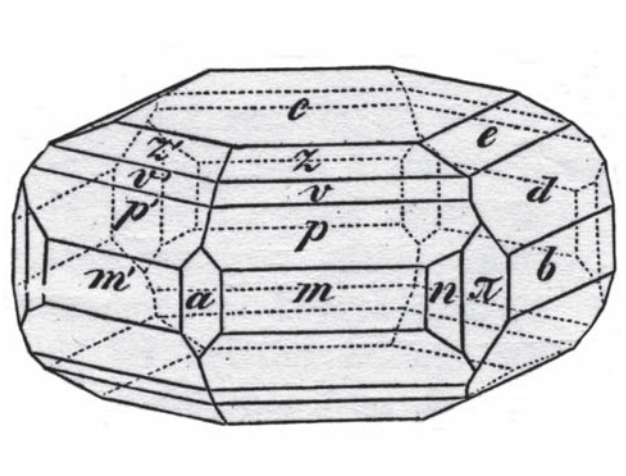

Fig. 50. Chalcocite crystal drawing by Vrba [362]. Crystal forms: c(001), e(012), d(021), b(010), z(113), v(112), p(111), m(110), n(230), π(130), a(100).

K. Vrba. Equant crystals of black *chalcocite* up to 3 mm in size are metallic and occur isolated or in groups [362]. A full succession in this paragenesis is as follows: *arsenic* aggregates are locally covered by small spheroidal aggregates of spongy *silver*, followed by a crust of *löllingite* crystals, covered by *calcite* in low rhombohedral crystals (Figs 48 and 49). *Chalcocite* crystals are dispersed between *calcite* crystals. This specimen comes from the Mineralogical collection, National Museum, Prague, No. NM9087.

Chalcocite also forms individual grains up to 0.3 mm long and larger aggregates up to 5 cm long, accompanied by *chalcopyrite*, *bornite*, *pyrite, tennantite,* and *silver* (Fig. 47). Replacement of these minerals by *chalcocite* was also observed. *Chalcocite* may be replaced by *bornite*.

Chemical analyses show a low and variable content of Fe.

Table 31. Calculated unit-cell parameters of chalcocite from Jáchymov for the space group $P2_1/c$.

sample	*a*	*b*	*c*	β
		(Å)		(°)
NM24596	15.263(7)	11.884(1)	13.513(1)	116.49(1)
J-571	15.291(1)	11.9007(10)	13.4968(10)	116.569(5)

Chalcopyrite $CuFeS_2$

Chalcopyrite from Jáchymov was studied by Mrňa and Pavlů (1967) [351]. They found *chalcopyrite* in ores of

Table 32. Chemical analyses of chalcocite.

sample	pt.	Cu	Ag	Fe	Zn	S	As	Total
					weight %			
MP112	2	74.18	0.14	4.32	0.43	20.71		99.78
MP112	3	75.54	0.44	3.36	0.25	20.76		100.35
MP112	a	74.84	0.39	3.99	0.48	18.97		98.67
MP112	b	74.68	0.84	3.74	0.64	19.08		98.98
MP112	c	74.94	0.47	4.29	0.75	18.79		99.24
MP112	1	80.04	0.52	0.31	0.15	19.83		100.85
MP112	4	78.61	0.71	0.33	1.02	19.81		100.48
MP112	d	79.13	0.37	0.57	0.37	20.44		100.88
NM24596	1	80.44				20.43		100.88
NM24596	2	80.40				20.25		100.64
NM24596	3	80.64				20.34		100.98
NM24596	4	79.96				20.42		100.39
NM24596	5	79.83				20.31		100.14
NM24596	6	79.83				20.45		100.28
J175P	C1	79.76		0.05		19.89		99.70
J175P	D1	80.30				20.22		100.52
J175P	E1	80.16	0.76			19.84	0.67	100.00
J013P	c	79.21	0.67	0.49		19.46	0.37	100.20
J010P	Ac	79.11	0.62	0.47		18.97	0.67	99.84
J019P	6a	79.18	0.79	0.37		19.67	0.59	100.60

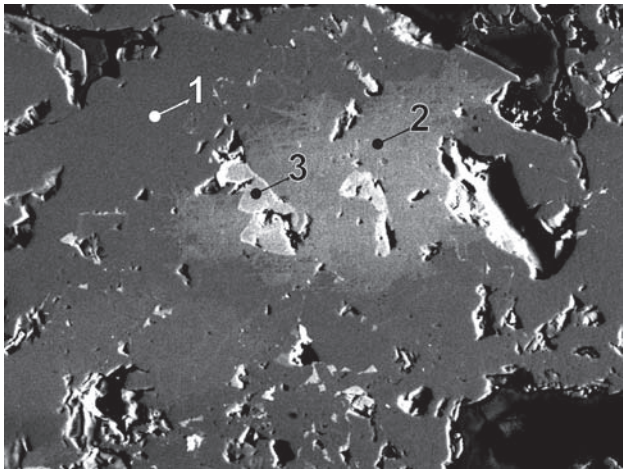

Fig. 51. J085P/D-5. 1 – chalcopyrite, 2 – Ag-chalcopyrite, 3 – freibergite. No. 1 Adit. BSE image. Magnification 115×.

sample	pt.	Cu	Ag	Fe	Zn	subtotal	S	As	subtotal	Total
						number of atoms				
MP112	2	1.85		0.12	0.01	1.98	1.02		1.02	3
MP112	3	1.87	0.01	0.10	0.01	1.98	1.02		1.02	3
MP112	a	1.91	0.01	0.12	0.01	2.04	0.96		0.96	3
MP112	b	1.90	0.01	0.11	0.02	2.04	0.96		0.96	3
MP112	c	1.90	0.01	0.12	0.02	2.05	0.95		0.95	3
MP112	1	2.00	0.01	0.01	0.00	2.02	0.98		0.98	3
MP112	4	1.97	0.01	0.01	0.03	2.02	0.98		0.98	3
MP112	d	1.96	0.01	0.02	0.01	1.99	1.01		1.01	3
NM24596	1	2.00				2.00	1.00		1.00	3
NM24596	2	2.00				2.00	1.00		1.00	3
NM24596	3	2.00				2.00	1.00		1.00	3
NM24596	4	1.99				1.99	1.01		1.01	3
NM24596	5	1.99				1.99	1.01		1.01	3
NM24596	6	1.99				1.99	1.01		1.01	3
J175P	C1	2.01				2.01	0.99		0.99	3
J175P	D1	2.00				2.00	1.00		1.00	3
J175P	E1	2.01				2.01	0.99		0.99	3
J022P	Ad	1.99	0.01	0.01		2.01	0.98	0.01	0.99	3
J013P	c	2.00	0.01	0.01		2.02	0.97	0.01	0.98	3
J010P	Ac	2.01	0.01	0.01		2.03	0.95	0.01	0.97	3
J019P	6a	1.99	0.01	0.01		2.01	0.98	0.01	0.99	3

Table 33. Calculated unit-cell parameters of chalcopyrite from Jáchymov.

sample	*a*	*c*
	(Å)	
J-702	5.2800(6)	10.416(2)

the *Sn-W sulpharsenide*, *arsenic-sulphide* and *sulphide* stages as a subordinate component. Minor *chalcopyrite* impregnates *quartz* of the *ore-free quartz* stage.

In sulphidic ores, it is usually associated with *pyrite*, *galena,* and especially s*phalerite*. In the latter mineral it forms anhedral aggregates. *Chalcopyrite* also occurs with

Table 34. Chemical analyses of chalcopyrite.

sample	pt.	Cu	Ag	Fe	Co	Ni	Bi	Hg	Zn	S	As	Sb	Sn	Total
							weight %							
MP295	1	33.26		30.32	0.13	0.33				33.64	0.79	0.96		99.43
MP295	1a	33.37		30.41	0.11	0.29				33.56	0.67	0.87		99.28
MP295	1b	33.18		30.31	0.19	0.34				33.71	0.85	0.79		99.37
MP112	5	34.55	0.30	30.45			0.97			33.34		0.16		99.77
J059P	3	34.94	0.49	27.77		0.19			0.70	33.44	1.74	0.46		99.73
J058P	6	37.69	0.99	23.81	0.21	0.30				32.57	3.85	0.18		99.60
J053P	4	34.03		29.60	0.31	0.67				34.64	2.20	0.55		102.00
J053P	7	34.27		29.56	0.12	0.05				33.74	1.30	0.65		99.69
J053P	8	33.79		29.82	0.34	0.46				34.29	0.88	0.55		100.13
J046P	1	34.42		29.95	0.23	0.30				34.08	0.88	0.35		100.21
J046P	2	36.38		21.91	0.36	0.22				32.04	8.64	0.55		100.10
J046P	3	35.15		27.75	0.10	0.24				33.98	2.48	0.65		100.35
J046P	4	36.32		21.75	0.28	0.29				32.69	8.39	0.52		100.24
J046P	5	37.14		22.19	0.15	0.29				32.56	7.56	0.48		100.37
J046P	7	36.82		22.20	0.24	0.38				32.33	7.69	0.48		100.14
J046P	8	37.25		24.42	0.32	0.39				33.86	3.18	0.22		99.64
J-702	a6	33.43	0.24	29.71		0.39			1.12	34.71	0.15	1.22		100.97
J041P	a2	34.54	0.11	30.60		0.29			0.87	34.06	0.35	0.58		101.40
J041P	a4	35.00	0.69	29.72		0.64			0.08	35.02	0.10	0.71		101.96
J014P	aa3	32.08	1.20	31.12				0.01		35.90				100.31
J014P	aa4	32.87	1.48	30.19						35.19				99.73
J022P	a3	32.11	0.78	31.20				0.02		35.41				99.52
J022P	a4	33.12	0.99	30.65				0.07		35.76				100.59
J010P	3	32.07	0.67	31.22						35.26				99.22
J010P	4	32.59	1.25	31.74				0.06		34.73				100.37
J118P	1	33.74	0.70	30.08				0.23	0.03	33.79	1.29		0.23	99.85

sample	pt.	Cu	Ag	subtotal	Fe	Ni	Zn	subtotal	S	As	Sb	subtotal	Total
						number of atoms							
MP295	1	0.98		0.98	1.01			1.01	1.96	0.02	0.02	2.00	4
MP295	1a	0.98		0.98	1.02			1.02	1.96	0.02	0.01	1.99	4
MP295	1b	0.98		0.98	1.01			1.01	1.96	0.02	0.01	2.00	4
MP112	5	1.02	0.01	1.03	1.02			1.02	1.95			1.95	4
J059P	3	1.03	0.01	1.04	0.93	0.01	0.02	2.00	1.95	0.04	0.01	2.00	4
J058P	6	1.13	0.02	1.15	0.81	0.01		1.97	1.93	0.10		2.03	4
J053P	4	0.98		0.98	0.97	0.02		1.97	1.97	0.05	0.01	2.03	4
J053P	7	1.01		1.01	0.99			2.00	1.96	0.03	0.01	2.00	4
J053P	8	0.98		0.98	0.99	0.01		1.99	1.98	0.02	0.01	2.01	4
J046P	1	1.00		1.00	0.99	0.01		2.01	1.96	0.02	0.01	1.99	4
J046P	2	1.09		1.09	0.75	0.01		1.86	1.91	0.22	0.01	2.14	4
J046P	3	1.03		1.03	0.92	0.01		1.96	1.97	0.06	0.01	2.04	4
J046P	4	1.09		1.09	0.74	0.01		1.84	1.94	0.21	0.01	2.16	4
J046P	5	1.11		1.11	0.75	0.01		1.88	1.93	0.19	0.01	2.12	4
J046P	7	1.10		1.10	0.76	0.01		1.88	1.92	0.20	0.01	2.12	4
J046P	8	1.10		1.10	0.82	0.01		1.94	1.98	0.08		2.06	4
J-702	a6	0.97		0.97	0.98	0.01	0.03	1.02	1.99		0.02	2.01	4
J041P	a2	1.00		1.00	1.00	0.01	0.02	1.04	1.95	0.01	0.01	1.97	4
J041P	a4	1.00	0.01	1.01	0.97	0.02	0.00	0.99	1.99		0.01	2.00	4
J014P	aa3	0.92	0.02	0.94	1.02			1.02	2.04			2.04	4
J014P	aa4	0.95	0.03	0.98	1.00			1.00	2.02			2.02	4
J022P	a3	0.93	0.01	0.94	1.03			1.03	2.03			2.03	4
J022P	a4	0.95	0.02	0.97	1.00			1.00	2.03			2.03	4
J010P	3	0.93	0.01	0.94	1.03			1.03	2.03			2.03	4
J010P	4	0.94	0.02	0.96	1.05			1.05	1.99			1.99	4
J118P	1	0.99		0.99	1.00			1.00	1.96	0.03		1.99	4

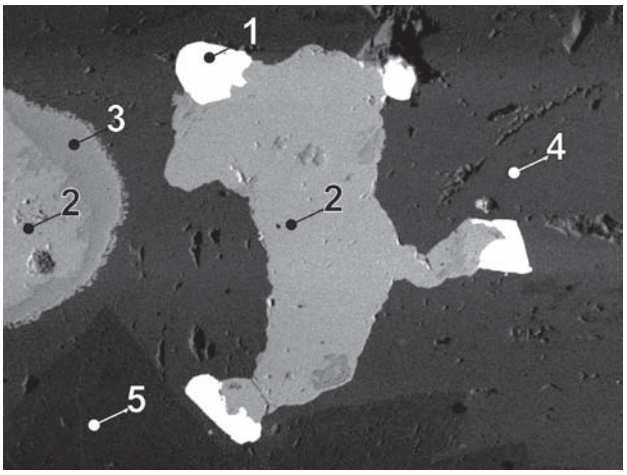

Fig. 52. MP190/E. 1 – galena, 2 – chalcopyrite, 3 – pyrite, 4 – calcite, 5 – dolomite. Svornost shaft. Daniel level, Anna vein. BSE image. Magnification 80×.

bornite in the form of enclosed irregular grains or orientated and probably exsolved domains. As a minor component it occurs with *tennantite*. Large massive lenses of *chalcopyrite* are rare. *Chalcopyrite* crystals may occur deposited on carbonate crystals. Together with other sulphides, *chalcopyrite* penetrates contraction fractures in *uraninite*, heals fractured arsenides and rarely fills vugs after leached *silver* [351].

The present study confirmed the above observations and documented rare *chalcopyrite* association with *stromeyerite* and *chalcopyrite* replacement by *silver*. It overgrows sulpharsenides and arsenides in rims 1–2 mm wide and in the form of small crystals. *Chalcopyrite* fills contraction fractures in *bornite* and may occur in a very fine-grained mixture with *bornite*. Botryoidal *chalcopyrite* contains some growth zones composed of *tennantite.*

Small grains of *silver-bearing chalcopyrite* containing 1.5 wt.% Ag were enclosed in ordinary *chalcopyrite*. Old generations of *chalcopyrite* are difficult to identify but the association with *stannite*, *mawsonite* or *roquesite* as well as the penetration by *nickeline* are indicative.

Chamosite $(Fe,Mg,Al)_6(Si,Al)_4O_{10}(OH)_8$

The mineral occurs in the central zone of carbonate veins in the form of rich accumulations with radiating structure. It is grey green, with a silky lustre, and intergrown with small *quartz* crystals enclosing *hematite* and spheroidal *pyrite* aggregates with *coffinite* in the central and marginal parts.

It was also found with *chalcopyrite* in a *quartz* vein, which contains *hyalophane* and *barian orthoclase*, at the Eliáš mine, and disseminated in *dolomite* gangue at the Rovnost I shaft.

Table 35. Chemical analyses of chamosite.

sample	pt.	SiO_2	TiO_2	Al_2O_3	FeO	MnO	MgO	CaO	BaO	Na_2O	K_2O	H_2O^*	Total
						weight %							
J186P	1	25.64	0.14	19.35	35.73		5.85	0.07	0.18	0.80		10.72	98.30
J186P	2	25.45		20.05	36.37	0.21	5.51	0.14	0.08	0.78		10.79	99.30
J186P	3	25.82		19.52	35.71		6.23	0.01		0.76	0.04	10.80	98.89
J112P	14	22.97	0.06	18.26	39.63	0.06	3.28			0.58			85.02
MP388	D1	25.17		20.69	31.46	0.04	7.30	0.30		0.60	0.01		85.63
J112P	12	24.42		17.31	40.47		2.90			0.52			85.61
J112P	13	24.25	0.10	17.76	39.88	0.04	2.83	0.11		0.54	0.02		85.53
MP388	D2	24.99		19.96	33.22	0.28	7.21	0.36		0.68			86.71
MP388	D3	24.83	0.07	19.31	33.95	0.14	7.18	0.32		0.57			86.37

sample	pt.	Mg	Fe	Mn	Ca	Na	Al	subtotal	Si	Ti	Al	subtotal	O	OH
							number of atoms							
J186P	1	0.98	3.34		0.01	0.17	1.50	6.00	2.87	0.01	1.05	3.93	10	8
J186P	2	0.91	3.38	0.02	0.02	0.17	1.50	6.00	2.83		1.12	3.95	10	8
J186P	3	1.03	3.32			0.16	1.48	6.00	2.87		1.07	3.94	10	8
J112P	14	0.47	4.00	0.01		0.14	1.37	5.99	2.77	0.01	1.22	4.00	14	
MP388	D1	0.99	3.00		0.04	0.13	1.64	5.81	2.87		1.13	4.00	14	
J112P	12	0.41	4.04			0.12	1.35	5.93	2.92		1.08	4.00	14	
J112P	13	0.40	3.97		0.01	0.12	1.39	5.91	2.89	0.01	1.10	4.00	14	
MP388	D2	0.98	3.16	0.03	0.04	0.15	1.52	5.89	2.85		1.15	4.00	14	
MP388	D3	0.99	3.26	0.01	0.04	0.13	1.47	5.90	2.85	0.01	1.14	4.00	14	

Number of atoms based on (O=14) or (O, OH =18)
* H_2O calculated from crystallochemical formula

Cinnabar Hg_2S

Mathesius [380], [392] reported *cinnabar* occurrence from the Dorota vein.

This study discovered that *cinnabar* forms anhedral grains up to 30 μm in size or granular aggregates 100 μm long, which are, however, visually indistinguishable from the more common *proustite*. It occurs in *quartz* gangue. In *dolomite* gangue, it is present on isolated *quartz* grains or along *dolomite-calcite* boundary. It was recorded in wall-rock next to carbonate vein. *Cinnabar* occurs in the proximity of dendritic *silver* crystals or in perimorphs after *silver*. It belongs to young hydrothermal minerals, and is younger than *nickeline*, *rammelsbergite*, *proustite* and *arsenpolybasite*.

It is closely associated with *acanthite*, *mercurian silver*, *imiterite* and *sternbergite.* One aggregate of *cinnabar* up to 200 μm long with *imiterite* and *acanthite* was observed. It was identified in samples from the Svornost shaft, below 5th level, Geschieber vein, from the Barbora shaft, 5th level, No. 32 vein and from the Eliáš mine. The mineral is rare at the ore deposit.

Clausthalite PbSe

Clausthalite was identified in two rounded grains 8 μm and 3 μm in size. It was deposited in a 30 μm cavity in *löllingite*, in association with *löllingite* and *arsenopyrite* enclosing *gold* and *aurostibite,* Bi-telluride and *bismuth.* The host rock is a dark, probably altered basic wall-rock from the Babora shaft, between 7th and 8th level, probably near vein 1S. In the second occurrence, *clausthalite* with *bornite* and *chalcocite* is enclosed in milky white *quartz* from the Giftkies adit.

Table 36. Chemical analyses of clausthalite.

sample	pt.	Pb	S	Se	Total	Pb	S	Se	Total
		weight %				number of atoms			
MP427	10	67.88	3.55	18.56	89.99	0.97	0.33	0.70	2
MP427	10	72.89	3.70	18.53	95.12	1.00	0.33	0.67	2

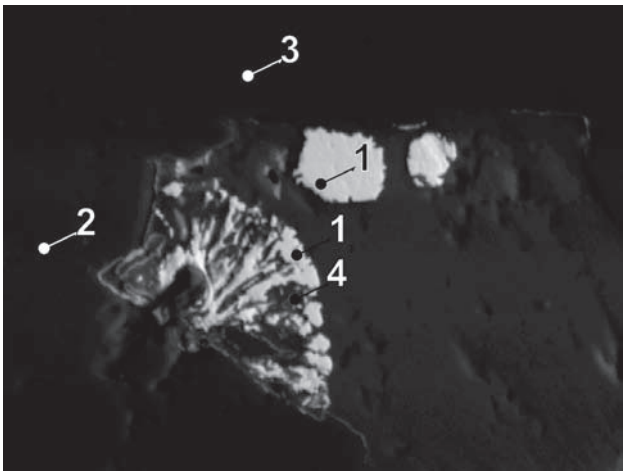

Fig. 53. MP271B/A-12. 1 – cinnabar, 2 – calcite, 3 – quartz, 4 – chlorite. Barbora shaft, 4th/5th level, No. 32 vein. BSE image. Magnification 680×.

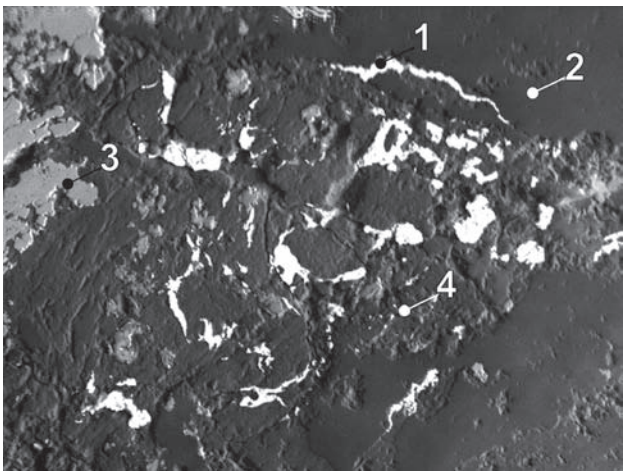

Fig. 54. MP271D/G. 1 – cinnabar, 2 – calcite, 3 – rammelsbergite, 4 – mineralized wall-rock. Barbora shaft, 4th/5th level, No. 32 vein. BSE image. Magnification 130×.

Clinosafflorite (Co,Fe,Ni)As_2

It forms highly lustrous, light grey radiating aggregates, with acicular crystals max. 5 mm in size. It is covered with white *dolomite* and associated with *skutterudite* in individual crystals and fine-grained aggregates. The sequence of crystallization of the two arsenides is uncertain. The composition of this *skutterudite* is near to ideal formula, it contains low S, Fe and minor Ni.

Clinosafflorite contains low amounts of S and often, low amounts of Cu. It occurs in parts of veins richer in Co, with *quartz* or carbonate gangue. *Clinosafflorite* crystals are rimmed by a narrow *löllingite* zone, which contains 0–6 wt.% Co.

The single safely localized find comes from the Svornost shaft, 5th level, Prokop vein.

Table 37. Calculated unit-cell parameters of clinosafflorite from Jáchymov for the space group $P2_1/n$.

sample	*a*	*b*	*c*	β
		(Å)		(°)
J-243	5.900(3)	5.906(2)	5.957(2)	116.16(4)
J108P/a (J-736)	5.962(4)	5.890(2)	5.960(4)	117.31(2)
J108P/b (J-736)	5.907(2)	5.833(1)	5.927(2)	115.48(2)
J042P	5.939(1)	5.862(1)	5.964(1)	116.27(1)
J108P (J-934)	5.9275(8)	5.8543(7)	5.9733(4)	116.371(7)

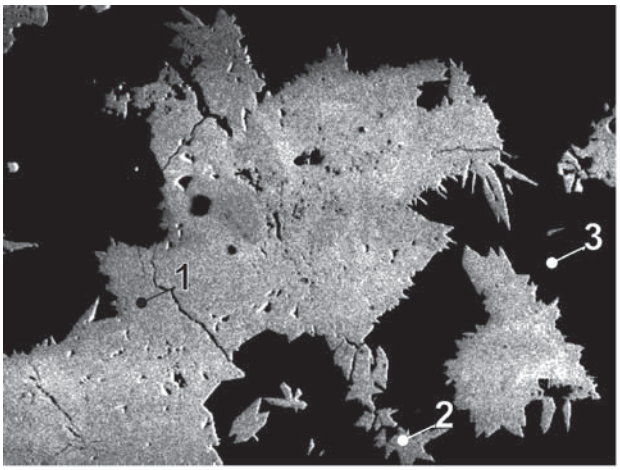

a

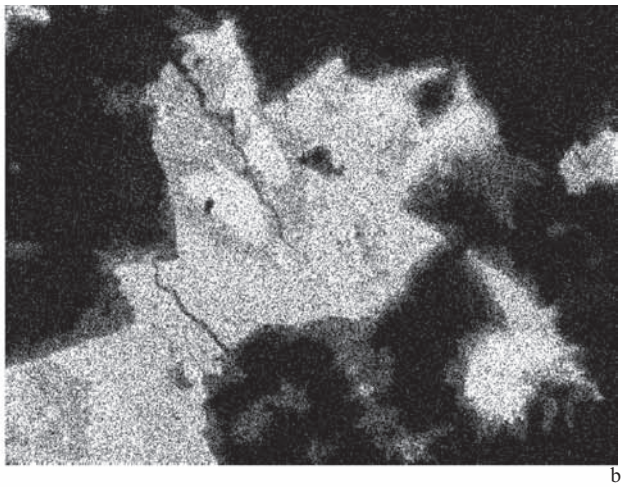

b

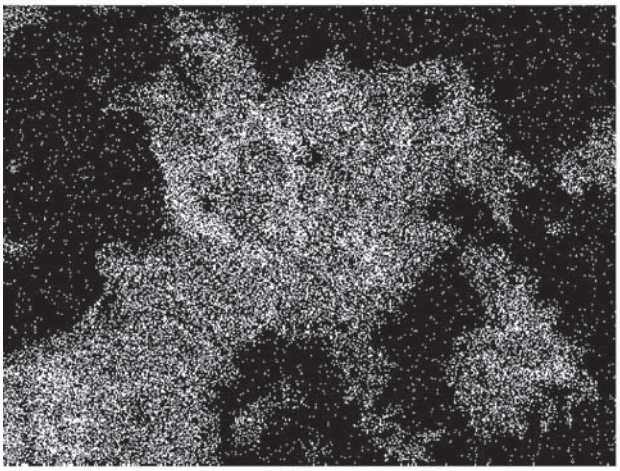

c

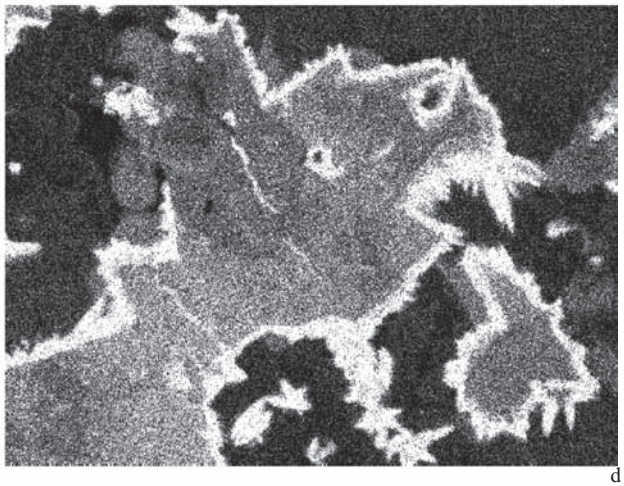

d

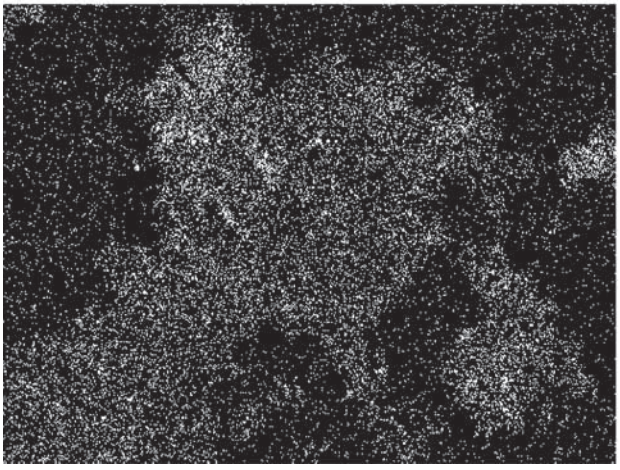

e

Fig. 55. J108P. 1 – clinosafflorite, 2 – löllingite, 3 – dolomite. Magnification 160×.
a) BSE image
b) Distribution of Co
c) Distribution of Cu
d) Distribution of Fe
e) Distribution of S

Table 38. Chemical analyses of clinosafflorite.

sample	pt.	Fe	Co	Ni	Cu	Zn	Ag	As	S	Sb	Total
						weight %					
J108P	3	6.92	21.07		1.13			69.42	2.00	0.05	100.59
J108P	1	6.85	20.09	1.10	0.42		0.06	70.48	1.11	0.28	100.39
J108P	2	5.77	20.21	2.62	0.24	0.04	0.19	71.24	0.91	0.22	101.44
J108P	4–1	6.27	19.45	2.99	0.20	0.07		69.10	2.35	0.00	100.43
J108P	4–2	6.96	19.51	1.94	0.19	0.04		68.67	2.18	0.14	99.62
J108P	4–3	9.58	16.55	0.03	1.50	0.11		71.69	0.33	0.00	99.79
J108P	4–4	10.14	16.07	0.05	1.29	0.12		72.18	0.19	0.22	100.25

sample	pt.	Fe	Co	Ni	Cu	subtotal	As	S	subtotal	Total
						number of atoms				
J108P	3	0.25	0.72		0.04	1.01	1.87	0.13	1.99	3
J108P	1	0.25	0.70	0.04	0.01	1.00	1.92	0.07	1.99	3
J108P	2	0.21	0.70	0.09	0.01	1.00	1.93	0.06	1.99	3
J108P	4–1	0.23	0.66	0.10	0.01	1.00	1.85	0.15	2.00	3
J108P	4–2	0.25	0.67	0.07	0.01	1.00	1.86	0.14	2.00	3
J108P	4–3	0.36	0.58		0.05	0.99	1.99	0.02	2.01	3
J108P	4–4	0.38	0.56		0.04	0.99	2.00	0.01	2.01	3

Coffinite $U(SiO_4)_{1-x}(OH)_{4x}$

Coffinite was known from Jáchymov for some time only from unpublished reports but later it was studied in detail by Janeczek [150]. The studied samples proved its presence in Ag- and Bi-paragenesis in the whole district, largely in places with the second generation of *uraninite*.

It also occurs without direct relation to *uraninite*, e. g., on the periphery of spheroidal *pyrite* aggregates set in

Table 39. Calculated unit-cell parameters of coffinite from Jáchymov for the space group $I4_1/amd$ and density.

sample	unit-cell parameters (Å)		density (g.cm^{-3})
	a	*c*	D_m
[150]	6.98(2)	6.22(3)	*6.31–6.52

* The value estimated from unit-cell dimensions and thermal analysis. Theoretical value for $USiO_4$ is 7.16 g.cm^{-3} [150].

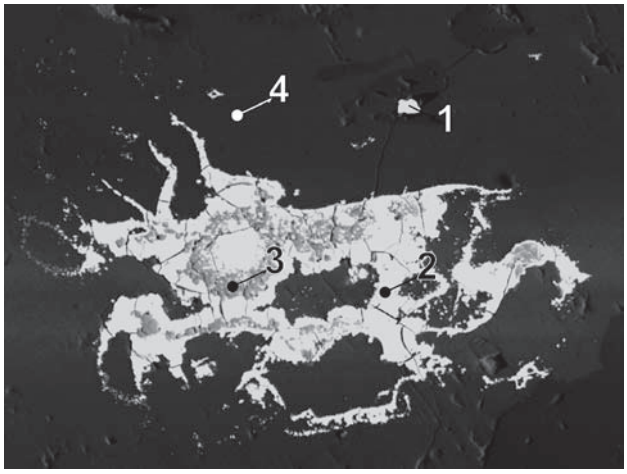

Fig. 57. MP271B/A-11. 1 – cinnabar, 2 – coffinite, 3 – pyrite, 4 – calcite. Barbora shaft, 4th/5th level, No. 32 vein. BSE image. Magnification 300×.

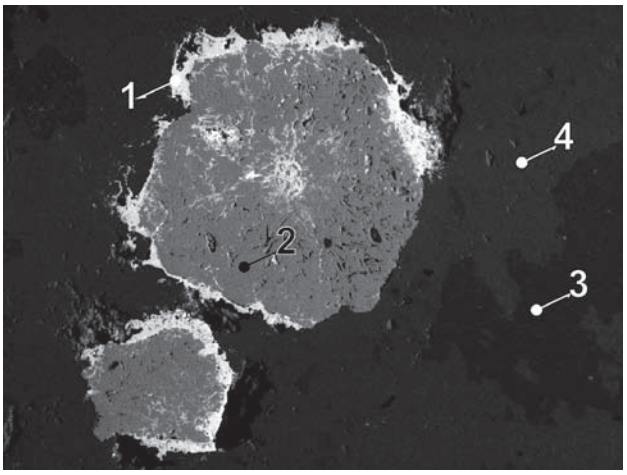

Fig. 56. J186P/1. 1 – coffinite, 2 – pyrite, 3 – chamosite, 4 – Fe-dolomite. Eliáš mine, AK vein. BSE image. Magnification 540×.

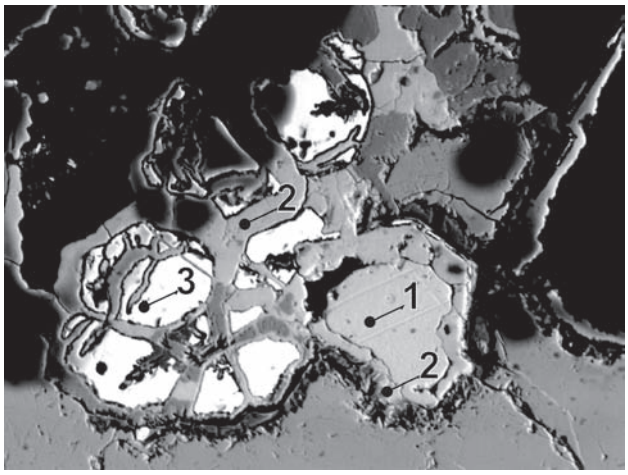

Fig. 58. MP390A/C. 1 – argentite, 2 – coffinite, 3 – uraninite. Rovnost I shaft, No. 13 vein. BSE image. Magnification 250×.

Table 40. Chemical analyses of coffinite.

sample	pt.	UO_2	ZrO_2	TiO_2	FeO	PbO	Y_2O_3	Ce_2O_3	SiO_2	P_2O_5	Bi_2O_3	BaO	CaO	Total
							weight %							
SR002	1	60.28	0.13	0.25		0.23	0.42		18.32	0.79	0.09	0.35	2.14	83.00
SR002	2	61.33	0.09	0.25		0.17	0.40		18.58	0.93	0.13	0.48	2.37	84.73
SR002	3	62.09	0.07	0.34	0.17	0.14	0.55		17.43	1.14	0.15	0.30	1.83	84.21
SR002	4	65.71	0.06	0.63	0.08	0.25	0.17		17.21	1.39	0.30	0.43	0.71	86.94
[150]	1	59.96	0.68		0.25	<0.01	0.80	0.32	17.89	1.43			3.05	84.38
[150]	2	61.93	0.75		0.29	0.48	0.17	0.31	18.02	1.25			3.08	86.28
[150]	3	62.84	0.10			0.42	<0.01	0.31	18.17	1.18			3.79	86.81

sample	pt.	U^{4+}	Zr^{4+}	Ca^{2+}	Ti^{4+}	Fe^{2+}	Y^{3+}	Ce^{3+}	Ba^{2+}	subtotal	Si^{IV}	P^{V}	subtotal	O
							number of atoms							
SR002	1	0.78		0.13	0.01		0.01		0.01	0.95	1.07	0.04	1.11	4
SR002	2	0.78		0.15	0.01		0.01		0.01	0.96	1.06	0.05	1.11	4
SR002	3	0.81		0.12	0.02	0.01	0.02		0.01	0.97	1.02	0.06	1.08	4
SR002	4	0.85		0.04	0.03		0.01		0.01	0.94	1.00	0.07	1.07	4
[150]	1	0.76	0.02	0.19		0.01	0.02	0.01		1.00	1.02	0.07	1.09	4
[150]	2	0.78	0.02	0.19		0.01	0.01	0.01		1.01	1.02	0.06	1.08	4
[150]	3	0.80	<0.01	0.23				0.01		1.05	1.04	0.06	1.10	4

chamosite. The chemistry of *coffinite* features a strong variation in the contents of U, Si, and Pb, P. Variation in grey hues in BSE images for domains with closely similar major element contents probably reflects variation in the content of water and the (OH) group.

The richest *coffinite* accumulations are in copper ores, particularly *bornite*, showing an extensive replacement of carbonate gangue by *quartz* and chalcedony and replacement of *uraninite* by spheroidal aggregates of *coffinite*.

The process of coffinitization [394], [454] is quite common at uranium deposits. Some authors described also de-coffinitization [454], [455]. This process is controlled mainly by pH, Eh and the activity of $(SiO_4)^{4-}$.

Based on the data by Brookins [456], it is possible to estimate conditions for *coffinite* formation at pH < 6, $Eh_{coff.} > Eh_{uraninite}$ (for 25 °C).

The alteration of *uraninite* to *coffinite* is either partial, with a proportion of *uraninite* relics in coffinite, or complete. The alteration proceeded in certain periods, as indicated by recurrent layering of thin laminae seen by the ore microscope or in BSE images.

The occurrence of concentric and radial fractures is probably due to the process of recrystallization of *uraninite* and *coffinite* – the density of *uraninite* is nearly doubled.

Covellite CuS

Covellite forms minor isolated grains up to 0.1 mm long in the assemblage of Cu-minerals. They show characteristic blue colour with an intense bireflection of various tints

Table 41. Calculated unit-cell parameters of covellite from Jáchymov for the space group $P6_3mmc$.

sample	*a*	*c*
	(Å)	
J-911	3.798(2)	16.396(7)

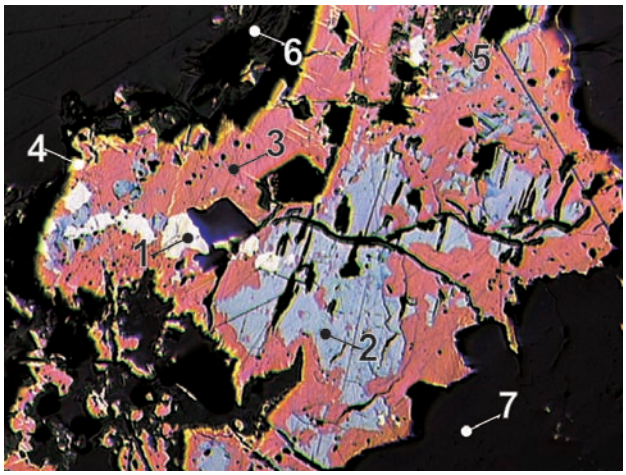

Fig. 59. Complicated texture of bornite enclosing silver and covellite. Fractures in bornite are filled by chalcopyrite and uraninite. 1 – silver, 2 – covellite, 3 – bornite, 4 – chalcopyrite, 5 – uraninite, 6 – roscoelite, 7 – quartz. Rovnost mine, 3rd level. Reflected light, single polarizer. Magnification 160×.

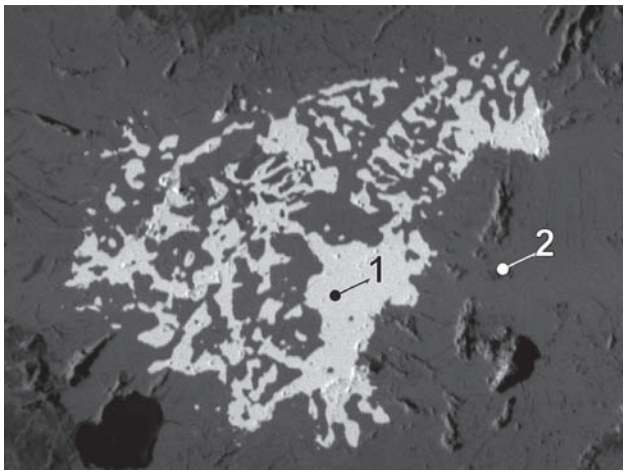

Fig. 60. J138P/B. 1 – galena, 2 – covellite. Shaft No. 14. BSE image. Magnification 320×.

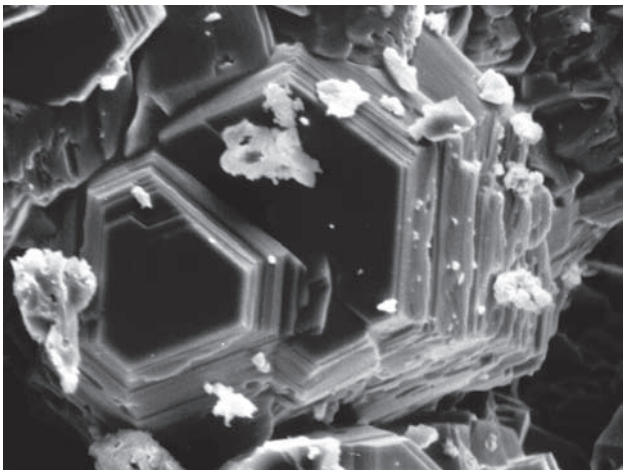

Fig. 61. J-928. Covellite crystals in cavity. SE image. Magnification 1100×. Photo A. Gabašová.

Table 42. Chemical analyses of covellite.

sample	pt.	Cu	Ag	Fe	Zn	S	Sb	As	Total
					weight %				
J063P	1	77.59	0.66	0.39	0.12	19.63	0.41	0.62	99.42
J063P	1a	77.64	0.59	0.27	0.23	19.71	0.37	0.46	99.27
J063P	1b	77.52	0.71	0.34	0.45	19.59	0.51	0.75	99.87
J063P	1c	77.69	0.55	0.44	0.09	19.81	0.67	0.83	100.08

sample	pt.	Cu	Ag	Fe	Zn	subtotal	S	As	subtotal	Total
						number of atoms				
J063P	1	1.97	0.01	0.01		1.99	0.99	0.01	1.00	3.00
J063P	1a	1.97	0.01	0.01	0.01	1.99	0.99	0.01	1.00	3.00
J063P	1b	1.96	0.01	0.01	0.01	2.00	0.98	0.02	1.00	3.00
J063P	1c	1.96	0.01	0.01		1.98	0.99	0.02	1.01	3.00

and strongly orange colour with crossed polarizers. Very good cleavage is characteristic. Although the optical properties of this *covellite* are standard, X-ray diffraction pattern shows poor crystallinity. This mineral occasionally forms larger aggregates and thin veinlets. Its presence indicates beginning alteration of the copper paragenesis (Fig. 60). *Covellite* was analysed in few samples but its occurrence in other samples with *djurleite* is probable.

Crandallite – goyazite $CaAl_3(PO_4)_2(OH)_5 \cdot H_2O$ – $SrAl_3(PO_4)_2(OH)_5 \cdot H_2O$

This mineral forms one 30 μm grain in intergrowth with *tennantite* in *quartz* in mineralized mica schist. It contains major Al, P, Ca and significant Sr, low Ce and sulphate group. The sample contains zoned W-rich *rutile, zircon*, and *arsenopyrite*, *sphalerite*, *chalcocite*, *covellite*, *chalcopyrite,* with inclusions of Zn-rich *stannite* and Fe-rich *gersdorffite.* The sample comes from the Giftkies adit.

Diaphorite $Pb_2Ag_3Sb_3S_8$

Diaphorite forms anhedral to subhedral grains of microscopic size in microcrystalline intergrowth with *pyrite* and *stephanite*. These coatings cover massive *stephanite* covered by *stephanite* crystals. The specimen collected in 1872 is in the Mineralogical collection, National Museum, Prague, No. NM9512 [333].

Table 43. Microhardness of diaphorite.

sample	mean	range	load
	[kp/mm^2]	[kp/mm^2]	[g]
[333]-NM9512	232	210–257	20

Dickite $Al_2Si_2O_5(OH)_4$

The recent data on *dickite* from Jáchymov were presented by Mrňa a Pavlů [351] and Mach [595]. They identified *dickite* in vein fillings, particularly in veins near granite pluton or directly in granite. Notable amounts of *dickite* occurred in the Geschieber vein, 10th and 12th level, Svornost shaft, as white to yellowish nests and coatings. Locally it amounts to 10 vol. % of the vein.

Table 44. Chemical analyses of diaphorite.

sample	Ag	Cu	Pb	Bi	Sb	S	As	Total
					weight %			
NM9512	23.73	0.08	29.90		27.48	19.31	0.07	100.57
NM9512	24.03	0.07	30.72	0.37	27.17	18.68		101.04
NM9512	23.82		30.35	0.11	27.30	19.10	0.10	100.78
NM9512	23.69		29.82		27.33	19.00	0.10	99.94
NM9512	24.22		29.69		27.56	18.75	0.11	100.33
NM9512	23.62	0.06	29.91	0.32	27.33	18.66		99.90

sample	Ag	Cu	Pb	Sb	As	Bi	S	Total
					number of atoms			
NM9512	2.95	0.02	1.93		3.02	8.07	0.01	16
NM9512	3.02	0.01	2.01	0.02	3.03	7.90		16
NM9512	2.97		1.97	0.01	3.02	8.02	0.02	16
NM9512	2.97		1.95		3.04	8.02	0.02	16
NM9512	3.04		1.94		3.07	7.93	0.02	16
NM9512	2.99	0.01	1.97	0.02	3.06	7.94		16

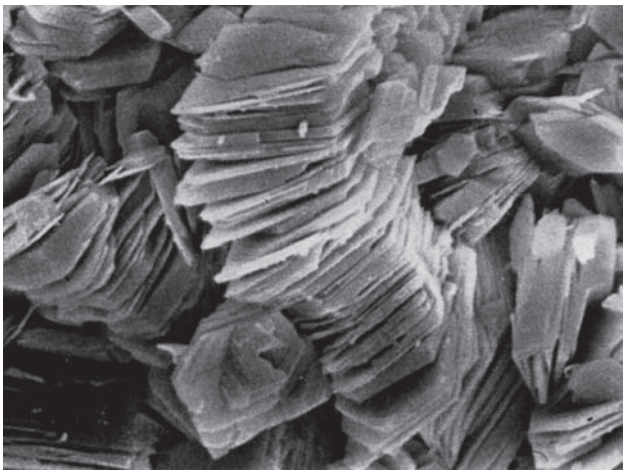

Fig. 62. Dickite crystals. SE image. Magnification 690×. Photo Z. Mach [595].

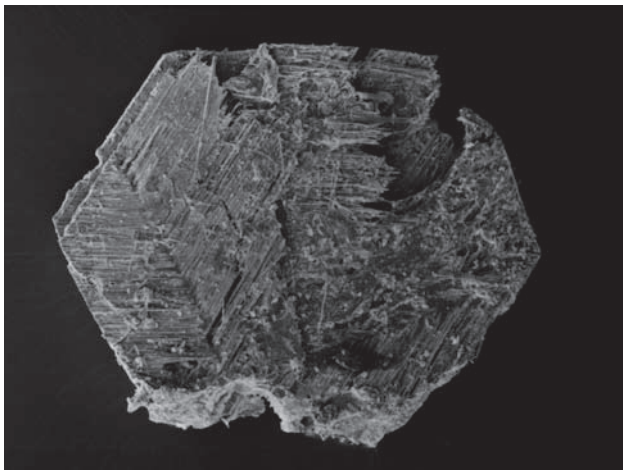

Fig. 63. NM4798. Pseudohexagonal crystal of djurleite. SE image. Magnification 45×. Photo A. Gabašová.

Dickite presence indicates a strong hydrothermal alteration of an original substrate, probably mylonitic clay [351].

Djurleite $Cu_{31}S_{16}$

Djurleite occurs in a mixture with *chalcocite* as small grains of a bluish steel colour, set in red hornfels-like *quartz*. It is associated with *chalcopyrite* and *tennantite*.

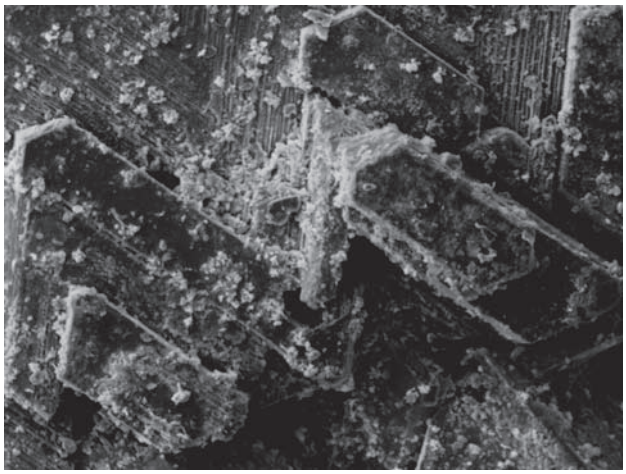

Fig. 64. NM4798. Accessories on the surface of pseudohexagonal crystal of djurleite. SE image. Magnification 200×. Photo A. Gabašová.

Table 45. Calculated unit-cell parameters of djurleite from Jáchymov for the space group $P2_1/n$.

sample	*a*	*b*	*c*	β
		(Å)		(°)
J013P	26.940(2)	15.689(1)	13.358(1)	90.17(1)

Table 46. Chemical analyses of djurleite.

sample	pt.	Cu	Ag	Fe	Zn	Ni	S	Sb	As	Total
						weight %				
J041P	a8	77.93	0.40	0.20	0.13	0.06	20.33	0.59	0.17	99.81
J041P	a1	77.71	0.67	0.19	0.13	0.16	20.67	0.44	0.32	100.29
99528	12	77.98	0.58	0.21	0.12	0.12	20.82	0.37	0.24	100.44
99528	14	78.55	0.37	0.43	0.15	0.34	20.76	0.25	0.53	101.38
J176P	A1	79.62		0.10			20.68			100.39
J176P	A2	79.02					20.62			99.64
J176P	A3	79.78					20.80			100.59
J003P	1	77.55		0.54			21.09			99.18

sample	pt.	Cu	Ag	Fe	Zn	Ni	subtotal	S	Sb	As	subtotal	Total
							number of atoms					
J041P	a8	30.69	0.09	0.09	0.05	0.03	30.95	15.87	0.12	0.06	16.05	47
J041P	a1	30.41	0.15	0.09	0.05	0.07	30.77	16.03	0.09	0.11	16.23	47
J176P	A1	30.99						16.01				47
J176P	A2	31.10						15.90				47
J176P	A3	30.98						16.02				47
99528	12	30.42	0.13	0.09	0.05	0.05	30.75	16.10	0.08	0.08	16.25	47
99528	14	30.39	0.08	0.19	0.06	0.14	30.86	15.92	0.05	0.17	16.14	47
J003P	1	30.38		0.24			30.62	16.38			16.38	47

In a single recorded case it formed thin tabular crystals of hexagonal appearance, reaching an impressive size of 2 cm. The large faces with pseudohexagonal outlines show striation indicating intergrowth of smaller crystals. *Djurleite* crystals are deposited on drape-like aggregates of white *quartz*. Vugs in the same specimen carry rare earthy *roxbyite*. The specimen is in the Mineralogical collection, National Museum, Prague, No. NM4798. Both minerals, especially *roxbyite*, indicate a low-temperature mineralization.

Dolomite $CaMg(CO_3)_2$

Mrňa a Pavlů (1967) [351] studied *dolomite* from the Jáchymov veins. They found out that *dolomite* is the most frequent gangue mineral in the carbonate veins. It originated mainly in the *carbonate-uraninite* and *arsenic-sulphide* stages. *Dolomite* associated with *uraninite* is pink, changing to a strong red colour in close proximity of *uraninite* aggregates. These two minerals occur in close association in parts of veins with bilateral symmetry. *Dolomite* is only weakly affected by younger mineralization stages.

Carbonates of the *arsenic-sulphide* stage are compositionally similar to *dolomite* of the *carbonate-uraninite* stage but they contain somewhat lower amount of Mn and lower amounts of *hematite* pigment. It is possible that some part of these carbonates represents regeneration of the older carbonate vein filling. A similar relation was considered for carbonates accompanying arsenide ores [351].

Pink *dolomite* enclosing *rammelsbergite* perimorphs after *silver* has 1 mm wide rim of buff coloured *dolomite* in proximity to the paramorphs, changing further away to pink colour.

Dolomite contains frequently some Fe and Mn. Rhombohedral crystal to 15 cm were observed occasionally.

Table 47. List of studied dolomite samples from Jáchymov.

sample	sample description	stage	composition	mine	level	vein
J005I 2	clear coarse-grained carbonate (perhaps younger than J005I/1) intergrown with J005I/1	*arsenide*	Ca>Mg>((Fe,Mn)), O,C	Svornost	5	Kryštof
J006I 1	coarse-grained milky-coloured carbonate (Fe oxides on the surface), with nickeline	*arsenide*	Ca>Mg=Fe((Mn)), O,C	Svornost	10	Kryštof
J007I 1	coarse-grained carbonate with red cloudy zones; stage arsenide	*arsenide*	Ca>Mg((Fe)), O,C	Svornost	Daniel	
J008I 1	coarse-grained carbonate, with inhomogeneous black colouring	*arsenide*?	Ca>Mg>((Mn,Fe)), O,C	Svornost		Prokop
J008I 2	yellowish rhombohedra partly covered with Fe-oxides/hydroxides in vugs (on J008I/1)	*arsenide*?	Ca>Mg>((Mn,Fe)), O,C	Svornost		Prokop
J009I 1	white coloured drusy zone in vugs with argentopyrite	*arsenic-sulphide*	Mg>Ca>((Fe)), O,C	Svornost		Geschieber (South)
J009I 2	clear coarse-grained carbonate (under J009I/1)	*arsenic-sulphide*	Ca>Mg>(Fe), O,C	Svornost		Geschieber (South)

Table 48. Homogenization temperature Th of fluid inclusions in dolomite from Jáchymov.

sample	mineral	Th	salinity	mineralization stage
		°C	wt.%	
J007I 1	dolomite		22–24	*arsenide*
J008I 1	dolomite	118–140	23	*arsenide*?
J008I 2	dolomite	126–144	22–24.5	*arsenide*?
J009I 1	dolomite		0.4	*arsenic-sulphide*
J005I 2	Fe-dolomite	96–112	23.5–24	*arsenide*
J009I 2	Fe-dolomite	112–138	23–23.5	*arsenic-sulphide*

Crystal structure refinement

The crystal structure was refined with the Rietveld method from powder diffraction patterns (start angle, step, end angle (°2θ Cu$K_{\alpha 1 \alpha 2}$): 18.0, 0.02, 120.0) obtained with the

Table 49. Rietveld structure refinement of carbonates from Jáchymov. Calculated unit-cell parameters, unit-cell volume, fraction.

sample	*a* (Å)	*c* (Å)	*V* (Å^3)	z_C	x_O	y_O	z_O	B_{ov} (Å^{-2})	R_p (%)	R_{wp} (%)	χ^2
J005I 1	4.8155(4)	16.068(2)	322.69(5)	0.238(2)	0.257(2)	–0.009(2)	0.243(1)	1.75(5)	9.6	13.6	2.03
J005I 2	4.8069(3)	16.012(1)	320.40(3)	0.239(3)	0.250(2)	–0.025(4)	0.2476(9)	1.41(7)	8.9	13.7	2.58
J006I 1	4.8130(4)	16.065(2)	322.28(5)	0.245(2)	0.257(3)	–0.025(4)	0.2501(8)	1.19(2)	8.5	12.2	1.88
J007I 1	4.8073(3)	16.013(1)	320.50(4)	0.254(1)	0.262(2)	–0.012(3)	0.2428(9)	1.49(5)	8.5	12.6	1.99
J008I 1	4.8090(4)	16.024(2)	320.93(5)	0.254(2)	0.257(3)	–0.019(4)	0.243(1)	1.47(7)	9.8	14.6	2.57
J008I 2	4.8092(4)	16.026(2)	321.00(5)	0.261(2)	0.251(2)	–0.028(3)	0.2432(9)	1.36(7)	9.2	13.3	2.23
J009I 1	4.8073(4)	16.024(2)	320.70(5)	0.242(2)	0.254(2)	–0.023(3)	0.2437(9)	1.31(7)	8.4	12.3	1.78
J009I 2	4.8142(3)	16.064(1)	322.44(4)	0.242(2)	0.267(2)	–0.009(3)	0.2440(9)	1.04(5)	8.7	13.2	2.35

Table 50. Calculated unit-cell parameters of dolomite from Jáchymov for the space group $R\bar{3}$.

sample	*a*	*c*
	(Å)	
G115A (J-822)	4.8284(5)	16.099(2)

Philips X'Pert diffractometer in Bragg-Brentano setting. FullProf 2k program [462] with graphic facility WinPlotr [464] was used.

Model structures used are those in Tables 1, 2, 7, and 8 in Reeder [465] – dolomite was refined in the trigonal space group $R\bar{3}$ with four fraction co-ordinates ($z_C \sim 0.243$; $x_O \sim 0.248$; $y_O \sim -0.035$; $z_O \sim 0.244$). In addition, total temperature factor, unit-cell parameters, parameters characterizing width and shape of diffractions (pseudo-Voigt profile function was used) and parameters describing microabsorption of X-ray radiation due to uneven sample surface were refined. Results are presented in Table 49.

Table 51. Chemical analysis of dyscrasite.

sample	pt.	S	Fe	Cu	As	Ag	Sb	Total
				weight %				
J105P	E1		0.12		0.89	76.20	22.99	100.20
J105P	E2				1.79	76.32	22.12	100.24
J105P	E3			0.02	1.05	75.24	23.10	99.40
J105P	E4				1.25	75.73	23.94	100.92
J105P	E5		0.08	0.09	2.06	74.20	21.98	98.41
J105P	E6	0.03			0.37	75.10	23.21	98.71
J105P	A1		0.17		2.47	72.79	23.13	98.56
J105P	A2	0.01	0.16		3.93	72.81	23.56	100.46

sample	pt.	Ag	Sb	As	subtotal	Total
			number of atoms			
J105P	E1	3.11	0.83	0.05	0.88	3.99
J105P	E2	3.10	0.80	0.10	0.90	4.00
J105P	E3	3.10	0.84	0.06	0.90	4.00
J105P	E4	3.07	0.86	0.07	0.93	4.00
J105P	E5	3.06	0.80	0.12	0.93	3.99
J105P	E6	3.12	0.85	0.02	0.88	4.00
J105P	A1	3.00	0.84	0.15	0.99	3.99
J105P	A2	2.92	0.84	0.23	1.06	3.99

Dyscrasite Ag_3Sb

Dyscrasite was identified as round 5 μm grains enclosed in *arsenic* containing 7 wt.% Sb, set in *dolomite* gangue. *Dyscrasite* is limited to 30–40 μm wide outer zones or aggregates of *arsenic*, which are deposited on larger aggregates of *arsenic* free of Sb (< 0.5 wt.% Sb) and free of *dyscrasite* inclusions (Fig. 65). The sample comes from the Svornost shaft, Adit level, Hildebrand vein.

Emplectite $CuBiS_2$

The mineral was identified as several acicular crystals to 0.5 mm long coated by an ultra-fine mixture of *emplectite* and *pyrite* surrounded by altered *uraninite*, and intergrown in porous brownish hornfelsic *quartz*. This sample comes from the Schweizer vein. On another sample, *emplectite* occurs in short prismatic crystals up to 20 μm long deposited on *rammelbergite* aggregate, with a

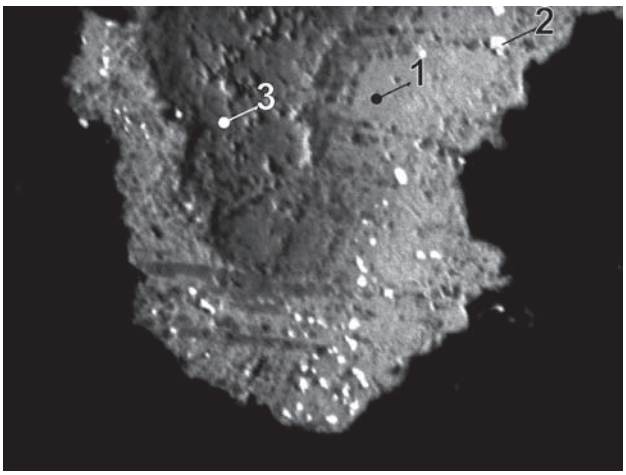

Fig. 65. J105P/A-5. 1 – arsenic, free of corrosion, 2 – dyscrasite, 3 – corroded arsenic. Svornost shaft, Adit level, Hildebrand vein. BSE image. Magnification 720×.

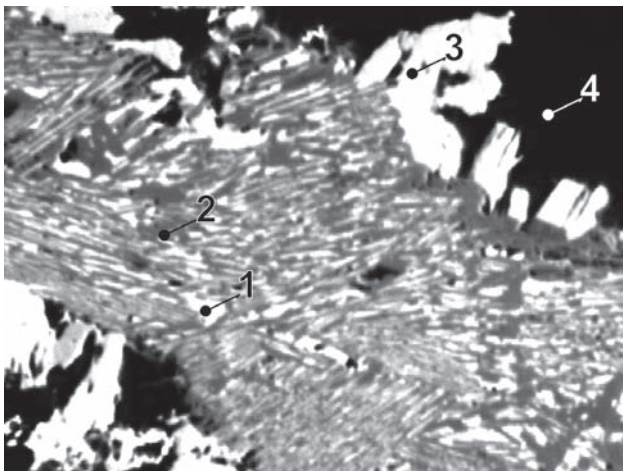

Fig. 66. MP290C/H-6. 1 – bismuth, 2 – rammelsbergite, 3 – emplectite, 4 – calcite. Barbora shaft, 5th level, vein No. 32. BSE image. Magnification 660×.

Table 52. Chemical analyses of emplectite.

sample	pt.	Cu	Ag	Pb	Bi	S	Total
				weight %			
MP290C	H6-13	16.58		0.85	61.04	18.54	97.02
MP290C	H6-2	16.34	0.06	0.97	59.37	19.08	95.82

sample	pt.	Cu	Pb	subtotal	Bi	S	Total
				number of atoms			
MP290C	H6-13	0.91	0.01	0.93	1.05	2.03	4
MP290C	H6-2	0.90	0.02	0.92	1.00	2.09	4

myrmekitic intergrowth of *bismuth* (Fig. 66). The intergrowth probably resulted from disintegration of an unstable phase. The sample comes from the Barbora shaft, 5th level, No. 32 vein.

Enargite Cu_3AsS_4

Enargite was reported by Zückert [423] as one of the minerals composing perimorphs after *silver* dendrites. It was not found in the present study, but *lautite* was identified outside the perimorphs. With regard to similar optical properties of *enargite* and *lautite* a possibility remains that Zückert observed *lautite*.

Ferberite $FeWO_4$

Mrňa and Pavlů [Mrňa, MS – written communication] described *wolframite* in a similar position as *cassiterite*, but as rare mineral. Tabular crystals up to 2 cm are accompanied by *molybdenite*, *muscovite* and *fluorite* in a *quartz* vein. The single occurrence comes from near granite contact with metamorphic mantle rocks in the Rovnost I shaft.

Ferberite in 1 cm crystals, partly replaced along cleavages by *hematite*, was newly identified. This greisen sample from the Rovnost I shaft (probably 8th level) contains also *annite*, *schorl*, *topaz*, *scheelite*, *molybdenite,* and *apatite.*

Fletcherite $Cu(Ni,Co)_2S_4$

Fletcherite forms 5 μm wide zone along *millerite–chalcopyrite* boundary. It is associated with *wittichenite*.

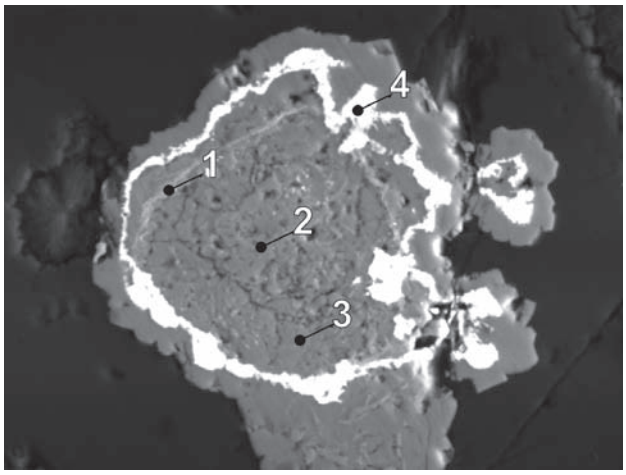

Fig. 67. MP230/A-1. 1 – fletcherite, 2 – millerite, 3 – chalcopyrite, 4 – wittichenite. Eva shaft, 5th level, vein No.32. BSE image. Magnification 1000×.

Table 53. Chemical analyses of ferberite.

sample	pt.	CaO	MnO	FeO	CuO	WO_3	ZnO	Total	Fe	Mn	Ca	subtotal	W	O
					weight %				number of atoms					
J012P	r6a	0.11	5.38	18.75	0.03	74.96	0.17	99.40	0.80	0.23	0.01	1.03	0.99	4
J012P	r6	0.10	5.19	19.27	0.09	75.24	0.29	100.18	0.81	0.22	0.01	1.04	0.98	4
J012P	r7	0.04	7.04	16.76	0.35	75.41	0.26	99.86	0.71	0.30		1.01	0.99	4

Table 54. Chemical analyses of fletcherite.

sample	pt.	S	Fe	Co	Ni	Cu	As	Total
					weight %			
MP27	D4	37.89	0.14	11.19	29.88	13.71	8.28	101.09
MP230	A	39.74	4.57	22.03	19.84	8.26	0.49	94.93

sample	pt.	Cu	Fe	Co	subtotal	Co	Ni	subtotal	S	As	subtotal	Total
						number of atoms						
MP27	D4	0.68	0.01	0.29	0.98	0.31	1.61	1.92	3.74	0.35	4.09	7
MP230	A	0.42	0.26	0.30	0.98	0.91	1.09	2.00	4.00	0.02	4.02	7

Fluorite CaF_2

Mrňa and Pavlů (1967) [351] studied *fluorite* from the Jáchymov deposit. They reported that *fluorite* has a rather limited occurrence. It is present in small amounts in lower parts of veins and in proximity of major fault zones.

Genetically it is related to the *Sn–W sulpharsenide*, *ore-free quartz*, *carbonate-uraninite*, and *post-ore* stages. *Fluorite* is usually light in colour (green, yellow, white) but *fluorite* of the *carbonate-uraninite* stage is violet turning to nearly black in proximity of *uraninite* lenses. In both cases, *fluorite* forms isolated grains, small aggregates or thin veinlets with euhedral crystals in vugs [351].

Fluorite veins up to 15 cm wide were observed during the present study. *Fluorite* has various colours: violet, yellow, white or colourless. Banded veins show palisade texture with crystal up to 5 cm long in open vugs. Such accumulations of *fluorite* occur in the north-eastern part of the district. *Fluorite* is common in small grains in greisen of the Rovnost shaft, probably 8th level. All these *fluorite* occurrences are related to the *Sn–W sulpharsenide* stage.

Table 55. Calculated unit-cell parameters of fluorite from Jáchymov for the space group $Fm\bar{3}m$.

sample	*a* (Å)
J-715	5.4630(1)
J-713	5.4632(3)
J-714	5.4642(3)

Table 56. Homogenization temperature Th of fluid inclusions in fluorite from Jáchymov.

sample	pt.	Th	salinity	mineralization stage
		°C	wt.%	
UNRUH	1	99–118	18–22.5	*sulphide*

Freibergite $(Ag,Cu)_6[(Cu, Ag)_4(Fe,Zn)_2](Sb,As)_4S_{13}$

Freibergite forms porous grains up to 0.5 mm enclosed in *chalcopyrite*. It encloses small *pyrargyrite* grains. The larger adjacent *pyrargyrite* crystals enclose sphalerite. *Freibergite* is slightly zoned, with the outer zone enriched in Sb. The paragenesis comprises *Sb-gersdorffite*, *löllingite*, *rammelsbergite* and *nickel-skutterudite*. All these minerals are enclosed in Fe-*dolomite* gangue of the Geschieber vein.

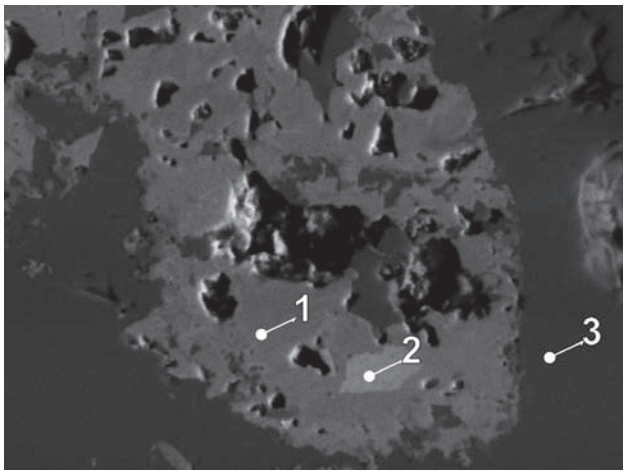

Fig. 68. G119C/D. 1 – freibergite, 2 – pyrargyrite, 3 – chalcopyrite. Svornost shaft, Geschieber vein. BSE image. Magnification 400×.

Table 57. Chemical analyses of freibergite.

sample	pt.	Ag	Cu	Fe	Zn	Ni	Sb	As	S	Total
						weight %				
G119C	D1	29.76	17.50	6.09	1.81	0.32	17.49	6.53	21.04	100.54
G119C	D2	29.41	18.24	4.96	1.93	0.22	16.55	7.52	21.64	100.48
J160P	7	19.73	24.27	4.94	2.15		17.50	8.20	23.35	100.14

sample	pt.	Ag	Cu	subtotal	Fe	Zn	Ni	subtotal	Sb	As	subtotal	S	Total
							number of atoms						
G119C	D1	5.06	5.05	10.11	2.00	0.51	0.10	2.61	2.64	1.60	4.23	12.04	29
G119C	D2	4.96	5.23	10.19	1.62	0.54	0.07	2.23	2.47	1.83	4.30	12.29	29
J160P	7	3.18	6.64	9.82	1.54	0.57		2.11	2.50	1.90	4.40	12.67	29

Galena PbS

Mrňa and Pavlů (1967) [351] studied the occurrence of *galena* in Jáchymov. They found that galena, similarly to other sulphides in the veins, forms fine-grained impregnation of isolated grains, irregular veinlets or lenses up to 10 cm scattered in the gangue.

Table 58. Calculated unit-cell parameters of galena from Jáchymov for the space group $Fm\bar{3}m$.

sample	*a* (Å)
J130P	5.935(1)

Apart from monomineralic accumulations, *galena* is associated with *sphalerite* in lenses of polymetallic ores. The sequence of crystallization of the two minerals varies. Less frequently, *galena* is accompanied by *chalcopyrite* or *arsenopyrite*. *Galena* occurrences are related to uranium and arsenide ores. It is deposited on older arsenides or fills vugs after leached *silver* [351].

Galena may occur as an exsolved phase in *covellite* or as myrmekitic aggregates in *bornite*. Replacement of *galen*a by *nickeline* indicates the existence of at least two generations of galena.

Samples affected by weathering carry fine-grained *cerussite* or *cerussite* fracture filling in *bornite, chalcopyrite* or in newly formed *covellite*.

Gersdorffite NiAsS

Gersdorffite occurs in rims around arsenides or as small grains. The mineral does not form voluminous accumulations, except the Zdař Bůh vein (Bratrství shaft, 5th level, block 531), where gersdorffite was documented in massive aggregates with well-formed crystals up to 1 cm (Geceva and Dubinkina [358], [424]), along contact of *rammelsbergite* with *millerite*.

Gersdorffite free of antimony was identified in several samples with *bismuth*, *nickel-skutterudite* and *safflorite*. *Gersdorffite* overgrows zoned crystals of *nickel-skutterudite* and its small accumulations may be replaced by *millerite*. Two types of *gersdorffite* occur in this association. The older *gersdorffite* overgrowing zoned *nickel-skutterudite* is grey and it has increased polishing hardness. Younger *gersdorffite* has a lighter colour.

Chemical analyses of Jáchymov *gersdorffite* (Table 59) show significant contents of Co in some samples and the Ni/Co ratio ranges to 5 : 3. *Co-gersdorffite* occurs in oval aggregates up to 0.2 mm, deposited on *skutterudite* with low Co content and enclosing skeletal *bismuth*. The sample comes from the No. 7 adit.

Some *gersdorffites* contain Sb. The highest content of 25 wt.% Sb was determined in an inhomogeneous *gersdorffite* deposited on *acanthite* in a rim on *nickel-skutterudite* at contact with *dolomite*. This composition corresponds to As/Sb atomic ratio of 2 : 1 and it is near the *gersdorffite–ullmannite* border. The sample comes from the Rovnost I shaft, 6th level, steep carbonate vein trending E–W, perpendicular to No. 16 vein.

Table 59. Calculated unit-cell parameters of gersdorffite from Jáchymov.

sample	*a* (Å)	*s.g.*
J100P (J-925)	5.6844(8)	$Pa\bar{3}$
J-771	5.685(1)	$Pa\bar{3}$
VS4238 (J-861)	5.689(1)	$Pa\bar{3}$
J-723	5.6902(2)	$Pca2_1$
J-233	5.692(1)	$P2_13$
J-236	5.692(1)	$Pa\bar{3}$

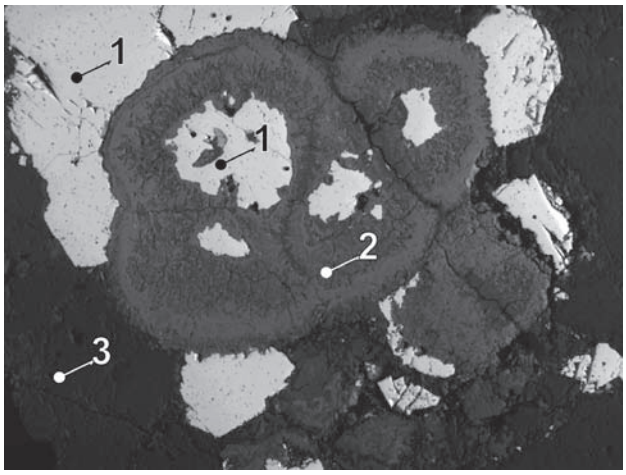

Fig. 69. J102P. 1 – galena, 2 – gersdorffite, 3 – quartz. Schönerz adit. BSE image. Magnification 16×.

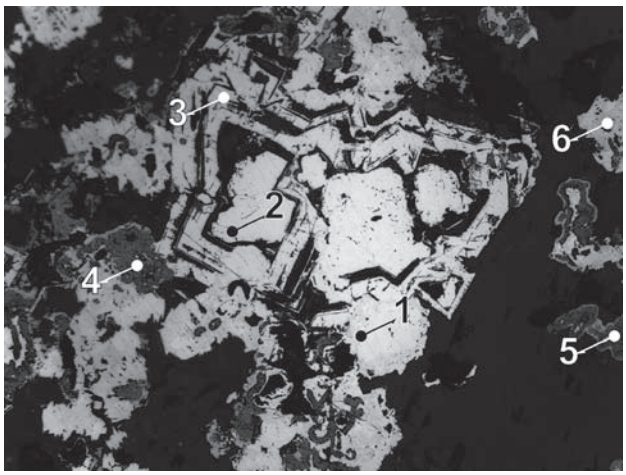

Fig. 70. J115P. Arsenides have internal structure emphasized by strong corrosion and they are gradually altered to gersdorffite with variable S content. Radial or botryoidal sphalerite is deposited on arsenides. Chalcopyrite and matildite are rare. 1 – galena, 2 – nickel-skutterudite, 3 – As-gersdorffite, 4 – sphalerite, 5 – matildite, 6 – chalcopyrite. Rovnost II shaft, 6th level, vein perpendicular to the vein No. 16. Reflected light, single polarizer. Objective 20×.

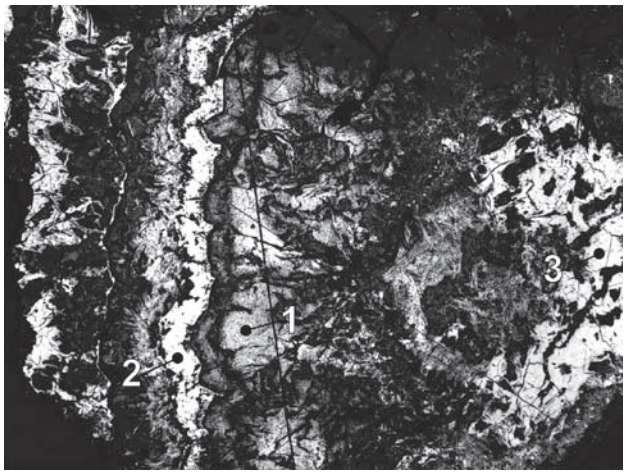

Fig. 71. J102P. Gersdorffite rims formed after skutterudite are rimmed by rammelsbergite. The association shows newly formed gersdorffite, transport of S is documented by galena grains. 1 – As-gersdorffite, 2 – rammelsbergite, 3 – galena. Schönerz adit. Reflected light, single polarizer. Objective 20×.

Fig. 72. J115P. Zone of crushed nickel-skutterudite, which is continuously replaced by a mixture of rammelsbergite and gersdorffite. 1 – nickel-skutterudite, 2 – rammelsbergite + gersdorffite. Rovnost II shaft, 6th level, vein perpendicular to the vein No. 16. Reflected light, single polarizer. Objective 20×.

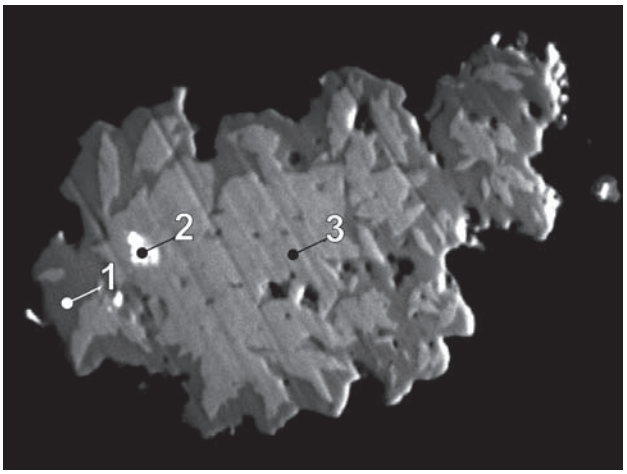

Fig. 73. MP230/A. 1 – gersdorffite, 2 – galena, 3 – löllingite. Eva shaft, 5th level, vein No. 32. BSE image. Magnification 1150×.

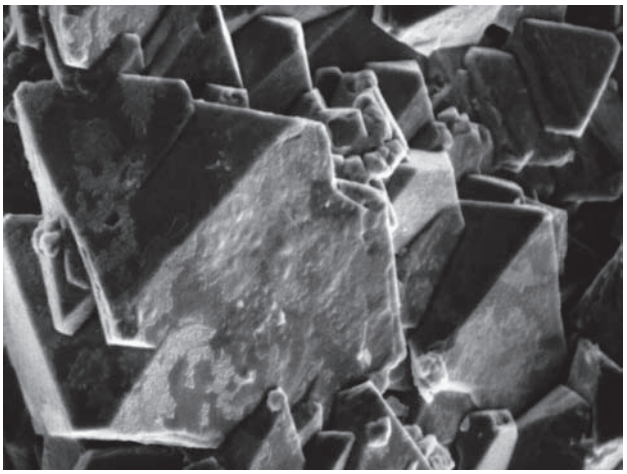

Fig. 74. J-723. Gersdorffite on nickeline. Svornost shaft, 10th level. SE image. Magnification 780×. Photo A. Gabašová.

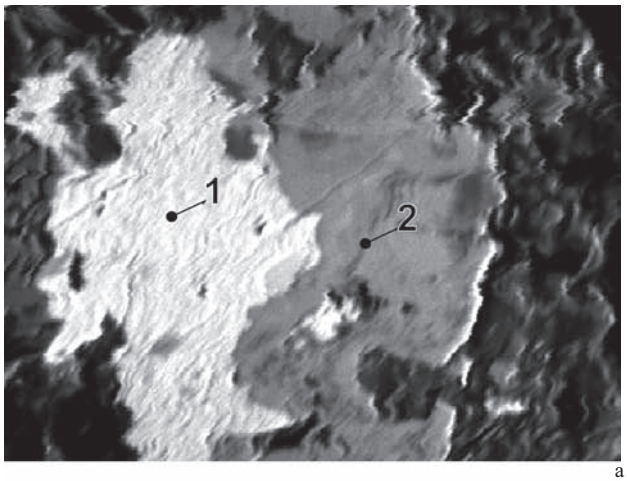

a

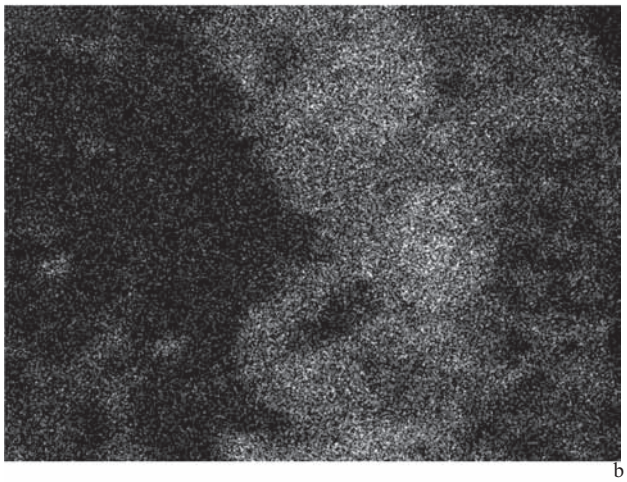

b

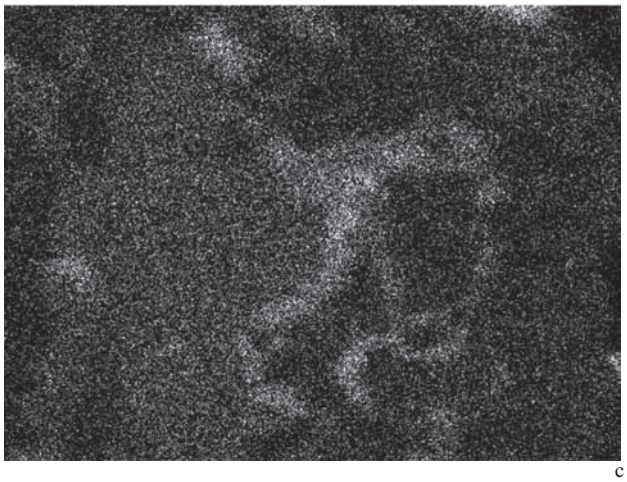

c

Fig. 75. MP511E/2. 1 – acanthite, 2 – gersdorffite. Rovnost II shaft, 6th level, vein No. 16. Magnification 1600×.
a) BSE image
b) Distribution of As
c) Distribution of Sb.

Other examples of *Sb-gersdorffite* include material containing 9–11 wt.% Sb, deposited on *sphalerite* and covered by *millerite*, in a sample from the Eliáš mine, No. 2A vein. *Gersdorffite* with 3 wt.% Sb overgrows clusters of *löllingite* crystals and *gersdorffite* with 1.5 wt.% Sb forms rims around hollow oval *löllingite* aggregates enclosed in *dolomite* or deposited on *nickel-skutterudite.* This sample comes from the Eva shaft, 5th level, No. 32 vein.

Gersdorffite is often associated with *rammelsbergite.* Intergrowth of the two minerals is so fine that even electron microprobe cannot tell them apart. As/S ratio in this material varies considerably [490] and in some cases it is not possible to distinguish *As-gersdorffite* from *S-rammelsbergite* just with chemical analyses, as composition of these minerals may overlap. In such cases it is necessary to use combination of optical properties and XRD identification (Table 59). This points to necessary caution in accepting published chemical analyses unless these minerals were examined by other methods as well.

Gersdorffite occurs in intergrowth with *rammelsbergite* in spheroidal aggregates with radiating structure (sample J100P). Observation of polished sections with optical microscope shows weakly defined concentric zoning with zones of variable porosity and a moderate to weak anisotropy of elongated grains with imperfect radial orientation. The intensity of anisotropy does not differ through the growth zones. This sample from the Schönerz adit was identified by XRD.

Gersdorffite is usually rare in hydrothermal veins but in the Jáchymov deposit it is a fairly common mineral.

Table 60. Chemical analyses of gersdorffite.

sample	pt.	Ni	Co	Fe	Cu	Ag	Zn	As	S	Sb	Total
						weight %					
J016P	a	32.94	0.62	0.31	0.30			50.67	16.19	0.68	101.71
J016P	b	34.59	0.51	0.42	0.39			47.35	17.29	0.71	101.26
J018P	a	33.49	0.94	0.87	1.10			48.21	14.68	0.57	99.86
J018P	b	33.67	0.84	0.86	1.12			48.96	14.54	0.76	100.75
J052P	7	21.31	4.18	8.31	0.55			43.09	22.57	0.27	100.28
J068P	D2	19.29	4.09	9.16	2.79	0.09	0.02	50.03	15.55	0.11	101.12
J068P	D1	18.47	3.68	10.11	3.24	0.16	0.20	48.92	16.02	0.00	100.81
J068P	D3	16.30	7.33	8.89	2.79		0.05	47.93	16.21	0.05	99.54
J068P	D4	18.06	5.35	9.27	1.10		0.06	48.83	17.00	0.04	99.71
J100P	2	27.35	0.66	2.77	0.11	0.32	0.01	58.93	9.77	0.29	100.21
J100P	3	28.79	0.41	1.50	0.05	0.08		61.09	8.00	0.39	100.31
J100P	1	27.42	1.18	1.03	0.13			65.16	4.23	0.27	99.42
J100P	1a	28.21	0.96	1.00	0.12		0.10	67.21	3.83		101.44
J100P	2a	27.36	0.94	0.85	0.33	0.14	0.08	67.11	3.43	0.07	100.31
J100P	1	29.77	1.06	2.59	0.20		0.07	49.71	15.04	1.13	99.56
J100P	1a	34.85	0.29	0.12				45.88	18.11	0.04	99.28
J115P	B1	19.92	12.00	1.32			0.08	52.93	12.78	0.06	99.10
J115P	B3	24.02	7.41	1.10	0.06	0.08		59.67	8.81		101.15
J115P	B2	28.34	1.79	0.31	0.06		0.16	67.68	2.98	0.03	101.34
J117P	A1	25.31	1.92	6.40	0.68	0.19	0.00	48.90	16.78	0.00	100.17
J117P	A2	26.36	0.64	1.55	0.53	0.14	0.09	66.85	3.16	0.13	99.46
J140P	1	26.60	1.56	0.24	0.02			66.10	4.43	0.00	98.95
J140P	2	27.73	0.88	0.17	0.03			67.20	4.09	0.00	100.10
J140P	3	26.08	1.39	0.62				68.77	2.93	0.00	99.80
J140P	4	26.76	1.47	0.48	0.03			68.62	3.01	0.03	100.39
J167P	1	32.31	2.18	0.04			0.17	49.16	15.86	0.02	99.70
J167P	2	32.59	2.12	0.07			0.12	47.98	16.38	0.13	99.40
J167P	3	25.63	7.48	0.20				51.92	13.99	0.12	99.30
MP230	A1	31.40	0.61	2.89				46.65	16.92	1.69	100.16
MP230	A2	30.25	1.35	2.93				45.60	17.37	3.03	100.53
MP287D	4	23.23	11.26	0.34	0.59			45.96	19.09	0.53	101.00
MP287D	5	22.59	11.93	0.36	0.42			45.17	19.22	0.32	100.01
MP287D	aa	22.76	11.10	0.35	0.44			45.84	19.11	0.22	99.82
MP287D	ab	22.64	10.87	0.37	0.39			45.24	19.34	0.29	99.14
MP290C	H5-1	33.44	0.46	0.86	0.11	0.13	0.10	47.19	16.84	0.46	99.60
MP290C	H5-2	33.10	0.61	0.77	0.18	0.07		47.80	16.12	1.16	99.82
MP511E	1	31.21	0.20	0.31	0.16			26.84	15.99	25.18	99.88
MP511E	2	32.47	0.17	0.24	0.11			28.90	16.28	21.04	99.21
MP511E	3	31.11	0.21	0.48	0.17			27.28	16.36	23.21	98.83
MP511E	4	31.37	0.50	0.70	0.23			30.55	16.32	21.82	101.50
MP511E	5	32.66	0.16	0.32	0.04			30.59	16.81	21.09	101.67
MP72	G1	33.36	0.06	1.39				45.49	16.68	3.11	100.10
MP72	G2	32.82	0.13	0.90	0.01			37.38	17.05	11.31	99.59
MP72	G3	33.22	0.07	1.44				39.28	17.03	8.83	99.87
MP72	F1	33.19	0.20	1.35	0.07			44.47	17.37	3.76	100.42
MP72	F2	33.69	0.21	1.30				46.54	17.90	0.73	100.38

Table 60. *(continued)*

sample	pt.	Ni	Co	Fe	Cu	subtotal	As	S	Sb	subtotal	Total
						number of atoms					
J140P	3	0.90	0.05	0.02		0.97	1.85	0.18		2.03	3
J140P	4	0.91	0.05	0.02		0.98	1.83	0.19		2.02	3
J117P	A2	0.90	0.02	0.06		0.98	1.80	0.20		1.99	3
J115P	B2	0.95	0.06	0.01		1.02	1.78	0.18		1.97	3
J100P	2a	0.93	0.03	0.03		0.99	1.78	0.21		1.99	3
J140P	2	0.94	0.03	0.01		0.97	1.78	0.25		2.03	3
J140P	1	0.90	0.05	0.01		0.97	1.76	0.28		2.03	3
J100P	1a	0.94	0.03	0.04		1.01	1.75	0.23		1.99	3
J100P	1	0.93	0.04	0.04		1.00	1.73	0.26		1.99	3
J100P	3	0.92	0.01	0.05		0.99	1.53	0.47		2.00	3
J115P	B3	0.75	0.23	0.04		1.02	1.47	0.51		1.97	3
J100P	2	0.86	0.02	0.09		0.97	1.45	0.56		2.01	3
J115P	B1	0.61	0.36	0.04		1.02	1.27	0.71		1.98	3
J167P	3	0.77	0.22	0.01		1.00	1.22	0.77		2.00	3
J100P	1	0.89	0.03	0.08		1.00	1.16	0.82		1.98	3
J016P	a	0.95	0.02	0.01	0.01	0.99	1.15	0.86	0.01	2.01	3
J018P	b	0.99	0.03	0.03	0.03	1.07	1.13	0.79	0.01	1.93	3
J167P	1	0.95	0.06			1.01	1.13	0.85		1.98	3
J018P	a	0.99	0.03	0.03	0.03	1.08	1.12	0.80	0.01	1.92	3
J117P	A1	0.73	0.06	0.19		0.98	1.11	0.89		2.00	3
MP290C	H5-2	0.97	0.02	0.02		1.01	1.10	0.87		1.97	3
J167P	2	0.95	0.06			1.02	1.10	0.88		1.98	3
MP290C	H5-1	0.97	0.01	0.03		1.01	1.08	0.90		1.97	3
MP230	A1	0.91	0.02	0.09		1.02	1.06	0.90	0.02	1.98	3
J016P	b	0.99	0.02	0.01	0.01	1.03	1.06	0.91	0.01	1.98	3
MP72	G1	0.98		0.04		1.02	1.04	0.89	0.04	1.98	3
MP72	F2	0.96	0.01	0.04		1.01	1.04	0.94		1.98	3
MP230	A2	0.88	0.04	0.09		1.00	1.03	0.92	0.04	2.00	3
J100P	1a	1.00	0.01	0.00		1.01	1.03	0.95		1.99	3
MP287D	aa	0.65	0.31	0.01	0.01	0.98	1.02	0.99		2.01	3
MP72	F1	0.96	0.01	0.04		1.01	1.01	0.92	0.05	1.99	3
MP287D	4	0.65	0.32	0.01	0.02	1.00	1.01	0.98		2.00	3
MP287D	ab	0.65	0.31	0.01	0.01	0.98	1.01	1.01		2.02	3
MP287D	5	0.64	0.34	0.01	0.01	1.00	1.00	1.00		2.00	3
J052P	7	0.58	0.11	0.24	0.01	0.94	0.92	1.13		2.05	3
MP72	G3	0.99		0.04		1.03	0.91	0.93	0.13	1.97	3
J068P	D4	0.52	0.15	0.28	0.03	0.99	0.90	1.11		2.01	3
MP72	G2	0.99		0.03		1.02	0.88	0.94	0.16	1.98	3
J068P	D3	0.48	0.21	0.27	0.08	1.04	0.87	1.10		1.96	3
J068P	D1	0.53	0.11	0.31	0.09	1.03	0.85	1.11		1.96	3
J068P	D2	0.56	0.12	0.28	0.07	1.03	0.83	1.14		1.96	3
MP511E	4	0.97	0.02	0.02		1.01	0.74	0.92	0.32	1.99	3
MP511E	5	1.00		0.01		1.01	0.73	0.94	0.31	1.98	3
MP511E	2	1.02	0.01	0.01		1.03	0.71	0.94	0.32	1.96	3
MP511E	3	0.99	0.01	0.02		1.01	0.68	0.95	0.36	1.98	3
MP511E	1	0.99	0.01	0.01		1.01	0.67	0.93	0.39	1.99	3

Glaucodot (Co,Fe)AsS

Glaucodot forms sheaf-like aggregates of thin prismatic crystals up to 2 cm long in vugs of dolomite or in matrix of vein breccia. The sample contains mainly crystals of *skutterudite* and fine-grained *rammelsbergite*, but no *bismuth*. With regard to the brittle character of the sample, *glaucodot* was identified using physical methods and chemical reactions. *Glaucodot* was found in 1947 in the Bratrství shaft, 2nd level, Zdař Bůh vein offshoot [424].

In the course of the present study, *glaucodot* was analysed in a sample from the Svornost shaft, 5th level, Prokop vein.

Table 61. Calculated unit-cell parameters of glaucodot from Jáchymov for the space group *Cmmm*.

sample	*a*	*b*	*c*
		(Å)	
J042P	6.628(1)	28.831(4)	5.705(1)
J043P	6.652(3)	28.68(1)	5.698(1)

Goethite FeO(OH)

Goethite forms acicular to thin prismatic crystals up to 4 mm long in radiating aggregates in vugs of carbonate gangue. It occurs in a large number of veins.

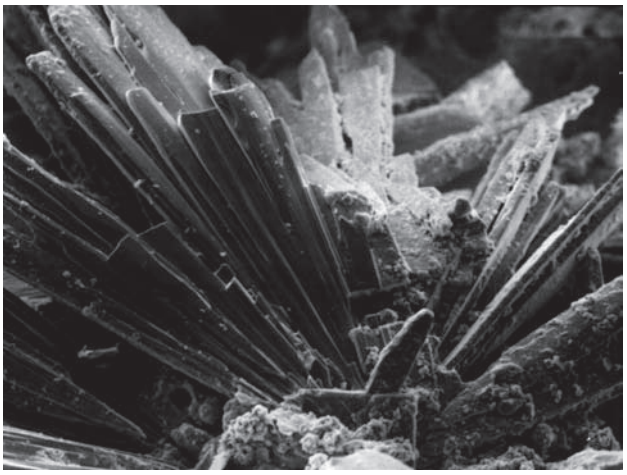

Fig. 76. J-927. Radiating goethite crystals. SE image. Magnification 120×. Photo A. Gabašová.

Gold Au

According to Agricola, it was assumed that *proustite* from the Barbora shaft contains Au [392]. The single reference of any reliability on finds of Au in this district [408], based on an old report, mentions high *gold* contents in *chalcopyrite* from a *quartz* vein in vicinity of the Sen Boží vein [386]. No evidence of *gold* finds in Jáchymov has been documented and panning prospection brought negative results (J. Šourek 2001 – personal communication).

A single round *gold* grain of 3 μm in diameter containing low Ag was identified during the present study, on the boundary of *löllingite* and *calcite* grains and associated with *bismuth*, *aurostibite* and an unidentified Bi-telluride. The last two minerals form mixture with *bismuth*. These ore minerals are enclosed in *arsenopyrite* and *löllingite*, not in *pyrite*, which is the main mineral in the sample. *Pyrite* is slightly corroded and rimmed by *hematite*, impregnating silicate matrix, which consists of chlorite, micas and feldspar. The chlorite-rich rock is probably related to the amphibolite layer shown in mine maps. The sample comes from the Barbora shaft, between 7th and 8th level, probably near 1S vein.

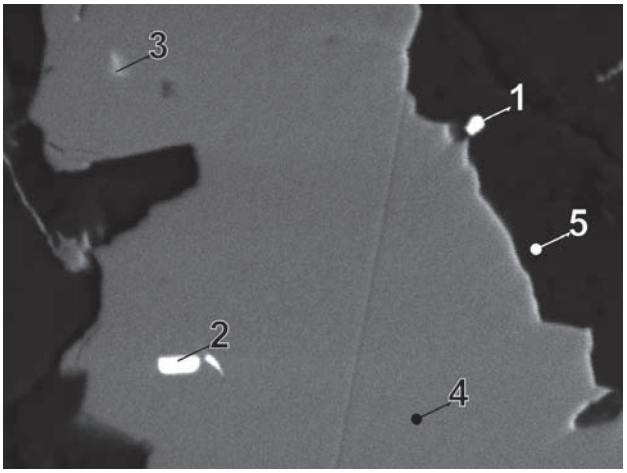

Fig. 77. MP427/2. 1 – gold, 2 – bismuth and Bi-telluride, 3 – finely dispersed bismuth, 4 – löllingite, 5 – calcite. Barbora shaft, 7th/8th level. BSE image. Magnification 1000×.

Table 62. Chemical analysis of gold.

sample	pt.	Ag	Au	Total	Ag	Au	Total
		weight %			number of atoms		
MP427	2	15.80	84.20	100.00	0.26	0.74	1

Greenockite CdS

Greenockite occurs in small grains usually enclosed in *sphalerite*. The sharp boundary between *sphalerite* and *greenockite* indicates that there are no transitions in Cd content between the two phases. *Greenockite* grains are up to 20 μm across, enclosed in oval *sphalerite* to 50 μm in size, rimmed by successive zones of *galena*, *wittichenite* and *bismuthinite.* The sample comes from the Barbora shaft, 5th level, No. 32 vein.

Another *greenockite* occurrence in grains up to 3 μm in *sphalerite* and 30 μm long grain in intergrowth with *tennantite* and *wittichenite*, in milky white *quartz* comes

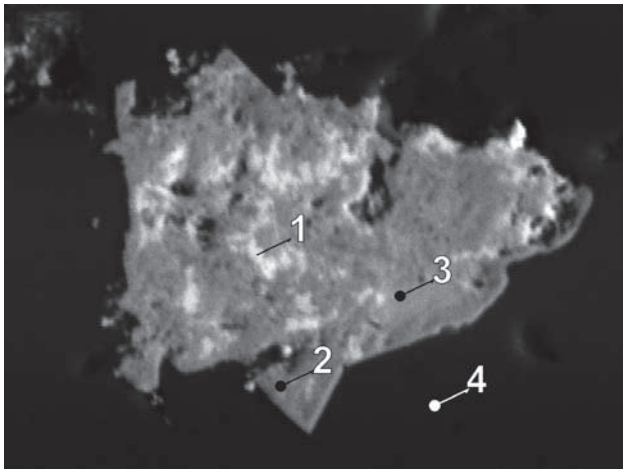

Fig. 78. MP27/D-4. 1 – greenockite, 2 – siegenite, 3 – tennantite, 4 – quartz. Eliáš mine. BSE image. Magnification 1200×.

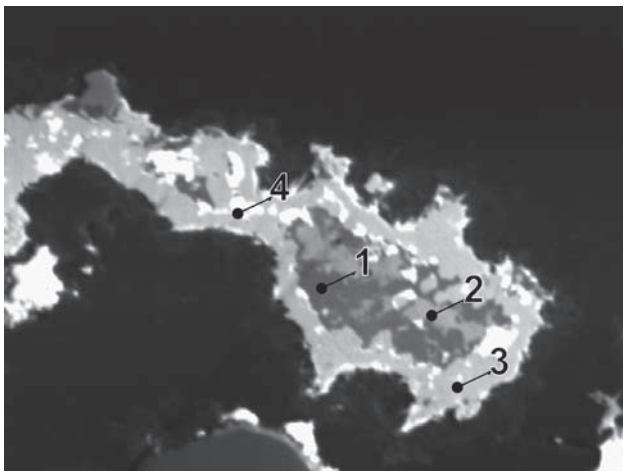

Fig. 79. MP290C/H-4. 1 – sphalerite, 2 – greenockite, 3 – wittichenite, 4 – galena. Barbora shaft, 5th level, vein No. 32. BSE image. Magnification 900×.

from Giftkies adit. It also occurred enclosed in *tennantite* intergrown with *siegenite* crystal in a sample from the Eliáš mine.

Vugs in milky white *quartz* from Giftkies adit carry secondary *greenockite* as bright yellow powdery coatings, formed probably by re-deposition of the primary *greenockite*.

Hematite Fe_2O_3

It forms fine aggregates dispersed in vein *quartz* or carbonates, resulting in brownish red colour of the gangue minerals. The strongest colouration is characteristic for *quartz* of the second generation – red hornfelsic *quartz*. Among carbonates, the strongest colouration is in *dolomite*. *Hematite* may be present in coarser aggregates of acicular or platy crystals, sometimes grouped in hollow spheroidal aggregates. *Hematite* is a common mineral in the Jáchymov ore district.

Hübnerite $MnWO_4$

Hübnerite occurs in 100 μm long grains, replaced along cleavage by *hematite* in greisen. It is accompanied by *ferberite*, *topaz*, *scheelite*, *molybdenite*, and *apatite*. The sample comes from the Rovnost I shaft, probably 8th level.

Minor crystals to 15 μm occur in mineralized mica schist, in association with *pyrite*, *chalcopyrite*, *bornite*, *tungstenian rutile*, *stannite*, *tennantite*, and *monazite-(Ce)*. The sample comes from Giftkies adit.

Hyalophane $(K,Ba)Al(Si,Al)_3O_8$

Hyalophane occurs as anhedral grains up to 0.25 mm enclosed in a *quartz–chalcopyrite* vein. It is enclosed mainly in *quartz* and may be intergrown with *barian orthoclase*, which is younger and it rims *hyalophane*. The boundary between *hyalophane* and *barian orthoclase* is sharp. The content of BaO in *barian orthoclase* is 7–10 wt.%. *Albite*, *chlorite,* minor *sphalerite,* and *galena* accompany Ba-feldspars. The sample comes from the Eliáš mine.

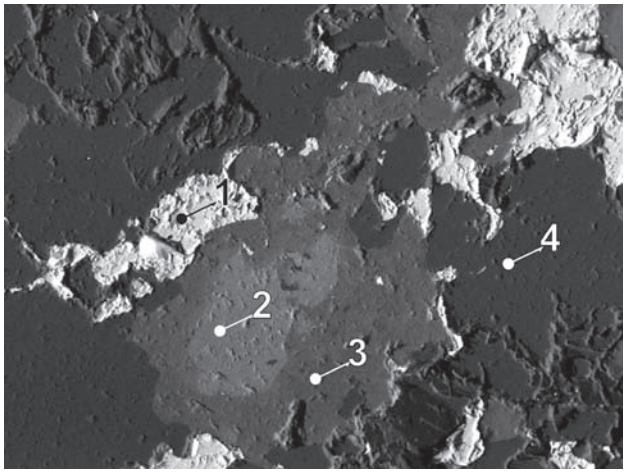

Fig. 80. J112P. 1 – chalcopyrite, 2 – hyalophane, 3 – Ba-orthoclase, 4 – quartz. Eliáš mine. BSE image. Magnification 400×.

Table 63. Chemical analyses of hübnerite.

sample	pt.	CaO	MnO	FeO	CuO	WO_3	ZnO	Total		Mn	Fe	Ca	subtotal	W	O
		weight %								number of atoms					
J012P	hr12	0.12	16.04	7.11	0.06	75.93	0.27	99.53		0.69	0.30	0.01	1.00	1.00	4
J012P	hr13	0.14	16.25	6.99	0.04	76.06	0.15	99.63		0.70	0.30	0.01	1.00	1.00	4

Table 64. Chemical analyses of hyalophane.

sample	pt.	Na_2O	K_2O	FeO	MnO	MgO	CaO	BaO	TiO_2	Al_2O_3	SiO_2	Total
						weight %						
J112P	1	1.81	7.10	0.22		0.16		19.72		22.14	48.42	99.57
J112P	1a	1.35	7.13				0.11	18.57		22.64	49.47	99.27
J112P	2	1.68	6.52	0.11	0.17	0.19		23.06		22.21	47.25	101.19
J112P	2a	1.12	7.53				0.03	18.26		22.88	50.07	99.89
J112P	3	1.52	7.39	0.14		0.05		21.32		21.98	48.66	101.06
J112P	3a	0.26	14.00					7.61		20.50	59.27	101.63
J112P	4	1.68	6.41	0.09		0.09		24.22		22.47	45.78	100.74
J112P	4a	0.23	14.37					7.32		20.21	58.34	100.48
J112P	5	1.70	6.66	0.11		0.14		22.58		22.26	46.73	100.18
J112P	5a	1.01	7.27				0.03	18.74		23.34	49.78	100.16
J112P	6	0.28	13.45					9.53		20.30	56.46	100.02
J112P	6a	0.52	13.39			0.14		9.39	0.26	19.76	56.43	99.90
J112P	7	1.82	6.73	0.15		0.20		22.05	0.31	22.26	47.46	100.98
J112P	7a	1.15	9.82					13.48		21.68	54.00	100.13
J112P	8	1.16	7.41					18.03		23.58	49.61	99.79
J112P	8a	0.41	13.06	0.15		0.13		10.34		20.42	56.29	100.80
J112P	9	0.52	14.34	0.11		0.09		7.38		19.08	58.38	99.91
J112P	10	0.68	12.89					11.20		20.13	56.20	101.10

Table 64. *(continued)*

sample	pt.	Na	K	Ba	subtotal	Al	Si	Ti	subtotal	O
					number of atoms					
J112P	1	0.19	0.48	0.41	1.08	1.39	2.58		3.96	8
J112P	1a	0.14	0.48	0.38	1.00	1.40	2.60		4.00	8
J112P	2	0.17	0.45	0.48	1.11	1.41	2.54		3.94	8
J112P	2a	0.11	0.50	0.37	0.99	1.40	2.61		4.01	8
J112P	3	0.16	0.50	0.44	1.10	1.37	2.58		3.95	8
J112P	3a	0.02	0.86	0.14	1.02	1.16	2.84		4.00	8
J112P	4	0.18	0.45	0.52	1.14	1.44	2.50		3.94	8
J112P	4a	0.02	0.89	0.14	1.05	1.16	2.83		3.99	8
J112P	5	0.18	0.46	0.48	1.12	1.42	2.53		3.95	8
J112P	5a	0.10	0.48	0.38	0.97	1.43	2.59		4.02	8
J112P	6	0.03	0.85	0.19	1.06	1.19	2.80		3.98	8
J112P	6a	0.05	0.85	0.18	1.08	1.16	2.80	0.01	3.97	8
J112P	7	0.19	0.46	0.46	1.11	1.40	2.53	0.01	3.95	8
J112P	7a	0.11	0.63	0.27	1.01	1.29	2.72		4.00	8
J112P	8	0.12	0.49	0.37	0.98	1.45	2.58		4.03	8
J112P	8a	0.04	0.82	0.20	1.06	1.19	2.78		3.97	8
J112P	9	0.05	0.90	0.14	1.09	1.10	2.86		3.96	8
J112P	10	0.07	0.82	0.22	1.10	1.18	2.79		3.96	8

number of atoms based on (O=8)

Imiterite Ag_2HgS_2

Imiterite occurs in anhedral, isolated grains and as lamellar crystals 12×4 μm in size enclosed in *arsenpolybasite*. It is black grey with a weak bireflection and its colour is somewhat different from that of *arsenpolybasite*, which is characterized by dark red internal reflections along cleavages. The *arsenpolybasite* sample occurs in *dolomite* gangue with *nickeline* and *rammelsbergite* in paragenesis with mercurian *silver* and *cinnabar*. *Imiterite* formed 200 μm long intergrowth aggregate with *cinnabar* and *acanthite* at the border of *dolomite* with *calcite.* The sample comes from the Barbora shaft, 5th level, No. 32 vein.

A smooth *imiterite* forms incomplete rim around mercurian *silver* showing a rough surface, in the same paragenesis with *nickeline* and *rammelsbergite* in quartz

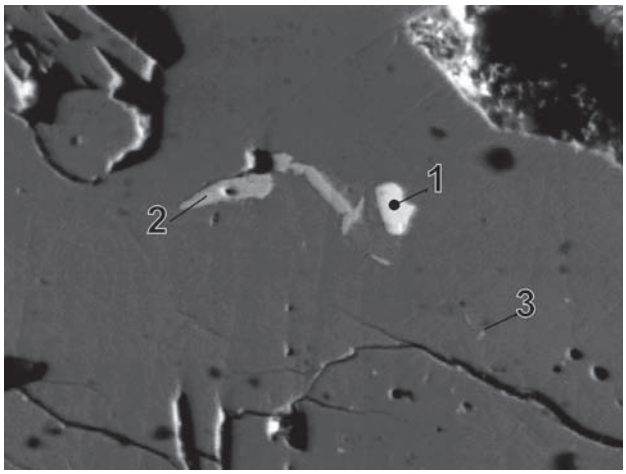

Fig. 81. MP271B/B-1. 1 – galena, 2 – imiterite, 3 – arsenpolybasite. Barbora shaft, 4th/5th level, vein No. 32. BSE image. Magnification 1200×.

Table 65. Chemical analyses of imiterite.

sample	pt.	Ag	Hg	Fe	Cu	S	Sb	As	Total
					weight %				
SR2712	12	43.29	40.91	0.14	0.65	13.42	0.84	0.87	100.12
SR2712	13	43.95	40.06	0.19	0.58	13.53	0.79	0.31	99.41
SR2712	14	43.75	41.11	0.10	0.48	13.41	0.54	0.22	99.61
SR2712	a	43.68	40.87	0.17	0.44	13.39	0.67	0.66	99.88
SR2712	b	43.55	40.61	0.15	0.67	13.43	0.59	0.48	99.48
SR2712	c	43.61	40.55	0.18	0.57	13.27	0.57	0.39	99.14

sample	pt.	Ag	Cu	subtotal	Hg	Fe	subtotal	S	As	Sb	subtotal	Total
						number of atoms						
SR2712	12	1.90	0.05	1.95	0.97	0.01	0.98	1.98	0.06	0.03	2.07	5
SR2712	13	1.94	0.04	1.98	0.95	0.02	0.97	2.01	0.02	0.03	2.06	5
SR2712	14	1.94	0.04	1.98	0.98	0.01	0.99	2.00	0.01	0.02	2.04	5
SR2712	a	1.93	0.03	1.96	0.97	0.01	0.98	1.99	0.04	0.03	2.06	5
SR2712	b	1.92	0.05	1.97	0.96	0.01	0.98	2.00	0.03	0.02	2.05	5
SR2712	c	1.94	0.04	1.98	0.97	0.02	0.99	1.99	0.03	0.02	2.03	5

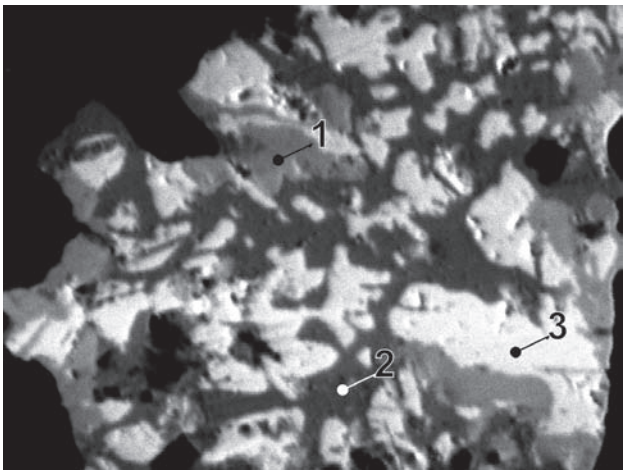

Fig. 82. MP271D/F-1. 1 – imiterite, 2 – argentite, 3 – cinnabar. Barbora shaft, 4th/5th level, vein No. 32. BSE image. Magnification 1000×.

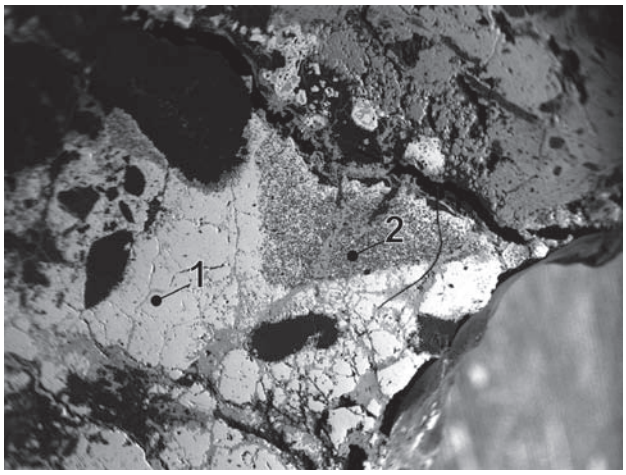

Fig. 84. J071P. 1 – nickel–skutterudite, 2 – nickel–skutterudite with kaolinite. Svornost shaft, 12th level. BSE image. Magnification 16×.

gangue from the Eliáš mine. *Imiterite* is a very rare mineral belonging to a low-temperature paragenesis.

Ixiolite $(Ta,Nb,Sn,Fe,Mn)_4O_8$

Ixiolite is identified in 15 μm long grain intergrown with *ferberite* in quartz gangue. It contains major Ta, Nb, lower Fe, Ti and W, and minor Mn and Sc. The neighbouring *ferberite* does not contain detactable Sc. Associated minerals include *bismuth* replaced by *bismuthinite* in *quartz*, *molybdenite* with lamellae of *bismuth* along cleavages, *cassiterite*, and *apatite.* The sample comes from the Klement shaft.

Kaolinite $Al_2Si_2O_5(OH)_4$

Sandberger [555] described crystallized *kaolinite* from the Morgenstern mine as pseudohexagonal tabular crys-

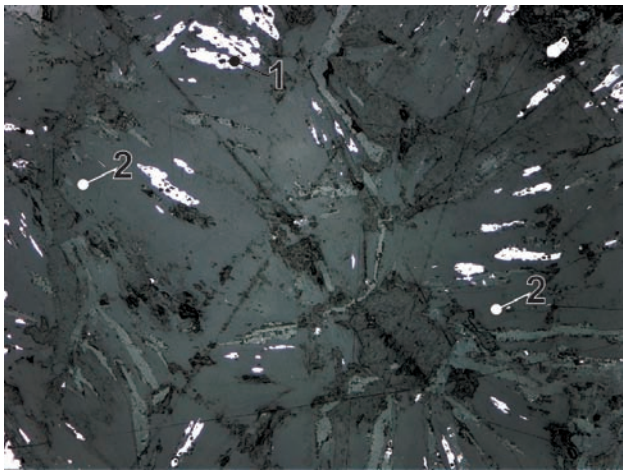

Fig. 85. J185P. Wall-rock fragment replaced by kaolinite. 1 – bornite, 2 – kaolinite of variable orientation. Svornost, Daniel level, Trojická vein. Reflected light, single polarizer. Objective 10×.

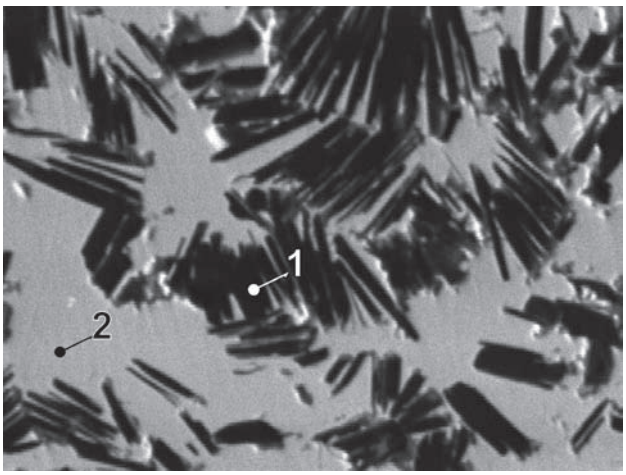

Fig. 83. J071P. 1 – kaolinite, 2 – nickel–skutterudite. Svornost shaft, 12th level. BSE image. Magnification 200×.

tals in fractures and drusy cavities of a hornfles-like vein at the contact of granite with schist.

Kaolinite occurs in coarse platy crystals to 2 mm long. Aggregates of crystals show radiating pattern with yellowish white colour changing locally to green. The colour differences do not correlate with chemical composition.

Kaolinite forms nests several cm across in *quartz* gangue and it accompanies ore minerals, which, however, are not intergrown directly with *kaolinite*. The sample comes from the Svornost shaft, Daniel level, Trojická vein.

Similar laminar *kaolinite* aggregates are enclosed in an internal growth zone of *nickel-skutterudite*. The sample comes from the Svornost shaft, 12th level, Geschieber vein.

Table 66. Chemical analyses of kaolinite.

sample	pt.	SiO_2	Al_2O_3	FeO	MnO	MgO	CaO	Na_2O	K_2O	H_2O*	Total
						weight %					
J185P	c	45.85	37.76	0.57	0.19	0.35	0.15	0.50	0.50	14.13	100.00
J185P	b	45.85	37.54	0.16		0.24	0.05	0.42	0.03	16.21	100.50
J185P	a	45.35	36.70	0.50	0.03	0.37		0.42	0.74	15.05	99.16
J071P	1	46.23	38.50	0.27		0.54	0.11	0.46		13.89	100.00
J071P	2	45.81	38.60	0.19		0.24	0.07	0.58	0.12	14.39	100.00
J071P	3	46.41	39.03	0.12		0.47	0.04	0.45		13.48	100.00

sample	pt.	Al	Fe	Mn	Mg	Ca	Na	K	subtotal	Si	O	OH
						number of atoms						
J185P	c	1.93	0.02	0.01	0.02	0.01	0.04	0.03	2.06	1.99	4.92	4.08
J185P	b	1.88	0.01		0.02		0.03	0.00	1.93	1.92	4.41	4.59
J185P	a	1.86	0.02		0.02		0.04	0.04	1.98	1.99	4.68	4.32
J071P	1	1.96	0.01		0.03	0.01	0.04		2.05	2.00	5.00	4.00
J071P	2	1.96	0.01		0.02		0.05	0.01	2.04	1.97	4.87	4.13
J071P	3	1.99			0.03		0.04		2.06	2.01	5.11	3.89

Number of atoms based on (O, OH = 9).
* H_2O calculated from crystallochemical formula.

Késterite $Cu_2(Zn,Fe)SnS_4$

Késterite forms grains to 40 μm long separated from *stannite*, which occur in the same paragenesis. It is rare compared to *stannite*. *Késterite* occurs in the eastern-most part of the deposit, but it was identified also in material from the Eliáš mine.

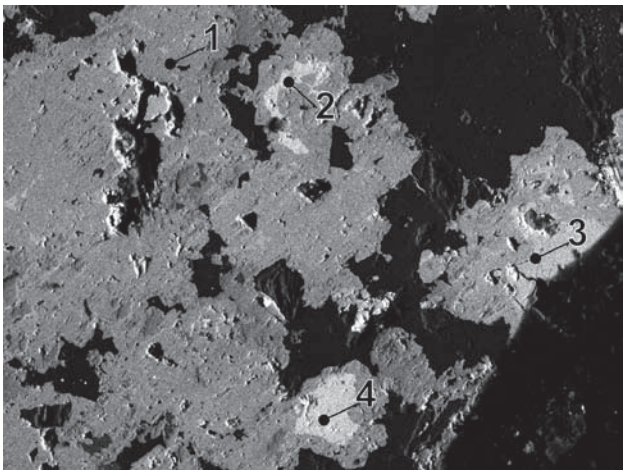

Fig. 86. J126P/D. 1 – chalcopyrite, 2 – késterite, 3 – Sb-tennantite, 4 – stannite. Schönerz adit. BSE image. Magnification 360×.

Table 67. Chemical analyses of késterite.

sample	pt.	Cu	Zn	Fe	Sn	S	As	Total
					weight %			
J066P	1	32.17	8.37	5.61	25.12	28.92		100.20
J066P	1a	32.26	7.89	5.82	24.77	29.04		99.79
J126P	1	28.96	13.56	2.43	26.76	28.38		100.10
J012P	ar2	28.82	10.01	6.52	24.59	29.26	0.15	99.44

sample	pt.	Cu	Zn	Fe	Sn	S	Total
				number of atoms			
J066P	1	2.19	0.55	0.44	0.92	3.90	8
J066P	1a	2.20	0.52	0.45	0.90	3.92	8
J126P	1	2.01	0.91	0.19	0.99	3.90	8
J012P	ar2	1.97	0.56	0.51	0.90	3.96	8

Krutovite $Ni_{(1-x)}As_2$

It was originally described as an "unusual" *gersdorffite* intergrown with *nickel-skutterudite* on *quartz* [489] and later as *krutovite* [335].

The mineral is granular, with a metallic lustre. It has a steel grey colour with a bluish tint. It is lighter than *nickel-skutterudite* and has a weaker lustre. It occurs in equant and/or irregular grains composing aggregates up to several mm long. Hardness is 5.5, microhardness VHN=630 kg/mm^2.

It also occurs in a spheroidal form, with individual spheres up to 2 mm which are hard (Fig. 88). The spheroidal structure becomes more striking after weathering of other Ni-arsenides and *krutovite* becomes soft. It associates with *chalcopyrite, pyrite*, *nickel-skutterudite, Ni-löllingite, rammelsbergite*, *sphalerite,* rarely with *tennatite.* The absence of S, only low Fe, Co and Cu contents near 1 wt.% are typical of *krutovite* composition. The low Cu content in *krutovite* is not unique among arsenides, since some *löllingites* from Jáchymov contain low Cu.

Krutovite was identified among arsenides from the Svornost shaft, 5th and 12th level, Geschieber vein.

Table 68. Calculated unit-cell parameters and density of krutovite from Jáchymov.

sample	unit–cell parameter	density
	a (Å)	D_m (g.cm^{-3})
[336]	5.794	
JA-62	5.7983(1)	
[337]		6.93

Table 69. Chemical analyses of krutovite.

sample	pt.	Ni	Co	Cu	Fe	Zn	Ag	As	S	Sb	Total
						weight %					
J029P	1	23.54	0.62	0.89	0.30	0.03		73.65	0.06		99.09
J029P	2	24.76	0.23	1.00	0.06	0.12		71.75	0.00		97.91
J029P	3	25.27	0.17	1.21	0.08	0.09		74.39	0.06		101.26
J029P	4	24.86	0.21	1.25	0.12			72.60	0.09		99.12
J133P	2–1	25.37	0.14	0.68	0.17		0.26	73.42	0.02		100.05
J133P	2–2	25.35	0.14	0.62	0.14	0.11	0.31	74.48	0.04	0.05	101.23
J133P	2–3	24.73	0.34	1.05	0.15		0.11	74.07	0.01	0.06	100.52
J133P	2–4	25.43	0.09	0.48	0.23	0.10	0.07	74.08		0.01	100.50
J133P	2–5	25.19	0.13	0.60	0.38	0.02	0.38	72.95		0.06	99.69
J133P	2–6	25.11	0.05	0.52	0.52		0.15	73.24		0.15	99.74
[335]	1	24.77	0.16	0.88	0.21			73.30	0.05		99.37
[335]	2	24.68	0.29	0.79	0.12			73.39	0.08		99.35
[335]	3	25.57	0.17	0.85	0.12			73.39	0.09		100.19
[335]	4	27.36	0.26	0.84	0.16			72.05	0.15		100.82
[335]	5	26.65	0.30	0.89	0.18			71.63	0.18		99.83
[335]	6	26.37	0.32	0.83	0.26			71.99	0.14		99.91

sample	pt.	Ni	Co	Cu	Fe	subtotal	x	As	S	As+S	Total
						number of atoms					
J029P	1	0.81	0.02	0.03	0.01	0.88	0.12	2.00		2.00	3
J029P	2	0.88	0.01	0.03		0.93	0.07	2.00		2.00	3
J029P	3	0.87	0.01	0.04		0.92	0.08	2.00		2.00	3
J029P	4	0.87	0.01	0.04		0.92	0.08	1.99	0.01	2.00	3
J133P	2–1	0.91		0.02	0.01	0.94	0.06	2.05		2.05	3
J133P	2–2	0.90		0.02	0.01	0.94	0.06	2.06		2.06	3
J133P	2–3	0.88	0.01	0.03	0.01	0.93	0.07	2.06		2.06	3
J133P	2–4	0.90		0.02	0.01	0.94	0.06	2.06		2.06	3
J133P	2–5	0.90		0.02	0.01	0.95	0.05	2.05		2.05	3
J133P	2–6	0.90		0.02	0.02	0.94	0.06	2.06		2.06	3
[335]	1	0.89	0.01	0.03	0.01	0.93	0.07	2.06		2.06	3
[335]	2	0.89	0.01	0.03		0.93	0.07	2.07	0.01	2.08	3
[335]	3	0.91	0.01	0.03		0.95	0.05	2.05	0.01	2.06	3
[335]	4	0.96	0.01	0.03	0.01	1.00	0.00	1.99	0.01	2.00	3
[335]	5	0.95	0.01	0.03	0.01	0.99	0.01	1.99	0.01	2.00	3
[335]	6	0.94	0.01	0.03	0.01	0.99	0.01	2.01	0.01	2.02	3

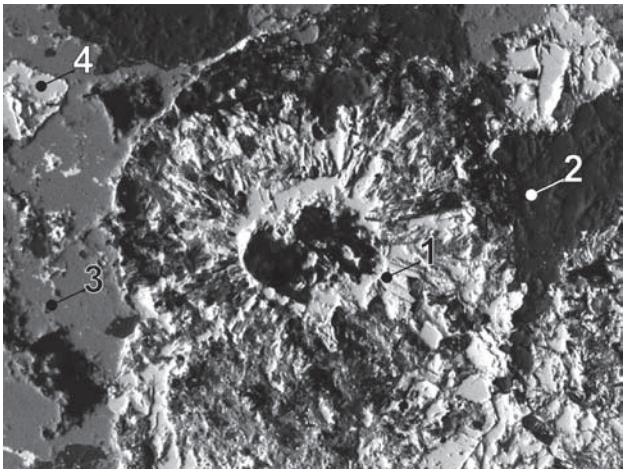

Fig. 87. J133P/2. 1 – krutovite, 2 – annabergite, 3 – pyrite, 4 – proustite. Svornost shaft, dump. BSE image. Magnification 230×.

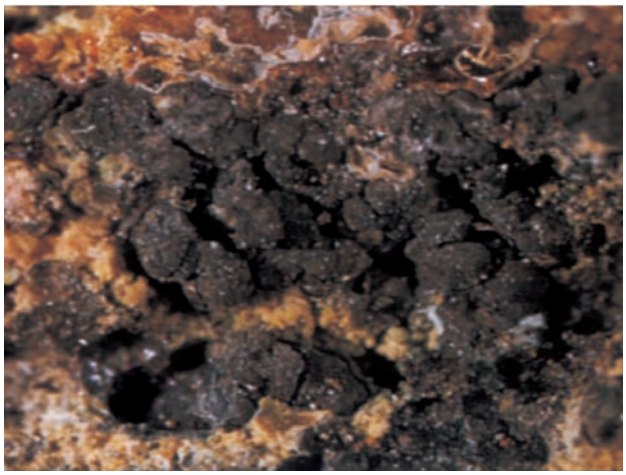
Fig. 88. Greyish black spherical krutovite aggregates (width of figure 2 cm). Photo J. & E. Sejkora.

Lautite CuAsS

Lautite was first described by Geceva a Dubinkina [424], who found an unknown mineral, identified on the basis of spectral analysis and after consultation with A. G. Betekhtin as *lautite*. It was identified in a massive ore with an appearance of cast iron. *Lautite* forms euhhedral crystals, party replaced by *chalcopyrite* and *calcite. Lautite* veinlets intersect older *löllingite* with inclusions of *sphalerite*, *pyrite* and *marcasite.* In other parts it forms fine intergrowth with *löllingite* and *chalcopyrite* in *calcite.* The succession is: *löllingite*, *lautite*, *chalcopyrite*, *calcite*, younger *löllingite. Lautite* occurs in the Schweizer vein, 6th level. Geceva and Dubinkina [424] and Mrňa et al. [408] reported in the blocks 609 and 611 parts composed exclusively of *löllingite*, *proustite*, *acanthite* and *lautite*.

A possibility remains that *enargite* replacing *bismuth*, reported by Zükert [423] in a polished section, was also *lautite*, because of similarity in optical properties of *enargite* and *lautite*.

Lautite forms isolated aggregates to 0.2 mm, compact, non-porous and producing well-polishable surface. It is always rimmed by *löllingite* enclosed in *bornite*. In this rim, minor anhedral *galena* is present among *löllingite* grains. *Lautite* is a rare mineral in the deposit. *Pyrite*, *chalcopyrite* and *tennantite* occur in the paragenesis with *lautite* in this quartz vein. The sample comes from the Svornost shaft, Daniel level, intersection of Trojická vein with Geschieber vein.

Lindströmite $Pb_3Cu_3Bi_7S_{15}$

Lindströmite in an intimate intergrowth with other sulphides forms exsolutions in *chalcopyrite* (Fig. 90). Its white colour makes *lindströmite* distinct from other copper sulphides and it has characteristic low polishing hardness. Size of aggregates does not exceed 20 μm. Representative spot analyses by electron microprobe could be obtained only after careful work, due to irregular concave shape of grains and numerous inclusions. The studied sample comes from the Rovnost I shaft, 6th level, Schweizer East vein.

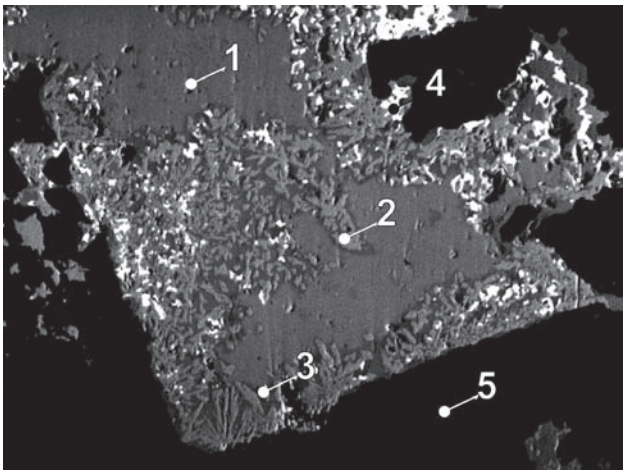

Fig. 89. J074P/A-3. 1 – lautite, 2 – löllingite, 3 – bornite, 4 – galena, 5 – quartz. Svornost shaft, Daniel level, intersection of Trojická vein with Geschieber vein. BSE image. Magnification 320×.

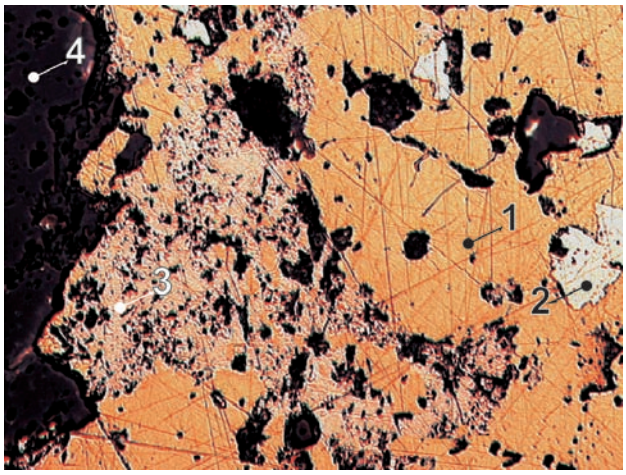

Fig. 90. MP150. Lindströmite forms radiating lamellae penetrating along interfaces of chalcopyrite. Chalcopyrite aggregate contains pyrite with irregular replacement. Minor pyrite and marcasite rim lindströmite. 1 – chalcopyrite, 2 – pyrite, 3 – lindströmite, 4 – dolomite. Rovnost shaft, 6th level, Schweizer vein. Reflected light, single polarizer. Magnification 260×.

Table 70. Chemical analyses of lautite.

sample	pt.	Cu	Fe	As	S	Total	Cu	Fe	As	S	Total
		weight %					number of atoms				
J074P	1	35.14	0.97	46.55	17.07	99.74	0.96	0.03	1.08	0.93	3
J074P	2	35.61	0.62	46.48	17.15	100.05	0.97	0.02	1.08	0.93	3
J074P	3	35.58	0.54	47.14	17.21	100.52	0.97	0.02	1.09	0.93	3
J074P	4	35.66	0.65	46.36	16.90	99.58	0.98	0.02	1.08	0.92	3
J074P	5	36.27	0.54	46.89	17.16	100.86	0.98	0.02	1.08	0.92	3
J074P	6	36.16	0.26	46.53	16.91	100.57	0.99	0.01	1.08	0.92	3

Table 71. Chemical analyses of lindströmite.

sample	pt.	Cu	Ag	Pb	Fe	Zn	Bi	S	Total
					weight %				
MP150	1	6.86	0.24	22.48	0.14	0.05	52.74	17.79	100.30
MP150	2	6.95	0.33	22.41	0.13	0.01	52.47	17.83	100.13
MP150	2a	6.82	0.14	22.31	0.10	0.14	53.01	17.56	100.08

sample	pt.	Pb	Fe	Zn	subtotal	Cu	Ag	subtotal	Bi	S	Total
						number of atoms					
MP150	1	2.95	0.07	0.02	3.04	2.94	0.06	3.00	6.87	15.10	28
MP150	2	2.94	0.06		3.01	2.97	0.08	3.06	6.82	15.11	28
MP150	2a	2.95	0.05	0.06	3.06	2.94	0.04	2.98	6.95	15.01	28

Löllingite $FeAs_2$

Mrňa a Pavlů (1967) [351] studied *löllingite* from Jáchymov. They found that *löllingite* does not form notable accumulations in the veins. Its limited occurrence is confined to arsenide ores with *bismuth*. *Löllingite* forms rims around *bismuth* or the youngest layers in polymineralic crusts. It also occurs in small amounts with ores of the *arsenic-sulphide* stage. Typical occurrence of *löllingite* is in the form of impregnations of small star-shaped crystals (Figs 96 and 97) at the margins of botryoidal *arsenic* [351].

The present study shows that *löllingite* is a quite common mineral in the deposit, but its occurrence in rims around *bismuth* [351] is not so common. Fine-grained aggregates, massive or slightly porous, often with euhedral rhomboidal crystals deposited in *quartz* or carbonate gangue are the most common modes of its presence (Figs 94, 95 and 98). It also occurs as a late mineral in radiating diarsenide aggregates.

Löllingite is often accompanied by *pyrite*, Ni and Co arsenides or copper minerals, including *chalcopyrite*, *bornite*, *tennantite*, and *lautite*. It is also associated with colloform *sphalerite* aggregates. There is probably more than one generation of *löllingite* – a younger generation is represented by the assemblage with Cu-minerals and by *löllingite* deposited on arsenic and spongy silver (see decription of *chalcocite*).

Löllingite in star-shaped triplets (Figs 96 and 97) contains 4–6 wt.% Ni only and its composition is near the *löllingite–safflorite* border, with some spot analyses corresponding to *safflorite*. The triplets are homogeneous with only limited compositional variations between individual crystals or the rim and the centre of the star. They probably belong to a younger *löllingite* generation, since they form rims with carbonate around decomposed and partly or completely leached crystals of a silver mineral, probably former *argentopyrite.*

Some *löllingites* contain approximately 2.5 wt.% Cu. In a general way, its crystallization was favoured by Fe-rich environment as indicated by common association with *marcasite* or pyrite.

Foshag and Short [467] described "*arsenoferrite*" from the Roebling collection (U. S. National Museum), specimen No. R-1063, from Jáchymov. The mineral forms fine-grained aggregates with a conchoidal fracture, it is isotropic in reflected light, density is 6.42 g/cm^3, hardness 5.5 and a chemical analysis gave 24.88 wt.% Fe and 66.84 wt.% As. Etching tests are identical with *skutterudite*. They concluded that the mineral is a cubic diarsenide. M. J. Buerger later re-determined "*arsenoferrite*" as *löllingite.* This situation may suggest that the analysis is in error or that another material was analysed, as it is difficult to accept that Short [467] would consider *löllingite* as an isotropic mineral. The status of "*arsenoferrite*" is not definitely clarified.

Table 72. Calculated unit-cell parameters of löllingite from Jáchymov for the space group *Pnnm*.

sample	*a*	*b*	*c*	*a/c*	*a/c* – tan(60)
		(Å)			
NM9087 (J-849)	5.2918(5)	5.9840(6)	2.8989(3)	1.825	–0.093
J171P (J-923)	5.157(1)	5.921(1)	3.0502(6)	1.691	0.041
MP473 (J-854)	5.2937(2)	5.9949(3)	2.9002(2)	1.825	–0.093
MP80B (J-913)	5.2728(6)	5.9713(8)	2.9221(4)	1.804	–0.072

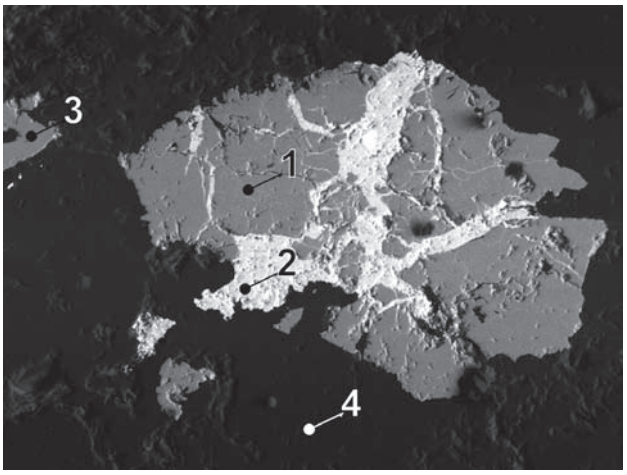

Fig. 91. J070P. 1 – löllingite, 2 – bismuth and bismuthinite, 3 – rammelsbergite, 4 – quartz. Adit No. 21. BSE image. Magnification 270×.

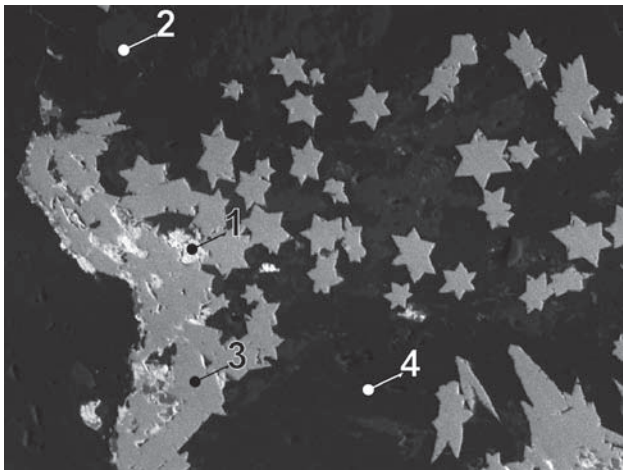

Fig. 92. J171P/I. 1 – argentite, 2 – siderite, 3 – löllingite, 4 – dolomite. Zimní Eliáš dump. BSE image. Magnification 230×.

Table 73. Chemical analyses of löllingite.

sample	pt.	Fe	Co	Ni	Zn	Cu	Ag	As	S	Sb	Total
						weight %					
J028P	a5	21.72	4.86	0.24		0.95		71.51	0.32	0.50	100.10
J028P	a6	20.08	3.75	0.29		1.23		73.73	0.41	0.51	100.00
J028P	b4	21.93	3.85	0.30		0.85		72.15	0.34	0.58	100.00
J028P	b1	20.98	4.97	0.26		1.04		71.70	0.42	0.62	99.99
J055P	2	22.48	0.76	4.78		0.51		68.28	3.79	0.09	100.69
J055P	4	26.13	0.08	0.42		0.11		72.04	1.04	0.14	99.96
J108P	4-6	21.31	5.09		0.03	0.34		72.07	0.40		99.24
J108P	4-5	26.14	0.24	0.04		0.92		72.44	0.39		100.19
J118P	1	23.76	1.15	0.09		2.62	0.21	71.08	0.29		99.21
J118P	2	26.11	0.18			2.54	0.15	72.07	0.11		101.16
J118P	3	25.04	0.30	0.01		3.17	0.16	71.89	0.07		100.64
J118P	4	23.13	1.40			3.11	0.20	71.18	0.31	0.11	99.43
J118P	5	27.27	0.17		0.10	1.17	0.16	70.09	0.29	0.01	99.26
J171P	e	11.67	9.22	5.80		0.47		72.29	0.07		99.54
J171P	ch2	11.33	10.91	4.13		0.63		71.68	0.30		98.97
J171P	ch4	11.70	10.01	4.73		0.46		71.92	0.33		99.15
J171P	ch5	11.24	10.63	4.82		0.53		72.42	0.41		100.05
J174P	M1	25.80				1.44	0.06	72.60	0.04		99.93
J174P	M2	25.16				2.29		72.85	0.15		100.45
J174P	L1	25.08				2.41	0.01	72.96	0.07		100.54
J174P	L2	24.75				2.56	0.07	72.15			99.54
J174P	L3	25.33				1.92	0.31	72.50	0.00		100.07
MP230	A1	27.20		0.62		0.32		71.28	1.24	0.10	100.75
MP230	A2	26.97		0.81		0.16		70.07	1.54		99.56
MP265A	3	19.77	2.21	4.45		0.08		71.32	0.72	1.12	99.67
MP290C	H5	26.78	0.05	0.43	0.01	0.62	0.03	70.07	1.49		99.49
MP36	C2	13.30	10.20	3.97		0.37	0.04	73.03	0.26		101.18
MP427	2	27.11						71.79	1.53		100.43
MP427	2	26.90						71.23	1.47		99.59
MP470	1	26.05	0.59	0.39		0.48		71.51	0.26	0.40	99.68
MP470	2	26.18	0.54	0.31		0.53		71.35	0.33	0.34	99.58
MP473	1	24.03		0.03		3.25		73.21	0.07		100.58
MP473	2	25.17	0.04		0.04	2.28		72.53	0.16	0.15	100.37
MP473	3	23.91	0.24	0.08	0.02	3.24		72.11		0.11	99.72
MP483	C1	26.86	0.06	0.55	0.02	0.64	0.00	70.26	0.97		99.35
MP483	C2	26.97	0.34	1.29	0.03	0.12	0.11	71.07	1.25	0.27	101.46

Table 73. *(continued)*

sample	pt.	Fe	Co	Ni	Cu	subtotal	As	S	Sb	subtotal	Total
						number of atoms					
J028P	a6	0.75	0.13	0.01	0.04	0.93	2.04	0.03	0.01	2.07	3
J171P	e	0.44	0.33	0.21	0.02	0.98	2.01			2.02	3
MP473	1	0.88			0.10	0.99	2.01			2.01	3
J171P	ch2	0.42	0.39	0.15	0.02	0.98	2.00	0.02		2.02	3
J171P	ch4	0.44	0.35	0.17	0.02	0.98	2.00	0.02		2.02	3
J171P	ch5	0.42	0.37	0.17	0.02	0.98	2.00	0.03		2.02	3
J174P	M1	0.95			0.05	1.00	2.00			2.00	3
J174P	L1	0.92			0.08	1.00	2.00			2.00	3
J174P	L2	0.92			0.08	1.00	2.00			2.00	3
J174P	L3	0.94			0.06	1.00	2.00			2.00	3
J028P	b4	0.81	0.14	0.01	0.03	0.98	1.99	0.02	0.01	2.02	3
J108P	4-6	0.79	0.18		0.01	0.98	1.99	0.03		2.02	3
MP473	2	0.92			0.07	1.00	1.99	0.01		2.00	3
MP473	3	0.89	0.01		0.11	1.00	1.99			2.00	3
MP36	C2	0.49	0.35	0.14	0.01	0.99	1.99	0.02		2.01	3
J174P	M2	0.92			0.07	1.00	1.99	0.01		2.00	3
J108P	4-5	0.96	0.01		0.03	1.00	1.98	0.02		2.00	3
J028P	b1	0.77	0.17	0.01	0.03	0.99	1.97	0.03	0.01	2.01	3
MP265A	3	0.73	0.08	0.16		0.97	1.97	0.05	0.02	2.03	3
MP470	1	0.96	0.02	0.01	0.02	1.01	1.97	0.02	0.01	1.99	3
J118P	1	0.88	0.04		0.09	1.01	1.97	0.02		1.99	3
J118P	4	0.86	0.05		0.10	1.01	1.97	0.02		1.99	3
J028P	a5	0.80	0.17	0.01	0.03	1.01	1.96	0.02	0.01	1.99	3
MP470	2	0.97	0.02	0.01	0.02	1.01	1.96	0.02	0.01	1.99	3
J118P	3	0.92	0.01		0.10	1.03	1.96			1.97	3
J055P	4	0.95		0.02		0.97	1.96	0.07		2.02	3
J118P	2	0.95	0.01		0.08	1.04	1.95	0.01		1.96	3
MP427	2	0.98				0.98	1.93	0.10		2.03	3
MP427	2	0.98				0.98	1.93	0.09		2.02	3
J118P	5	1.01	0.01		0.04	1.05	1.93	0.02		1.94	3
MP230	A1	0.98		0.02	0.01	1.01	1.91	0.08		1.99	3
MP483	C1	0.98		0.02	0.02	1.02	1.91	0.06		1.98	3
MP290C	H5	0.97		0.01	0.02	1.01	1.90	0.09		1.99	3
MP230	A2	0.98		0.03	0.01	1.01	1.89	0.10		1.99	3
MP483	C2	0.96		0.04		1.01	1.89	0.08		1.97	3
J055P	2	0.79	0.03	0.16	0.02	0.99	1.78	0.23		2.01	3

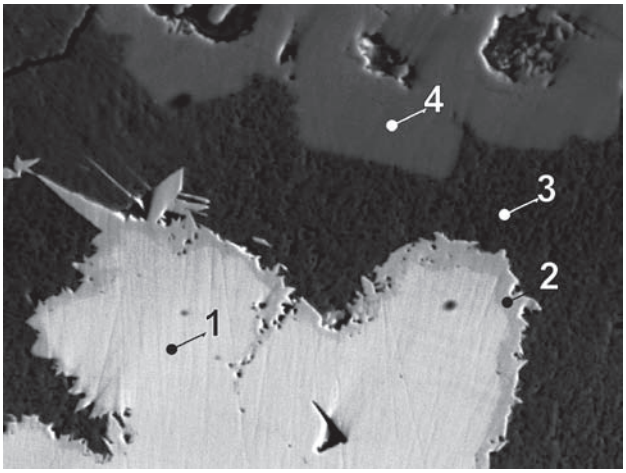

Fig. 93. MP41/D. 1 – rammelsbergite, 2 – löllingite, 3 – pyrite, 4 – sphalerite. Rovnost I shaft, 8th level, Bergkittler vein. BSE image. Magnification 40×.

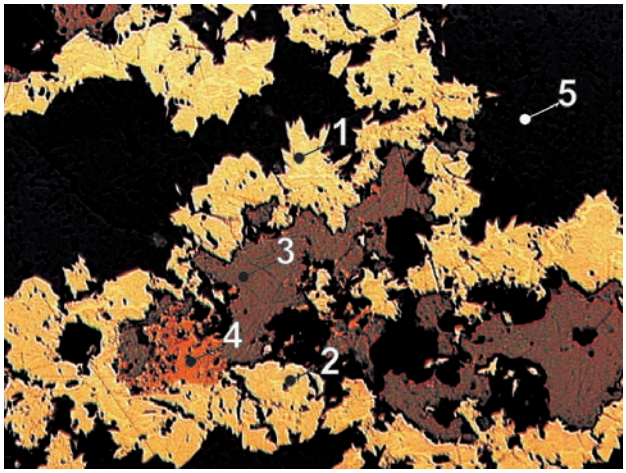

Fig. 94. MP265A. Radial aggregates of löllingite formed at the expense of nickel-skutterudite. Both minerals rim centres of proustite corroded by chalcopyrite. 1 – löllingite, 2 – nickel-skutterudite, 3 – proustite, 4 – chalcopyrite, 5 – dolomite. Svornost shaft, 5th level, Geschieber vein. Reflected light, single polarizer. Magnification 200×.

Fig. 95. MP470. Euhedral and compositionally homogeneous löllingite crystals in gangue minerals. 1 – löllingite, 2 – dolomite. Rovnost shaft, Schweizer vein, 6th level. Reflected light, single polarizer. Magnification 260×.

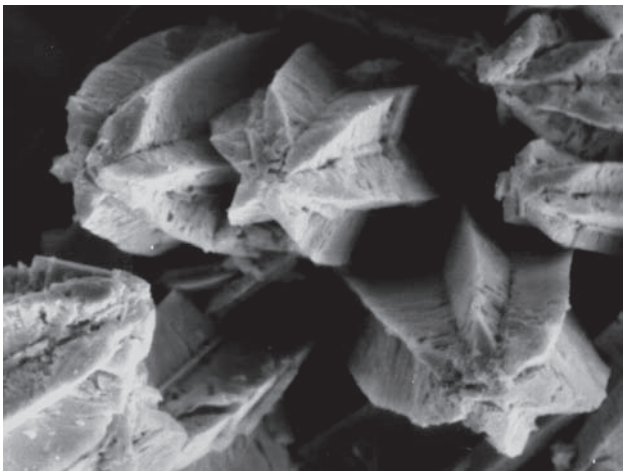

Fig. 96. J171P. Ni-löllingite triplets on (101) plane in the shape of six-pointed star. Zimní Eliáš dump. SE image. Magnification 1550×. Photo A. Gabašová.

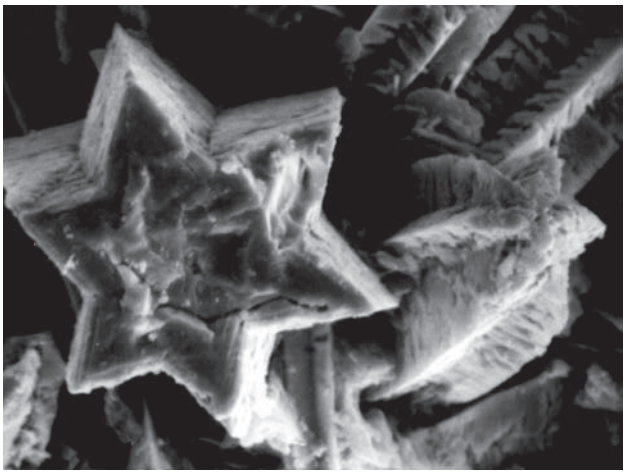

Fig. 97. J171P. Ni-löllingite triplets on (101) plane in the shape of six-pointed star (detail of broken triplets). Zimní Eliáš dump. SE image. Magnification 1890×. Photo A. Gabašová.

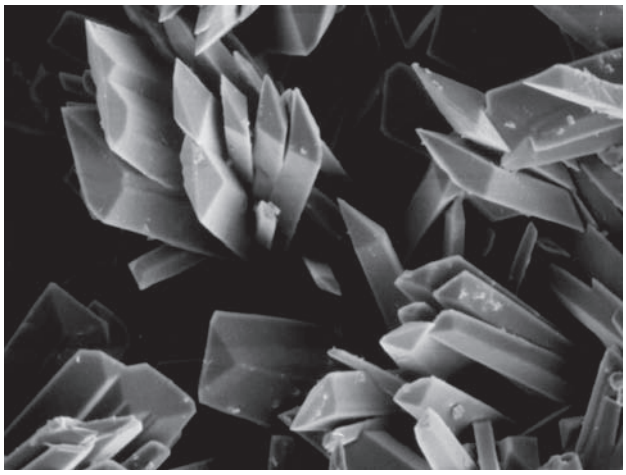

Fig. 98. NM9087. Lath-shaped löllingite crystals on native arsenic. SE image. Magnification 550×. Photo A. Gabašová.

Magnetite Fe_3O_4

Magnetite was found in *actinolite* skarn mineralized with *chalcopyrite.* It also forms a thin rim around *pyrite* relics enclosed in *smythite* aggregates. This indicates rather intensive oxidation prior to *smythite* crystallization.

Table 74. Calculated unit-cell parameters of magnetite from Jáchymov for the space group $Fd\bar{3}m$.

sample	*a* (Å)
J-444	8.5052(5)

Marcasite FeS_2

The mineral occurs in small aggregates or isolated grains in paragenesis with *pyrite*, *chalcopyrite* and *galena*. Some thin prismatic crystals contain 0.6 wt.% As in their cores and up to 10 wt.% As in outer rims. *Mar*

Table 75. Calculated unit-cell parameters of marcasite from Jáchymov for the space group *Pnnm*.

sample	*a*	*b*	*c*
		(Å)	
J-444	4.4384(4)	5.4711(8)	3.4359(4)
J-721	4.4429(7)	5.4322(6)	3.3848(6)
J035P	4.4459(2)	5.4258(2)	3.3867(1)
J034P	4.4462(2)	5.4239(2)	3.3831(2)
VS7651	4.4540(5)	5.4310(6)	3.3750(3)
J-771	4.4610(2)	5.4440(3)	3.3880(2)

Table 76. Chemical analyses of marcasite.

sample	pt.	Fe	Ni	Co	Ag	Cu	S	As	Sb	Total
					weight %					
J034P	1	45.41	0.61	0.27	0.16	0.34	53.63	0.06	0.39	100.87
J034P	2	45.41	0.48	0.41	0.17	0.49	53.32	0.13	0.49	100.90
J034P	3	41.44	4.20	0.30	0.33	0.37	53.04	0.15	0.44	100.27
J034P	4	44.51	0.50	0.35	0.29	0.16	53.15	0.19	0.35	99.50
J034P	5	35.61	8.34	0.85	0.26	0.60	51.63	2.18	0.35	99.82
J034P	6	34.49	10.05	0.59	0.31	0.44	52.78	0.38	0.62	99.66
J034P	7	36.26	8.37	0.52	0.25	0.16	52.91	1.14	0.58	100.19
J034P	8	38.10	6.54	0.76	0.31	0.37	53.18	0.83		100.09
J034P	9	36.17	8.83	0.57	0.41	0.56	52.78	0.92	0.68	100.92
J034P	11	23.86	21.18	1.07	0.85	0.46	46.51	6.07	0.54	100.54
J034P	18	44.57	0.27	0.37	0.19	0.26	53.20	0.64	0.29	99.79
J034P	19	45.25	0.12	0.56	0.08	0.46	53.26	0.73	0.33	100.79
J034P	20	44.97	0.25	0.30	0.19	0.12	53.25	1.39	0.17	100.64
J034P	21	45.04	0.29		0.11	0.23	52.76	2.00	0.39	100.82
J034P	22	45.22	0.28	0.13	0.14	0.16	53.18	0.23	0.45	99.79
J113P	E-1	47.27		0.11			52.31	0.64		100.34
J113P	E-2	42.80	0.06				46.63	10.23		99.73
J113P	E-3	44.01	0.04				46.79	8.99		99.83
J019P	ba	42.17	0.56	0.76		0.48	45.16	10.21	0.48	99.82
J019P	bb	41.76	0.19	0.69		0.37	44.12	10.27	0.43	97.83
J028P	aa	42.76	0.49	0.64		0.39	45.13	10.98	0.34	100.73
J028P	ab	41.32	0.23	0.57		0.31	45.00	11.46	0.21	99.10
J019P	a1	42.71	0.21	0.71		0.31	45.12	10.39	0.56	100.01
J028P	a2	42.30	0.19	0.65		0.29	45.37	10.68	0.52	100.00
J028P	a3	42.47	0.17	0.68		0.39	45.30	10.51	0.48	100.00
J028P	a4	42.69	0.26	0.63		0.35	44.96	10.56	0.54	99.99
J028P	b2	42.62	0.27	0.72		0.28	44.91	10.63	0.57	100.00
J028P	b3	42.55	0.11	0.62		0.41	45.95	9.89	0.47	100.00

sample	pt.	Fe	Co	Ni	Cu	subtotal	S	As	Sb	subtotal	Total
						number of atoms					
J034P	1	0.97	0.01	0.01	0.01	1.00	2.00	0.00	0.00	2.00	3
J034P	2	0.97	0.01	0.01	0.01	1.00	1.99	0.00	0.01	2.00	3
J034P	3	0.90	0.01	0.09	0.01	1.00	2.00	0.00	0.00	2.00	3
J034P	4	0.96	0.01	0.01	0.00	0.99	2.01	0.00	0.00	2.01	3
J034P	5	0.78	0.02	0.17	0.01	0.99	1.97	0.04	0.00	2.01	3
J034P	6	0.75	0.01	0.21	0.01	0.98	2.00	0.01	0.01	2.02	3
J034P	7	0.79	0.01	0.17	0.00	0.98	2.00	0.02	0.01	2.02	3
J034P	8	0.82	0.02	0.13	0.01	0.98	2.00	0.01		2.02	3
J034P	9	0.78	0.01	0.18	0.01	0.99	1.99	0.02	0.01	2.01	3
J034P	11	0.54	0.02	0.46	0.01	1.05	1.85	0.10	0.01	1.96	3
J034P	18	0.96		0.01		0.97	2.00	0.01		2.01	3
J034P	19	0.97		0.00		0.97	1.99	0.01		2.00	3
J034P	20	0.97		0.01		0.97	1.99	0.02		2.02	3
J034P	21	0.97		0.01		0.98	1.98	0.03		2.01	3
J034P	22	0.98		0.01		0.98	2.00	0.00		2.01	3
J113P	E-1	1.02				1.02	1.97	0.01		1.98	3
J113P	E-2	0.97				0.97	1.85	0.17		2.02	3
J113P	E-3	1.00				1.00	1.85	0.15		2.00	3
J019P	ba	0.97	0.02	0.01	0.01	1.01	1.81	0.18		1.99	3
J019P	bb	0.98	0.02	0.00	0.01	1.01	1.81	0.18		1.99	3
J028P	aa	0.98	0.01	0.01	0.01	1.01	1.80	0.19		1.99	3
J028P	ab	0.96	0.01	0.01	0.01	0.98	1.82	0.20		2.02	3
J019P	a1	0.98	0.02	0.01	0.01	1.01	1.81	0.18	0.01	1.99	3
J028P	a2	0.97	0.01		0.01	1.00	1.82	0.18	0.01	2.00	3
J028P	a3	0.98	0.02		0.01	1.00	1.81	0.18	0.01	2.00	3
J028P	a4	0.98	0.01	0.01	0.01	1.01	1.80	0.18	0.01	1.99	3
J028P	b2	0.98	0.02	0.01	0.01	1.01	1.80	0.18	0.01	1.99	3
J028P	b3	0.97	0.01		0.01	1.00	1.83	0.17	0.01	2.00	3

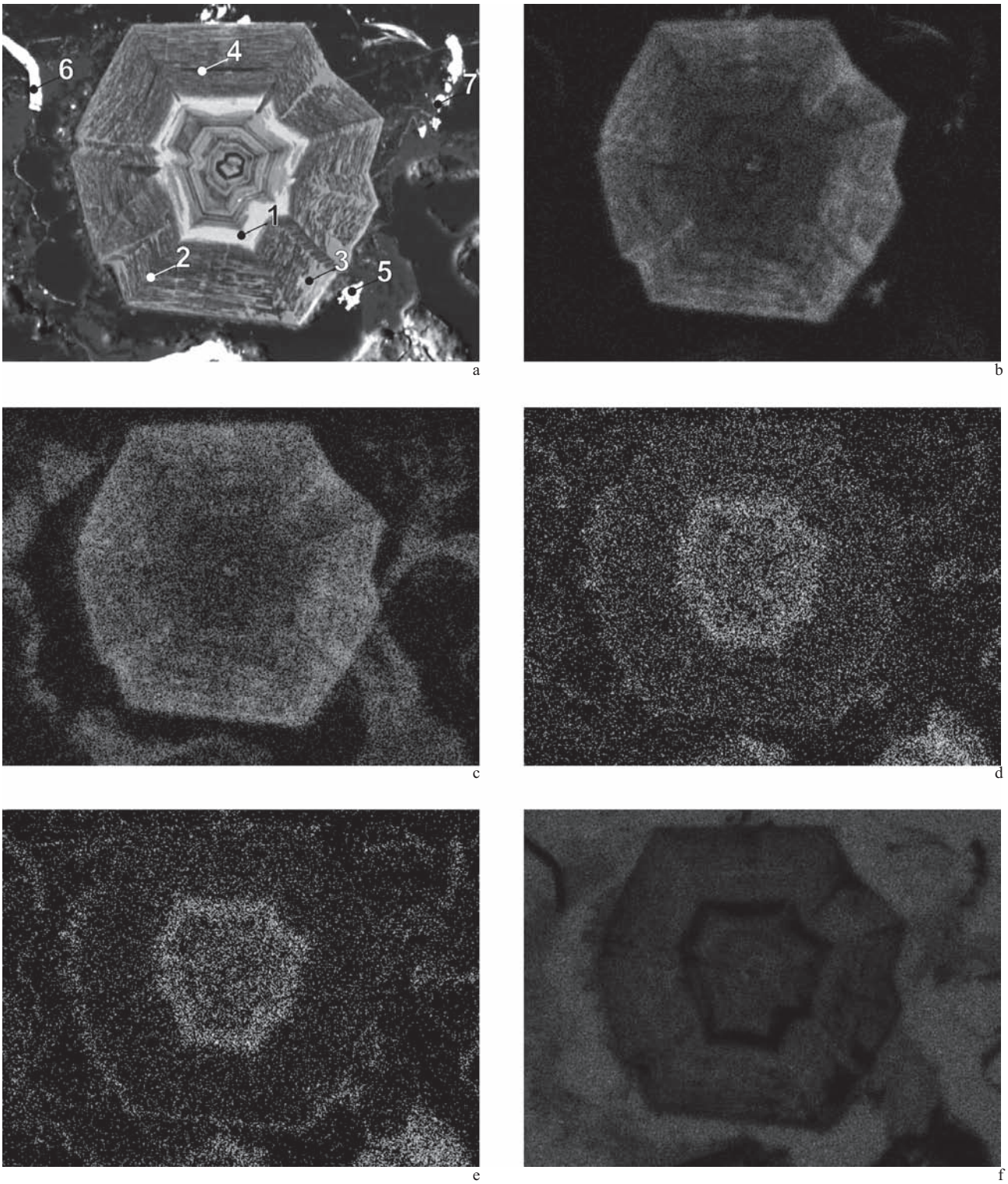

Fig. 99. J083P. 1 – rammelsbergite, 2 – marcasite, 3 – sphalerite, 4 – quartz, 5 – bismuth, 6 – uraninite, 7 – matildite. Rovnost I shaft, Geister level. Magnification 160×.
a) BSE image.
b) Distribution of S.
c) Distribution of Fe.
d) Distribution of Ni.
e) Distribution of As.
f) Distribution of Si.

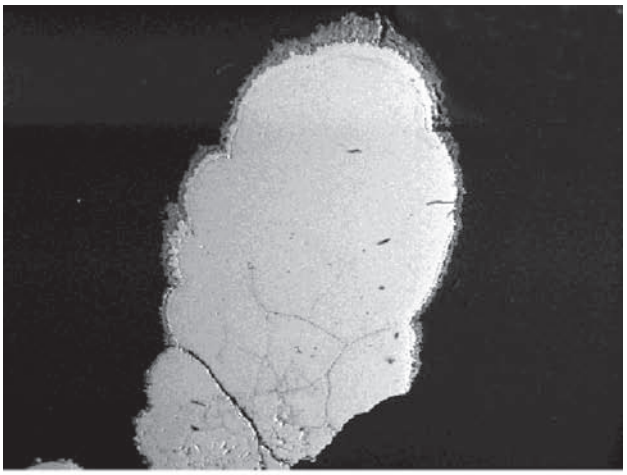

a

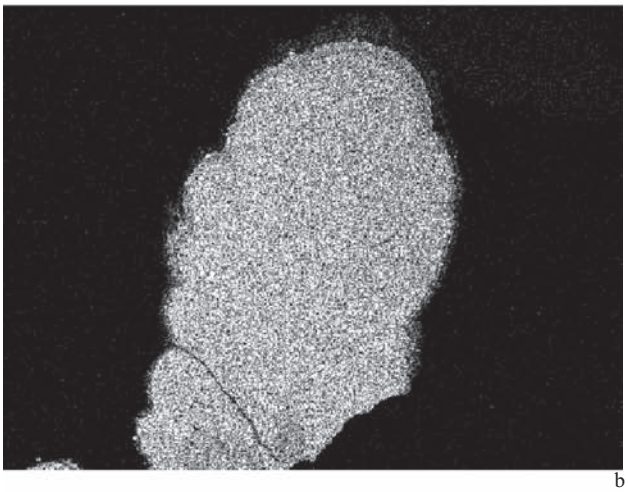

b

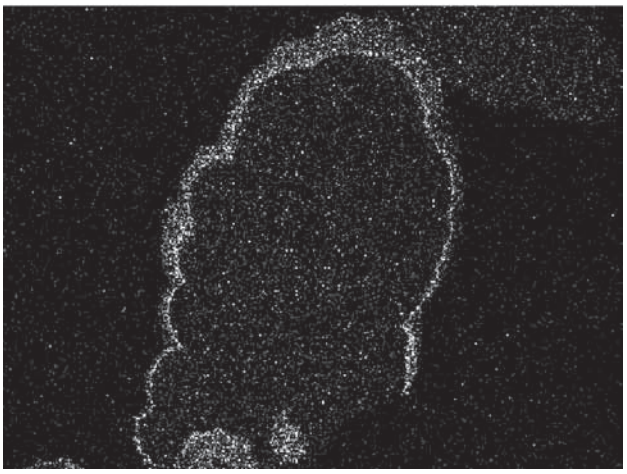

c

Fig. 100. J034P. Marcasite. Svornost shaft, 12th level, Geschieber vein. Magnification 16×.
a) BSE image.
b) Distribution of Fe.
c) Distribution of Ni.

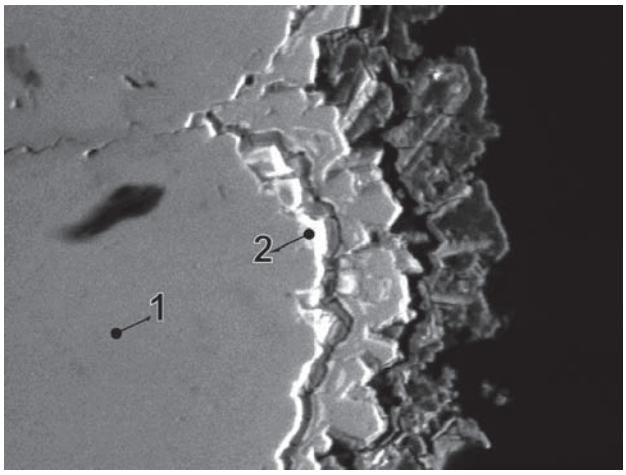

Fig. 101. J034P/1. 1 – marcasite, 2 – gersdorffite. Svornost shaft, 12th level, Geschieber vein. BSE image. Magnification 100×.

casite is common in association with *stephanite* and less frequently with *argentopyrite* in the whole ore district. Marcasite accompanying *stephanite* may form spheroidal aggregates in vugs, with increased Ni and As in outer rim, overgrown by *gersdorffite*. According to Zepharovich [391], density of *marcasite* is 4.865 g/cm^3.

Twinned *marcasite* crystals 2 mm long are deposited on *dolomite* from the Svornost shaft, 5th level, Prokop vein. A complicated cyclic twin was found in a sample from the Geister vein. *Marcasite* is not a common mineral in the district.

Matildite AgBiS$_2$

Matildite forms small equant grains with *pyrite*, intergrown in *quartz*. It composes a greater part of a grey yellow aggregate 4 cm long, collected in the Geister vein. Together with *aikinite* it replaces several *bismuth* grains enclosed in *uraninite*, which is surrounded by *rammelsbergite*. The sample comes from the Eliáš mine.

Table 77. Calculated unit-cell parameters of matildite from Jáchymov for the space group $P\bar{3}m1$.

sample	*a*	*c*
	(Å)	
J047P	4.051(4)	18.859(7)

Table 78. Chemical analyses of matildite.

sample	pt.	Ag	Cu	Fe	Co	Zn	Bi	Sn	Pb	S	As	Sb	Total
							weight %						
J061P	5	28.68	0.17	0.07	0.17		54.18			16.88		0.14	100.29
J061P	6	28.02	0.15	0.09	0.13		54.27			16.81	0.31	0.14	99.92
J061P	1	26.46	0.24	2.12	0.12					17.37	54.54	0.32	101.17
J061P	2	27.00	0.27	1.02	0.15					17.23	54.16	0.46	100.29
J061P	3	27.52	0.34	0.91	0.24					17.17	54.28	0.29	100.75
J061P	8	27.79	0.08	0.78	0.27					17.23	54.41	0.29	100.85
J012P	aa	27.03	0.79	0.12		0.32	53.98	0.69	0.47	16.59		0.48	100.47
J012P	ab	24.06	0.37	0.65		0.59	54.68	0.12	0.60	17.65		0.88	99.60
MP36	1	26.24	0.01				55.01		1.22	17.52			100.00
MP27	B1	26.73	0.18				55.42		0.10	17.38			99.82
MP291B	1	27.79					53.33		0.27	17.66			99.04

sample	pt.	Ag	Cu	Fe	Zn	Co	subtotal	Bi	Pb	Sn	As	subtotal	S	Sb	subtotal	Total
							number of atoms									
J061P	5	1.00	0.01	0.01		0.01	1.03	0.98				0.98	1.99		1.99	4
J061P	6	0.99	0.01	0.01		0.01	1.01	0.98			0.02	1.00	1.99		1.99	4
J061P	1	0.90	0.12	0.02	0.01		1.05	0.96				0.96	1.99		1.99	4
J061P	2	0.93	0.06	0.03	0.01		1.03	0.97	0.01			0.97	2.00		2.00	4
J061P	3	0.95	0.05	0.02	0.01		1.04	0.97	0.01			0.97	1.99		1.99	4
J061P	8	0.96	0.05	0.02	0.02		1.04	0.97				0.97	2.00		2.00	4
J012P	aa	0.95	0.05	0.01	0.02		1.02	0.98	0.01	0.02		1.01	1.96	0.02	1.97	4
J012P	ab	0.83	0.02	0.04	0.03		0.93	0.98	0.01			0.99	2.05	0.03	2.08	4
MP36	1	0.92					0.92	0.99	0.02			1.02	2.06			4
MP27	B1	0.94					0.95	1.00				1.00	2.05		2.05	4
MP291B	1	0.97					0.97	0.96				0.96	2.07		2.07	4

Mawsonite $Cu_6Fe_2SnS_8$

Mawsonite grains up to 30 μm long are usually intergrown with *stannite* and *chalcopyrite* in the northeastern part of the ore district. It is older than *stannite* and encloses small grains of *roquesite*. *Mawsonite,* without *stannite*, occured in rims around *chalcopyrite*. It belongs to the *Sn–W sulpharsenide* stage.

Mawsonite originates from the Giftkies adit.

Table 79. Chemical analyses of mawsonite.

sample	pt.	Cu	Fe	Zn	Sn	S	Total
				weight %			
J066P	1	42.59	13.51	0.83	14.05	7.90	100.02
J066P	7	40.99	12.23	2.06	16.36	7.94	100.66
J066P	3	41.90	12.75	1.81	16.09	7.86	101.51
J090P	1	42.39	13.51		13.85	8.02	99.08

sample	pt.	Cu	Zn	subtotal	Fe	Sn	S	Total
				number of atoms				
J066P	1	5.85	0.11	5.96	2.11	1.03	7.90	17
J066P	7	5.66	0.28	5.93	1.92	1.21	7.94	17
J066P	3	5.74	0.24	5.98	1.99	1.18	7.86	17
J090P	1	5.84		5.84	2.12	1.02	8.02	17

Miargyrite $AgSbS_2$

The mineral occurs as aggregates of small, dark steel grey crystals with dark red internal reflections and a grey red streak. The aggregates set in pink *dolomite* are up to 1 cm across. Some aggregates contain grains of native *antimony*, indicating an equilibrium state of the system Ag–Sb–S [444], in which these minerals crystallized. *Stibnite*, *pyrite*, *arsenic*, *stibarsen*, *pyrargyrite*, *sphalerite*, *dyscra-*

Table 80. Microhardness of miargyrite.

sample	mean	range	load
	[kp/mm^2]	[kp/mm^2]	[g]
[333]-NM9526	132	116–143	20

Table 81. Calculated unit-cell parameters of miargyrite from Jáchymov for the space group *Aa*.

sample	*a*	*b*	*c*	β
		(Å)		(°)
J-797 (J-804)	13.2385(7)	4.4168(3)	12.8747(8)	98.471(4)
[333]-NM9526	13.17(1)	4.409(4)	12.89(1)	98.47(9)

Table 82. Chemical analyses of miargyrite.

sample	pt.	Ag	Fe	Cu	Pb	Bi	Sb	S	As	Total
						weight %				
J105P	D1	36.62					41.11	20.94	0.27	98.93
J105P	D2	36.80	0.06	0.03			42.23	21.10	0.19	100.41
J105P	D3	36.22					41.66	21.22	0.13	99.24
J105P	D4	36.27		0.01			41.98	21.04	0.07	99.36
J105P	G5	36.61		0.03			41.80	21.03	0.09	99.56
J105P	G6	36.98	0.01				41.21	21.05	0.11	99.36
J105P	E	37.18	0.14				40.73	20.96	0.37	99.38
NM-9526	1	36.33			0.26	0.15	41.93	21.51	0.24	100.42
NM-9526	2	36.48			0.10		41.86	22.07	0.25	100.76
NM-9526	3	36.60			0.10	0.09	41.29	21.84	0.33	100.25
NM-9526	4	36.70			0.21		41.39	22.08	0.50	100.88
NM-9526	5	36.69			0.25		41.54	22.89	0.17	101.54
NM-9526	6	36.55			0.13		41.82	22.57	0.26	101.33
NM-9526	7	36.40				0.07	42.17	22.16	0.39	101.19
NM-9526	8	36.55			0.18		42.11	22.55	0.26	101.65
NM-9526	9	36.42			0.10	0.24	42.06	22.04	0.34	101.20
NM-9526	10	37.06			0.13	0.09	41.53	22.13	0.30	101.24
NM-9526	11	36.84			0.10		41.17	22.53	0.92	101.56
NM-9526	12	36.22			0.07		41.96	22.07	0.23	100.55
NM-9526	13	36.45			0.07		42.03	21.86	0.14	100.55

sample	pt.	Ag	Sb	As	S	Total
			number of atoms			
J105P	D1	1.02	1.01	0.01	1.96	4
J105P	D2	1.01	1.03	0.01	1.95	4
J105P	D3	1.00	1.02	0.01	1.97	4
J105P	D4	1.00	1.03	0.01	1.96	4
J105P	G5	1.01	1.02	0.01	1.96	4
J105P	G6	1.02	1.01	0.01	1.96	4
J105P	E	1.03	1.00	0.01	1.95	4
NM-9526	1	0.99	1.02	0.01	1.98	4
NM-9526	2	0.98	1.00	0.01	2.00	4
NM-9526	3	0.99	0.99	0.01	2.00	4
NM-9526	4	0.99	0.99	0.02	2.00	4
NM-9526	5	0.97	0.98	0.01	2.04	4
NM-9526	6	0.97	0.99	0.01	2.03	4
NM-9526	7	0.98	1.00	0.02	2.00	4
NM-9526	8	0.97	0.99	0.01	2.02	4
NM-9526	9	0.98	1.00	0.01	2.00	4
NM-9526	10	1.00	0.99	0.01	2.00	4
NM-9526	11	0.98	0.97	0.04	2.01	4
NM-9526	12	0.98	1.00	0.01	2.01	4
NM-9526	13	0.99	1.01	0.01	1.99	4

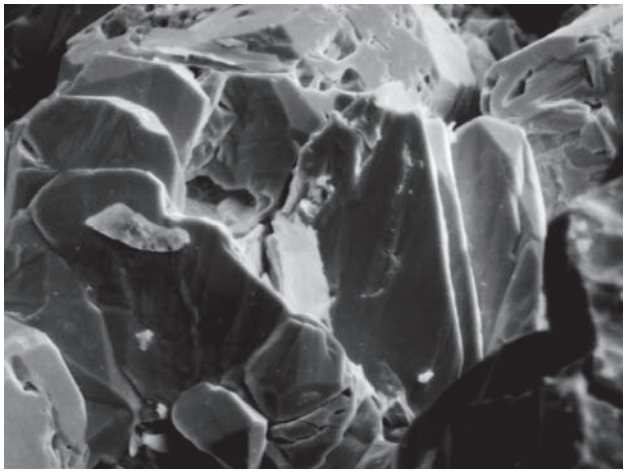

Fig. 102. J-804. Surface of subhedral miargyrite crystals. Svornost shaft, Adit level, Hildebrad vein. SE image. Magnification 670×. Photo A. Gabašová.

site, *robinsonite,* and an undescribed intermetallic Bi–Sb phase occur in paragenesis with the above minerals. This specimen comes from the Svornost shaft, Adit level, Hildebrand vein.

Miargyrite also forms microscopic anhedral to subhedral grains showing a mosaic structure in a massive aggregate with *pyrargyrite*. A half-spheroidal *pyrite* aggregate 4 cm in diameter, deposited on the *miargyrite–pyrargyrite* matrix, is in turn covered by 1 cm long *argentopyrite* crystals. Some vugs in the matrix carry *miargyrite* crystals up to 2 mm long. This exceptional specimen is in the Mineralogical exposition, National Museum, Prague, No. NM9526. It was acquired in 1835 with the collection of count K. Sternberk [333].

Millerite NiS

In 1854, Haidinger mentioned *millerite* to occur in Jáchymov [357]. In 1854 Kenngott [370] descibed *millerite* from Jáchymov.

Fig. 103. Group of acicular millerite crystals in the gangue cavities (width of figure 2.6 cm). Photo J. & E. Sejkora.

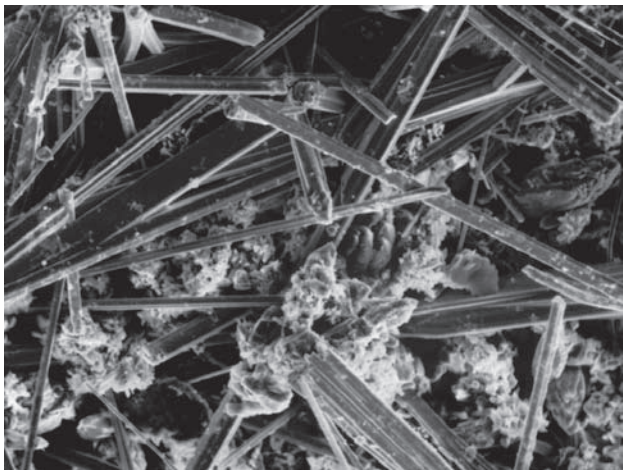

Fig. 104. J-905. Acicular crystals of millerite on dolomite. Svornost shaft, 5th level, Prokop vein. SE image. Magnification 220×. Photo A. Gabašová

Millerite occurs in long acicular crystals of golden colour, up to 2 cm long, often grouped in radiating aggregates (Fig. 103). Mostly it is intergrown in gangue minerals. Rich aggregates of *millerite* crystals are usually in vugs of *quartz.*

Microscopic *millerite* is quite common, intergrown in arsenides in association with *nickel-skutterudite* and *gersdorffite* or with other sulphides – *pyrite*, *sphalerite*, *siege-*

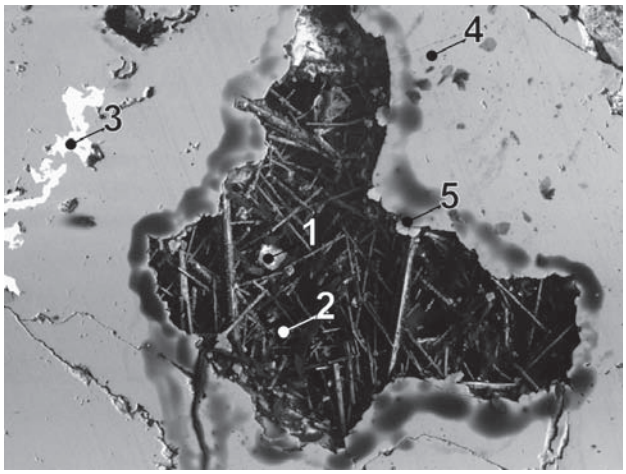

Fig. 105. MP72/E. 1 – siderite, 2 – millerite, 3 – galena, 4 – nickel-skutterudite, 5 – Sb-gersdorffite. Eliáš mine, 2A vein. BSE image. Magnification 72×.

Table 83. Calculated unit-cell parameters of millerite from Jáchymov for the space group *R*3*m*.

sample	*a*	*c*
	(Å)	
J130P	9.6146(2)	3.1486(2)
J-233	9.616(1)	3.1508(3)

Table 84. Chemical analyses of millerite.

sample	pt.	Ni	Co	Zn	Fe	Ag	Cu	S	Sb	As	Total
						weight %					
J042P	a1	62.04	1.84		0.57	0.26	0.18	35.18	0.55	0.31	100.93
99453	aa	58.00	5.98	0.02	0.45			34.67		0.97	100.09
99453	ab	57.68	5.98	0.07	0.64			35.06		0.73	100.16
99454	aa	58.69	5.26	0.34	0.32			35.21		1.01	100.83
99454	ab	59.59	0.59	0.09	0.46			34.49		1.97	97.19
99453	2	57.97	5.44	0.01	0.73			34.92		0.93	100.00
99453	8	58.43	5.33	0.04	0.52			34.83		0.85	100.00
99454	1	58.04	5.37	0.03	0.68			34.85		1.04	100.01
99454	2	60.22	3.46	0.03	0.64			34.91		0.74	100.00
99454	3	61.35	2.50	0.06	0.62			34.87		0.60	100.00
99454	4	60.49	3.42	0.01	0.59			34.94	0.03	0.56	100.01
J057P	11	59.90	0.50	0.12	2.77		0.92	34.65	0.22	0.44	99.52
J057P	12	61.42	0.23		2.05		0.20	34.92	0.55	0.25	99.62
J130P	1	63.85	1.23		0.02			35.02			100.15
J130P	2	64.27	0.76		0.17			35.21			100.41
J130P	3	55.40	9.96		0.02		0.24	35.21	0.13		100.84
J130P	4	54.42	10.04		0.13			35.56	0.36		100.28
J130P	5	63.03	1.34		0.03			35.37			100.12
J130P	6	52.75	10.72		0.06		0.17	36.22			99.92
J141P	D1	47.33				12.65		27.65		2.06	89.69
J141P	D2	44.93				15.24	0.15	27.32		2.14	89.77
MP230	A1	58.31	0.37		3.27		2.80	35.15		0.66	100.56
MP230	A2	48.06	3.38		5.68		6.48	36.38		1.01	100.99

Table 84. *(continued)*

sample	pt.	Ni	Co	Fe	Cu	Ag	subtotal	S	As	subtotal	Total
					number of atoms						
J042P	a1	0.96	0.03	0.01			0.99	0.99		0.99	2
99453	aa	0.90	0.09	0.01			1.00	0.99	0.01	1.00	2
99453	ab	0.89	0.09	0.01			1.00	0.99	0.01	1.00	2
99454	aa	0.90	0.08	0.01			1.00	0.99	0.01	1.01	2
99454	ab	0.95	0.01	0.01			0.97	1.01	0.03	1.03	2
99453	2	0.90	0.08	0.01			1.00	0.99	0.01	1.00	2
99453	8	0.91	0.08	0.01			1.00	0.99	0.01	1.00	2
99454	1	0.90	0.08	0.01			1.00	0.99	0.01	1.00	2
99454	2	0.94	0.05	0.01			1.00	0.99	0.01	1.00	2
99454	3	0.95	0.04	0.01			1.00	0.99	0.01	1.00	2
99454	4	0.94	0.05	0.01			1.00	0.99	0.01	1.00	2
J057P	11	0.94		0.05			0.99	0.99		0.99	2
J057P	12	0.96		0.03			0.99	1.00		1.00	2
J130P	1	0.99	0.02				1.01	0.99		0.99	2
J130P	2	0.99	0.01				1.00	0.99		0.99	2
J130P	3	0.85	0.15				1.00	0.99		0.99	2
J130P	4	0.84	0.15				0.99	1.00		1.00	2
J130P	5	0.97	0.02				1.00	1.00		1.00	2
J130P	6	0.81	0.16				0.98	1.02		1.02	2
J141P	D1	0.89				0.13	1.02	0.95	0.03	0.98	2
J141P	D2	0.86				0.16	1.01	0.95	0.03	0.98	2
MP230	A1	0.90	0.01	0.05	0.04		1.00	0.99	0.01	1.00	2
MP230	A2	0.73	0.05	0.09	0.09		0.97	1.02	0.01	1.03	2

nite, *bismuthinite.* Its chemical composition is simple but central parts of some crystals contain up to 10 wt.% Co.

Millerite is the youngest mineral of the *arsenide* mineralization stage. Beautiful specimens of *millerite* in drusy *quartz* vugs originated from the Svornost shaft, 5th level, Prokop vein.

Molybdenite MoS_2

Rare *molybdenite* occurs in *quartz* veinlets in Klement shaft or in greisen [420] in crystals up to 1 cm. In both cases it is associated with *wolframite* and interlayered with lamellae of *bismuth*. Greisen with *molybdenite* comes from the Rovnost shaft, probably 8th level.

Monazite-(Ce) $(Ce,La,Nd,Th)PO_4$

Monazite-(Ce) was identified by its chemical composition: major P, O, Ce, La. *Monazite-(Ce)* with a low Th content was found as a minor component in some rocks, including a specimen from dump at the Rovnost I shaft, mineralized rock from Giftkies adit and a wall–rock at the Geschieber vein.

It forms anhedral to subhedral grains up to 30 μm, intergrown with *synchysite-(Ce)* in chlorite-rich rock containing minor *gold*. The sample comes from the Barbora shaft, between 7th and 8th level.

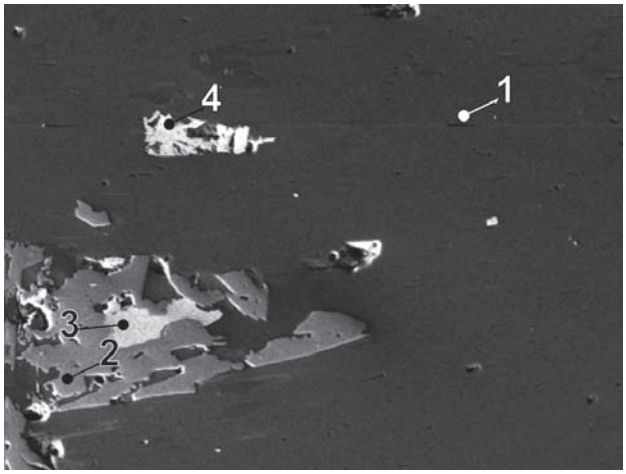

Fig. 106. SR99147/r. Monazite-(Ce) along fractures in rutile in muscovite schist. Synchisite-(Ce) aggregate in quartz-muscovite matrix. 1 – mica, 2 – rutile, 3 – monazite-(Ce), 4 – synchysite-(Ce). Skarn. Plavno mine. BSE image. Magnification 217×.

Muscovite $KAl_2(Si_3Al)O_{10}(OH,F)_2$

Phengitic *muscovite* forms compact soft aggregates of a deep grey green colour in *quartz* gangue along fractures or along contact of vein with wall–rock. It is rarely intergrown with younger *chalcopyrite*. The sample comes from the Svornost shaft, 5th level, Trojická vein.

Table 85. Calculated unit–cell parameters of muscovite from Jáchymov for the space group *C*2.

sample	*a*	*b*	*c*	β
		(Å)		(°)
J-881	5.235(1)	9.046(2)	10.176(2)	101.35(2)

Nickeline NiAs

Nickeline from Jáchymov was studied by Mrňa and Pavlů [351] a [421]. They found out that it is usually accompanied by *rammelsbergite* and *nickel-skutterudite*. It is one of the minerals of botryoidal arsenide lenses, containing dendritic *silver* and alternating zones of *rammels-*

Table 86. Chemical analyses of muscovite.

sample	pt.	K	Na	Ca	Fe	Mn	Mg	Al	Si	Ti	O	H*	Total
							weight %						
J184P	1	6.86	0.57	0.13	5.85	0.00	1.09	13.34	25.23	0.05	50.05	0.417	103.60
J184P	2	6.40	0.71	0.60	9.01	0.12	1.67	10.61	23.38	0.08	46.12	0.325	99.04
J184P	3	6.73	0.46	0.01	6.38	0.00	0.97	12.97	24.58	0.12	49.02	0.429	101.66

sample	pt.	K_2O	Na_2O	CaO	FeO	MnO	MgO	Al_2O_3	SiO_2	TiO_2		H_2O*	Total
							weight %						
SR98554	m1	11.29	0.38	0.06	2.21	0.15	2.28	30.80	49.04	0.28		4.48	100.97
SR98554	m2	10.75	0.49	0.19	2.63	0.17	2.39	30.97	48.30	0.47		4.47	100.83
SR98554	m4	11.18	0.38	0.07	2.68	0.32	2.33	31.25	47.84	0.45		4.46	100.96
SR98554	m5	10.36	0.60	0.06	3.81	0.27	2.37	30.63	47.86	0.42		4.45	100.83
SR98554	m6	10.33	0.54	0.22	2.38	0.26	1.33	34.58	46.37	0.49		4.48	100.98
SR98554	m7	11.11	0.36	0.07	2.17	0.24	2.33	31.01	48.31	0.47		4.48	100.55
SR98554	m10	11.26	0.50	0.13	2.64	0.07	2.30	30.57	48.72	0.30		4.47	100.95
SR98554	m11	11.02	0.45	0.13	2.23	0.19	2.48	30.51	48.64	0.62		4.48	100.75
SR98553	m1	11.09	0.08	0.04	2.41	0.06	2.23	30.68	49.21	0.69		4.49	100.98
SR98553	m2	11.08	0.42	0.11	2.43	0.17	2.48	30.61	48.60	0.61		4.47	100.98
SR98553	m3	10.80	0.33	0.06	2.53	0.23	2.56	30.50	48.94	0.56		4.48	100.99
SR98553	m4	10.68	0.36	0.07	2.81	0.17	3.45	27.13	51.44	0.40		4.49	101.00
SR98553	m6	10.86	0.39	0.11	3.12	0.27	2.67	29.80	48.74	0.54		4.46	100.96
SR98552	m1	10.96	0.44	0.06	2.87	0.25	2.15	31.42	47.62	0.58		4.46	100.81
SR98552	m2	10.93	0.45	0.22	2.78	0.22	1.90	32.06	47.24	0.70		4.46	100.96
SR98552	m3	10.71	0.48	0.12	3.55	0.12	2.02	31.95	46.93	0.62		4.45	100.95
SR98552	m4	10.78	0.58	0.10	3.06	0.22	2.20	31.53	48.04			4.46	100.97
SR98552	m5	11.11	0.46	0.08	2.41	0.31	2.02	31.84	47.63	0.55		4.46	100.87
SR98552	m6	10.21	0.23	0.11	10.70	0.17	0.85	32.94	40.83	0.47		4.27	100.78

sample	pt.	K^+	Na^+	Ca^{2+}	H_3O^+	subtotal X	Al^{3+}	Fe^{2+}	Mg^{2+}	Mn^{2+}	Ti^{IV}	subtotal Y	Si^{IV}	Ti^{IV}	Al^{III}	subtotal Z	$(OH)^-$	O
									number of atoms									
J184P	1	0.68	0.10	0.01	0.21	1.00	1.44	0.41	0.17			2.02	3.50		0.49	4.00	2.00	10
J184P	2	0.69	0.13	0.06	0.12	1.00	1.16	0.68	0.29	0.01		2.14	3.50	0.01	0.49	4.00	2.00	10
J184P	3	0.69	0.08	0.00	0.23	1.00	1.42	0.46	0.16			2.04	3.49	0.01	0.50	4.00	2.00	10
SR98554	m1	0.96	0.05	0.01		1.01	1.66	0.13	0.23	0.01	0.02	2.03	3.25		0.75	4.00	2.00	10
SR98554	m2	0.91	0.07	0.02		0.99	1.64	0.15	0.24	0.01	0.03	2.06	3.21		0.79	4.00	2.00	10
SR98554	m4	0.95	0.05	0.01		1.01	1.64	0.15	0.23	0.02	0.03	2.06	3.19		0.82	4.00	2.00	10
SR98554	m5	0.89	0.08	0.01		0.97	1.61	0.22	0.24	0.02	0.02	2.10	3.20		0.81	4.00	2.00	10
SR98554	m6	0.88	0.07	0.02		0.96	1.77	0.13	0.13	0.02	0.03	2.07	3.07		0.93	4.00	2.00	10
SR98554	m7	0.95	0.05	0.01		1.00	1.65	0.12	0.23	0.02	0.03	2.04	3.22		0.79	4.00	2.00	10
SR98554	m10	0.96	0.07	0.01		1.03	1.64	0.15	0.23	0.01	0.02	2.03	3.24		0.76	4.00	2.00	10
SR98554	m11	0.94	0.06	0.01		1.00	1.63	0.13	0.25	0.01	0.03	2.04	3.24		0.77	4.00	2.00	10
SR98553	m1	0.94	0.01	0.01		0.95	1.65	0.14	0.22	0.01	0.04	2.04	3.26		0.75	4.00	2.00	10
SR98553	m2	0.94	0.06	0.01		1.00	1.62	0.14	0.25	0.01	0.03	2.04	3.23		0.78	4.00	2.00	10
SR98553	m3	0.92	0.05	0.01		0.96	1.63	0.14	0.26	0.02	0.03	2.06	3.24		0.76	4.00	2.00	10
SR98553	m4	0.90	0.05	0.01		0.96	1.52	0.16	0.34	0.01	0.02	2.04	3.40		0.60	4.00	2.00	10
SR98553	m6	0.93	0.05	0.01		0.98	1.59	0.18	0.27	0.02	0.03	2.07	3.25		0.76	4.00	2.00	10
SR98552	m1	0.94	0.06	0.01		1.00	1.65	0.16	0.22	0.02	0.03	2.06	3.18		0.83	4.00	2.00	10
SR98552	m2	0.93	0.06	0.02		1.01	1.66	0.16	0.19	0.02	0.04	2.06	3.15		0.86	4.00	2.00	10
SR98552	m3	0.91	0.06	0.01		0.99	1.65	0.20	0.20	0.01	0.03	2.09	3.14		0.87	4.00	2.00	10
SR98552	m4	0.92	0.08	0.01		1.00	1.67	0.17	0.22	0.02	0.00	2.07	3.20		0.81	4.00	2.00	10
SR98552	m5	0.95	0.06	0.01		1.01	1.67	0.14	0.20	0.02	0.03	2.05	3.17		0.83	4.00	2.00	10
SR98552	m6	0.91	0.03	0.01		0.95	1.55	0.63	0.09	0.01	0.03	2.30	2.85		1.16	4.00	2.00	10

Number of atoms based on (O, OH = 12).
* H_2O or H calculated from crystallochemical formula.

bergite and *nickeline*. *Nickeline* aggregates in *rammelbergite* are usually irregular but sometimes show arborescent shapes or outlines similar to ice crystals. In samples with *nickeline* prevailing above *rammelsbergite*, *nickeline* forms an internal zone bordering *silver*. *Nickeline* aggregates show at least a thin *rammelsbergite* rim (Fig. 112). On the other hand, *nickeline* is rarely seen to rim *bismuth* crystals [383].

Nickeline aggregates have a subhedral granular structure, sometimes with a radiating pattern of granular aggregates [351]. Compared to other arsenides, *nickeline* shows the least tendency to well-formed crystals.

The present study confirmed the observations by Mrňa and Pavlů [351] and [421]. In polished sections, *nickeline* in typical granular aggregates shows distinct bireflection brownish red and light pink, and a strong anisotropy with anomalous brownish and blue green colours (Fig. 111). It is often separated from younger arsenides (*pararammelsbergite*, *gersdorffite*) by a narrow zone of *uraninite* spherolites.

An exceptional *nickeline* sample from the Adam shaft represents a large anhedral single crystal about 5 mm in diameter, rimmed by *rammelsbergite* in the same optical orientation. This suggests epitactic growth of *rammelsbergite* on *nickeline.*

Nickeline is quite common mineral in Jáchymov. Typical are botryoidal aggregates showing alternating narrow

Table 87. Calculated unit-cell parameters of nickelite from Jáchymov for the space group $P6_3/mmc$.

sample	*a*	*c*
	(Å)	
J-774	3.6159(1)	5.0406(2)
J-781	3.6165(1)	5.0412(1)
J-758	3.6151(2)	5.0393(3)
J-782	3.61710(6)	5.0396(1)
J-842	3.6186(2)	5.0360(2)
J-723	3.6210(3)	5.0366(6)
J-759	3.6163(3)	5.0427(7)
MP259D (J-802)	3.6221(3)	5.0382(7)
MP511C (J-922)	3.6190(5)	5.036(1)
J100P (J-925)	3.6085(4)	5.0437(5)

Table 88. Chemical analyses of nickelite.

sample	pt.	Ni	Cu	Fe	Co	Zn	Ag	As	S	Sb	Total
						weight %					
J016P	aa	44.26	0.58	0.31	0.40			52.59	1.29	0.23	99.66
J016P	ab	44.12	0.47	0.56	0.12			52.76	1.59	0.67	100.29
J017P	aa	41.23	0.68	0.34	0.48	0.15		56.68	0.21		99.77
J017P	ab	42.16	0.57	0.26	0.48	0.48		56.46	0.39		100.80
J018P	aa	41.67	0.76	0.26	0.42	0.27		56.29	0.26		99.93
J018P	ab	42.15	0.56	0.22	0.37	0.49		56.47	0.42		100.68
J117P	A	42.58			0.60			55.89	1.58	0.22	57.68
J140P	1	44.05		0.06	0.17		0.18	52.75	0.09		53.07
J146P	1	44.71	0.10	0.07	0.11		0.04	54.81		0.10	55.13
MP27	D	43.03	0.34	0.03	0.30			55.77	0.18		56.32
MP287D	3	43.14	0.76	0.34	0.49			55.09	0.29	0.17	100.28
MP431	2	43.12	0.61	0.27	0.84			54.35	0.47	0.66	100.32
MP483	C	43.58		0.04	0.05	0.09	0.15	55.17	0.02		55.47
MP511C	B1	42.66	0.09	0.02	0.43	0.00		56.07	0.28	0.05	99.62
MP511C	B2	42.63	0.00	0.03	0.42	0.02		55.49	0.40	0.13	99.12
MP511C	B3	42.60	0.04	0.00	0.44	0.02		55.87	0.41	0.06	99.44

sample	pt.	Ni	Cu	Fe	Co	subtotal	As	S	Sb	subtotal	Total
						number of atoms					
J017P	aa	0.94	0.01			0.96	1.01	0.01		1.02	2
MP27	D	0.98				0.98	1.00	0.01		1.00	2
MP511C	B1	0.97	0.00	0.00	0.01	0.99	1.00	0.01		1.01	2
MP511C	B2	0.98	0.00	0.00	0.01	0.99	1.00	0.02		1.01	2
MP511C	B3	0.97	0.00	0.00	0.01	0.98	1.00	0.02		1.02	2
J018P	aa	0.95	0.02			0.96	1.00	0.01		1.02	2
J018P	ab	0.95	0.01			0.96	1.00	0.02		1.01	2
J017P	ab	0.95	0.01			0.96	1.00	0.02		1.01	2
MP483	C	1.00				1.00	0.99			0.99	2
J146P	1	1.02				1.02	0.98			0.98	2
MP287D	3	0.98	0.02	0.01	0.01	1.01	0.98	0.01		0.99	2
J117P	A	0.95				0.95	0.97	0.06		1.04	2
J140P	1	1.03				1.03	0.96			0.97	2
MP431	2	0.97	0.01	0.01	0.02	1.01	0.96	0.02	0.01	0.99	2
J016P	aa	0.99	0.01			1.00	0.92	0.05		0.98	2
J016P	ab	0.98	0.01			0.99	0.92	0.07		0.99	2

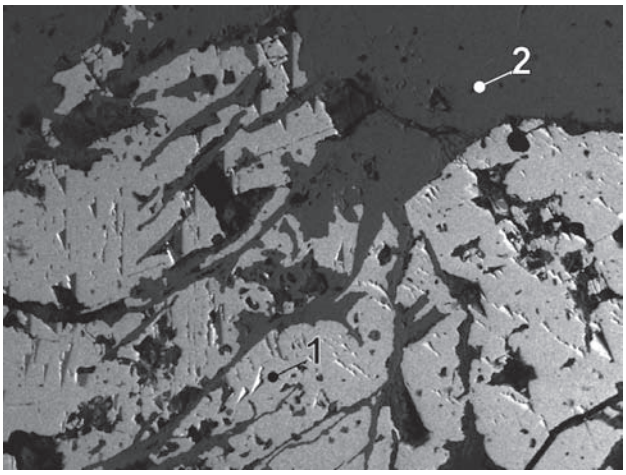

Fig. 107. J117P/A-10. 1 – galena, 2 – nickeline. Eliáš mine, 2A vein. BSE image. Magnification 32×.

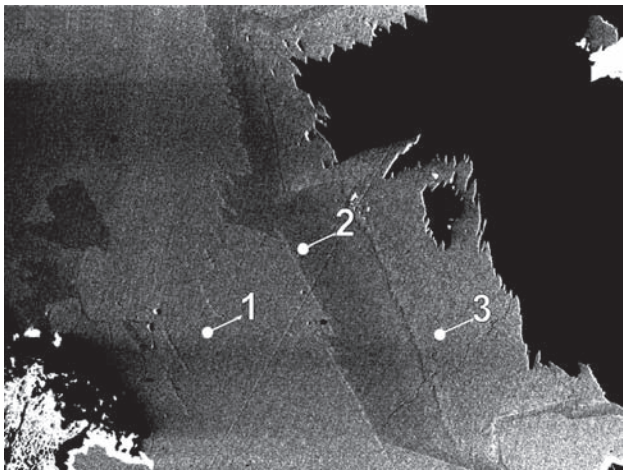

Fig. 110. MP483/C. 1 – nickeline, 2 – rammelsbergite, 3 – löllingite. Eva shaft, N-2 vein. BSE image. Magnification 200×.

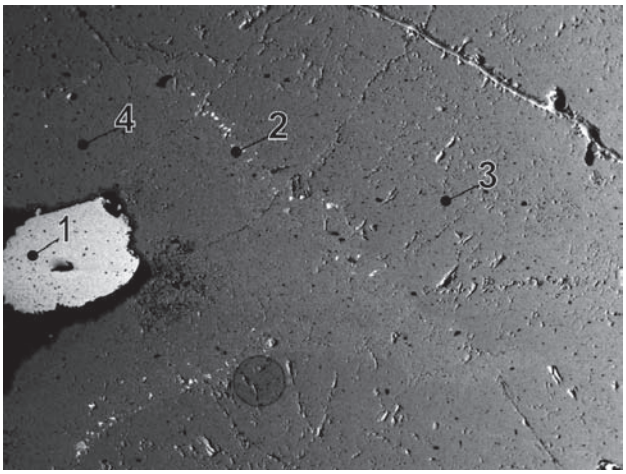

Fig. 108. MP390A/B-1. 1 – argentite, 2 – uraninite, 3 – nickeline, 4 – rammelsbergite. Rovnost I shaft. BSE image. Magnification 1150×.

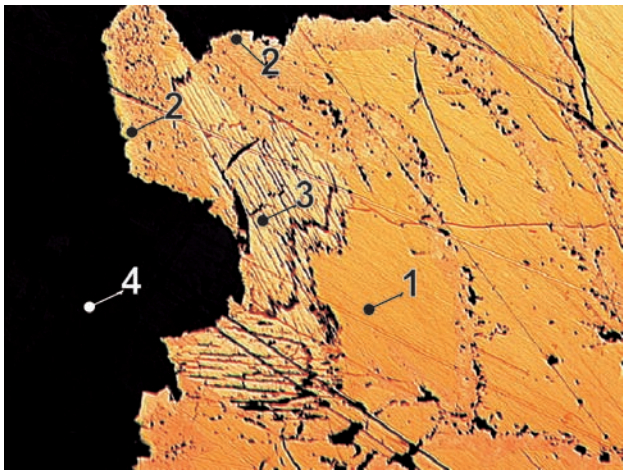

Fig. 111. MP287D. Fractured nickeline aggregate replaced by gersdorffite with varying S content. 1 – nickeline, 2 – gersdorffite, 3 – pararammelsbergite, 4 – dolomite. Barbora shaft, 5th level, vein No. 32. Reflected light, single polarizer. Magnification 65×.

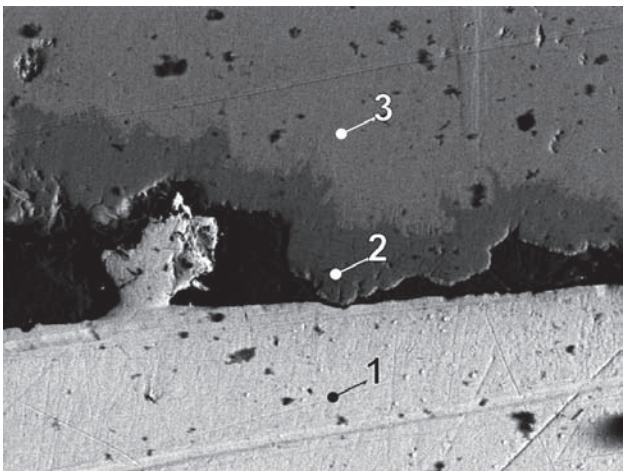

Fig. 109. MP390A/B-2. 1 – argentite, 2 – gersdorffite, 3 – rammelsbergite. Rovnost I shaft. BSE image. Magnification 1000×.

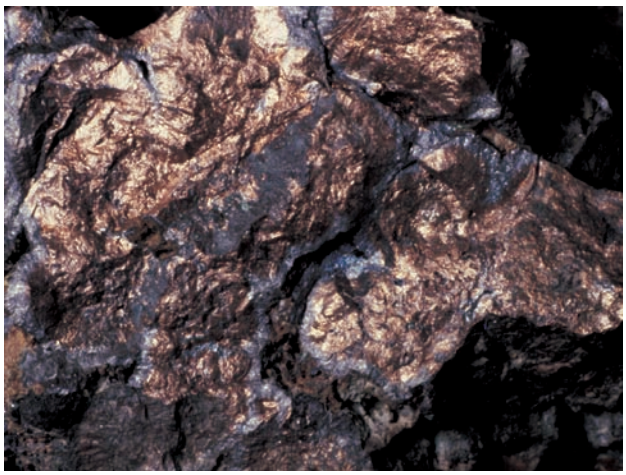

Fig. 112. Nickeline aggregates with light grey rammelsbergite rim (width of figure 3.8 cm). Photo J. & E. Sejkora.

zones of *nickeline* and *rammelsbergite.* Less common are irregular *nickeline* grains up to 5 cm, rimmed by *rammelsbergite* and overgrown by carbonates.

Nickel-skutterudite $NiAs_3$

Nickel-skutterudite from Jáchymov was described by Mrňa and Pavlů [351], [378], who could not reliably distinguish *skutterudite* and *nickel-skutterudite* with the methods they used. For this reason, they presented their observation under *skutterudite.* Pavlů [381] noted *nickel-skutterudite* occurrence in Geschieber vein from borehole HG-1, which penetrated granite approximately 100 m below the 12th level of the Svornost shaft.

Kvaček (1965) [429] presented a detailed study of *nickel-skutterudite* from Bi paragenesis in the Bratrství mine. He described two types – the first type includes large fine-grained aggregates with metallic lustre and tin-white colour on fresh fracture. It is intergrown with grey compact *quartz* and *bismuth* grains. The material is in part porous. A second type of *nickel-skutterudite* is represented by small cubic crystals up to 1 cm, intergrown in gangue or freely grown in drusy cavities (Fig. 121). They turn dark and partly iridescent on exposure to air.

Nickel-skutterudite aggregates are composed of zoned, euhedral to subhedral grains. Zoning can be seen by observation in air with a single polarizer due to variation in relief, reflectance, and somewhat different colour shades or a weak anisotropy of some zones (Fig. 120). Zoning is clearly defined after etching with 1:1 HNO_3.

It encloses skeletal or rounded crystals of *bismuth*, partly replaced by *bismuthinite* and rare minute *nickeline.* Rare *bismuth* veinlets heal fractures in *nickel-skutterudite.* Some anisotropic domains, visible mainly with oil immersion, are not safely identified – they may represent anomalously anisotropic *nickel-skutterudite* or domains of orthorhombic diarsenides.

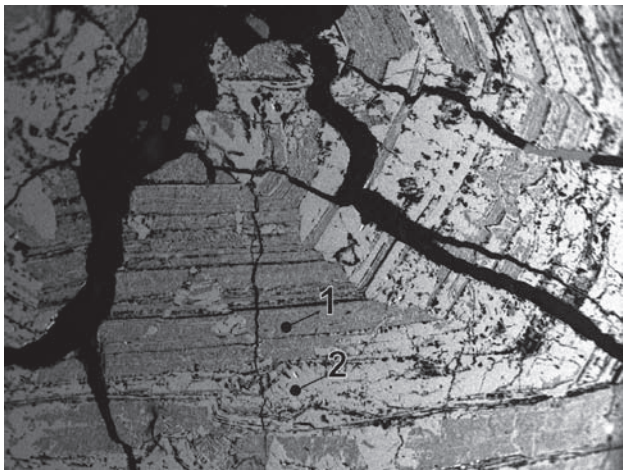

Fig. 114. MP274A. 1 – nickel-skutterudite, 2 – porous rammelsbergite. Eva shaft. BSE image. Magnification 16×.

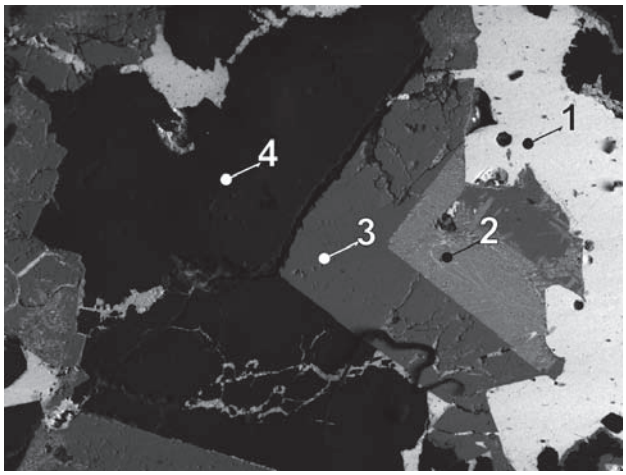

Fig. 115. MP344B. 1 – galena, 2 – orientated intergrowths of rammelsbergite and bismuth, 3 – nickel-skutterudite, 4 – quartz. Bratrství shaft, 5th level, Františka vein. BSE image. Magnification 660×.

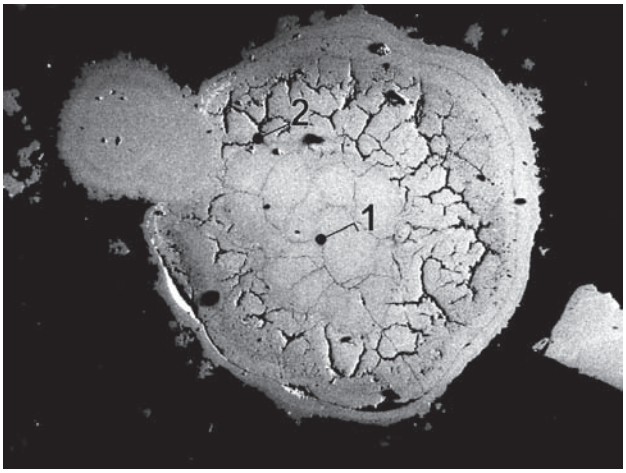

Fig. 113. J113P/A. 1 – nickel-skutterudite, 2 – contraction fissures. Svornost shaft, 8th level, Geschieber vein. BSE image. Magnification 115×.

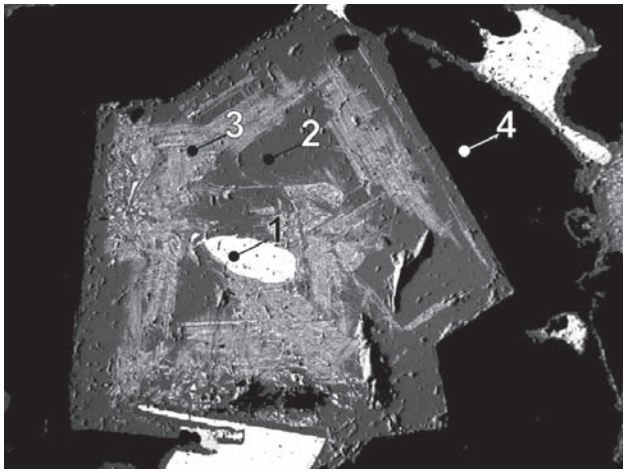

Fig. 116. MP346D/4. 1 – galena, 2 – nickel-skutterudite, 3 – rammelsbergite and bismuth, 4 – quartz. Bratrství shaft, 3rd level, Pomoc Boží vein. BSE image. Magnification 40×.

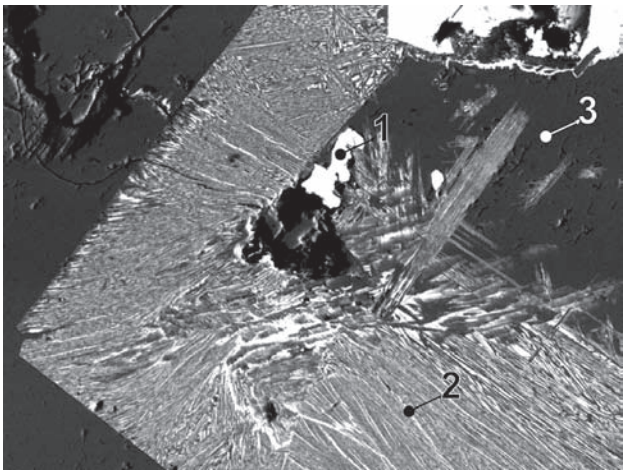

Fig. 117. MP344B/1. 1 – bismuth, 2 – orientated intergrowths of rammelsbergite and bismuth, 3 – nickel-skutterudite. Bratrství shaft, 5th level, Františka vein. BSE image. Magnification 2000×.

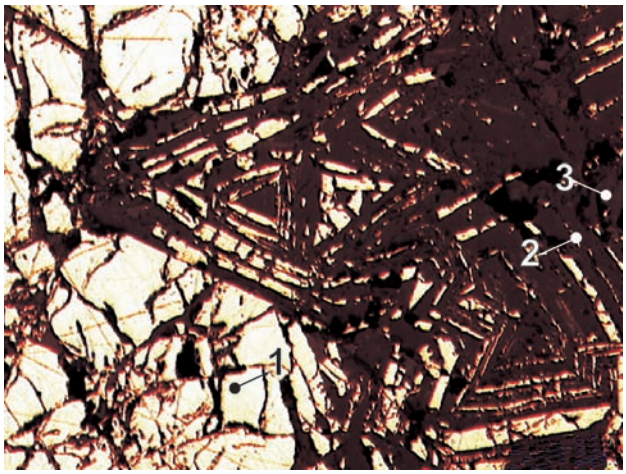

Fig. 120. J057P. Replacement of corroded nickel-skutterudite by calcite. Nickel-skutterudite zones displaced in the process are continuously altered in acicular millerite aggregates. 1 – nickel-skutterudite, 2 – millerite, 3 – calcite. Svornost shaft, 5th level, Prokop vein. Reflected light, single polarizer. Magnification 130×.

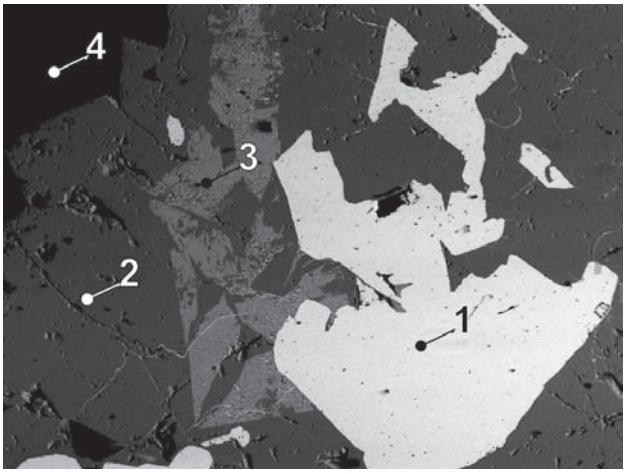

Fig. 118. MP346D/2. 1 – bismuth, 2 – nickel-skutterudite, 3 – rammelsbergite and bismuth, 4 – quartz. Bratrství shaft, 3rd level, Pomoc Boží vein. BSE image. Magnification 72×.

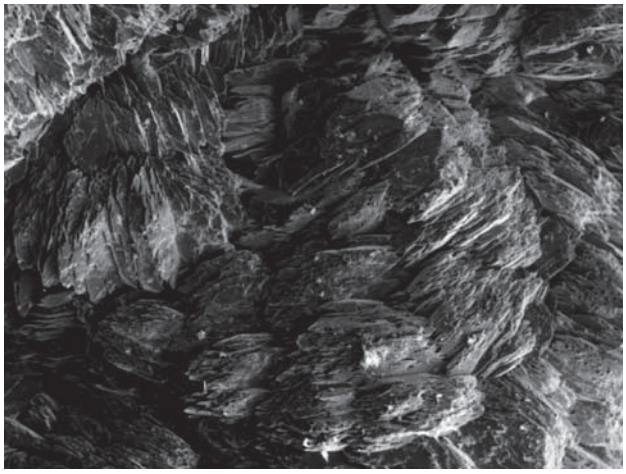

Fig. 121. Well-formed nickel-skutterudite crystals (width of figure 6.7 mm). Photo J. & E. Sejkora.

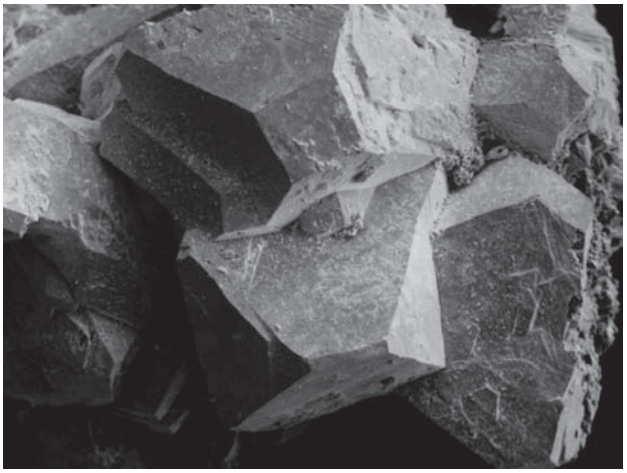

Fig. 119. J-902. Euhedral cubic crystals of nickel-skutterudite on dolomite. Zimní Eliáš dump. SE image. Magnification 50×. Photo A. Gabašová.

Table 89. Calculated unit-cell parameters of nickel-skutterudite from Jáchymov for the space group $Im\bar{3}$.

sample	*a* (Å)
[429]/1	8.273(5)
J-764	8.2776(2)
[429]/2	8.279(2)
J050P	8.2801(5)
J051P	8.2830(4)
J048P	8.2838(6)
J049P	8.3251(2)

The second type of *nickel-skutterudite* – cubic crystals or rather their relics partly replaced by *bismuth* and *quartz*, and some anhedral crystals, associate not only with *bismuth* and *bismuthinite* but also with *tennantite*, *chalcopyrite* and younger sulphides. Density corrected for content of *bismuth* and *quartz* was 6.23 g/cm^3 [429]. According to Zepharovich [391], density of *nickel-skutterudite* is 6.89 g/cm^3.

Table 90. Chemical analyses of nickel-skutterudite.

sample	pt.	Ni	Co	Fe	Cu	Ag	Bi	As	S	Sb	Total
						weight %					
[429]	1	10.54	7.81	1.46	0.03		3.08	70.21	2.73		98.09
[429]	2	11.63	6.32	2.14	0.03		3.18	67.81	3.66		99.91
J016P	9	17.78	2.97	0.44	0.42			75.58	2.43	0.38	100.00
J016P	11	14.24	3.00	4.15	0.58			75.69	2.24	0.10	100.00
J016P	12	18.35	2.08	1.38	0.29			75.33	2.13	0.44	100.00
J016P	13	16.26	2.68	2.36	0.69			74.92	2.72	0.37	100.00
J026P	aa	16.49	2.48	0.59	0.29			75.32	2.64	0.21	98.02
J026P	ab	18.06	3.01	0.34	0.64			77.21	2.67	0.39	102.32
J048P	1	11.00	3.59	4.65	1.03			79.08	0.17		99.52
J048P	2	12.69	3.63	4.17	0.12			78.11	0.32		99.04
J048P	3	10.84	3.55	4.87	1.12			78.77	0.35		99.50
J048P	4	10.48	3.11	5.19	2.02			79.04	0.23		100.07
J048P	9	8.32	6.15	4.47	0.55			79.63	0.19		99.31
J048P	10	17.68	1.45	0.57	0.44			79.16	0.24		99.54
J048P	12	16.26	1.90	1.31	0.76			79.47	0.16		99.86
J048P	13	10.36	5.22	3.72	0.56			79.68	0.12		99.66
J049P	1	15.09	3.15	2.20	0.86			78.76	0.33		100.39
J049P	2	13.56	3.56	2.54	0.74			79.25	0.34	0.11	100.10
J049P	3	18.40	0.38	0.37	0.99			79.31	0.19	0.07	99.71
J049P	5	14.87	4.13	2.52	0.37			78.10	0.37		100.36
J049P	6	19.05	0.76	0.60	0.62			78.95	0.17		100.15
J050P	1	9.56	6.85	3.03	1.76			78.32	0.64		100.16
J050P	2	13.12	3.98	3.45	0.67			78.36	0.63		100.21
J050P	3	14.54	3.17	3.13	0.55			78.21	0.76		100.36
J051P	1	16.61	2.27	0.71	0.24			78.96	0.16	0.28	99.23
J051P	2	15.53	3.71	1.02	0.47			78.85	0.42	0.12	100.12
J051P	3	10.88	6.36	3.25	0.59			78.79	0.53	0.24	100.64
J051P	4	12.95	4.44	3.12	0.68			78.39	0.41	0.22	100.21
J051P	5	12.03	4.60	3.04	0.28			79.51	0.23	0.17	99.86
J051P	6	12.99	4.57	3.46	0.34			78.46	0.52	0.17	100.51
J057P	1	7.58	6.94	5.58				77.67	1.09	0.48	99.34
J057P	2	8.09	7.86	5.10	0.51			77.43	1.11	0.31	100.41
J057P	4	8.81	7.76	3.69	0.49			77.44	1.09	0.31	99.59
J057P	5	7.93	6.29	5.99	0.14			77.79	0.81	0.49	99.44
J060P	1	9.01	5.32	6.06	0.94			76.89	2.06	0.46	100.74
J060P	2	8.95	5.43	6.02	0.67			76.72	2.16	0.41	100.36
J060P	3	8.93	5.18	5.99	0.98			76.93	1.82	0.29	100.12
J113P	a1	18.79	0.22	1.07	0.49			79.40			99.96
J113P	a2	20.38	0.15	0.10				79.03			99.66
J113P	a3	20.15	0.18	0.20	0.12			80.03			100.68
J113P	a4	20.18	0.16	0.19	0.09			79.68			100.30
J113P	a5	18.74	0.86	0.58	0.10			79.26	0.01		99.55
J113P	a6	7.28	5.67	6.78	0.48			79.28	0.32		99.80
J124P	3	13.65	7.06	0.63		0.06		76.94	0.75		99.19
J133P	1	20.76	0.05		0.17	0.09		79.98			101.03
J140P	1	9.15	8.38	2.68	0.09			79.22	1.24	0.08	100.85
J148P	2	9.74	7.68	2.94	0.12			77.05	2.13		99.66
MP265A	1	18.75	0.49	0.85	0.32			78.72	0.30	0.31	99.74
MP265A	1	11.41	2.13	6.19	0.22			79.58	0.10	0.58	100.21
MP265A	2	11.54	3.19	5.81	0.10			78.73	0.18	0.40	99.95
MP265A	2	11.67	2.95	5.73	0.44			78.53	0.18	0.59	100.09
MP265A	3	10.10	2.80	6.90	0.49			78.73	0.10	0.43	99.55
MP296	E	10.18	8.59	2.85	0.21			76.38	2.18		100.39
MP430	1	17.75	2.82	0.30	0.64			76.98	0.47	0.67	99.63
MP430	3	14.77	5.34	0.54	0.33			76.90	1.01	0.58	99.47
MP431	1	19.41	0.45	0.38	0.08			78.71	0.34	0.49	99.86
MP431	5	20.56	0.38	0.27	0.15			77.98	0.20	0.46	100.00
MP80B	B3-6	11.35	3.16	4.62	1.05			80.25	0.01		100.44
MP80B	B3-5	19.55	0.54	0.62				78.21	0.22		99.14
MP80B	B2-4	23.47	0.12	0.09	0.74			75.56	0.00		99.97
MP80B	B2-3	24.08	0.15	0.16	0.61			75.17	0.07		100.24
MP80B	B2-2	20.60	0.06					79.47	0.00		100.12
MP80B	B1-1	20.82	0.05	0.02				79.23	0.04		100.17

Table 90. *(continued)*

sample	pt.	Ni	Co	Fe	Cu	subtotal	As	S	Sb	subtotal	Total
						number of atoms					
J048P	9	0.40	0.30	0.23	0.03	0.95	3.03	0.02		3.05	4
MP80B	B3-6	0.55	0.15	0.23	0.05	0.98	3.02			3.02	4
J048P	13	0.50	0.25	0.19	0.03	0.97	3.02	0.01		3.03	4
J113P	a1	0.91	0.01	0.05	0.02	0.99	3.01			3.01	4
J113P	a3	0.97	0.01	0.01	0.01	0.99	3.01			3.01	4
J113P	a4	0.97	0.01	0.01		0.99	3.01			3.01	4
J113P	a5	0.91	0.04	0.03		0.98	3.01			3.01	4
J048P	12	0.79	0.09	0.07	0.03	0.98	3.01	0.01		3.02	4
J049P	3	0.89	0.02	0.02	0.04	0.97	3.01	0.02		3.03	4
J051P	1	0.81	0.11	0.04	0.01	0.97	3.01	0.01		3.03	4
J051P	5	0.58	0.22	0.15	0.01	0.97	3.01	0.02		3.03	4
MP80B	B2-2	0.99				0.99	3.00			3.00	4
J113P	a2	0.99	0.01			0.99	3.00			3.00	4
J133P	1	0.99				0.99	3.00			3.00	4
MP265A	1	0.55	0.10	0.31	0.01	0.98	3.00	0.01	0.01	3.03	4
J048P	1	0.53	0.17	0.24	0.05	0.99	3.00	0.02		3.01	4
J048P	10	0.86	0.07	0.03	0.02	0.98	3.00	0.02		3.03	4
MP80B	B1-1	1.00				1.00	2.99			2.99	4
J113P	a6	0.35	0.27	0.34	0.02	0.99	2.99	0.03		3.01	4
MP265A	3	0.49	0.14	0.35	0.02	1.00	2.99	0.01	0.01	3.00	4
MP265A	1	0.91	0.02	0.04	0.01	0.99	2.98	0.03	0.01	3.01	4
MP431	1	0.94	0.02	0.02	0.00	0.98	2.98	0.03	0.01	3.02	4
J048P	3	0.52	0.17	0.25	0.05	0.99	2.98	0.03		3.01	4
J048P	4	0.50	0.15	0.26	0.09	1.01	2.98	0.02		3.00	4
J049P	2	0.65	0.17	0.13	0.03	0.98	2.98	0.03		3.01	4
J049P	6	0.92	0.04	0.03	0.03	1.01	2.98	0.02		2.99	4
MP80B	B3-5	0.95	0.03	0.03		1.01	2.97	0.02		2.99	4
MP265A	2	0.56	0.15	0.29		1.01	2.97	0.02	0.01	2.99	4
J051P	2	0.75	0.18	0.05	0.02	0.99	2.97	0.04		3.00	4
MP265A	2	0.56	0.14	0.29	0.02	1.01	2.96	0.02	0.01	2.99	4
J048P	2	0.62	0.18	0.21	0.01	1.01	2.96	0.03		2.99	4
J049P	1	0.72	0.15	0.11	0.04	1.02	2.95	0.03		2.98	4
MP431	5	0.99	0.02	0.01	0.01	1.03	2.94	0.02	0.01	2.97	4
J051P	3	0.52	0.30	0.16	0.03	1.01	2.94	0.05		2.99	4
J051P	4	0.62	0.21	0.16	0.03	1.02	2.94	0.04		2.98	4
J140P	1	0.43	0.39	0.13		0.96	2.93	0.11		3.04	4
J050P	1	0.46	0.33	0.15	0.08	1.01	2.93	0.06		2.99	4
J050P	2	0.63	0.19	0.17	0.03	1.02	2.93	0.06		2.98	4
J051P	6	0.62	0.22	0.17	0.02	1.02	2.93	0.05		2.97	4
J057P	5	0.38	0.30	0.30	0.01	0.99	2.93	0.07		3.00	4
J049P	5	0.71	0.20	0.13	0.02	1.05	2.92	0.03		2.95	4
J057P	1	0.36	0.33	0.28		0.98	2.92	0.10		3.01	4
MP430	1	0.86	0.14	0.02	0.03	1.04	2.91	0.04	0.02	2.97	4
J050P	3	0.69	0.15	0.16	0.02	1.02	2.91	0.07		2.98	4
J124P	3	0.66	0.34		0.03	1.03	2.90	0.07		2.97	4
J057P	4	0.42	0.37	0.19	0.02	1.00	2.90	0.10		3.00	4
MP430	3	0.71	0.26	0.03	0.02	1.01	2.89	0.09	0.01	2.99	4
J057P	2	0.38	0.37	0.25	0.02	1.03	2.87	0.10		2.96	4
J148P	2	0.46	0.36	0.15	0.01	0.97	2.85	0.18		3.03	4
J060P	3	0.42	0.24	0.30	0.04	1.00	2.84	0.16		2.99	4
MP80B	B2-4	1.12	0.01		0.03	1.16	2.83			2.83	4
J026P	aa	0.79	0.12	0.03	0.01	0.95	2.82	0.23	0.01	3.05	4
J060P	1	0.42	0.25	0.30	0.04	1.00	2.81	0.18		2.99	4
J060P	2	0.42	0.25	0.30	0.03	1.00	2.81	0.19		3.00	4
MP80B	B2-3	1.15	0.01	0.01	0.03	1.19	2.80	0.01		2.81	4
MP296	E	0.47	0.40		0.14	1.01	2.79	0.19		2.98	4
J016P	9	0.83	0.14	0.02	0.02	1.01	2.77	0.21	0.01	2.99	4
J016P	11	0.67	0.14	0.20	0.03	1.04	2.77	0.19	0.00	2.97	4
J016P	12	0.86	0.10	0.07	0.01	1.04	2.77	0.18	0.01	2.96	4
[429]	1	0.53	0.39	0.08		0.99	2.76	0.25		3.01	4
J026P	ab	0.83	0.14	0.02	0.03	1.01	2.76	0.22	0.01	3.00	4
J016P	13	0.76	0.12	0.12	0.03	1.03	2.73	0.23	0.01	2.97	4
[429]	2	0.58	0.31	0.11		1.01	2.66	0.33		2.99	4

Interesting is common presence of minor Mo, and often Cr, indicated in *nickel-skutterudite* samples by spectral analyses. Kvaček [429] did not find the source of these elements but considered them as anisomineral, possibly due to *koechlinite* presence.

The present study shows no difference in *nickel-skutterudite* in two parageneses, i.e., with *silver* and with *bismuth.* This suggests that processes which precipitated these two metals were rather similar, or may be considered as a single process.

The highest Co content in zoned *nickel-skutterudite* is in its outer zone, Fe is distributed evenly.

Some zones in *nickel-skutterudite* showing variable porosity are replaced by other minerals, including *quartz*, *carbonate*, *rammelsbergite*, *siegenite*, *nickeline*, *pararammelsbergite*. Some *nickel-skutterudites* contain zones consisting of myrmekitic unmixed particles of *bismuth* in *rammelsbergite.* The structures probably formed via decomposition of an unstable phase. Orientation of vermiform *bismuth* particles may indicate some structural direction of the original mineral. Similar particles also occur in cores of some *nickel-skutterudite* crystals or sharply bound domains elsewhere in the crystals.

A sample with spheroidal *nickel-skutterudite* aggregates up to 0.5 mm has abundant contraction fractures in an intermediate zone. This zone contains domains with very fine, dispersed *bismuth* particles. It is possible that this *nickel-skutterudite* formed by recrystallization of colloids. In chemical composition, all zones represent practically pure *nickel-skutterudite* nearly free of Co and Fe, except the outer zone, containing equal Ni and Fe and somewhat lower Co. This sample comes from the Svornost shaft, Geschieber vein.

Orthoclase $KAlSi_3O_8$

Barian orthoclase forms anhedral grains up to 0.3 mm long, intergrown with *hyalophane* or rimming *hyalophane.* It is associated with *quartz*, *chalcopyrite*, *chlorite*, *sphalerite*, *galena,* and *albite*. The sample of *quartz* vein with *chalcopyrite*, containing these assemblages, comes from the Eliáš mine.

Barian orthoclase showing a strong compositional zoning occurs with *grossular*, *titanite*, *allanite*, *epidote*, *sphalerite*, and *smithsonite* in skarn at the elevation point Stráž [433].

Pararammelsbergite $NiAs_2$

Pararammelsbergite occurs in indistinct, dim radiating aggregates of grey colour. Cleavage is orientated parallel to elongation of acicular crystals. The outer shape of these aggregates, up to 3 cm long, is botryoidal. Quite rare are axe-shaped crystals protruding to free spaces (Figs 122, 123). In one particular sample, there were three zones of granular *pararammelsbergite* below the upper zone of radiating *pararammelsbergite.* Minute bismuth inclusions occur in the middle of the three granular zones. Still older than granular *pararammelsbergite* is a zone of somewhat lighter grey, massive or slightly porous *rammelsbergite*, intergrown with *nickeline*. This sample comes from the Bratrství mine, Zdař Bůh vein.

Another type of *pararammelsbergite* forms rectangular isolated grains up to 2 mm with distinct cleavage, enclosed in fine-grained *rammelsbergite*. In contrast to the fresh enclosing mineral, grey *pararammelsbergite* crystals are dim and corroded. The same contrast is seen on freshly broken surfaces of samples recently removed from the vein. This indicates that the corrosion took place at a time when the sample was part of the vein (not afterwards). This type of material comes from the Barbora shaft, below 5th level, No. 32 vein.

Pararammelsbergite has a simple composition, it is free of increased Fe, Co, and Cu but it contains low sulphur.

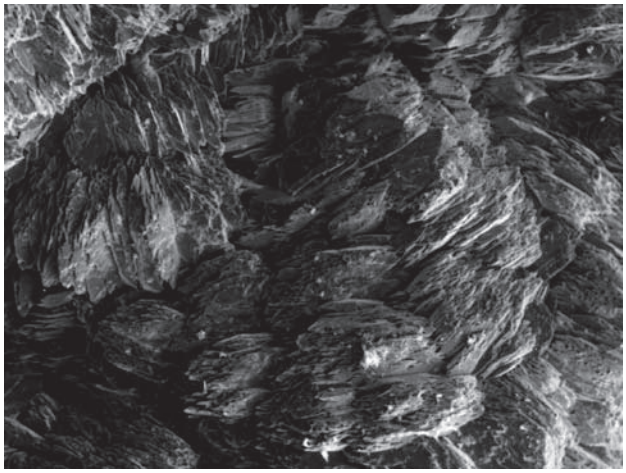

Fig. 122. J-838. Surface of radial aggregate of pararammelsbergite. Bratrství shaft, Zdař Bůh vein. SE image. Magnification 120×. Photo A. Gabašová.

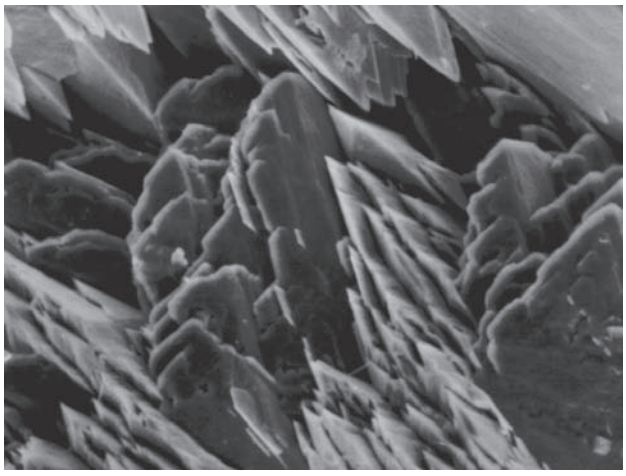

Fig. 123. J-838. Detail of the surface of radial aggregate of pararammelsbergite. Bratrství shaft, Zdař Bůh vein. SE image. Magnification 1110×. Photo A. Gabašová.

Table 91. Calculated unit-cell parameters of pararammelsbergite from Jáchymov for the space group *Pbca*.

sample	*a*	*b*	*c*
		(Å)	
J-775	5.785(1)	5.854(1)	11.448(1)
J-838	5.7787(4)	5.8491(4)	11.395(1)

Table 92. Chemical analyses of pararammelsbergite.

sample	pt.	Ni	Co	Fe	Cu	Zn	Ag	As	S	Sb	Total
						weight %					
J146P	2	28.81	0.11	0.01	0.00	0.00	0.00	70.19	0.37	0.04	99.53
J146P	3	28.94	0.10	0.03	0.00	0.12	0.04	69.59	0.45	0.00	99.28
J146P	4	28.72	0.06	0.05	0.13	0.00	0.22	70.30	0.34	0.01	99.82
J146P	5	28.94	0.05	0.01	0.11	0.07	0.00	70.88	0.11	0.00	100.17
J104P	1	27.92	0.00	0.06	0.04	0.03	0.00	71.24	0.08	0.13	99.51

sample	pt.	Ni	As	S	subtotal	Total
			number of atoms			
J146P	2	1.02	1.95	0.02	1.97	1.02
J146P	3	1.03	1.93	0.03	1.96	1.03
J146P	4	1.02	1.95	0.02	1.97	1.02
J146P	5	1.02	1.96	0.01	1.97	1.02
J104P	1	1.00	1.99	0.00	2.00	1.00

Parkerite $Ni_3Bi_2S_2$

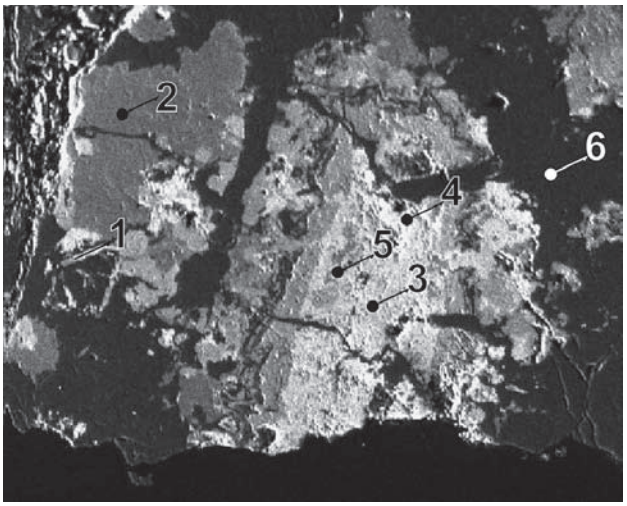

Fig. 124. J057P. Millerite formed by alteration of skutterudite, in association with native bismuth and bismuthinite. Parkerite grain is identified in proximity of coffinitizated uraninite. 1 – millerite, 2 – skutterudite, 3 – bismuth, 4 – parkerite, 5 – uraninite and coffinite, 6 – dolomite. Svornost shaft, 5th level, Prokop vein. Reflected light, single polarizer. Magnification 150×.

Parkerite occurs in grains several microns long. In reflected light, the mineral is white to light yellow. *Parkerite* is intergrown with *uraninite* and *coffinite.* Radiating *millerite* aggregates deposited on *nickel-skutterudite* occur in close proximity. The sample comes from the Svornost shaft, 5th level, Prokop vein.

Phlogopite $KMg_3AlSi_3O_{10}(OH,F)_2$

Phlogopite is identified in *quartz* vein with *molybdenite* from the Klement shaft and in skarn from the shaft Vladimír in association with *chlorite*, *cassiterite*, *amphibole*, *sphalerite*, *pyrite* and *magnetite* [433].

Table 94. Calculated unit-cell parameters of phlogopite from Jáchymov for the space group *C*2/*m*.

sample	*a*	*b*	*c*	β
		(Å)		(°)
J-800	5.319(1)	9.192(2)	10.110(1)	99.22(1)

Plumbogummite $PbAl_3(PO_4)_2(OH)_5 \cdot H_2O$

The mineral forms oval grains up to 200 μm, disseminated in some samples of micaceous gneiss. In addition to micas, *quartz* and feldspars, the rock contains *dravite*, *zircon*, *rutile* and minute *chalcopyrite*, *covellite* and *tennantite*. Chemical composition corresponds to rather pure *plumbogummite,* with a low Ba, Ca, and Fe. The sample comes from the Giftkies adit.

Table 93. Chemical analyses of parkerite.

sample	pt.	Ni	Bi	S	Co	Fe	Zn	Pb	Sb	Cu	Ag	Total
							weight %					
J057P	14	26.89	58.24	10.30	0.52	0.49	1.48	0.65	0.62	0.99	0.48	100.66
J057P	15	24.40	62.95	9.98	0.65	0.32	1.27	0.79	0.53	1.53	0.31	102.73
J057P	16	26.79	59.82	9.77	0.27	0.32	0.42	0.92	0.71	0.44	0.46	99.92
J057P	17	24.75	62.35	9.75	1.32	0.00	0.22	1.08	0.23	0.11	0.35	100.16

sample	pt.	Ni	Co	Fe	Zn	Cu	subtotal	Bi	Pb	Sb	Cu	Ag	subtotal	S	Total
								number of atoms							
J057P	14	2.85	0.05	0.05	0.14		3.10	1.73	0.02	0.03	0.10	0.03	1.91	2.00	7
J057P	15	2.65	0.07	0.04	0.12	0.15	3.03	1.92	0.02	0.03		0.02	1.99	1.98	7
J057P	16	2.94	0.03	0.04	0.04		3.05	1.85	0.03	0.04	0.04	0.03	1.98	1.96	7
J057P	17	2.78	0.15	0.00	0.02		2.95	1.97	0.03	0.01	0.01	0.02	2.05	2.00	7

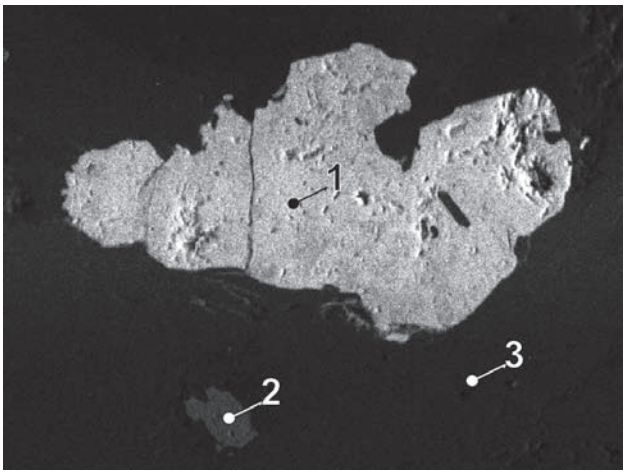

Fig. 125. J191P/1. 1 – plumbogummite, 2 – rutile, 3 – quartz. Giftkies adit. BSE image. Magnification 320×.

Polybasite $(Ag,Cu)_{16}Sb_2S_{11}$

Polybasite occurs as tabular and rare prismatic crystals. Characteristic is a triangular striation seen on basal faces of tabular crystals and striation parallel to basal face on prismatic faces. This produces an aspect of crystals composed of thin wafers. The mineral is black with a steel grey or greenish tint. Thin flakes are dark red in transmitted

Table 95. Calculated unit-cell parameters of polybasite from Jáchymov for the space group $P\bar{3}$.

sample	*a*	*c*
	(Å)	
J033P	15.00(1)	23.52(2)

Table 96. Chemical analyses of polybasite.

sample	pt.	Ag	Cu	Fe	Ni	Co	Zn	S	Sb	As	Total
						weight %					
21019	4	74.89	0.69	0.12			0.03	16.06	8.86	1.30	101.95
21019	4a	74.76	0.36	0.17			0.02	15.88	9.15	1.50	101.84
21019	4b	74.69	0.72	0.14			0.14	15.87	8.67	1.56	101.79
21019	c4	74.91	0.74	0.18			0.09	15.85	8.77	1.49	102.03
J-702	a1	73.65	0.57	0.44	0.16		0.16	15.65	10.22	0.86	101.71
J-702	a2	73.17	0.85	0.19	0.30		0.02	15.69	10.24	0.35	100.81
J-702	a3	74.05	0.65	0.16	0.23		0.13	15.34	10.02	0.52	101.10
J031P	7	69.55	4.14	0.50	0.14	0.13		15.89	7.52	2.03	99.90
J031P	8	69.53	4.63	0.55	0.11	0.07		16.15	7.38	2.36	100.78
J031P	9	71.82	2.89	0.52	0.13	0.10		15.88	6.55	2.78	100.67
J031P	10	69.90	3.94	0.51	0.14	0.20		15.96	7.84	2.16	100.65
J117P	A1	69.75	5.49	0.01				14.38	9.83	0.82	100.28
J117P	A2	67.60	7.48	0.55				14.38	9.57	0.81	100.39
J-840	1	62.99	10.72					16.54	6.09	3.06	99.40
J-840	2	62.53	10.36					16.39	6.59	3.24	99.11
J-840	3	62.74	9.83					16.34	8.72	1.83	99.46

sample	pt.	Ag	Cu	Fe	Co	Ni	Zn	subtotal	Sb	As	subtotal	S	Total
						number of atoms							
21019	4	15.50	0.24	0.05			0.01	15.80	1.63	0.39	2.01	11.19	29
21019	4a	15.55	0.13	0.07			0.01	15.75	1.69	0.45	2.14	11.11	29
21019	4b	15.50	0.25	0.06			0.05	15.86	1.59	0.47	2.06	11.08	29
21019	c4	15.53	0.26	0.07			0.03	15.89	1.61	0.45	2.06	11.05	29
J-702	a1	15.37	0.20	0.18		0.06	0.06	15.86	1.89	0.26	2.15	10.99	29
J-702	a2	15.38	0.30	0.08		0.12	0.01	15.89	1.91	0.11	2.01	11.10	29
J-702	a3	15.64	0.23	0.07		0.09	0.05	16.07	1.88	0.16	2.03	10.90	29
J031P	7	14.30	1.44	0.20	0.05	0.05		16.04	1.37	0.60	1.97	10.99	29
J031P	8	14.10	1.59	0.22	0.03	0.04		15.97	1.33	0.69	2.01	11.02	29
J031P	9	14.73	1.01	0.21	0.04	0.05		16.03	1.19	0.82	2.01	10.96	29
J031P	10	14.28	1.37	0.20	0.08	0.05		15.98	1.42	0.64	2.05	10.97	29
J117P	A1	14.73	1.97					16.70	1.84	0.25	2.09	10.21	29
J117P	A2	14.06	2.64	0.22				16.93	1.76	0.24	2.01	10.07	29
J-840	1	12.46	3.60					16.06	1.07	0.87	1.94	11.00	29
J-840	2	12.44	3.50					15.94	1.16	0.93	2.09	10.97	29
J-840	3	12.57	3.34					15.91	1.55	0.53	2.08	11.01	29

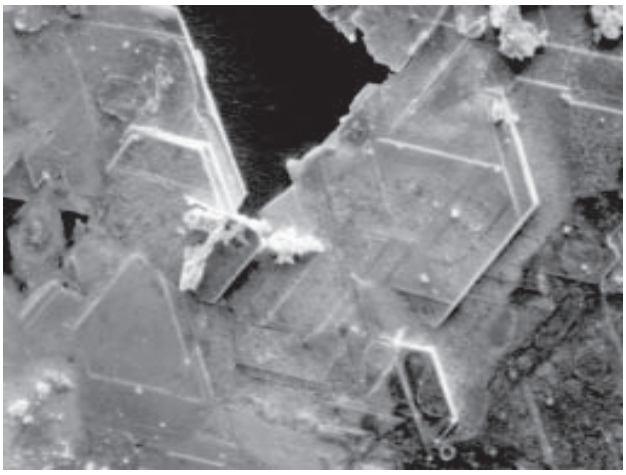

Fig. 126. J-701. Vicinal forms on basal face of polybasite. Svornost shaft, 12th level, Geschieber vein. SE image. Magnification 330×. Photo A. Gabašová.

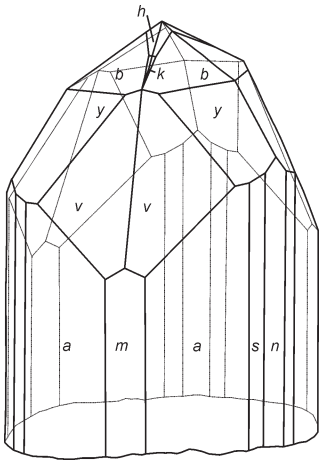

Fig. 128. Drawing of proustite crystal by Kašpar [379]. Crystal forms: v(21$\bar{3}$1), y(31$\bar{4}$1), a(11$\bar{2}$0), b(31$\bar{4}$2), m(10$\bar{1}$0), n(01$\bar{1}$0), s(12$\bar{3}$0), h(7,6,$\bar{13}$,10), k(3257)

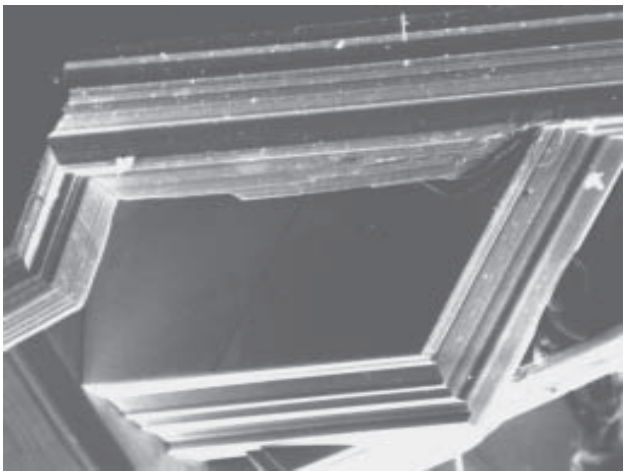

Fig. 127. J-701. Detail of vicinal growth on basal face of polybasite. Svornost shaft, 12th level, Geschieber vein. SE image. Magnification 330×. Photo A. Gabašová.

light. Fracture is uneven, cleavage imperfect parallel to the basal face in hexagonal setting. *Polybasite* in crystals up to 2 mm is a rare mineral in Jáchymov.

The sample from the Svornost shaft, 12th level, Geschieber vein, carries *polybasite* crystals with *stephanite* and *proustite–pyrargyrite* in vugs of brecciated hornfelsic *quartz*.

Proustite Ag_3AsS_3

Mrňa a Pavlů [351] studied p*roustite* from Jáchymov. They found *proustite* occurrence in small amounts in numerous veins and at various depth levels. Previous data document notable accumulations of *proustite* in upper levels of the deposit. Zepharovich [391] noted more common occurrence of *proustite* in the eastern part of the district; *argentite* was more common in the western part. At present, the best occurrences are in the Svornost shaft, Geschieber vein.

Proustite is intergrown with other silver minerals and enclosed in arsenic or carbonate gangue. Druses with crystals exceptionally up to several cm long crystallized in gangue cavities. *Proustite* aggregates fill spaces after dendritic *silver*. The mineral is light red, with a glassy lustre (Figs 134–136). Crystals with perfect faces are prismatic, with a fine striation in the vertical zone [351]. Kašpar [379] published the crystallographic study of Jáchymov *proustite* featuring several crystal types. *Proustite* specimens of the best aesthetic quality were collected in 1817 and 1822 in the Marie vein (Zippe [527]). In 1814, the Emperor presented to the National Museum in Prague (Patriotic Museum by that time) an exceptional *proustite* specimen 3 kg in weight, 15×13×10 cm in size, composed entirely of *proustite*, except a small part of arsenic and dolomite. According to Zippe [528], the absence of *pyrite* in this sample provided a guarantee that the specimen would not disintegrate.

Proustite crystallization belongs to the *arsenic-sulphide* stage, during which rich arsenic accumulations formed with cavities filled by crystal aggregates of silver minerals, including *proustite–pyrargyrite and stephanite* (relatively abundant at lower levels of the Geschieber vein) at slightly increased Eh and in the temperature range of 60–180 °C. Less common are *silver*, *argentite*, *polybasite*, *arsenpolybasite*, *xanthoconite* and minute crystalline aggregates or isolated single crystals of *sternbergite* and *argentopyrite*. In this paragenesis, *löllingite* rims *arsenic* aggregates. During the *sulphidic* stage, *proustite* is intensively replaced by *chalcopyrite*, *bornite*, *tennantite*, and *pyrite*.

Chemical and crystal structure study of the series proustite–pyrargyrite

Proustite and *pyragyrite* form an isostructural solid-solution series. The crystal structure features a trigonal unit-cell with the space group *R*3*c*; the unit–cell parameters range from a_{proust} = 10.77 Å to $a_{pyrar.}$ = 11.05 Å and c_{proust} = 8.69 Å to $c_{pyrar.}$ = 8.73 Å. Correlation of calculated unit–cell parameters (*a*, *c*) and As/(As+Sb) ratio for Jáchymov *proustite* and *pyrargyrite* are expressed in Fig. 137. A complete miscibility between As and Sb members should occur above 90 °C. Phase relations of this system were published: [495], [407], [401], [393], [397]. Zepharovich [391] determined Jáchymov *proustite* density of 5.55 g/cm^3.

Proustite and *pyragyrite* solid solutions in some deposits of the Bohemian Massif (Příbram sulphidic ore and uranium ore districts, Měděnec deposit in the Krušné hory Mts.) were recently studied by Řídkošil et al. [373]. The authors determined compositions with nearly equal proportions of *proustite* and *pyrargyrite* in samples from Třebsko (Příbram district) and from Měděnec. *Proustite* with notable compositional zoning was described from Měděnec.

Proustite and *pyrargyrite* samples used in the present study are from the Geschieber vein, Svornost shaft, 10th level (sample J-843) and 12th level (sample J-842). Crystals showing complex twinning and compositional zoning, with zones corresponding to *Sb-proustite* and *As-pyrargyrite*, with lamellar and lenticular domains showing variable As/Sb ratio are most common.

Variation in chemical composition is well seen in BSE images (Figs 131–133). The lamellar polysynthetic twinning is most common on (10$\bar{1}$4), pressure twinning is also assumed [487]. The zoned crystals are often imperfect, with *proustite* zones partly replaced by *pyrargyrite*, which also replaced cores of crystals and forms their outer growth zones. Individual zones represent various members of the solid-solution series, which are closer to *proustite* or *pyrargyrite.*

Although the two end-members are isostructural, the *proustite–pyragyrite* crystals from Jáchymov show limited miscibility (Figs 129 and 130). The limited miscibility at this locality is probably a function of quite low temperature, possibly lower than 150 °C (see section *Ore-forming processes and mineral parageneses of the Jáchymov ore district* – stability of *argentopyrite*) or a presence of additional elements in crystals structure with possibly favoured relative separation of As and Sb in a single crystal. Our data show that at temperature lower than 150 °C, *proustite* can not accept more than 20 mol.% Sb, in correspondence with the empirical formula of *Sb-proustite* $Ag_3(As_{0.80}Sb_{0.20})S_3$. In *pyrargyrite*, up to 44 mol. % Sb in the Sb(As) position was observed, in correspondence with the empirical formula of *As-pyrargyrite* $Ag_3(Sb_{0.56}As_{0.44})S_3$. The range of the As content in pyrargyrite (up to 6.02 wt.% As) is more extensive than Sb range in *proustite* (Sb up to 4.98 wt.%).

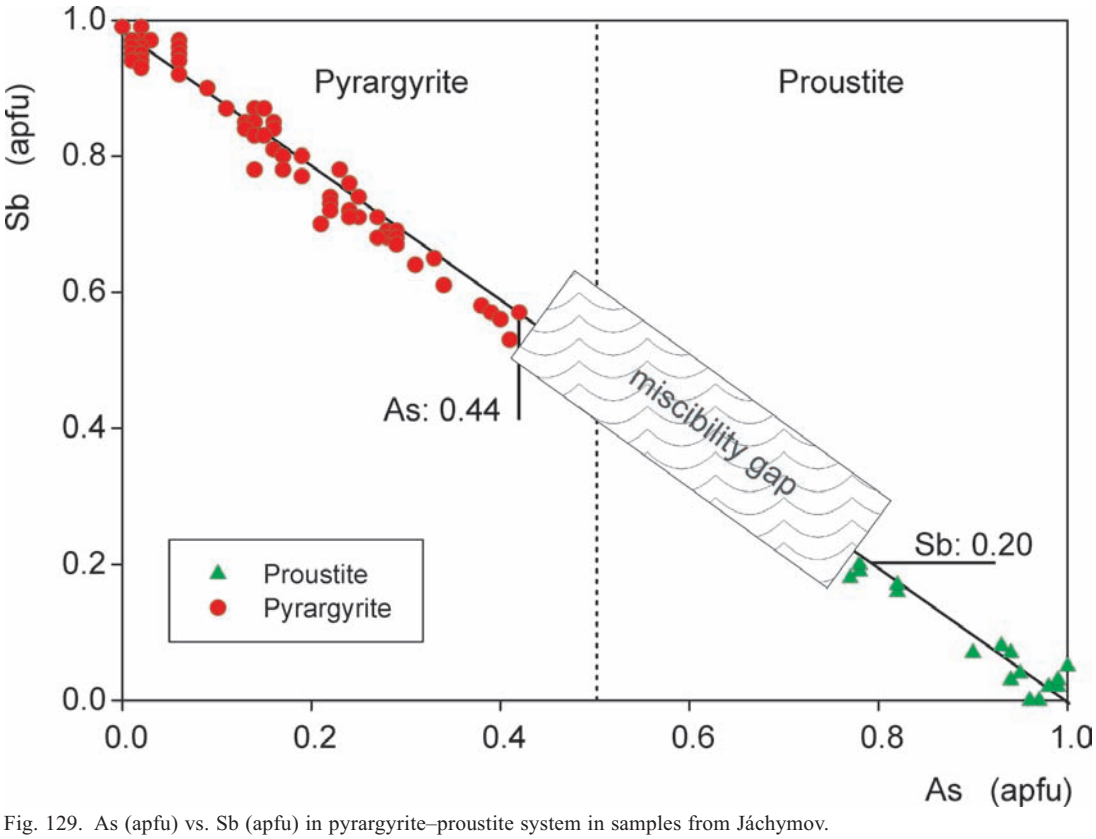

Fig. 129. As (apfu) vs. Sb (apfu) in pyrargyrite–proustite system in samples from Jáchymov.

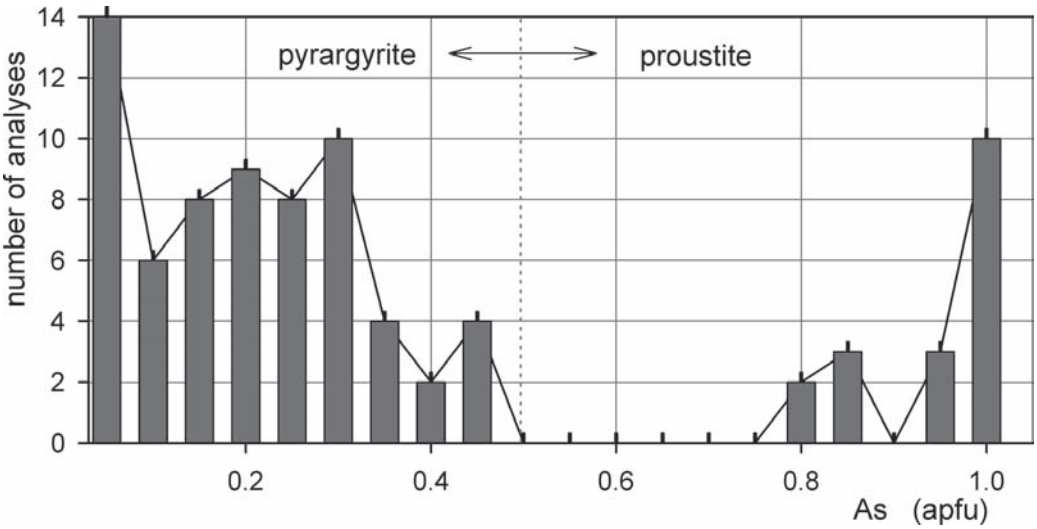

Fig. 130. Diagram of As content frequency in pyrargyrite–proustite series in Jáchymov.

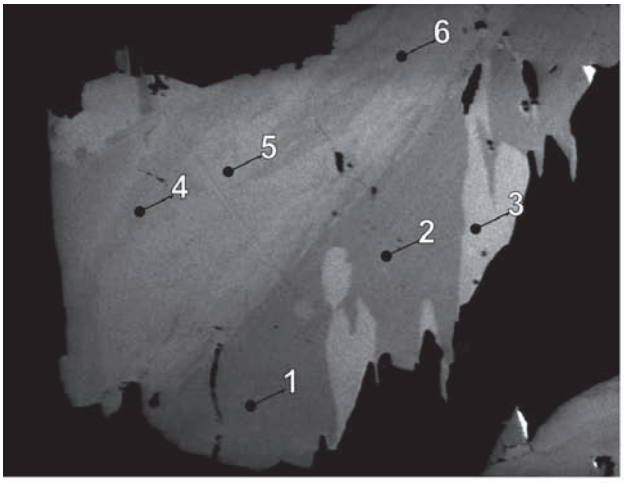

a

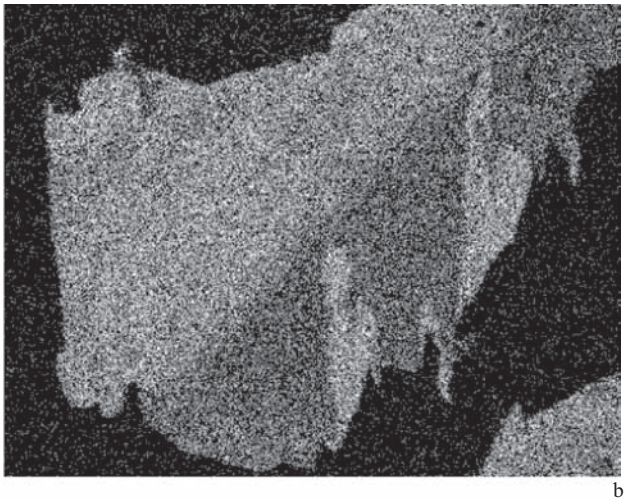

b

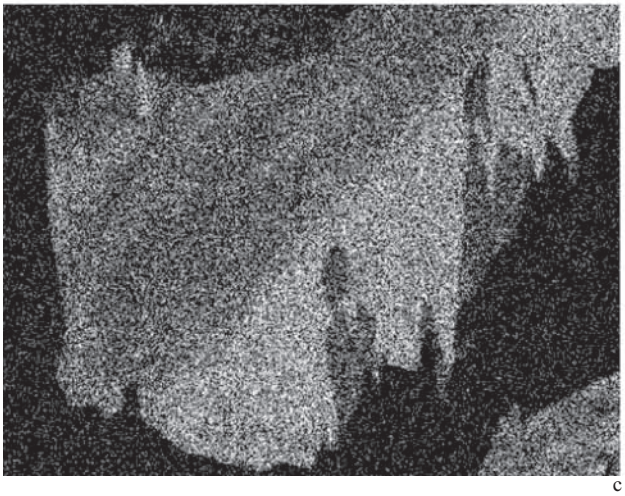

c

Fig. 131. J-843. 1, 2 – proustite, 3 – pyrargyrite, 4, 5, 6 – domains with intermediate composition. Svornost shaft, the 10th level, Geschieber vein. Magnification 800×.
a) BSE image.
b) Distribution of Sb.
c) Distribution of As.

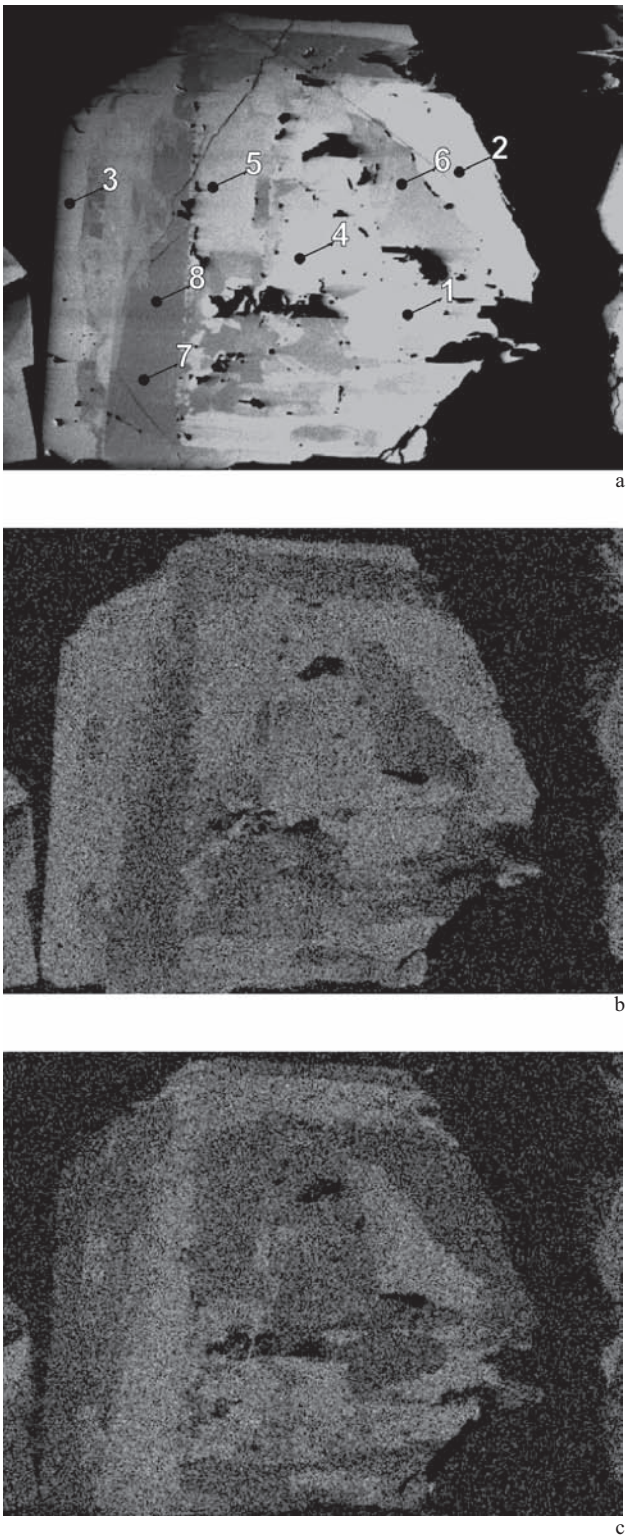

Fig. 132. J-842/4. 1, 2, 4 – As-pyrargyrite, 3, 5, 6 – domains with intermediate composition, 7, 8 – proustite. Svornost shaft, 12th level, Geschieber vein. Magnification 1600×.
a) BSE image.
b) Distribution of Sb.
c) Distribution of As.

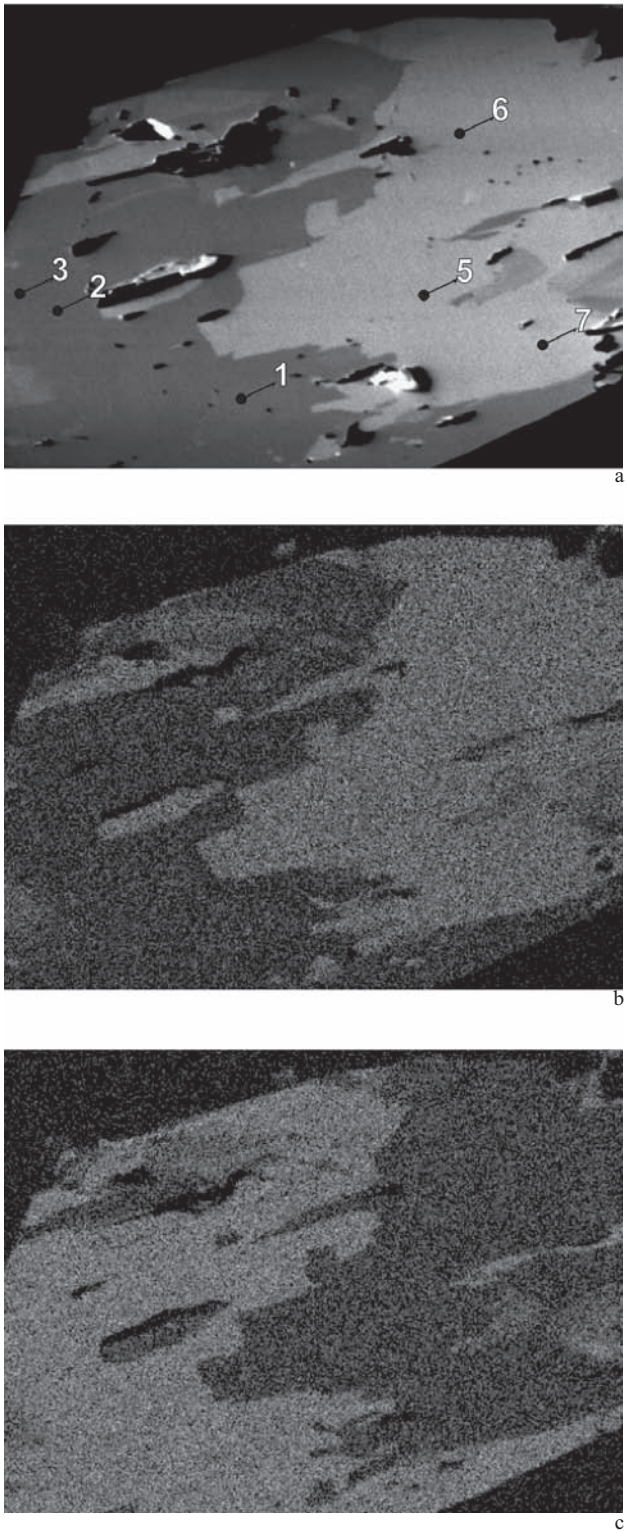

Fig. 133. J-842/1. 1, 2, 3 – proustite, 5,6,7 – pyrargyrite. Svornost shaft, 12th level, Geschieber vein. Magnification 1200×.
a) BSE image.
b) Distribution of Sb.
c) Distribution of As.

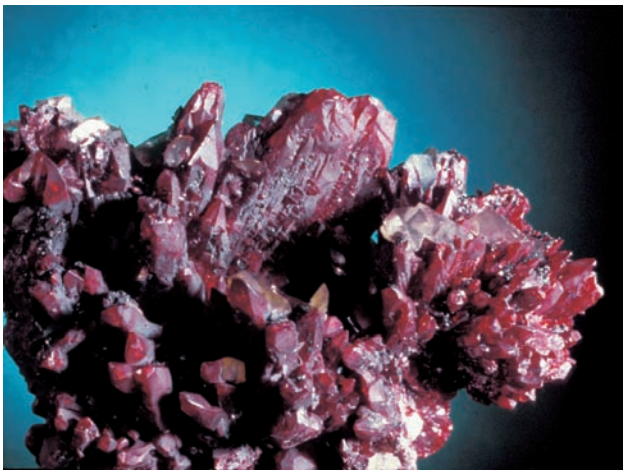

Fig. 134. Group of dark red proustite crystals up to 1–2 cm (width of figure 5 cm). Photo J. & E. Sejkora.

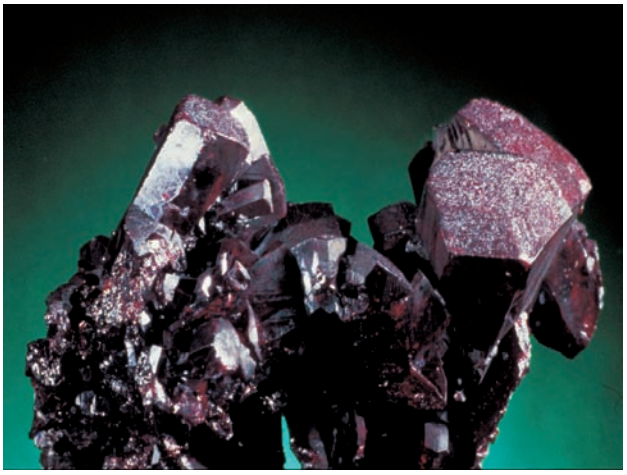

Fig. 135. Group of proustite crystals up to 1 cm (width of figure 3 cm). Photo J. & E. Sejkora.

Fig. 136. The proustite pseudomorphoses after skeletal silver crystals (width of figure 9 mm). Photo J. & E. Sejkora.

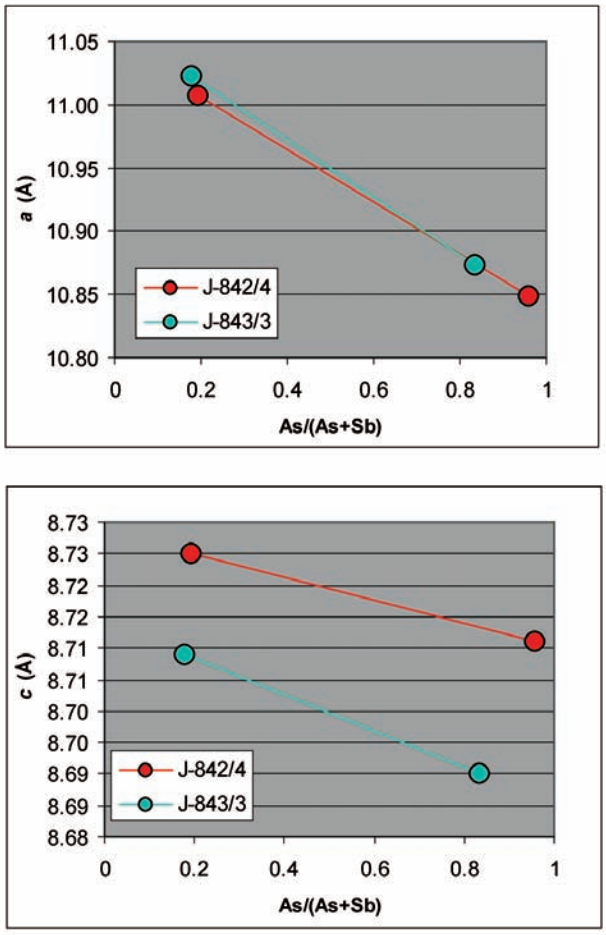

Fig. 137. Correlation of unit-cell parameters (*a*, *c*) and As/(As+Sb) ratio for proustite and pyrargyrite from Geschieber vein, Svornost shaft (sample No. J-842: 12th level, sample No. J-843: 10th level).

Table 97. Calculated unit-cell parameters of proustite from Jáchymov for the space group *R*3*c*.

sample	unit-cell parameters (Å)		density (g.cm^{-3})	
	a	*c*	D_m	D_X
[340]	10.800	8.7229	5.59	5.592
J-843(average)	10.832(4)	8.670(1)		
J-842/4	10.849(1)	8.711(2)		
J-843/3	10.874(4)	8.690(1)		
J-842(average)	10.9119(7)	8.724(1)		

Proustite-pyragyrite minerals close in composition to the end-members occur only exceptionally in the Jáchymov ore veins. *Pyrargyrite* has at least a minor As content, with minimum at 0.2 wt.% As. Both minerals tend to form intergrowth in crystallographic orientation and single crystals of pure *proustite* and *pyrarargyrite* have not been found. Ramdohr [487] described crystallographically orientated intergrowth of the two minerals from Andreasberg in Harz, Germany. From Jáchymov, Ramdohr mentioned

Table 98. Chemical analyses of proustite.

sample	pt.	Ag	Cu	Fe	As	Sb	S	Total	Ag	As	Sb	As+Sb	S	Total
					weight %						number of atoms			
J-842	1–1	64.37			14.86	1.11	18.78	99.13	3.01	1.00	0.05	1.04	2.95	7
J-842	1–2	65.42			14.78	0.46	18.96	99.62	3.03	0.99	0.02	1.01	2.96	7
J-842	1–4	66.00			15.01	0.64	19.32	100.97	3.02	0.99	0.03	1.01	2.97	7
J-842	4–8	65.54			14.87	0.49	19.62	100.52	2.99	0.98	0.02	1.00	3.01	7
J-842	5–10	65.31			14.54		19.26	99.11	3.03	0.97		0.97	3.00	7
J-842	5–7	66.15			14.72		19.57	100.44	3.02	0.97		0.97	3.01	7
J-842	5–9	65.57			14.62	0.10	19.38	99.67	3.02	0.97		0.97	3.00	7
J122P	B	66.31	0.11		14.20		18.65	99.27	3.10	0.96		0.96	2.93	7
J-842	4–7	65.04			14.42	0.87	19.56	99.89	2.99	0.95	0.04	0.99	3.02	7
J-842	1–3	65.53			14.11	1.60	18.94	100.17	3.04	0.94	0.07	1.01	2.95	7
J-842	5–8	65.55			14.12	0.64	19.42	99.73	3.02	0.94	0.03	0.96	3.01	7
J106P	B	64.92	0.36	0.93	13.97	1.86	18.57	100.60	3.03	0.93	0.08	1.00	2.89	7
J-842	4–6	65.07			13.50	1.77	19.38	99.72	3.01	0.90	0.07	0.97	3.02	7
J-843	3–1	65.01			12.26	3.91	19.16	99.13	3.02	0.82	0.16	0.98	3.00	7
J-843	3–2	64.29			12.33	4.17	19.50	100.97	2.97	0.82	0.17	0.99	3.03	7
J-843	4–3	65.12			11.64	4.59	19.26	100.61	3.02	0.78	0.19	0.97	3.01	7
J-843	4–5	64.48			11.58	4.82	19.10	99.98	3.02	0.78	0.20	0.98	3.01	7
J-843	4–1	64.40			11.75	4.98	19.40	100.53	2.99	0.78	0.20	0.99	3.03	7
J-843	4–4	65.16			11.42	4.45	19.10	100.13	3.04	0.77	0.18	0.95	3.00	7

As content

intergrowth of *proustite* with *arsenic.* Recently, crystallographic intergrowths of nearly pure *proustite* with *acanthite* pseudomorphs after *argentite* were found in Jáchymov.

Pyrargyrite Ag_3SbS_3

Mrňa and Pavlů (1967) found out that *pyrargyrite* is a subordinate mineral, as Sb is not typical of the Jáchymov ore veins. In ores of *arsenic-sulphide* stage it takes a similar position as *proustite* – minute prismatic crystals in ore vugs, dominated by rhombohedral and scalenohedral faces [351] (Fig. 138). Crystallization conditions (mineralization stage) and position in mineral assemblages are very close to, or corresponding to those of *proustite.* Chemical relations and crystal structure characteristics in the *proustite–pyrargyrite* series are discussed in detail under *proustite*.

Correlation of unit-cell parameters and As/(As+Sb) ratio is in Fig. 137.

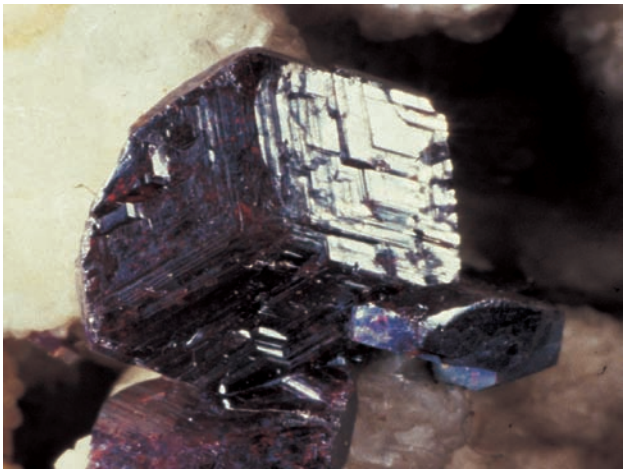

Fig. 138. Pyrargyrite crystal in cavity of carbonate gangue (width of figure 3.8 cm). Photo J. & E. Sejkora.

Table 99. Calculated unit-cell parameters of pyrargyrite from Jáchymov for the space group *R*3*c*.

sample	point	*a*	*c*
		(Å)	
J-843	average	10.964(2)	8.727(2)
J-842	4	11.007(1)	8.725(1)
[333]	(NM9512)	11.022(1)	8.722(1)
J-843	3	11.023(4)	8.709(4)
J-842	average	11.030(1)	8.706(1)
[333]	(NM9512)	11.033(1)	8.721(1)

Pyrite FeS_2

Mrňa and Pavlů [351] observed that *pyrite* is present as a component of hydrothermal ores as well as fine-grained impregnation in some rocks.

There are several generations *of pyrite*, crystallized with ores of individual mineralization stages. The identification of *pyrite* generation is possible only in cases where *pyrite* is associated with minerals characteristic of a mineralization stage. Observations on succession relations indicate that *pyrite* is associated with minerals of the *Sn–W sulpharsenide* stage, with uranium ores (coarse-grained, skeletal, in euhedral crystals), and particularly with minerals of the sulphidic stage. In the latter case, *pyrite* is a common component in carbonate gangue, occurs in polymetallic ore lenses and sometimes forms monomineralic accumulations with radiating or botryoidal aggregates. *Pyrite* in arsenide ores is deposited on arsenides and has a similar position as other younger minerals – *galena*, *sphalerite* and *arsenic. Pyrite* is sometimes accompanied by *marcasite* [351].

Younger *pyrite* fills extension fractures in *skutterudite*, replaces *proustite* and *skutterudite* along their contacts, or locally rims silver minerals [431].

Table 100. Chemical analysis of pyrargyrite.

sample	pt.	Ag	Cu	Fe	As	Sb	S	Total	Ag	Cu	Fe	As	Sb	subtotal	S	Total
		weight %							number of atoms							
J105P	g2	58.59	0.00	0.11	0.19	22.68	16.99	98.57	3.01			0.01	1.03	1.05	2.93	7
NM9730	a3	59.09	0.63	0.15	0.18	22.63	17.52	100.20	2.96	0.05	0.02	0.01	1.01		2.95	7
NM9725	a4	59.12	0.22	0.15	0.25	22.55	18.10	100.39	2.94	0.02	0.01	0.02	0.99		3.02	7
J105P	g3	60.66	0.18	0.17	0.27	21.80	16.64	99.72	3.10	0.02		0.02	0.99	1.01	2.86	7
J105P	g1	60.87		0.11	0.03	22.09	17.06	100.16	3.09				0.99	0.99	2.91	7
NM9725	a2	59.38	0.12	0.07	0.39	22.02	18.02	100.00	2.96	0.01	0.01	0.03	0.97		3.02	7
NM9725	a1	59.45	0.82	0.10	0.26	22.18	18.11	100.92	2.93	0.07	0.01	0.02	0.97		3.00	7
NM9730	a4	59.71	0.19	0.68	0.14	22.06	17.71	100.49	2.97	0.02	0.07	0.01	0.97		2.97	7
J-842	1–5	60.14			0.85	21.74	17.34	100.07	3.03			0.06	0.97	1.03	2.94	7
NM9726	a1	59.21	0.60	0.52	0.16	21.68	17.66	99.83	2.96	0.05	0.05	0.01	0.96		2.97	7
NM4843	b1	59.56	0.11	0.33	0.25	21.67	17.79	99.71	2.98	0.01	0.03	0.02	0.96		3.00	7
J-842	1–6	60.74			0.81	21.57	17.29	100.41	3.05			0.06	0.96	1.02	2.93	7
NM4843	b2	59.39	0.23	0.45	0.85	21.34	17.54	99.80	2.97	0.02	0.04	0.06	0.95		2.96	7
NM9730	a2	59.76	0.13	0.45	0.22	21.43	17.78	99.77	2.99	0.01	0.04	0.02	0.95		2.99	7
NM9730	a1	59.85	0.64	0.69	0.11	21.60	17.57	100.46	2.98	0.05	0.07	0.01	0.95		2.94	7
NM9726	a2	59.17	1.06	0.39	0.23	21.47	17.89	100.21	2.93	0.09	0.04	0.02	0.94		2.98	7
NM9726	a4	59.77	0.73	0.38	0.14	21.22	17.70	99.94	2.98	0.06	0.04	0.01	0.94		2.97	7
J-842	1–8	60.71			0.80	20.96	17.40	99.87	3.06			0.06	0.94	0.99	2.95	7
NM9726	a3	59.95	0.67	0.28	0.28	20.80	17.55	99.53	3.01	0.06	0.03	0.02	0.93		2.96	7
J106P	c	61.07	0.09	0.09	0.77	20.55	17.21	99.78	3.08	0.01		0.06	0.92	0.98	2.92	7
J-842	5–4	60.24			1.27	20.40	18.08	99.99	2.99			0.09	0.90	0.99	3.02	7
J-842	4–2	60.24			1.48	19.80	18.07	99.59	3.00			0.11	0.87	0.98	3.02	7
J-842	1–7	60.48			1.97	19.42	17.42	99.39	3.04			0.14	0.87	1.01	2.95	7
J106P	d	60.71	0.11	0.01	2.05	19.75	17.87	100.51	3.00	0.01		0.15	0.87	1.01	2.97	7
J-842	7–6	59.81			2.28	19.28	17.97	99.34	2.98			0.16	0.85	1.01	3.01	7
J-842	8–3	60.62			1.99	19.45	18.10	100.16	3.00			0.14	0.85	0.99	3.01	7
J-842	4–1	60.63			1.88	19.28	17.97	99.76	3.01			0.13	0.85	0.98	3.00	7
J-842	7–3	60.28			2.18	19.23	18.05	99.74	2.99			0.16	0.84	1.00	3.01	7
J-842	8–2	60.91			1.76	19.25	18.17	100.09	3.01			0.13	0.84	0.97	3.02	7
J-842	8–1	61.59			1.78	19.30	18.17	100.84	3.03			0.13	0.84	0.97	3.01	7
J-842	5–5	60.11			2.15	18.84	18.13	99.23	2.99			0.15	0.83	0.98	3.03	7
J-843	3–3	60.62			2.00	19.55	19.55	100.17	2.89			0.14	0.83	0.96	3.14	7
J-843	3–4	60.59			2.30	18.50	18.00	99.62	3.01			0.16	0.81	0.98	3.01	7
J-842	7–4	60.55			2.41	18.40	18.40	99.76	2.98			0.17	0.80	0.97	3.05	7
J-843	3–5	61.54			2.65	18.54	18.26	99.39	3.01			0.19	0.80	0.99	3.00	7
NM4843	a5	61.11	0.80	0.47	2.44	18.23	18.64	101.69	2.94	0.07	0.04	0.17	0.78		3.01	7
NM9725	a3	61.20	0.33	0.89	2.07	18.16	18.44	101.09	2.96	0.03	0.08	0.14	0.78		3.00	7
J-843	1–3	61.80			3.20	17.83	17.83	100.66	3.04			0.23	0.78	1.00	2.95	7
NM4843	1	60.99	0.20	0.24	2.71	18.09	18.78	101.01	2.95	0.02	0.02	0.19	0.77		3.05	7
J-842	4–3	60.57			3.37	17.33	18.12	99.39	2.99			0.24	0.76	1.00	3.01	7
NM4843	a8	61.48	0.18	0.37	3.09	17.16	18.45	100.73	2.98	0.02	0.04	0.22	0.74		3.01	7
J122P	a2	61.83			3.45	16.73	17.36	99.37	3.09			0.25	0.74	0.99	2.92	7
J-843	3–6	62.08			3.17	17.07	18.45	100.41	3.02			0.22	0.74	0.96	3.02	7
NM4843	2	61.19	0.78	0.51	3.10	17.18	18.48	101.24	2.95	0.06	0.05	0.22	0.73		2.99	7
NM4843	4	61.03	0.59	0.44	3.12	16.57	18.11	99.86	2.99	0.05	0.04	0.22	0.72		2.98	7
J-842	4–4	61.37			3.41	16.57	18.37	99.72	3.01			0.24	0.72	0.96	3.03	7
NM4843	a9	61.05	0.17	0.34	3.55	16.41	18.43	99.95	2.98	0.01	0.03	0.25	0.71		3.02	7
J-842	7–5	61.40			3.77	16.13	18.02	99.32	3.03			0.27	0.71	0.97	2.99	7
NM4843	a7	61.43	0.95	0.68	3.59	16.90	18.72	102.27	2.92	0.08	0.06	0.25	0.71		2.99	7
J-842	4–5	61.85			3.41	16.49	18.40	100.15	3.02			0.24	0.71	0.95	3.02	7
NM4843	3	60.56	0.71	0.35	3.04	16.24	18.53	99.43	2.95	0.06	0.03	0.21	0.70		3.04	7
J-842	7–2	61.42			3.97	15.81	18.02	99.22	3.03			0.28	0.69	0.97	2.99	7
J122P	a1	61.73			4.11	15.63	17.58	99.04	3.07			0.29	0.69	0.98	2.94	7
NM4843	a6	61.16	0.50	0.66	3.93	15.99	18.65	100.89	2.94	0.04	0.06	0.27	0.68		3.01	7
J-842	5–6	62.00			4.05	15.66	18.42	100.13	3.02			0.28	0.68	0.96	3.02	7
J-843	2–5	62.38			4.09	15.92	18.49	100.88	3.02			0.29	0.68	0.97	3.01	7
J-843	2–2	61.86			4.13	15.39	18.21	99.59	3.03			0.29	0.67	0.96	3.01	7
J-843	2–3	61.91			4.18	15.40	18.32	99.81	3.03			0.29	0.67	0.96	3.01	7
J-842	7–a	61.28			4.63	15.07	18.36	99.34	3.00			0.33	0.65	0.98	3.02	7
J-843	2–4	62.29			4.50	14.97	18.57	100.33	3.02			0.31	0.64	0.96	3.03	7
NM4843	a10	62.50	0.07	0.38	4.86	14.42	18.81	101.04	2.99	0.01	0.04	0.34	0.61		3.03	7
J-843	1–6	62.52			5.47	13.64	18.48	100.11	3.03			0.38	0.58	0.97	3.01	7
J-843	1–5	62.20			5.53	13.38	18.54	99.65	3.02			0.39	0.57	0.96	3.02	7
J-843	1–1	62.82			6.02	13.39	18.40	100.63	3.03			0.42	0.57	0.99	2.98	7
J-843	1–2	63.15			5.79	13.28	18.81	101.03	3.02			0.40	0.56	0.96	3.02	7

Sb content

The present work confirmed that *pyrite* occurs with a majority of ore minerals, in aggregates of variable size and crystal form. It belongs to the most abundant minerals in the ore district.

Some small *pyrite* aggregates show perfect spherical form, several microns up to 20 μm in diameter. The size of *pyrite* crystals in a sphere correlates with diameter of the sphere, with approximately 15 *pyrite* crystals per section of a sphere (Figs 142–144). Microprobe analyses of such small object are not reliable, but a small admixture of As is indicated. The spheroidal aggregates are similar to framboidal *pyrite*, for which a role of bacteria is assumed, but in the Jáchymov deposit the mode of formation of this *pyrite* is uncertain. It seems that distribution of such *pyrite* aggregates does not follow textures of vein filling.

Some samples carry *pyrite* of at least two generations. A sample from the Svornost shaft, Geschieber vein contains an older, porous *pyrite,* producing surface with poor quality polish, overgrown by younger, compact *pyrite* giving good polish. Boundary between the two types of *pyrite* is sharp and the old generation may show euhedral shape. Both types of *pyrite* contain 5–5.5 wt.% As and their compositions are comparable.

A younger *pyrite* containing 4 wt.% As and 4 wt.% Ni occurs in paragenesis with *violarite*, *Sb-gersdorffite* and *millerite.* The sample comes from the Eliáš mine, No. 2A vein. *Pyrite* containing several per cent As was reported from adit No. 7, veins Ro and Co [416, 522]. Maximum content of As reaches 17.35 wt.% in pyrite from Svornost shaft, Prokop vein, 5th level (Fig. 140). Correlation of calculated unit-cell parameter *a* and As content for pyrites enriched in As from Jáchymov is expressed in Figs 146 and 147.

Examples of solid solutions in the system FeS_2–NiS_2 *(pyrite–vaesite)* exist in spherical aggregates deposited on

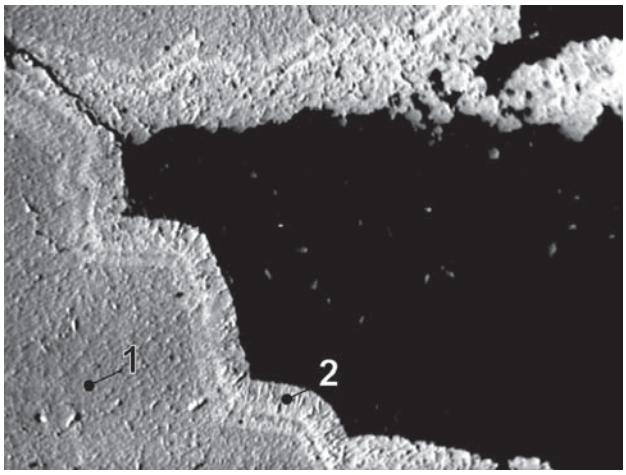

Fig. 140. J064P. 1 – pyrite, 2 – As-pyrite. Eliáš mine, sludge bed. BSE image. Magnification 40×.

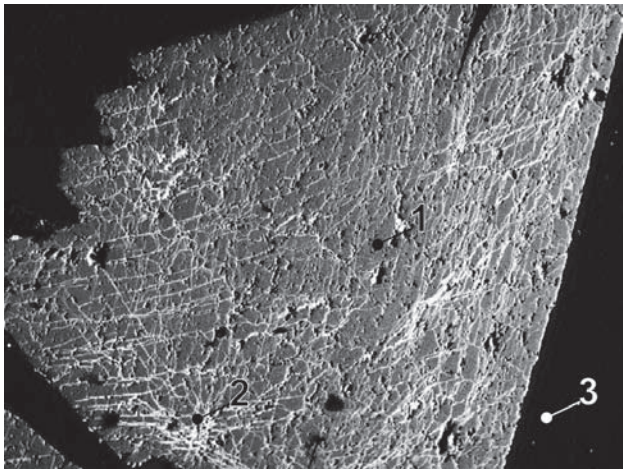

Fig. 141. J075P. 1 – pyrite, 2 – bornite, 3 – quartz. Svornost shaft, Daniel level, Trojická or Geschieber vein. BSE image. Magnification 54×.

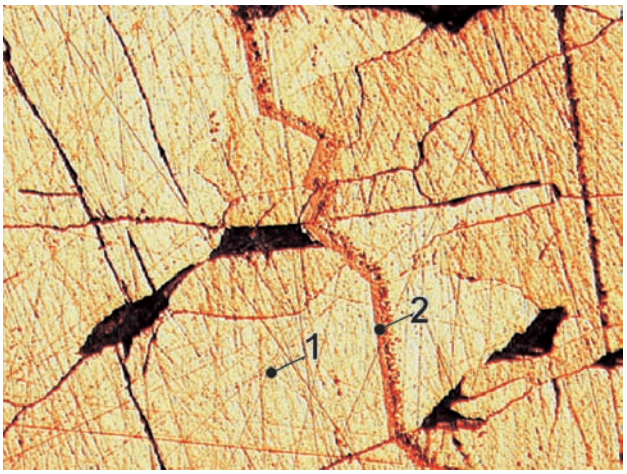

Fig. 139. J054P. Narrow darker growth zones of uniform width in pyrite are enriched in Ni. Content of Ni is up to 17 wt.%. 1 – pyrite, 2 – Ni-pyrite. Svornost shaft, 5th level, Prokop vein. Reflected light, single polarizer. Magnification 260×.

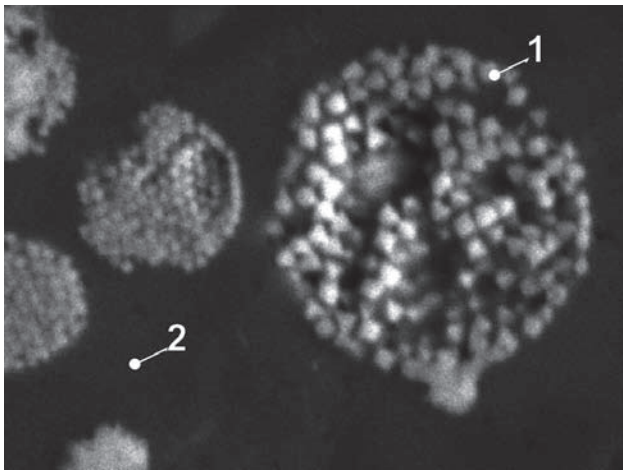

Fig. 142. J105P/B-1. 1 – pyrite, 2 – dolomite. Svornost shaft, Adit level, Hildebrand vein. BSE image. Magnification 2300×.

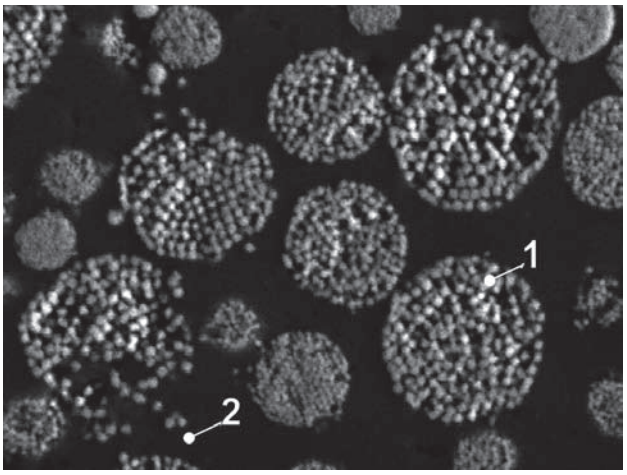

Fig. 143. J105P/B-3. 1 – pyrite, 2 – dolomite. Svornost shaft, Adit level, Hildebrand vein. BSE image. Magnification 900×.

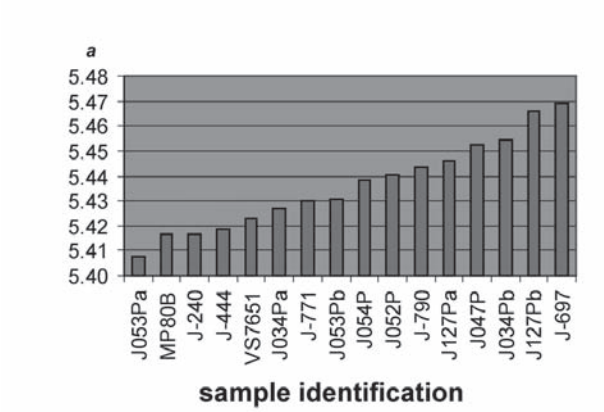

Fig. 146. Variation of unit-cell parameter *a* in a set of pyrite samples enriched in As from Jáchymov.

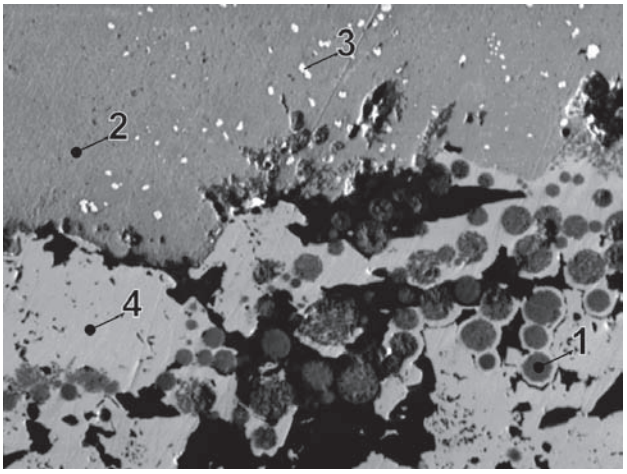

Fig. 144. J105P/E-1. 1 – pyrite, 2 – Sb-arsenic, 3 – dyscrasite, 4 – miargyrite. Svornost shaft, Adit level, Hildebrand vein. BSE image. Magnification 60×.

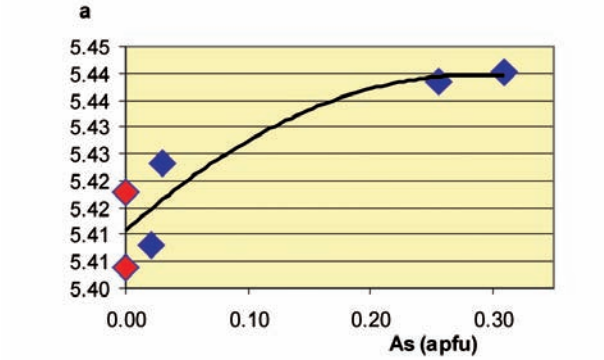

Fig. 147. Correlation of unit-cell parameter *a* and As content for pyrites enriched in As from Jáchymov. Red symbols show data for As-free pyrite, taken from [499].

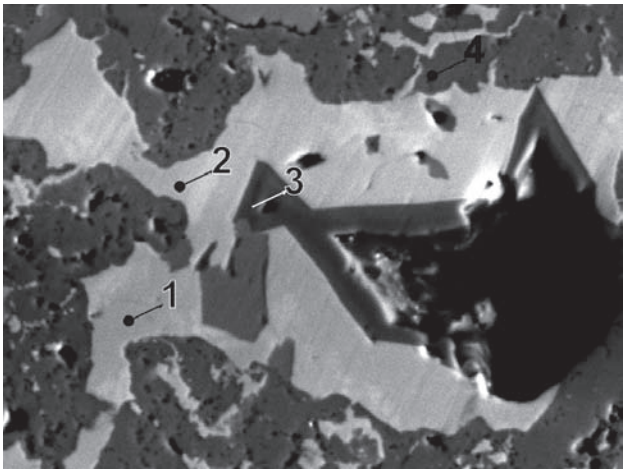

Fig. 145. MP72/G-1. 1 – Sb-gersdorffite (3 wt.% Sb), 2 – Sb-gersdorffite (11 wt.% Sb), 3 – As-Ni-pyrite, 4 – violarite. Eliáš mine, 2A vein. BSE image. Magnification 1150×.

Table 101. Calculated unit-cell parameters of pyrite from Jáchymov for the space group $Pa\bar{3}$.

sample	*a* (Å)
J034Pa	5.4267(5)
J034Pb	5.4543(5)
J-240	5.4169(2)
J-444	5.4185(4)
J-697	5.469(1)
J052P	5.4402(4)
J053Pa	5.408(2)
J053Pb	5.431(1)
J054P	5.4384(3)
J047P	5.4528(3)
J127Pa	5.4458(4)
J127Pb	5.466(2)
J-771	5.4299(3)
MP80B	5.4168(9)
J-790	5.4438(1)
VS7651	5.4232(4)

Table 102. Chemical analyses of pyrite.

sample	pt.	Fe	Co	Ni	Cu	Zn	Ag	S	As	Sb	Total
						weight %					
99453	1	43.63	1.01	1.01		0.92		52.87	0.56		100.00
99454	ab	42.81	0.67	1.06		0.59		52.89	0.75		98.77
99454	aa	43.29	0.59	1.02		0.14		53.06	0.98		99.08
99454	5	43.52	1.05	1.03		0.89		53.01	0.50		100.00
99454	6	43.69	1.11	1.06		0.94		52.51	0.68		99.99
99454	7	43.90	0.09	1.01		0.91		52.67	1.41		99.99
J017P	r13	42.92	0.80	0.81	0.42	0.79		47.43	6.45		99.62
J017P	r12	41.27	0.56	0.57	0.34	0.61		47.24	9.51		100.10
J017P	ar6	45.25	0.51	0.51	0.29	0.79		48.66	3.78		99.79
J017P	ar5	43.94	0.21	0.43		0.81		47.86	6.53		99.78
J042P	1	43.33		0.14		0.55	0.58	49.51	4.87	0.71	99.69
J052P	1	43.64	0.56	0.64	0.19			49.18	5.49	0.25	99.95
J052P	2	43.89	0.40	0.46	0.48			49.25	5.57	0.10	100.15
J052P	3	43.86	0.47	0.54	0.41			49.28	5.54	0.17	100.27
J052P	6	27.10	2.95	10.05	0.43			41.38	17.35		99.26
J053P	1	45.13	0.66	0.86	0.15			52.42	1.08	0.56	100.86
J053P	2	44.93	0.57	0.37	0.41			52.36	1.13	0.39	100.16
J053P	3	32.18	4.29	10.34	1.27			51.47	0.28	0.52	100.35
J053P	6	29.21	5.64	11.42	0.88			51.42	1.56	0.53	100.66
J053P	9	21.95	7.35	16.68	0.32			51.29	1.91	0.31	99.81
J053P	10	23.24	7.17	17.39	0.28			51.47	0.23	0.55	100.33
J053P	11	24.25	6.45	14.98	1.76			50.59	1.89	0.21	100.13
J053P	12	22.22	7.11	17.33	1.62			51.72	0.37	0.09	100.46
J054P	1	45.40	0.27	0.15	0.23			50.39	2.40	0.46	99.30
J054P	2	42.55	0.38	0.78	0.22			47.44	7.34	0.70	99.41
J054P	3	43.62	0.53	0.45	0.38			48.69	5.09	0.76	99.52
J054P	4	43.83	0.57	0.44	0.32			49.67	3.92	0.56	99.31
J054P	5	44.76	0.18	0.33	0.17			49.66	3.59	0.62	99.31
J054P	6	43.86	0.82	0.64	0.38			49.34	3.91	0.46	99.41
J054P	7	42.96	0.55	0.92	0.36			48.55	5.14	0.72	99.20
J054P	8	30.23	0.90	9.56	0.84			43.30	14.94	0.56	100.33
J054P	9	29.95	1.36	9.95	0.66			44.16	13.49	0.71	100.28
J054P	10	43.82	0.08	0.29	0.16			50.06	4.20	0.47	99.08
J054P	11	24.75	2.48	14.23	1.19			44.47	12.72	0.84	100.68
J054P	12	22.06	2.18	16.72	0.24			42.95	15.53	0.56	100.24
J054P	13	22.62	2.66	14.43	0.97			41.85	16.42	1.40	100.35
J066P	1	47.51						54.96			54.96
J099P	1	45.51					0.07	51.15	2.47	0.55	54.24
J099P	2	45.93					0.02	50.81	2.02	0.32	53.16
J099P	3	45.91					0.02	51.35	2.58	0.34	54.29
J118P	1	46.74		0.02		0.03		51.50	2.88		101.17
J181P	1	44.98	0.01		0.10			50.67	5.17		100.92
J181P	2	44.81						50.29	5.31		100.41
J181P	3	45.26						50.91	5.26		101.43
J181P	4	44.80						50.97	4.59		100.36
J183P	1	46.44						52.94	0.47		99.85
J183P	2	47.75						53.21	0.26		101.22
J183P	3	46.83		0.06	0.01			53.66	0.35		100.91
J183P	4	46.20	0.10		0.17			53.71	0.88		101.05
MP295	2	33.10	1.17	14.02	0.23			49.76	0.30	0.74	99.32
MP295	3	22.25	1.65	22.13	1.25			46.98	1.85	1.07	97.18
MP296	E1	42.14	0.19	2.37	0.06			49.44	6.59		56.03
MP296	E1a	22.65	3.34	19.49	0.14			48.95	5.15		99.73
MP296	B2	20.93	5.25	19.75	0.03			48.93	5.51		100.40
MP427	2	45.48						52.78	0.02		98.28
MP72	G	41.47	0.10	3.63				51.11	3.60	0.01	54.73
NM9520	1	45.29			0.07			51.86	1.63	0.14	98.99
NM9527	7	45.98					2.28	49.63	1.33		99.22
NM9527	8	45.56					3.61	48.94	1.25		99.36
NM9527	9	46.34					1.50	50.73	1.17		99.74
NM9527	10	46.59					2.07	50.79	1.25		100.70
NM9527	11	45.63					2.49	50.05	1.17		99.34
VS7651	1	47.49					0.91	50.23	1.56		100.20
VS7651	2	47.13					0.59	50.62	1.55		99.89
VS7651	3	47.41					0.45	50.22	1.53		99.61

Table 102. *(continued)*

sample	pt.	Fe	Co	Ni	Cu	Ag	Zn	subtotal	S	As	Sb	subtotal	Total
							number of atoms						
MP427	2	0.99						0.99	2.01			2.01	3
J066P	1	1.00						1.00	2.00			2.00	3
J183P	2	1.02						1.02	1.98			1.98	3
J053P	10	0.51	0.15	0.36	0.01			1.03	1.97		0.01	1.98	3
99454	ab	0.93	0.01	0.02			0.01	0.98	2.01	0.01		2.02	3
J183P	4	0.99						0.99	2.00	0.01		2.01	3
J183P	1	1.00						1.00	1.99	0.01		2.00	3
J183P	3	1.00						1.00	1.99	0.01		2.00	3
99454	5	0.94	0.02	0.02			0.02	1.00	1.99	0.01		2.00	3
99453	1	0.94	0.02	0.02			0.02	1.00	1.99	0.01		2.00	3
99454	6	0.95	0.02	0.02			0.02	1.01	1.98	0.01		1.99	3
J053P	12	0.49	0.15	0.36	0.03			1.02	1.97	0.01		1.98	3
J053P	3	0.70	0.09	0.22	0.02			1.03	1.96	0.01	0.01	1.97	3
MP295	2	0.74	0.03	0.30				1.06	1.93	0.01		1.93	3
99454	aa	0.94	0.01	0.02			0.00	0.98	2.01	0.02		2.02	3
99454	7	0.95		0.02			0.02	0.99	1.99	0.02		2.01	3
J053P	2	0.97	0.01	0.01	0.01			1.00	1.98	0.02		2.00	3
J053P	1	0.97	0.01	0.02				1.00	1.97	0.02	0.01	1.99	3
NM9527	9	1.02				0.02		1.04	1.94	0.02		1.96	3
NM9527	10	1.02				0.02		1.04	1.94	0.02		1.96	3
NM9527	11	1.01				0.03		1.04	1.94	0.02		1.96	3
NM9527	7	1.02				0.03		1.05	1.93	0.02		1.95	3
NM9527	8	1.02				0.04		1.07	1.91	0.02		1.93	3
NM9520	1	0.99						0.99	1.98	0.03		2.01	3
J053P	9	0.48	0.15	0.35	0.01			0.99	1.97	0.03		2.00	3
J053P	6	0.64	0.12	0.24	0.02			1.01	1.96	0.03	0.01	1.99	3
J099P	2	1.01						1.01	1.95	0.03		1.98	3
J053P	11	0.54	0.14	0.32	0.03			1.02	1.95	0.03		1.98	3
VS7651	2	1.03				0.01		1.04	1.93	0.03		1.96	3
VS7651	3	1.04				0.01		1.05	1.93	0.03		1.96	3
VS7651	1	1.04				0.01		1.05	1.92	0.03		1.95	3
MP295	3	0.52	0.04	0.49	0.03			1.06	1.89	0.03		1.93	3
J099P	3	1.00						1.00	1.95	0.04		1.99	3
J099P	1	1.00						1.00	1.95	0.04		2.00	3
J054P	1	1.00	0.01					1.01	1.94	0.04	0.01	1.98	3
J118P	1	1.01						1.01	1.94	0.05		1.99	3
MP72	G	0.91		0.08				0.99	1.95	0.06		2.01	3
J054P	5	1.00		0.01				1.00	1.92	0.06	0.01	1.99	3
J017P	ar6	1.01	0.01	0.01	0.01		0.02	1.05	1.89	0.06		1.95	3
J054P	10	0.98		0.01				0.98	1.94	0.07	0.01	2.02	3
J181P	4	0.98						0.98	1.94	0.07		2.02	3
J054P	4	0.98	0.01	0.01	0.01			1.00	1.93	0.07	0.01	2.00	3
J054P	6	0.98	0.02	0.01	0.01			1.02	1.92	0.07	0.01	1.99	3
J042P	1	0.97				0.01	0.01	0.99	1.93	0.08	0.01	2.01	3
J181P	1	0.98						0.98	1.93	0.08		2.01	3
J181P	2	0.99						0.99	1.93	0.09		2.01	3
J181P	3	0.98						0.98	1.93	0.09		2.02	3
J052P	2	0.97	0.01	0.01	0.01			1.00	1.91	0.09		2.00	3
J052P	1	0.97	0.01	0.01				1.00	1.91	0.09		2.00	3
MP296	E1a	0.51	0.07	0.42				1.00	1.91	0.09		2.00	3
MP296	B2	0.47	0.11	0.42				1.00	1.91	0.09		2.00	3
J054P	7	0.97	0.01	0.02	0.01			1.01	1.90	0.09	0.01	2.00	3
J054P	3	0.98	0.01	0.01	0.01			1.01	1.90	0.09	0.01	1.99	3
J052P	3	0.97	0.01	0.01	0.01			1.00	1.90	0.09		2.00	3
MP296	E1	0.93		0.05				0.99	1.90	0.11		2.01	3
J017P	r13	0.97	0.02	0.02	0.01		0.02	1.03	1.87	0.11		1.97	3
J017P	ar5	0.99		0.01			0.02	1.02	1.87	0.11		1.98	3
J054P	2	0.97	0.01	0.02				0.99	1.87	0.12	0.01	2.01	3
J017P	r12	0.93	0.01	0.01	0.01		0.01	0.98	1.86	0.16		2.02	3
J054P	11	0.58	0.06	0.32	0.02			0.97	1.80	0.22	0.01	2.03	3
J054P	9	0.70	0.03	0.22	0.01			0.96	1.80	0.24	0.01	2.04	3
J054P	8	0.71	0.02	0.21	0.02			0.96	1.77	0.26	0.01	2.04	3
J054P	12	0.52	0.05	0.38	0.01			0.95	1.77	0.27	0.01	2.05	3
J054P	13	0.54	0.06	0.33	0.02			0.95	1.74	0.29	0.02	2.05	3
J052P	6	0.65	0.07	0.23	0.01			0.96	1.73	0.31		2.04	3

crystals of *skutterudite* or as rims on *rammelsbergite*. Nickel content increases from the core of a sphere *(pyrite)* to the rim *(vaesite)*. The sample comes from the Bratrství shaft, 5th level, Františka vein.

Some specimens carry Fe and Ni disulphides in a close intergrowth. Two distinct types were recognized. Crystals with predominance of *pyrite* contain growth zones with variable Ni content and low variable Co content (*cattierite* component) (Fig. 139). Some large radiating *pyrite* aggregates contain growth zones with several mol.% of *vaesite* component. Patches with increased Ni occur near the base of *pyrite* aggregate.

Pyrite occurs in minor relics rimmed by narrow *magnetite* zone in *smythite* aggregates. An older *pyrite* in Fe-dolomite below *smythite* aggregates forms a rim around *sphalerite*. Both types of *pyrite* represent pure FeS_2.

Pyrostilpnite Ag_3SbS_3

According to Ježek [189], in the Museum of Natural History (Naturhistorisches Museum) in Vienna, there is a specimen of *pyrostilpnite*. A *pyrostilpnite* specimen is also in the National Museum, Prague, but this specimen comes from Příbram, though the label gives Jáchymov as the locality. It is possible that identification of this mineral is an error stemming from usage of old type mineral names. The name "Feuerblende" was used both for *xanthoconite* and *pyrostilpnite*, in a similar way as "Rotgültigerz" was used both for *proustite* and *pyragyrite*.

Pyrrhotite $Fe_{(1-x)}S$

Small columnar crystals described in the older literature [59], [391] as "*Magnetkies*" correspond clearly to *argentopyrite*, not *pyrrhotite*. *Pyrrhotite* was found as a rare mineral in the form of thin hexagonal plates, sometimes grouped in radiating aggregates. It is free of a notable contant of Ni, Co and As.

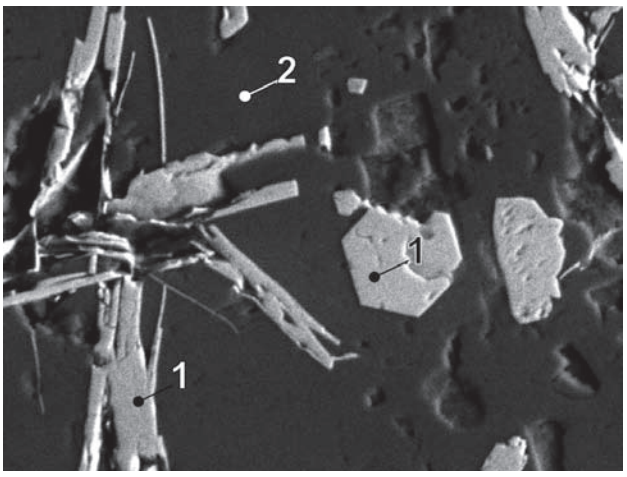

Fig. 148. G115A/E-1. 1 – pyrrhotite, 2 – carbonate. Svornost shaft, Geschieber vein. BSE image. Magnification 540×.

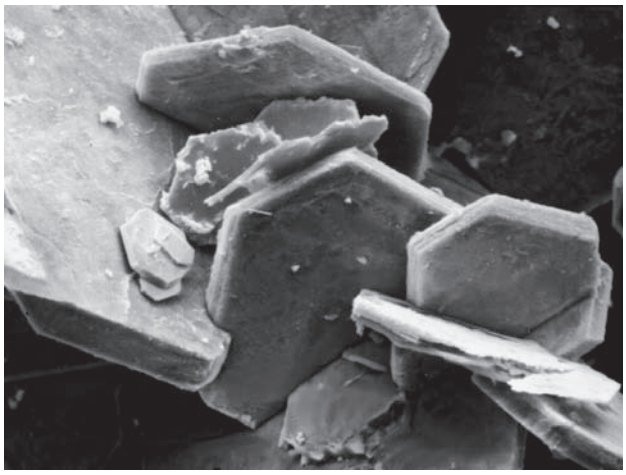
Fig. 149. Tabular crystal of pyrrhotite. Zimní Eliáš dump, SEM. Magnification 550×. Photo A. Gabašová.

Table 103. Calculated unit-cell parameters of pyrrhotite from Jáchymov for the space group $P3_121$.

sample	*a*	*c*
	(Å)	
G115A (J-822)	6.8705(6)	17.224(2)

Table 104. Chemical analyses of pyrrhotite.

sample	pt.	S	Fe	Cu	As	Total	Fe	S	x
		weight %					number of atoms		
G115A	E1	38.43	61.38		0.11	99.92	0.92	1.00	0.08
G115A	E2	39.40	60.88	0.06	0.15	100.49	0.89	1.00	0.11
G115A	E3	38.89	62.41	0.08	0.06	101.44	0.92	1.00	0.08
G115A	B	38.83	59.98	0.12	0.24	99.18	0.89	1.00	0.11
G115A	F	38.77	61.24	0.06	0.01	100.08	0.91	1.00	0.09

Pyrrhotite occurs in *dolomite* gangue of the Eliáš mine, and Svornost shaft (Geschieber vein), along contact of *dolomite* with *calcite.*

Quartz

Geceva and Dubinkina [358] studied in detail *quartz* and its generations. They classified *quartz* into the following types: pre-ore *quartz* (in relation to the U-mineralization) – hornfelsic and palisade *quartz* (followed by *dolomite* and older sulphides), intra-ore quartz of the chalcedony type (present only in the marginal parts of the ore district), and post-ore *quartz* (smoky *quartz*).

Mrňa and Pavlů (1967) [351] came to similar conclusions. They found out that *quartz* is the most common gangue mineral in the deposit. Especially in the deeper parts of veins, it is often the single vein-filling mineral. Significant quantities of *quartz* crystallized before deposition of the *carbonate–uraninite* mineralization stage. This includes mainly chalcedony-type *quartz*, ferruginous *quartz* and palisade *quartz*, classified in the *ore-free quartz* stage of mineralization.

The chalcedony type *quartz*, strongly brecciated, is compact, grey, with abundant microscopic clay mineral and *pyrite* inclusions. Ferruginous *quartz*, the most widespread variety in the veins, contains unevenly distributed pigment of *hematite* spherolites. Rare examples of pseudomorphs of ferruginous *quartz* after carbonates and barite were recorded. Ferruginous *quartz* was affected by an intense brecciation and healed by younger minerals, especially the palisade *quartz*, which partly fills even very narrow fractures. Palisade *quartz* overgrows fragments of wall-rock and contacts of vein with wall-rock and it fills cavities in *quartz* of older generations. Such rims, up to 0.5 cm wide, consist of euhedral crystals deposited on granular *quartz* matrix. Small transparent *quartz* crystals show sometimes amethystine tint in their tips, due to zoned distribution of hematite pigment. In some vein sections, a thin rim of *albite* takes the place of this *quartz* generation.

While for the chalcedony-type *quartz* and ferruginous *quartz* a deposition from solution of a colloidal character can be assumed, the palisade *quartz* crystallized from true solutions, though participation of residual solutions after deposition of the main part of colloidal silica is also possible.

The arsenide ores are associated with fine- to medium-grained, so-called "ore-quartz". This variety is semi-transparent, grey to black, with the dark portions carrying disseminated ore minerals. Main volumes of this *quartz* were deposited after crystallization of arsenide ores.

Later *quartz*, rarely accompanying ores of the *sulphidic* stage, shows characteristics similar to that of ore-quartz. Small amounts of chalcedony-like *quartz* grading to opal and ferruginous *quartz* were deposited in closing stages of the whole mineralization process.

Rammelsbergite $NiAs_2$

Mrňa and Pavlů (1967) [351] studied r*ammelsbergite* from Jáchymov. They found out that it accompanies dendritic *silver*, mainly as rims around *silver*, which can be separated from *silver* by a narrow zone of *uraninite* spherolites. *Rammelsbergite* frequently encloses irregular aggregates of *nickeline*, alternates with *nickeline* in thin aggregate growth zones, and fills fractures in large *nickeline* aggregates.

Table 105. Calculated unit-cell parameters of rammelsbergite from Jáchymov for the space group *Pnnm*.

sample	*a*	*b*	*c*
		(Å)	
HK24077	4.905(3)	5.854(3)	3.302(2)
J055P	4.7328(5)	5.7734(6)	3.5450(5)
J056P	4.7408(4)	5.7818(5)	3.5541(4)
J060P	4.843(2)	5.802(2)	3.434(2)
J100P (J-925)	4.7374(9)	5.781(1)	3.5504(9)
J-695	4.76(1)	5.790(5)	3.310(3)
J-719	4.727(1)	5.754(1)	3.537(1)
J-723	4.7577(7)	5.7858(8)	3.5266(7)
J-758	4.7220(5)	5.7672(5)	3.5579(4)
J-759	4.661(1)	5.771(2)	3.574(1)
J-775	4.771(1)	5.803(1)	3.542(1)
J-778	4.7540(4)	5.7880(4)	3.5380(3)
J-838	4.7535(3)	5.7918(2)	3.5522(3)
J-842	4.7498(2)	5.7894(2)	3.5474(2)
MP259D (J-802)	4.747(1)	5.796(1)	3.5461(9)
MP511C (J-922)	4.7525(5)	5.7893(6)	3.5428(4)

Fig. 150. Light grey rammelsbergite rims around nickeline aggregates (width of figure 2.4 cm). Photo J. & E. Sejkora.

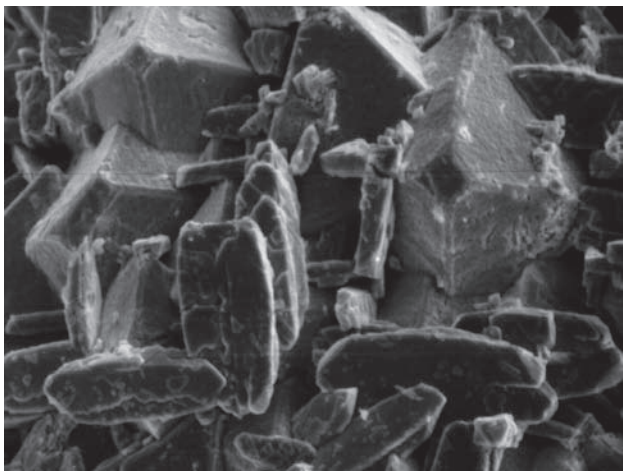

Fig. 151. J-723. Crystals of rammelsbergite and gersdorffite on nickeline. Svornost shaft, 10th level. SE image. Magnification 670×. Photo A. Gabašová.

Fig. 152. J-723. Detail of rammelsbergite crystal. Svornost shaft, 10th level. SE image. Magnification 280×. Photo A. Gabašová.

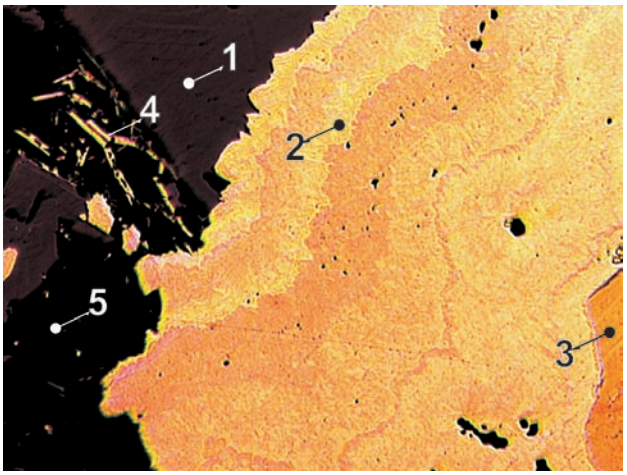

Fig. 153. J016P. Aggregates of nickeline are rimmed by zonal rammelsbergite with varying content of S. Lath-shaped lamellae of löllingite are in carbonate near margin of sphalerite aggregates. 1 – sphalerite, 2 – rammelsbergite, 3 – nickeline, 4 – löllingite, 5 – carbonate. Bratrství shaft. Reflected light, single polarizer. Magnification 160×.

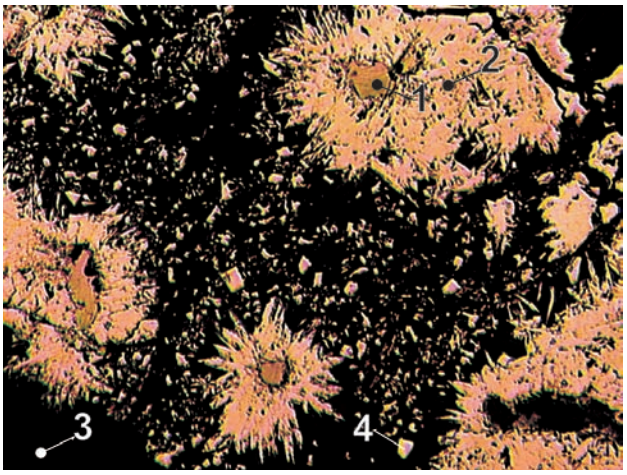

Fig. 154. J027P. Cores of radiating rammelsbergite aggregates, originally formed by native bismuth were later replaced by bismuthinite. Sporadic Ni-pyrite crystals are enclosed in carbonate. 1 – bismuthinite, 2 – rammelsbergite, 3 – carbonate, 4 – Ni-pyrite. Svornost shaft, 10th level. Reflected light, single polarizer. Magnification 130×.

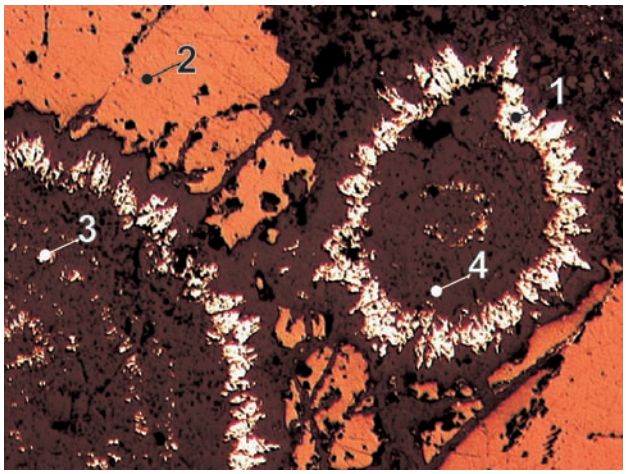

Fig. 155. J060P. Radiating rammelsbergite replaced botryoidal uraninite which was at an earlier stage partly replaced by gangue with nickel-skutterudite. Arsenides are in turn replaced by galena and botryoidal sphalerite. Individual pyrite grains occur in gangue. 1 – rammelsbergite, 2 – sphalerite, 3 – nickel-skutterudite, 4 – quartz. Rovnost I shaft, Geister vein. Reflected light, single polarizer. Magnification 160×.

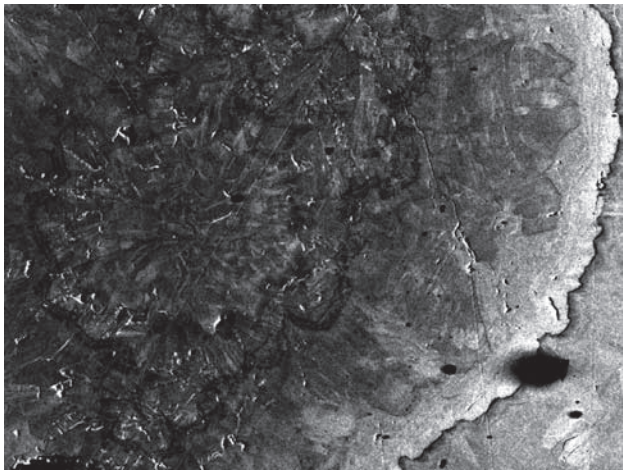

Fig. 156. J120P/A. Rammelsbergite. Barbora shaft, 5th level, vein No. 32. BSE image. Magnification 130×.

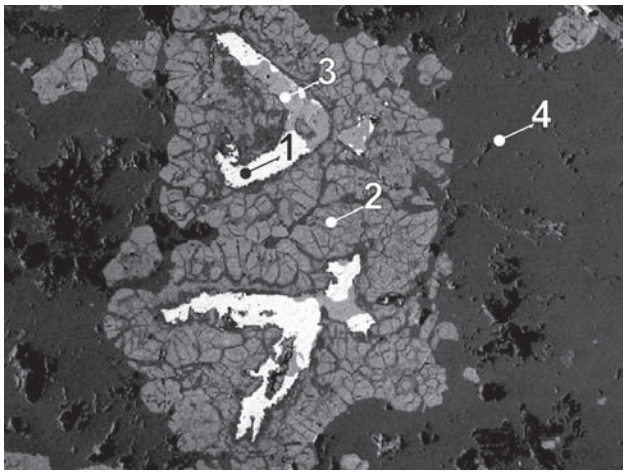

Fig. 157. MP27/B. 1 – bismuth, 2 – uraninite, 3 – aikinite and matildite, 4 – rammelsbergite. Eliáš mine. BSE image. Magnification 60×.

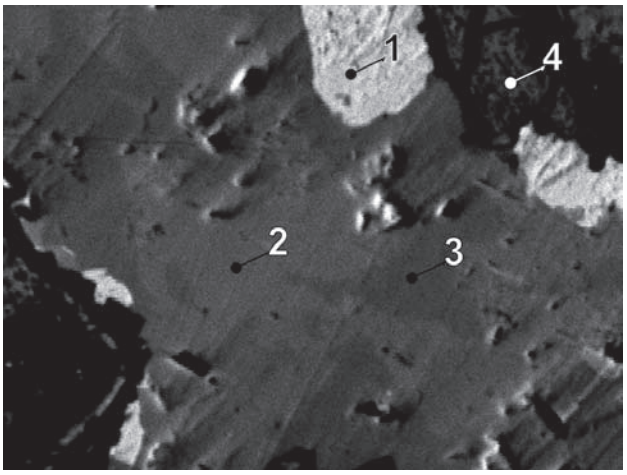

Fig. 158. MP27/B-1. 1 – bismuth, 2 – aikinite, 3 – matildite, 4 – uraninite. Eliáš mine. BSE image. Magnification 750×.

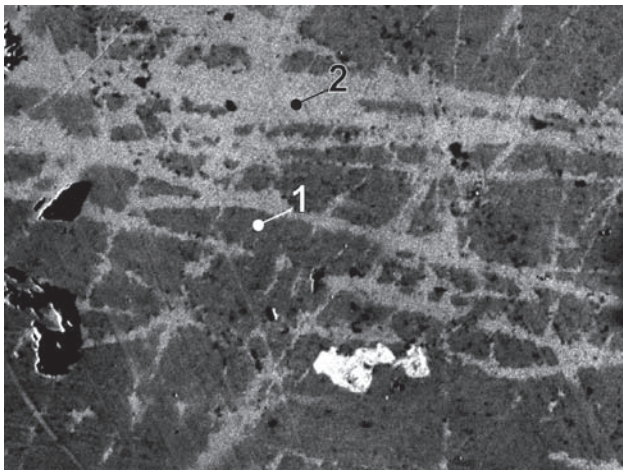

Fig. 159. MP27/C. 1 – S-rammelsbergite, 2 – rammelsbergite. Eliáš mine. BSE image. Magnification 60×.

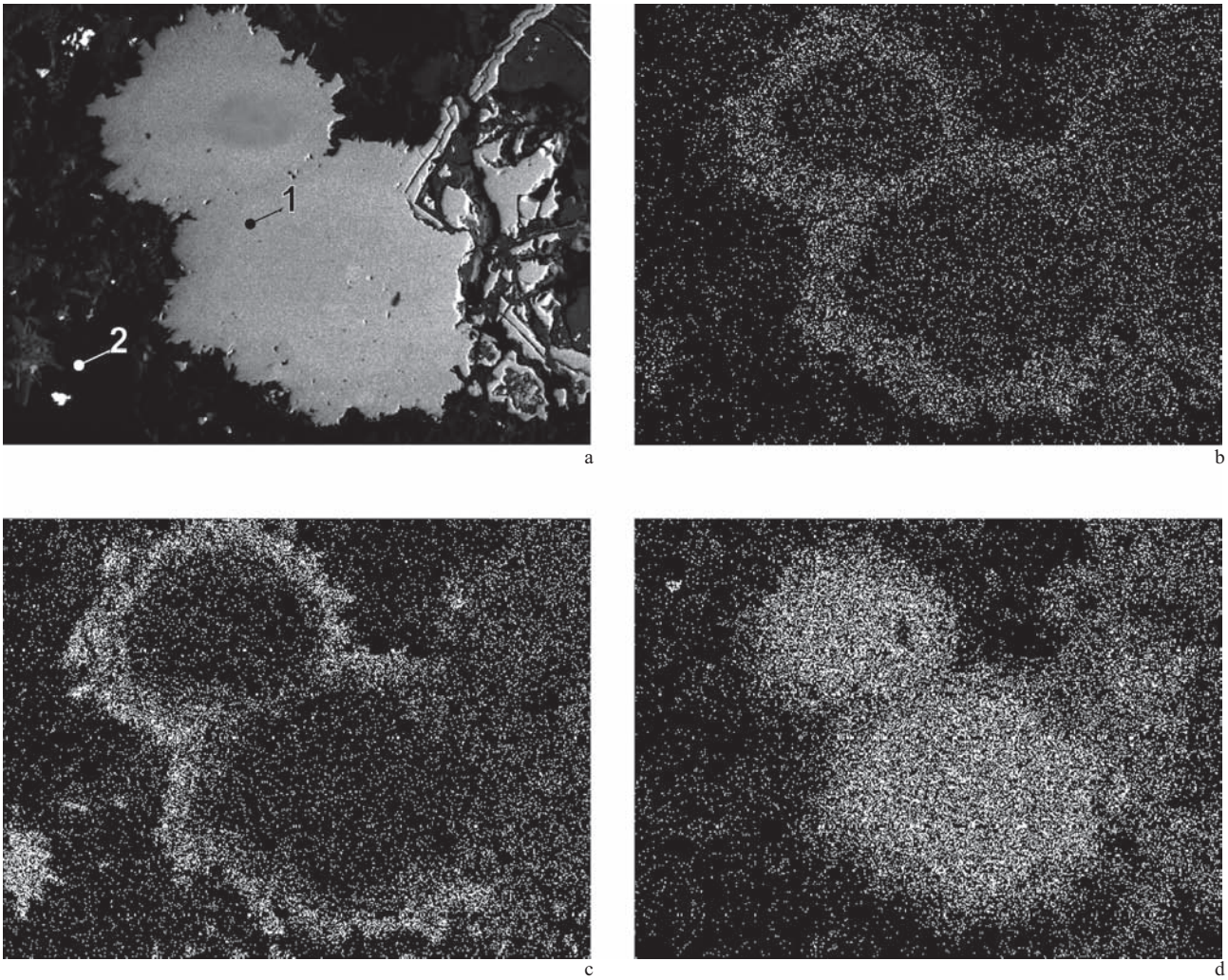

Fig. 160. MP36/C. 1 – rammelsbergite, 2 – calcite. Svornost shaft, 10th level, Geschieber vein. Magnification 130×.
a) BSE image.
b) Distribution of Co.
c) Distribution of Fe.
d) Distribution of Ni.

Table 106. Chemical analyses of rammelsbergite.

sample	pt.	Ni	Co	Fe	Zn	Cu	Ag	As	S	Sb	Total
						weight %					
J015P	aaa	27.00	0.42	0.54	0.35	0.21		70.21	0.79		99.52
J015P	aab	26.98	0.67	1.02	0.21	0.75		70.26	0.76		100.65
J017P	aa	27.34	0.59	0.48	0.19	0.33		70.62	0.67		100.22
J017P	ab	27.11	0.68	0.87	0.29	0.76		70.26	0.99		100.96
J017P	ar7	30.75	1.89	0.61		0.40		53.78	12.36		99.79
J017P	ar8	30.42	2.05	0.51		0.38		51.86	15.00		100.22
J017P	r5	27.54	0.45	0.69	0.28	0.50		69.02	0.79		99.27
J017P	r6	26.41	4.75	1.25	0.60	0.62		58.66	8.33		100.62
J017P	r7	27.12	5.23	1.14	0.88	0.71		55.09	9.99		100.16
J017P	r8	27.65	3.41	0.87	0.33	0.51		58.16	9.00		99.93
J024P	aaa	27.12	0.65	0.78	0.27	0.32		70.34	0.54		100.02
J024P	aab	27.31	0.48	0.78	0.34	0.71		69.99	1.01		100.62
J034P	10	32.60	0.55	2.38		0.49	0.28	42.68	18.97	2.77	100.72
J034P	13	17.93	7.99	1.86		0.13	0.07	70.33	0.43	0.66	99.40
J034P	14	24.65	1.33	0.79		0.73	0.03	71.26	0.29	0.68	99.76
J034P	15	23.59	1.18	2.27		0.67	0.07	71.72	0.35	0.74	100.59
J034P	16	22.62	2.75	1.74		0.61	0.07	72.20	0.45	0.47	100.91
J034P	17	26.96	0.53	0.46		0.05	0.08	72.08	0.07	0.55	100.78
J042P	a2	16.56	7.81	3.98	0.39	0.40	0.17	69.80	0.70	0.27	100.08
J042P	a6	12.97	10.09	4.07	0.49	0.83	0.39	69.67	0.68	0.60	99.79
J042P	3	11.15	10.18	4.21	0.49	0.58	0.13	71.58	0.86	0.41	99.59
J042P	4	13.70	9.44	3.61	0.24	0.60	0.25	70.62	0.62	0.68	99.76
J048P	5	24.89	0.94	0.57		1.28		72.07	0.25	0.14	100.14
J048P	6	24.68	0.84	0.49		1.46		72.13	0.26	0.12	99.98
J048P	7	24.65	0.59	0.55		1.77		72.69	0.28	0.15	100.68
J048P	8	17.84	4.96	3.79		0.85		72.28	0.27	0.17	100.16
J048P	11	23.98	1.46	0.79		1.05		72.13	0.20	0.13	99.74
J050P	4	20.54	5.91	0.70		0.98		71.68	0.20	0.24	100.25
J055P	1	25.25	2.67	0.34		0.44		70.34	1.55	0.18	100.77
J055P	3	25.59	1.82	0.24		0.55		70.12	1.18	0.28	99.78
J055P	5	25.38	0.78	0.40		0.61		70.65	1.47	0.27	99.56
J056P	13	26.88	0.94	0.60		0.61		69.08	2.39	0.19	100.69
J056P	16	27.62	0.69	0.27		0.33		69.60	2.10	0.17	100.78
J056P	17	27.46	0.86	0.13		0.42		69.27	2.06	0.13	100.33
J057P	10	26.55	1.65	0.17	0.76	0.64		68.65	1.68	0.36	100.46
J057P	13	25.96	1.57	0.24	0.52	0.57		69.40	1.73	0.51	100.50
J059P	4	12.76	3.93	10.24	0.46	1.38		70.62	0.19	0.36	99.94
J060P	4	14.56	8.08	5.47	0.19	0.29		65.37	5.74		99.70
J060P	5	14.63	7.82	5.48	0.61	0.33		65.80	4.83	0.28	99.78
J060P	6	14.91	7.93	5.72	0.54	0.58		64.10	5.02	0.69	99.49
J060P	7	16.20	7.48	4.73	0.65	0.77		64.94	4.83	0.22	99.82
J060P	8	15.70	7.72	5.39	0.94	0.66		64.53	4.33	0.44	99.71
J060P	9	15.52	7.90	5.12	0.11	0.19		64.85	5.43	0.33	99.45
J060P	10	16.61	4.39	7.27	0.74	0.54		64.27	5.75	0.18	99.75
J060P	11	18.83	3.30	5.05	0.18	0.31		67.52	3.73	0.59	99.51
J060P	13	11.62	9.78	9.08	0.26	0.39		63.13	5.06	0.38	99.70
J060P	17	20.41	4.47	2.68	0.12	0.49		68.75	2.24	0.38	99.54
J060P	18	18.39	6.14	3.34	0.35	0.33		67.32	3.52	0.27	99.66
J060P	19	15.06	7.64	5.24	0.52	0.36		66.15	4.50	0.20	99.67
J060P	21	14.51	7.83	6.31		0.66		64.71	5.05	0.50	99.57
J060P	22	17.99	6.39	4.06	0.28	0.32		65.45	4.79	0.40	99.68
J060P	23	18.62	3.53	5.28	0.51	0.33		67.04	3.41	0.85	99.57
J104P	1	27.85	0.13				0.10	71.63		0.12	99.83
J117P	A	28.15	2.75	0.18				64.36	4.14	0.17	99.75
J123P	A	16.17	10.01	2.25		0.21		71.98	0.56		101.19
J140P	B1	23.00	4.56	1.37		0.13		67.46	4.13	0.02	100.67
J140P	B2	24.20	5.57	0.67				62.77	6.90	0.19	100.30
J140P	B3	23.04	3.87	1.10				68.26	2.64	0.11	99.02
J140P	B4	23.26	4.19	1.19		0.02		69.48	2.88	0.09	101.12
MP27	A	28.10	1.22	0.17				70.06	0.99		100.53
MP27	C	28.32	0.49	0.00		0.03		70.94	0.53	0.18	100.49
MP27	C1	27.89	2.06	0.02				65.51	3.50		98.97
MP287D	1	27.48	0.95	0.20		0.53		68.95	0.90	0.57	99.58
MP287D	2	27.26	1.08	0.14		0.53		69.87	0.82	0.39	100.09

(continued)

Table 106. *(continued)*

sample	pt.	Ni	Co	Fe	Zn	Cu	Ag	As	S	Sb	Total
						weight %					
MP287D	6	26.68	1.44	0.45		0.56		68.61	1.26	0.52	99.52
MP296	B	29.54	0.01	0.10		0.23		70.86	0.22		100.95
MP36	C1	16.57	7.75	3.87	0.11	0.04		71.22	0.22		99.77
MP36	C3	25.79	1.32	0.39	0.04	0.77	0.09	71.68	0.03		100.11
MP430	2	28.03	1.00	0.43		0.49		69.13	0.63	0.58	100.29
MP430	4	24.09	6.89	0.45		0.75		60.13	7.91	0.23	100.45
MP430	5	24.38	7.27	0.59		0.43		59.32	8.16	0.56	100.71
MP430	6	25.03	7.97	0.86		0.61		56.03	8.84	0.47	99.81
MP431	3	28.12	0.75	0.44		0.65		69.81	0.25	0.38	100.40
MP431	4	30.03	0.53	0.71		0.72		61.08	7.84	0.80	101.71
MP483	C1	29.46	2.79	0.08	0.02		0.02	60.77	7.83	0.18	101.15
MP483	C2	29.79	2.44	0.16	0.18			61.73	7.03		101.32
MP511C	A1	26.97	1.13	0.79	0.01			70.38	1.92		101.21
MP511C	A2	26.59	1.07	0.70	0.06			68.75	1.83	0.24	99.24
MP511C	A3	26.52	1.15	0.80		0.10		69.12	1.47	0.09	99.25
MP511C	A4	26.90	1.08	0.60				69.07	1.58	0.16	99.39
MP511C	A5	27.56	0.41	0.13		0.02		71.66	0.62	0.05	100.45
MP511C	An1	27.38	0.35	0.59	0.06	0.20		71.05	0.69		100.33
MP511C	An2	27.11	0.65	0.60		0.26		71.49	0.37		100.48
MP511C	An3	27.95	0.08	0.01	0.18			72.27	0.09		100.59
MP511C	B1	27.02	0.39	0.41		0.30		71.19	0.65	0.01	99.97
MP511C	B2	26.94	0.54	0.23		0.45		71.83	0.34	0.14	100.47
MP511C	B3	27.08	0.76	0.22	0.04	0.06		71.10	0.80		100.06

sample	pt.	Ni	Co	Fe	Zn	Cu	Ag	subtotal	As	S	Sb	subtotal	Total
							number of atoms						
J048P	11	0.86	0.05	0.03		0.04		0.97	2.01	0.01		2.03	3
J048P	6	0.88	0.03	0.02		0.05		0.97	2.01	0.02		2.03	3
J048P	7	0.87	0.02	0.02		0.06		0.97	2.01	0.02		2.03	3
J034P	17	0.95	0.02	0.02				0.99	2.00	0.01	0.01	2.01	3
MP511C	An3	0.99			0.01			1.00	2.00	0.01		2.00	3
J104	1	0.99						1.00	2.00	0.01		2.00	3
J048P	8	0.63	0.18	0.14		0.03		0.98	2.00	0.02		2.02	3
J048P	5	0.88	0.03	0.02		0.04		0.98	2.00	0.02		2.02	3
J050P	4	0.73	0.21	0.03		0.03		0.99	1.99	0.01		2.00	3
MP36	C3	0.92	0.05	0.01	0.03			1.00	1.99	0.01		2.00	3
J034P	14	0.88	0.05	0.03		0.02		0.98	1.99	0.02	0.01	2.02	3
J034P	16	0.80	0.10	0.06		0.02		0.98	1.99	0.03	0.01	2.02	3
J042P	3	0.40	0.36	0.16	0.02	0.02		0.95	1.99	0.06	0.01	2.05	3
MP36	C1	0.59	0.27	0.14				1.01	1.98	0.01		1.99	3
J034P	15	0.83	0.04	0.08		0.02		0.98	1.98	0.02	0.01	2.02	3
MP511C	B2	0.95	0.02	0.01		0.01		0.99	1.98	0.02		2.01	3
MP511C	An2	0.95	0.02	0.02		0.01		1.01	1.97	0.02		1.99	3
MP511C	B1	0.95	0.01	0.02		0.01		0.99	1.97	0.04		2.01	3
MP511C	A5	0.97	0.01					0.99	1.97	0.04		2.01	3
J034P	13	0.64	0.28	0.07				1.00	1.96	0.03	0.01	2.00	3
J042P	4	0.49	0.33	0.14	0.01	0.02	0.01	0.99	1.96	0.04	0.01	2.01	3
J123	A	0.56	0.35	0.08	0.01			1.00	1.96	0.04		2.00	3
MP511C	B3	0.95	0.03	0.01				0.99	1.96	0.05		2.01	3
J059P	4	0.45	0.14	0.38	0.02	0.05		1.03	1.95	0.01		1.97	3
MP27	C	0.99		0.02				1.01	1.95	0.03		1.98	3
MP511C	An1	0.96	0.01	0.02		0.01		1.00	1.95	0.04		2.00	3
J055P	5	0.89	0.03	0.02		0.02		0.95	1.95	0.10		2.04	3
MP296	B	1.03						1.04	1.94	0.01		1.96	3
J024P	aaa	0.96	0.02	0.03	0.01	0.01		1.03	1.94	0.04		1.98	3
J017P	aa	0.96	0.02	0.02	0.01	0.01		1.02	1.94	0.04		1.99	3
J015P	aaa	0.95	0.02	0.02	0.01	0.01		1.01	1.94	0.05		1.99	3
J042P	a6	0.46	0.36	0.15	0.02	0.03	0.01	1.02	1.93	0.04	0.01	1.98	3
J055P	3	0.90	0.06	0.01		0.02		0.99	1.93	0.08		2.01	3
MP431	3	0.99	0.03	0.02		0.02		1.05	1.92	0.02	0.01	1.95	3
J042P	a2	0.58	0.27	0.15	0.01	0.01		1.03	1.92	0.05	0.01	1.97	3

(continued)

Table 106. *(continued)*

sample	pt.	Ni	Co	Fe	Zn	Cu	Ag	subtotal	As	S	Sb	subtotal	Total
						number of atoms							
J015P	aab	0.94	0.02	0.04	0.01	0.02		1.03	1.92	0.05		1.97	3
MP287D	2	0.96	0.04	0.01		0.02		1.02	1.92	0.05	0.01	1.98	3
J017P	r5	0.97	0.02	0.03	0.01	0.02		1.04	1.91	0.05		1.96	3
MP27	A	0.98	0.01	0.04				1.03	1.91	0.06		1.97	3
J024P	aab	0.95	0.02	0.03	0.01	0.02		1.03	1.91	0.06		1.97	3
J017P	ab	0.94	0.02	0.03	0.01	0.02		1.03	1.91	0.06		1.97	3
MP287D	1	0.97	0.03	0.01		0.02		1.03	1.91	0.06	0.01	1.97	3
J055P	1	0.87	0.09	0.01		0.01		0.99	1.91	0.10		2.01	3
MP430	2	0.98	0.04	0.02		0.02		1.05	1.90	0.04	0.01	1.95	3
MP511C	A3	0.93	0.04	0.03		0.00		1.00	1.90	0.09		2.00	3
MP287D	6	0.94	0.05	0.02		0.02		1.02	1.89	0.08	0.01	1.98	3
MP511C	A4	0.94	0.04	0.02		0.00		1.00	1.89	0.10		2.00	3
J057P	13	0.90	0.05	0.01	0.02	0.02		1.00	1.89	0.11		2.00	3
MP511C	A1	0.92	0.04	0.03		0.00		0.99	1.89	0.12	0.00	2.01	3
MP511C	A2	0.93	0.04	0.03		0.00		0.99	1.88	0.12		2.01	3
J056P	17	0.95	0.03	0.01		0.01		1.00	1.87	0.13		2.00	3
J056P	16	0.95	0.02	0.01		0.01		0.99	1.87	0.13		2.01	3
J060P	17	0.71	0.16	0.10		0.02		0.98	1.87	0.14	0.01	2.02	3
J057P	10	0.92	0.06	0.01	0.02	0.02		1.03	1.86	0.11		1.97	3
J140P	B3	0.80	0.13	0.04				0.97	1.86	0.17		2.03	3
J056P	13	0.92	0.03	0.02		0.02		0.99	1.85	0.15		2.00	3
J140P	B4	0.79	0.14	0.04				0.97	1.85	0.18		2.03	3
J060P	11	0.64	0.11	0.18	0.01	0.01		0.95	1.81	0.23	0.01	2.05	3
J060P	23	0.64	0.12	0.19	0.02	0.01		0.97	1.80	0.21	0.01	2.03	3
J060P	18	0.63	0.21	0.12	0.01	0.01		0.98	1.80	0.22		2.02	3
J140P	B1	0.77	0.15	0.05				0.98	1.77	0.25		2.02	3
MP27	C1	0.95		0.07				1.03	1.76	0.22		1.97	3
J060P	19	0.51	0.26	0.19	0.02	0.01		0.98	1.74	0.28		2.02	3
J060P	5	0.49	0.26	0.19	0.02	0.01		0.97	1.73	0.30	0.01	2.03	3
J060P	22	0.60	0.21	0.14	0.01	0.01		0.98	1.72	0.29	0.01	2.02	3
J117P	A	0.95	0.01	0.09				1.05	1.70	0.25		1.95	3
J060P	8	0.53	0.26	0.19	0.03	0.02		1.03	1.70	0.27	0.01	1.97	3
J060P	7	0.54	0.25	0.17	0.02	0.02		1.00	1.70	0.30		2.00	3
J060P	21	0.49	0.26	0.22		0.02		0.99	1.70	0.31	0.01	2.01	3
J060P	4	0.48	0.27	0.19	0.01	0.01		0.96	1.70	0.35		2.05	3
J060P	9	0.52	0.26	0.18		0.01		0.97	1.69	0.33	0.01	2.03	3
J060P	6	0.50	0.27	0.20	0.02	0.02		1.00	1.68	0.31	0.01	2.00	3
J060P	10	0.55	0.15	0.25	0.02	0.02		0.99	1.66	0.35		2.02	3
J060P	13	0.39	0.32	0.32	0.01	0.01		1.05	1.64	0.31	0.01	1.95	3
J140P	B2	0.79	0.18	0.02				0.99	1.60	0.41		2.01	3
MP483	C2	0.95	0.01	0.08				1.04	1.55	0.41		1.96	3
MP431	4	0.95	0.02	0.02		0.02		1.02	1.52	0.46	0.01	1.99	3
MP483	C1	0.94		0.09				1.03	1.51	0.46		1.97	3
MP430	4	0.77	0.22	0.02		0.02		1.03	1.51	0.46		1.97	3
MP430	5	0.78	0.23	0.02		0.01		1.04	1.48	0.48	0.01	1.96	3
J017P	r6	0.84	0.15	0.04	0.02	0.02		1.06	1.46	0.48		1.94	3
J017P	r8	0.88	0.11	0.03	0.01	0.02		1.04	1.44	0.52		1.96	3
MP430	6	0.79	0.25	0.03		0.02		1.09	1.39	0.51	0.01	1.91	3
J017P	r7	0.84	0.16	0.04	0.03	0.02		1.09	1.34	0.57		1.91	3
J017P	ar7	0.94	0.06	0.02		0.01		1.03	1.29	0.69		1.98	3
J017P	ar8	0.90	0.06	0.02		0.01		0.99	1.20	0.81		2.01	3
J034P	10	0.93	0.02	0.07		0.01		1.03	0.95	0.99	0.04	1.97	3

The outer shape of *rammelsbergite* aggregates is usually irregular or botryoidal and euhedral crystals are rare. *Rammelsbergite* rims around native metals show a zoning structure (Fig. 150), with individual zones showing different resistence to oxidation in air. The internal structure of zoned aggregates indicates that the zones mimic shape of dendritic *silver*, serving as matrix for *rammelsbergite.* It sometimes forms radiating aggregates [351].

The present study confirmed observations by Mrňa and Pavlů [351] and characterizes rammelsbergite as belonging to abundant minerals in the deposit. It is newly found in rims around bismuth. It also forms individual grains or larger aggregates. It shows a strong anisotropy and aggregate extinction in polished sections. It is often associated with *nickel-skutterudite.* Reported zoning of *rammelsbergite* aggregates may be explained by variation in

Table 107. Unusual X-ray diffraction pattern of (Co,Fe)-rammelsbergite sample No. J060P.

h	*k*	*l*	I_{obs}	d_{obs}
1	1	0	18	3.716
0	1	1	8	2.938
0	2	0	13	2.897
1	0	1	70	2.788
1	1	1	68	2.512
1	2	0	72	2.486
2	0	0	9	2.422
2	1	0	29	2.234
1	2	1	14	2.009
2	1	1	60	1.8688
2	2	0	4	1.8579
1	3	0	15	1.7937
0	0	2	24	1.7048
0	3	1	31	1.6803
2	2	1	24	1.6314
1	3	1	21	1.5875
3	1	0	4	1.5552
1	1	2	8	1.5495
2	3	0	5	1.5098
3	0	1	1	1.4591

sulphur content or by intergrowth with *löllingite* or *gersdorffite*.

Rammelsbergite occasionally occurs in extremely fine intergrowth with *gersdorffite*, impossible to separate by electron microprobe. As the As/S ratio varies the analyses do not allow distinguishing *S-rammelsbergit* from *As-gersdorffite*. Both minerals contain (atomic values) As+S twice the total of (Ni+Co+Fe) and their compositions may overlap. Observation of optical properties helps in identification (Fig. 153), but it is optimal to use X-ray diffraction, where possible, for identification (Tables 105 and 107). Thus, published chemical analyses should be considered with reservation if the analysed minerals were not identified by other methods as well.

Some radiating spheroidal aggregates show distinct zoning in BSE images (Fig. 154). With optical microscope, such aggregates show poorly defined zones with variation in porosity and a weak anisotropy of flame-shaped domains with radiating pattern. The aggregate is identified by XRD as a mixture of *gersdorffite* a *rammelsbergite.* The sample comes from the Schönerz adit.

A branching network of younger *rammelsbergite* veinlets penetrates *rammelsbergite* in one sample. Older generation contains 0.5 wt.% S, the younger one 3.5 wt.% S. The sample comes from the Eliáš mine.

Rammelsbergite also occurs as a matrix intergrown with myrmekitic *bismuth,* corresponding probably to domains of an unstable unidentified mineral. Such aggregates occur as zones or cores in *nickel-skutterudite* (Fig. 155). *The* orientation of *bismuth* particles may indicate structural orientation of the original phase.

Rammelsbergite aggregates as perimorphs after *silver* are deposited on matrix of crystallized palisade *quartz* next to wall-rock. This assemblage was later partly covered with pinkish *dolomite*. *Argentite*, deriving Ag probably from dendritic native *silver*, is deposited on *dolomite* and itself partly covered by *dolomite* and by coarse-grained *calcite*. Low-temperature minerals including *imiterite*, *acanthite*, *cinnabar* and *sternbergite* are often deposited at the contact of pink *dolomite* with light *calcite*.

Realgar AsS

Zippe [239] mentioned *realgar* as small prismatic crystals accompanied by *calcite* and deposited on *arsenic*. It was also studied by Mrňa and Pavlů [351]. Notable

Table 108. Calculated unit-cell parameters of realgare from Jáchymov for the space group $P2_1/n$.

sample	*a*	*b*	*c*	β
		(Å)		(°)
J-212	9.343(1)	13.581(1)	6.5939(5)	106.34(1)
VS4231	9.340(1)	13.583(1)	6.5963(4)	106.47(5)

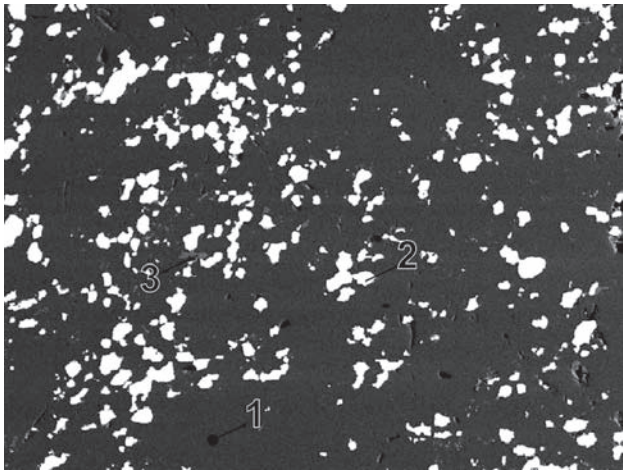

Fig. 161. VS4231. 1 – realgar, 2 – bismuth, 3 – arsenic. BSE image. Magnification 115×.


Fig. 162. Red realgar crystals on arsenic gangue (width of figure 4.4 mm). Photo J. & E. Sejkora.

quantities of this mineral were recorded in historic works in upper levels of the Geschieber vein, Svornost shaft [119].

It was also found in new works in upper levels of the Geschieber vein. *Realgar* in earthy coatings and anhedral grains in botryoidal aggregates is associated with *arsenic* or fills fractures in carbonate gangue. Prismatic crystals up to several mm long also occur [351].

The present study of samples collected at various periods shows that *realgar* occurs always in proximity of *arsenic*, usually deposited directly on botryoidal *arsenic*. The crystals are equant to short prismatic, with typical flame-like, orange-red colour (Fig. 162). *Realgar* in ore breccia with *arsenic* and *nickel-skutterudite* is rare. Some grains of this type are dark red to black, due to finely dispersed anhedral inclusions of *bismuth*.

Robinsonite $Pb_4Sb_6S_{13}$

Robinsonite was found as a single 5 μm grain of round shape, intergrown with *bismuth* in a small vug in *arsenic*, filled by *calcite*. The sample contains the paragenesis of *arsenic–miargyrite–antimony–stibnite*. It was collected in the Svornost shaft, Adit level, Hildebrand vein.

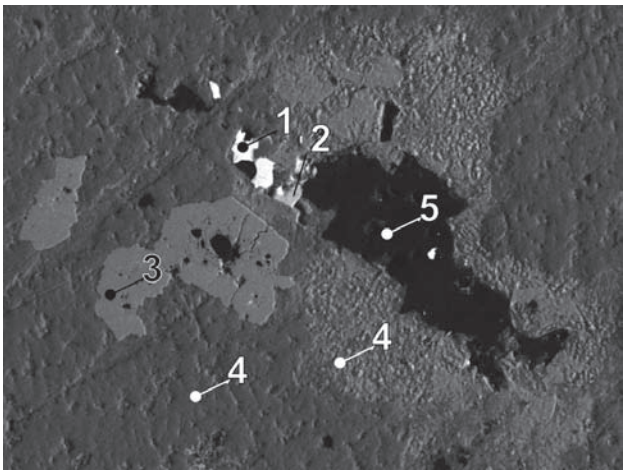

Fig. 163. J105P/A-2. 1 – bismuth, 2 – robinsonite, 3 – nickel-skutterudite, 4 – arsenic, 5 – calcite. Svornost shaft, Adit level, Hildebrand vein. BSE image. Magnification 160×.

Table 109. Chemical analysis of robinsonite.

sample	pt.	Pb	Ag	Cu	Fe	Sb	As	S	Total
					weight %				
J105P	A2	42.21	0.30	0.08	0.01	34.42	0.60	22.39	100.00

sample	pt.	Pb	Cu	Ag	subtotal	Sb	As	S	subtotal	S	Total
						number of atoms					
J105P	A2	3.91	0.02	0.05	3.99	5.43	0.15	0.41	6.00	13.01	23

Roquesite $CuInS_2$

Roquesite forms isolated grains up to 5 μm, always enclosed in *mawsonite* rimming *stannite*. These aggregates are enclosed in *chalcopyrite* deposited on crystals of smoky *quartz*. *Roquesite* contains low Fe. It is a very rare mineral limited to the southeastern part of the deposit, in paragenesis with *arsenopyrite*, *cassiterite*, *chalcopyrite*, *bornite*, *pyrite*, *tennantite*, and *galena*.

The sample with *roquesite* contains two types of *stannite* – grains enclosed in *chalcopyrite*, and myrmekitic particles exsolved from *chalcopyrite*. The two types show similar compositions with Fe/Zn ratio varying up to *kësterite.* In contrast, *mawsonite* in rims around *stannite* of the first type contains low Zn up to 2 wt.%. This may indicate that domains with myrmekitic *stannite* represent a former unstable phase. The sample comes from the Giftkies adit.

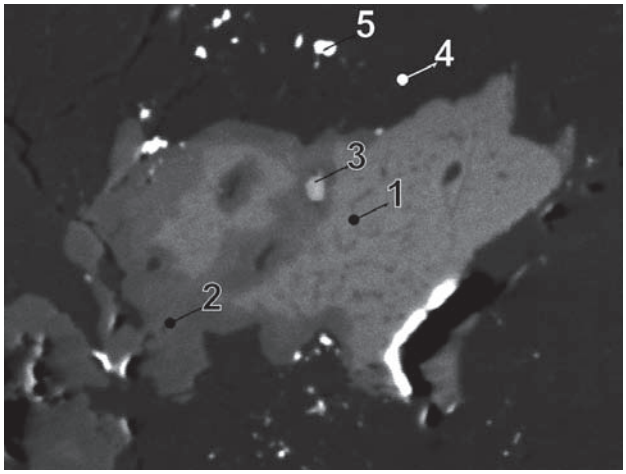

Fig. 164. J066P/2. 1 – stannite, 2 – mawsonite, 3 – roquesite, 4 – chalcopyrite, 5 – galena. Adit No. 21. BSE image. Magnification 800×.

Roscoelite $(K,\square)(V,Al)_2AlSi_3O_{10}(OH)_2$

Roscoelite occurs in graphitic mica schist next to the vein, impregnated by sulphides, mainly *pyrite*, *chalcopyrite, tennantite,* and *uraninite* with *coffinite* [345]. Vanadium is released by weathering, giving rise to *tyuyamunite*, whose contrasting yellow colour marks *roscoelite*-bearing bands in the rock.

This type of weathering is typical of upper parts near surface, characterized by faster reactions. In lower parts of the Geister vein, characterized by *mottramite*, a connection to *roscoelite* is not estabilished.

It also occurred as soft black aggregates up to 0.5 cm in red hornfelsic quartz from the Geister vein.

Table 110. Chemical analyses of roscoelite.

sample	pt.	Na_2O	MgO	Al_2O_3	SiO_2	K_2O	CaO	TiO_2	V_2O_3	MnO	FeO	CuO	ZnO	Total
							weight %							
J021P	1	0.45	2.52	17.04	50.40	7.27	0.47	0.29	10.59	0.52	5.80	1.91		97.26
J021P	2	0.17	1.83	13.41	47.76	8.58	0.49	0.28	21.10	0.21	3.57	1.63		99.03
J021P	3	0.30	1.89	13.70	48.59	8.07	0.33	0.39	18.53	0.34	4.18	1.71		98.03
J021P	4		1.84	13.43	49.56	8.49	0.30	0.22	20.87	0.30	3.12	1.31		99.44
J021P	5		1.93	13.16	48.63	8.14	0.27	0.26	20.38	0.54	3.54	1.31		98.16
J021P	6	0.55	3.08	17.94	51.67	7.52	0.39	0.17	9.80	0.40	4.79	2.17		98.48
J021P	7	0.56	3.11	17.75	51.78	6.95	0.59	0.25	8.60	0.36	5.90	2.95		98.80
J021P	8	0.52	1.97	13.95	47.99	6.74	0.47	0.28	16.37	0.58	6.72	1.96		97.55
[345]	1	0.18	1.27	11.39	45.94	7.03	0.46	0.19	18.44	0.32	8.74	3.82	0.74	98.52
[345]	2	0.13	1.40	11.80	46.88	6.92	0.52	0.24	18.02	0.28	8.75	3.01	0.55	98.50
[345]	3	0.10	1.29	11.55	46.33	6.75	0.49	0.27	16.96	0.23	10.68	3.01	0.83	98.49
[345]	4	0.06	1.10	11.14	43.31	6.95	0.67	0.30	16.77	0.41	10.94	3.15	0.69	98.49
[345]	5		1.15	11.82	46.59	6.95	0.63	0.23	15.61	0.28	10.89	3.71	0.67	98.50
[345]	6		1.02	11.53	47.60	7.63	0.52	0.31	17.86	0.44	8.92	1.95	0.70	98.48
[345]	7	0.15	1.11	11.10	46.68	6.32	0.51	0.31	16.33	0.47	11.77	3.03	0.71	98.49
[345]	8	0.18	1.35	11.83	47.28	6.76	0.50	0.30	18.30	0.34	8.24	2.59	0.83	98.50
[345]	9	0.24	1.62	12.36	48.34	6.52	0.49	0.31	18.86	0.33	7.13	1.76	0.54	98.50

sample	pt.	K^+	Na^+	Ca^{2+}	Cu^{2+}	Fe^{2+}		sub-total	V^{3+}	Al^{3+}	Fe^{2+}	Mn^{2+}	Mg^{2+}	sub-total	Al^{3+}	Ti^{4+}	Si^{4+}	sub-total	O
								number of atoms											
J021P	1	0.64	0.06	0.04	0.10	0.06	0.10	1	0.58	0.86	0.27	0.03	0.26	2	0.52	0.02	3.46	4	11
J021P	2	0.76	0.02	0.04	0.09	0.03	0.06	1	1.18	0.44	0.18	0.01	0.19	2	0.66	0.02	3.32	4	11
J021P	3	0.72	0.04	0.03	0.09	0.02	0.10	1	1.04	0.52	0.22	0.02	0.20	2	0.60	0.02	3.38	4	11
J021P	4	0.74		0.02	0.07	0.02	0.15	1	1.15	0.48	0.16	0.02	0.19	2	0.60	0.01	3.39	4	11
J021P	5	0.72		0.02	0.07	0.05	0.14	1	1.14	0.47	0.16	0.03	0.20	2	0.61	0.01	3.38	4	11
J021P	6	0.65	0.07	0.03	0.11	0.04	0.10	1	0.53	0.91	0.23	0.02	0.31	2	0.51	0.01	3.48	4	11
J021P	7	0.60	0.07	0.04	0.15	0.03	0.11	1	0.46	0.91	0.30	0.02	0.31	2	0.50	0.01	3.49	4	11
J021P	8	0.60	0.07	0.04	0.10	0.12	0.08	1	0.92	0.55	0.28	0.04	0.21	2	0.61	0.02	3.37	4	11
[345]	1	0.65	0.03	0.04	0.21	0.53	0.02	1	1.07	0.97	0.48	0.02	0.14	2	0.68	0.01	3.31	4	11
[345]	2	0.63	0.02	0.04	0.16	0.52	0.12	1	1.03	0.99	0.49	0.02	0.15	2	0.64	0.01	3.35	4	11
[345]	3	0.62	0.01	0.04	0.16	0.64	0.06	1	0.98	0.98	0.53	0.01	0.14	2	0.64	0.02	3.34	4	11
[345]	4	0.64	0.01	0.05	0.17	0.66	0.04	1	0.97	0.95	0.57	0.03	0.12	2	0.63	0.02	3.35	4	11
[345]	5	0.64		0.05	0.20	0.66	0.04	1	0.90	1.00	0.59	0.02	0.12	2	0.63	0.01	3.36	4	11
[345]	6	0.69		0.04	0.11	0.53	0.13	1	1.02	0.97	0.50	0.03	0.11	2	0.59	0.02	3.39	4	11
[345]	7	0.58	0.02	0.04	0.17	0.71	0.04	1	0.94	0.94	0.56	0.03	0.12	2	0.60	0.02	3.38	4	11
[345]	8	0.61	0.03	0.04	0.14	0.49	0.10	1	1.04	0.99	0.41	0.02	0.14	2	0.62	0.02	3.36	4	11
[345]	9	0.58	0.03	0.04	0.09	0.42	0.19	1	1.06	1.02	0.35	0.02	0.17	2	0.59	0.02	3.39	4	11

Number of atoms based on (O = 11).

Roxbyite Cu_9S_5

Roxbyite sample consists of variously orientated plates of white *quartz* with isolated, flat crystals of *djurleite*, 2 cm long. Some vugs in *quartz* are filled by bluish black powdery substance, in part aggregated to a soft coherent mass. This material is pure *roxbyite,* which could be analysed with microprobe and gave a good X-ray diffraction pattern. No crystal shapes were revealed with electron microscope but *roxbyite* contains small milky white, doubly terminated *quartz* crystals; small *chalcopyrite* and *bornite* were also noted. This mineral assemblage relates to low-temperature mineralization. A single specimen is deposited in the Mineralogical collection, National Museum, Prague, sample No. NM4798.

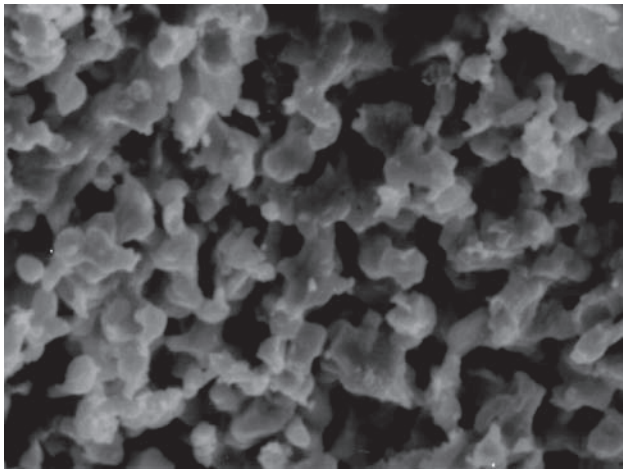

Fig. 165. NM4798. Texture of earthy aggregates of roxbyite. SE image. Magnification 2780×. Photo A. Gabašová

Table 111. Calculated unit-cell parameters of roxbyite from Jáchymov for the space group *P2/m*.

sample	*a*	*b*	*c*	β
		(Å)		(°)
NM4798	53.84(2)	30.958(9)	13.313(5)	89.59(4)

Table 112. Chemical analyses of roxbyite.

sample	pt.	Cu	Fe	S	Total
			weight %		
J177P	K2	69.80	6.55	24.05	100.40
J177P	K3	74.37	2.68	21.76	98.80
J177P	L1	74.41	2.61	22.91	99.94
J177P	L2	74.95	3.31	22.26	100.53
J177P	L3	74.89	3.25	22.84	100.98
J177P	M1	76.40	1.76	22.09	100.25
J177P	M2	71.90	5.20	23.14	100.24
J177P	M3	74.40	3.22	22.29	99.91

sample	pt.	Cu	Fe	subtotal	S	Total
				number of atoms		
J177P	K2	7.82	0.83	8.66	5.34	14
J177P	K3	8.64	0.35	8.99	5.01	14
J177P	L1	8.48	0.34	8.82	5.18	14
J177P	L2	8.54	0.43	8.97	5.03	14
J177P	L3	8.46	0.42	8.88	5.12	14
J177P	M1	8.75	0.23	8.98	5.02	14
J177P	M2	8.14	0.67	8.81	5.19	14
J177P	M3	8.52	0.42	8.94	5.06	14

Rutile TiO_2

Common accessory rutile is widespread in metamorphic rocks of the region.

Samples from the southeastern part of the district, which is characteristic of *Sn–W sulpharsenide* mineralization stage, contain *rutile* up to 100 μm long, showing sharply defined growth zones in BSE images. Light zones correspond to *rutile* with 4–6 wt.% W, 2–2.5 wt.% Fe, 1–1.5 % Sn and dark zones have 0.2–0.7 wt.% W, 0.9–2.4 wt.% Fe, and 0.8–1.4 % Sn. Rocks containing this zoned W-rich *rutile* carry *topaz*. A similar W-rich *rutile* was described from Western Australia [387] both from *muscovite* schist and *quartz* vein. It contains 7 wt.% WO_3, 2 wt.% Sb_2O_5 and 1 wt.% FeO.

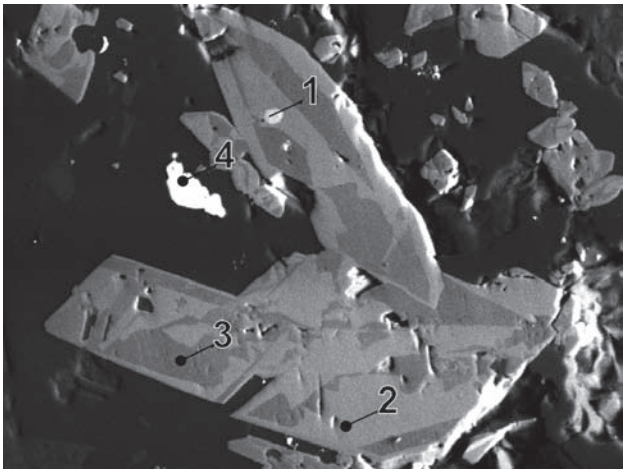

Fig. 166. J068P/D-7. 1 – xenotime-(Y), 2 – W-Sn-rutile, 3 – rutile, 4 – galena. Giftkies adit. BSE image. Magnification 720×.

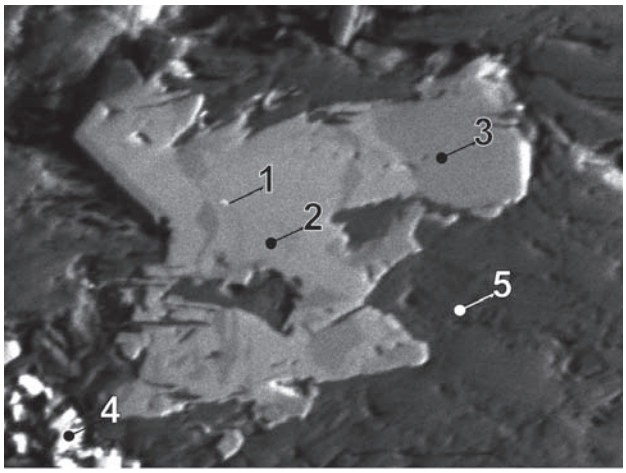

Fig. 167. MP544B/G. 1 – ferberite, 2 – W-Sn-rutile, 3 – rutile, 4 – pyrite, 5 – mica. Nikolaj shaft, cross-cut to Rovnost I. BSE image. Magnification 480×.

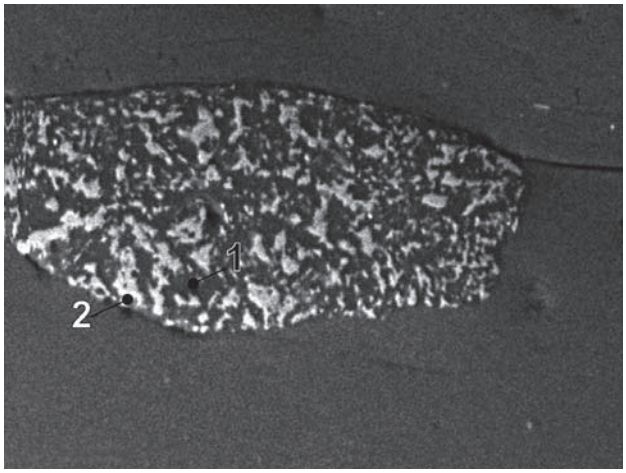

Fig. 168. SR98553/i. Aggregate of myrmekitic intergrowth of rutile and quartz located at contact of two muscovite crystals. Variation in grey shade of rutile (resp. quartz) inclusions indicates differences in content of SiO_2 in rutile (resp. TiO_2 in quartz). 1 – quartz, 2 – rutile. Skarn. Plavno. BSE image. Magnification 600×.

Table 113. Calculated unit-cell parameters of W-Sn rutile from Jáchymov for the space group $P4_2/mnm$.

sample	*a*	*c*
	(Å)	
J-912	4.6036(1)	2.9634(2)

Table 114. Chemical analyses of rutile.

sample	pt.	Ti	Fe	Sn	W	O	Total
				weight %			
J068P	D1-1tm	56.23	2.43	1.38	0.72	38.82	99.57
J068P	D1-1sv	52.59	2.44	1.42	6.08	37.80	100.32
J068P	D1-2tm	55.35	2.15	1.34	1.70	38.40	98.95
J068P	D2-1sv	53.15	2.06	1.25	5.66	37.91	100.03
J068P	D2-1tm	54.50	2.24	1.14	3.86	38.37	100.11
J068P	D3-1tm	56.82	1.70	1.11	0.52	38.88	99.02
J068P	D3-1sv	54.10	2.26	1.74	4.45	38.42	100.96
MP544B	G1tm	57.10	2.44	0.98	0.62	39.27	100.40
MP544B	G2tm	57.45	1.99	0.78	0.22	39.22	99.65
MP544B	G3tm	57.99	0.85	0.89	0.46	39.34	99.53
MP544B	G1sv	52.59	1.84	0.74	6.45	37.54	99.16
MP544B	G2sv	53.26	2.08	0.83	6.29	38.04	100.51
MP544B	G3sv	52.71	2.17	0.95	7.21	37.97	101.00
MP544B	G4sv	53.62	1.81	0.93	5.55	38.03	99.93
MP544B	G5sv	52.63	2.16	1.14	6.52	37.79	100.24
MP544B	G6sv	54.90	1.34	1.05	3.91	38.36	99.57
J090P	1	53.84	1.76	1.08	4.44	37.92	99.04
J090P	2	54.40	1.31	1.23	4.06	38.10	99.09
J090P	3	53.87	1.58	1.37	5.30	38.19	100.31
J090P	4	53.84	1.53	1.08	5.27	38.08	99.81

sample	pt.	TiO_2	FeO	Al_2O_3	SiO_2	K_2O	CaO	MnO	Total
					weight %				
SR98553	q4	94.39	0.41	0.07	4.62	0.25	0.09	0.17	100.00
SR98553	q5	95.17	0.46	0.53	3.49	0.12	0.13	0.11	100.00
SR98553	q6	92.09	0.53	0.87	5.99	0.25	0.16	0.11	100.00

sample	pt.	Ti	Fe	Sn	W	Si	subtotal	O	Total
					number of atoms				
J068P	D1-1	0.96	0.04	0.01			1.01	1.99	3
J068P	D1-1a	0.93	0.04	0.01	0.03		1.00	2.00	3
J068P	D1-2	0.96	0.03	0.01	0.01		1.01	1.99	3
J068P	D2-1	0.94	0.03	0.01	0.03		1.00	2.00	3
J068P	D2-1a	0.95	0.03	0.01	0.02		1.01	1.99	3
J068P	D3-1	0.97	0.02	0.01			1.01	1.99	3
J068P	D3-1a	0.94	0.03	0.01	0.02		1.00	2.00	3
SR98553	q4	0.93	0.01			0.06	1.01	2.00	3
SR98553	q5	0.94	0.01			0.05	1.01	2.00	3
SR98553	q6	0.91	0.01			0.08	1.01	2.00	3
MP544B	G1tm	0.97	0.04	0.01			1.01	1.99	3
MP544B	G2tm	0.97	0.03	0.01			1.01	1.99	3
MP544B	G3tm	0.98	0.01	0.01			1.00	2.00	3
MP544B	G1sv	0.94	0.03	0.01	0.03		1.00	2.00	3
MP544B	G2sv	0.94	0.03	0.01	0.03		1.00	2.00	3
MP544B	G3sv	0.93	0.03	0.01	0.03		1.00	2.00	3
MP544B	G4sv	0.94	0.03	0.01	0.03		1.00	2.00	3
MP544B	G5sv	0.93	0.03	0.01	0.03		1.00	2.00	3
MP544B	G6sv	0.96	0.02	0.01	0.02		1.00	2.00	3
J090P	1	0.95	0.03	0.01	0.02		1.00	2.00	3
J090P	2	0.95	0.02	0.01	0.02		1.00	2.00	3
J090P	3	0.94	0.02	0.01	0.02		1.00	2.00	3
J090P	4	0.95	0.02	0.01	0.02		1.00	2.00	3

Safflorite $CoAs_2$

The literature on Jáchymov reports *safflorite* as a common mineral. The present study indicates that minerals previously described as *safflorite* correspond in fact to *rammelsbergite* and sometimes possibly to *löllingit*e. The identification of *rammelsbergite* from *safflorite* without direct analytical evidence was uncertain. Thus already Zückert [423] noted that he used the term "*safflorite*" for orthorhombic diarsenides, while some of the material might have been *rammelsbergite*. The contention suggested by Zückert [423] proved to be correct with regard to predominance of Ni above Co, *rammelsbergite* is more abundant than *safflorite*.

Mrňa and Pavlů (1967) [351] also studied s*afflorite* from Jáchymov. The main occurrence of this mineral is in arsenide ores with *bismuth*. *Safflorite* holds here a similar position as *rammelsbergite* in Ag-paragenesis. It rims skeletal *bismuth* crystals as a narrow zone, which mimics the outer shape of *bismuth* matrix. In some instances, the diarsenide rim on *bismuth* is polymineralic with a local succession of the type Co–Ni–Fe. *Safflorite* also occurs as large subhedral aggregates or as a fine-grained impregnation of star-shaped triplets in gangue adjacent to margins of ore lenses. Aggregates constituting impregnatitons are younger than *safflorite* rim around *bismuth* [351].

The present work shows that optical identification of *rammelsbergite* from *safflorite* [351] was not completely reliable. Rims of *bismuth* crystals are dominantly of *rammelsbergite*, though in the literature they are erroneously described as *safflorite*. *Safflorite* is a fairly rare mineral in Jáchymov; only several examples of *safflorite* rim around *bismuth* were identified.

One example of *safflorite* rim around *nickel-skutterudite* was identified. Since *safflorite* shows transitions to *löllingite* or *rammelsbergite,* it also occurs in aggregates consisting of euhedral to subhedral crystals, often in star-shaped triplets (see the section Substitution trends – interpretation of chemical analyses).

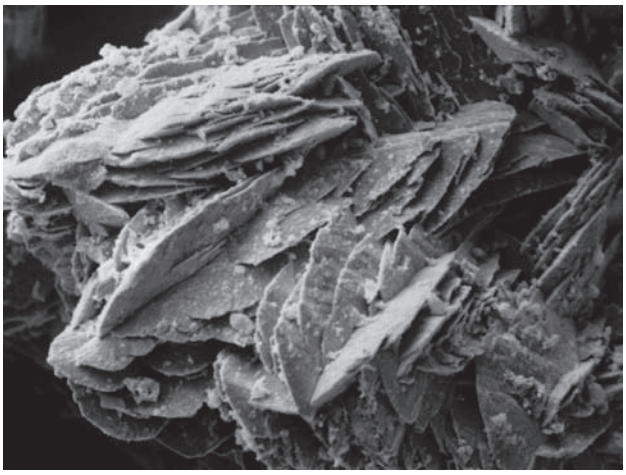

Fig. 169. VS20291. Crystals of Fe-safflorite on native bismuth. SE image. Magnification 330×. Photo A. Gabašová.

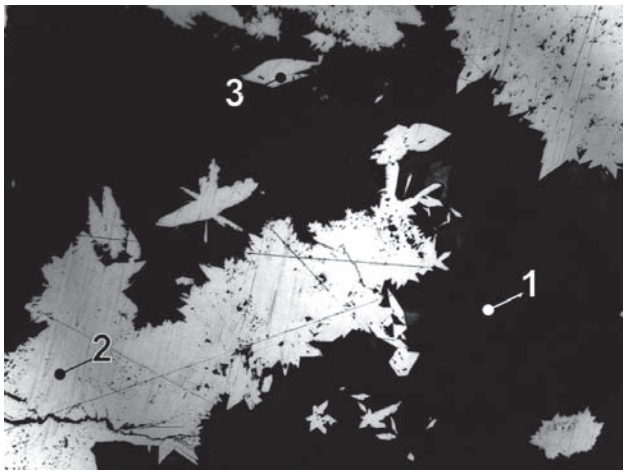

Fig. 170. J108P. Massive safflorite is rimmed by fine-grained radiating löllingite crystals. 1 – carbonate, 2 – safflorite, 3 – löllingite. Reflected light, single polarizer. Objective 20×.

Table 115. Calculated unit-cell parameters of safflorite from Jáchymov for the space group *Pnnm*.

sample	*a*	*b*	*c*	*a/c*	*a/c* – tan(60)
		(Å)			
J-695	5.266(3)	5.965(2)	2.942(1)	1.790	–0.058
J-696	5.271(2)	5.973(1)	2.926(1)	1.801	–0.069
MP473 (J-854)	5.1595(5)	5.9156(9)	3.0156(6)	1.711	0.021
MP80B (J-913)	5.1171(5)	5.9025(4)	3.0675(3)	1.668	0.064
J108P (J-934)	5.1158(9)	5.8960(6)	3.0707(3)	1.666	0.066
J-855	5.233(1)	5.969(1)	2.977(1)	1.758	–0.026
VS20291 (J-872)	5.248(2)	5.988(2)	2.944(1)	1.783	–0.051
J123P (J-921)	5.119(3)	5.904(3)	3.039(2)	1.684	0.048

Table 116. Chemical analyses of safflorite.

sample	pt.	Co	Ni	Fe	Zn	Cu	Ag	As	S	Sb	Total
						weight %					
MP80B	B3-7	16.68	0.18	10.05		0.90		72.27	1.04		101.13
MP80B	B3-8	16.42	0.07	10.13		0.98		72.70	0.56		100.86
J171P	CH1	10.43	8.68	7.65		0.40		72.55	0.28		100.00
J171P	CH3	10.97	6.51	9.41		0.57		72.61	0.22		100.30
MP329C	1	13.75	6.97	7.52		0.25		70.32	0.54	0.35	99.70
MP329C	2s	21.13	3.62	3.84		0.36		69.95	0.63	0.36	99.89
MP329C	3	19.88	5.10	3.26		0.12		70.82	0.39	0.37	99.94
J042P	d1	13.62	7.96	5.72	0.37	0.46	0.53	70.60	0.71	0.30	100.27
J042P	e1	12.80	12.11	3.11	0.22	0.25	0.42	68.40	1.90	0.43	99.64
J042P	a5	20.35	12.88	1.54	0.22	0.29	0.37	48.86	15.80	0.50	100.81
J042P	a7	21.24	10.59	1.33	0.33	0.30	0.38	53.50	12.85	0.17	100.69
J034P	12	12.40	11.06	4.35		0.09	0.28	72.08	0.09	0.44	100.79
J056P	4	16.57	8.08	3.53		0.47		70.55	1.30	0.15	100.65
J056P	5	19.71	3.65	3.81				70.84	2.18	0.10	100.29
J056P	6	15.96	4.96	5.92		0.13		72.36	0.86	0.24	100.43
J056P	7	18.23	8.84	3.52		0.49		61.51	7.82	0.08	100.49
J056P	8	14.09	1.48	10.85		1.04		72.32	0.31	0.36	100.45
J056P	9	18.14	4.15	5.18				72.17	0.37	0.12	100.13
J056P	10	19.42	3.18	3.19		0.43		70.08	2.70	0.05	99.05
J056P	11	16.87	8.51	1.58		0.56		70.55	1.52	0.05	99.64
J056P	12	15.94	3.19	7.96		0.41		70.52	1.63	0.08	99.73
J059P	5	8.64	8.04	7.61	0.29	2.42		70.25	1.21	0.45	98.91
J060P	14	11.86	11.27	6.76	0.16	0.58		64.11	4.28	0.59	99.61
J060P	15	13.16	8.77	8.19	0.58	0.70		63.93	3.97	0.46	99.76
J060P	16	11.10	10.67	7.75	0.15			65.60	3.85	0.41	99.53
J060P	24	10.92	10.44	6.91	0.64	0.21		65.61	4.29	0.65	99.67
J123P	A1	16.97	1.10	9.96		0.93		69.55	1.31		99.83
J123P	A1a	17.73	1.33	8.28	0.02	0.90	0.02	70.49	0.65		99.42

Table 116. *(continued)*

sample	pt.	Co	Ni	Fe	Zn	Cu	Ag	subtotal	As	S	Sb	subtotal	Total
						number of atoms							
MP80B	B3-7	0.57	0.01	0.37		0.03		0.98	1.96	0.07		2.02	3
MP80B	B3-8	0.57		0.37		0.03		0.97	1.99	0.04		2.02	3
J171P	CH1	0.37	0.31	0.28		0.01		0.97	2.01	0.02		2.03	3
J171P	CH3	0.38	0.23	0.35		0.02		0.98	2.00	0.01		2.02	3
MP329C	1	0.48	0.25	0.28		0.01		1.02	1.94	0.04	0.01	1.98	3
MP329C	2s	0.74	0.13	0.14		0.01		1.02	1.93	0.04	0.01	1.98	3
MP329C	3	0.70	0.18	0.12				1.01	1.96	0.03	0.01	1.99	3
J042P	a5	0.59	0.38	0.05	0.01	0.01	0.01	1.03	1.12	0.84	0.01	1.97	3
J042P	a7	0.64	0.32	0.04	0.01	0.01	0.01	1.02	1.26	0.71		1.98	3
J042P	d1	0.48	0.28	0.21	0.01	0.02	0.01	1.01	1.94	0.05	0.01	2.00	3
J042P	e1	0.44	0.42	0.11	0.01	0.01	0.01	1.00	1.87	0.12	0.01	2.00	3
J034P	12	0.44	0.39	0.16			0.01	1.00	1.99	0.01	0.01	2.01	3
J056P	10	0.67	0.11	0.12		0.01			1.91	0.17		2.08	3
J056P	11	0.59	0.30	0.06		0.02			1.94	0.10		2.04	3
J056P	12	0.55	0.11	0.29		0.01			1.93	0.10		2.03	3
J056P	4	0.57	0.28	0.13		0.02			1.92	0.08		2.00	3
J056P	5	0.68	0.13	0.14					1.92	0.14		2.06	3
J056P	6	0.56	0.17	0.22					1.99	0.06		2.04	3
J056P	7	0.58	0.28	0.12		0.01			1.54	0.46		2.00	3
J056P	8	0.49	0.05	0.40		0.03			1.99	0.02	0.01	2.02	3
J056P	9	0.64	0.15	0.19					2.00	0.02		2.02	3
J059P	5	0.31	0.29	0.28	0.01	0.08		0.96	1.95	0.08		2.03	3
J060P	14	0.40	0.38	0.24	0.01	0.02		1.04	1.69	0.26	0.01	1.96	3
J060P	15	0.44	0.30	0.29	0.02	0.02		1.07	1.68	0.24	0.01	1.94	3
J060P	16	0.37	0.36	0.28	0.01			1.02	1.74	0.24	0.01	1.99	3
J060P	24	0.37	0.35	0.25	0.02	0.01		0.99	1.73	0.27	0.01	2.01	3
J123P	A1	0.59	0.04	0.36		0.03		1.02	1.90	0.08		1.98	3
J123P	A1a	0.62	0.05	0.31		0.03		1.01	1.95	0.04		1.99	3

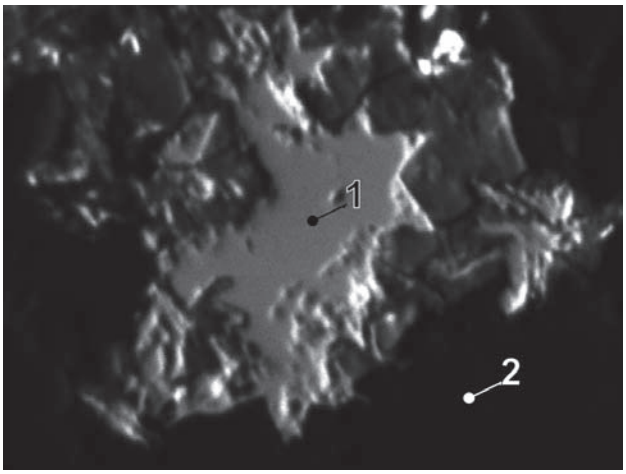

Fig. 171. J123P/A. 1 – safflorite, 2 – quartz. Svornost shaft, 10th level. BSE image. Magnification 1000×.

Fe-safflorite occurs as a rim of skeletal *bismuth* in a sample from the Bratrství shaft, Adit level, Zdař Bůh vein.

In another sample from the Eliáš mine, 2A vein, the zone of *Fe-safflorite* is deposited on several zones of pure *nickel-skutterudite,* but the uppermost zone of *nickel-skutterudite,* directly below *safflorite*, contains 4 wt.% Fe and 4 wt.% Co.

Scheelite $CaWO_4$

Chrt et al. [517] described fine-grained *scheelite* impregnations in skarn of the Plavno shaft.

Scheelite was observed as common in *pyroxene*-rich parts of *garnet–pyroxene* skarn in the Vladimír shaft, 6th level. Grey-white, highly lustrous and weakly corroded *scheelite* grains are up to 2 mm long. Some grains show tetragonal cross sections or imperfect steep pyramidal shapes.

A second type of *scheelite* with a small Mo component is represented by grains up to 1 cm long, enclosed in greisen, usually in proximity of *wolframite*, and surrounded by *chlorite*. The sample comes from the Rovnost I shaft, probably 8th level.

Schorl $NaFe_3Al_6(BO_3)_3Si_6O_{18}(OH)_4$

Clusters and radiating aggregates of prismatic crystals up to 2 cm long occur in pegmatite in the A adit. Greenish-black *schorl* also occurs in greisen but this tourmaline aggregates contain abundant hematite. Greisen sample comes from the Rovnost I shaft, probably 8th level.

Table 117. Chemical analyses of schorl.

sample	pt.	Na_2O	K_2O	FeO	MnO	MgO	CaO	TiO_2	Al_2O_3	SiO_2	Total
						weight %					
J143P	1	2.67	0.03	16.22	0.24	0.74	0.01	0.68	30.59	34.82	85.99
J143P	2	2.61	0.01	16.97		0.70	0.07	0.75	30.79	34.86	86.76
J143P	3	2.55	0.08	15.68		0.67	0.15	0.61	31.64	34.24	85.63
J143P	4	2.58	0.01	16.94	0.03	0.59	0.03	0.66	30.53	34.00	85.37
J190P	1	2.27	0.12	9.46	0.14	3.55	0.20	0.29	34.82	35.79	86.64
J192P	1	2.71	0.02	13.00	0.00	3.92	0.92	0.62	29.13	34.72	85.05
J192P	2	2.23	0.03	15.40	0.03	3.07	1.51	0.19	28.88	35.04	86.38

sample	pt.	Na	K	Ca	subtotal	Fe^{2+}	Mn^{2+}	Mg	Al	subtotal	Al	$*(BO_3)^{3-}$	Ti^{IV}	Al	subtotal	Si^{IV}	O
					X-site					Y-site	Z-site					T-site	
J190P	1	0.74	0.02	0.04	0.80	1.33	0.02	0.89	0.77	2.23	6.00	2.75	0.04	0.12	2.91	6	29.31
J192P	1	0.91		0.17	1.08	1.88		1.01	0.11	2.89	5.82	2.95	0.08		3.03	6	28.95
J192P	2	0.74	0.01	0.28	1.02	2.21		0.78	0.01	2.99	5.82	3.04	0.02		3.07	6	28.90
J143P	1	0.89	0.01	0.00	0.90	2.34	0.04	0.19	0.44	2.56	5.78	2.99	0.09		3.08	6	29.00
J143P	2	0.87		0.01	0.89	2.44		0.18	0.38	2.62	5.87	2.91	0.10		3.01	6	29.00
J143P	3	0.87	0.02	0.03	0.91	2.30		0.18	0.53	2.47	6.01	2.73	0.08		2.81	6	29.00
J143P	4	0.88		0.01	0.89	2.50		0.16	0.34	2.66	6.01	2.79	0.09		2.88	6	29.00

Number of atoms based on (Si = 6) in T-site.
* B calculated from empirical formula

Siderite $FeCO_3$

Coarse-grained light brown or dark brown *siderite* is a minor and scattered representative of early carbonates. Relatively well-formed rhombohedra of *siderite* are usually enclosed in younger carbonates, but *ankerite* may be enclosed in cores of some *siderite* crystals. *Siderite* in Jáchymov contains minor Mn.

Table 118. Calculated unit-cell parameters of siderite from Jáchymov for the space group $R\bar{3}c$.

sample	*a*	*c*
	(Å)	
J-855	4.6920(1)	15.473(5)
J-797 (J-804)	4.6868(7)	15.475(3)
NM4854 (J-844)	4.6730(3)	15.490(2)

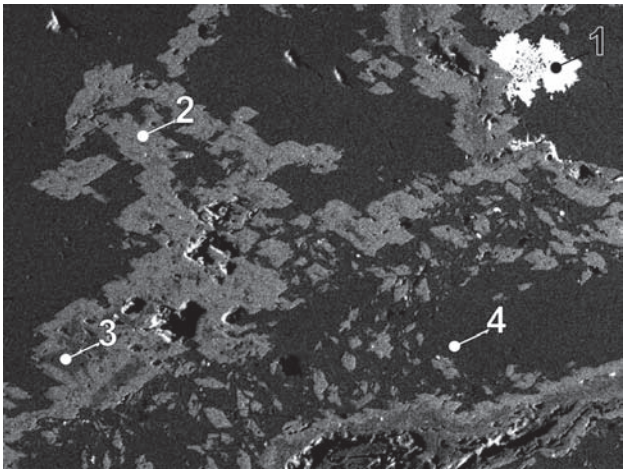

Fig. 172. G73A/B. 1 – rammelsbergite, 2 – siderite, 3 – ankerite, 4 – calcite. Svornost shaft, Geschieber vein. BSE image. Magnification 130×.

Siegenite $(Ni,Co)_3S_4$

Siegenite occurs in individual grains up to 50 μm long and in aggregates of light pink yellow, bronze brown or violet grey colour. It is the most common member of the *linneite* group in the Jáchymov district. It is often associated with *millerite* and other sulphides. One sample documents a selective replacement of certain zones in zonal *nickel-skutterudite* by *siegenite.*

Table 119. Calculated unit-cell parameters of siegenite from Jáchymov for the space group $Fd\bar{3}m$.

sample	*a* (Å)
J-243	9.4148(9)
J-233	9.415(1)

Table 120. Chemical analyses of siegenite.

sample	pt.	Ni	Co	Fe	Cu	S	As	Sb	Total
					weight %				
99452	r4V	39.17	10.28	7.48	0.37	41.66	0.85		99.81
99452	r2	38.49	10.76	7.84	0.43	41.74	0.34		99.60
99452	r5V	38.22	11.28	8.20	0.26	41.89	0.04		99.89
99452	r3V	37.85	10.49	8.87	0.32	41.28	0.85		99.66
99452	r1	37.34	10.70	8.85	0.44	41.26	0.96		99.55
99453	r1a	38.99	17.26	0.74	0.27	41.94	0.56		99.76
99453	r2a	38.91	18.01	0.31	0.20	42.17	0.35		99.95
99453	r5	38.34	18.98	0.25	0.34	41.68	0.17		99.76
99453	r4	37.86	18.81	0.54	0.62	41.82	0.42		100.07
99453	r3	37.38	17.74	1.85	0.59	41.63	0.49		99.68
J056P	14	38.45	15.51	2.48	0.76	42.40	0.36	0.17	100.13
J056P	15	39.45	15.62	2.39	0.41	41.48	0.65	0.12	100.12
J-404	1	29.86	27.36	0.49		42.29			100.00
MP175B	A1	38.81	15.97	1.98	0.35	41.70	0.71		99.52
MP175B	A3	33.13	19.40	4.25	0.22	41.65	0.91		99.55
MP175B	A2	30.47	14.58	12.05	0.16	42.08	0.50		99.84
MP27	D2-2	22.10	22.19	10.39	2.54	41.47	0.34	0.17	99.20
MP27	D2-1	22.40	22.97	9.91	2.69	42.23	0.67	0.21	101.09
MP511A	1	38.68	17.21	1.41	0.23	41.57	0.61		99.71
MP511E	B4	24.86	17.82	14.10		42.53	2.38	0.02	101.72
MP511E	B1	23.77	20.29	11.32		41.21	4.17		100.76
MP511E	B2	23.70	15.61	16.47	0.08	40.79	4.17	0.12	100.94
MP511E	B3	23.61	14.87	17.42		41.35	3.13	0.02	100.41

sample	pt.	Ni	Co	Fe	Cu	subtotal	S	As	Sb	subtotal	Total
						number of atoms					
J056P	15	2.05	0.81	0.13	0.02	3.02	3.96	0.03		3.98	7
99452	r4V	2.04	0.53	0.41	0.02	3.00	3.97	0.03		4.00	7
99453	r1a	2.03	0.90	0.04	0.01	2.98	4.00	0.02		4.02	7
MP175B	A1	2.03	0.83	0.11	0.02	2.98	3.99	0.03		4.02	7
99453	r2a	2.02	0.93	0.02	0.01	2.98	4.01	0.01		4.02	7
MP511A	1	2.02	0.89	0.08	0.01	3.00	3.97	0.02		4.00	7
99452	r2	2.00	0.56	0.43	0.02	3.01	3.98	0.01		3.99	7
99453	r5	2.00	0.99	0.01	0.02	3.01	3.98	0.01		3.99	7
J056P	14	1.99	0.80	0.13	0.04	2.96	4.02	0.01		4.04	7
99452	r5V	1.98	0.58	0.45	0.01	3.02	3.98	0.00		3.98	7
99453	r4	1.97	0.97	0.03	0.03	3.00	3.98	0.02		4.00	7
99452	r3V	1.97	0.55	0.49	0.02	3.02	3.94	0.03		3.98	7
99453	r3	1.95	0.92	0.10	0.03	3.00	3.98	0.02		4.00	7
99452	r1	1.95	0.56	0.49	0.02	3.01	3.95	0.04		3.99	7
MP175B	A3	1.73	1.01	0.23	0.01	2.98	3.98	0.04		4.02	7
MP175B	A2	1.58	0.75	0.66	0.01	2.99	3.99	0.02		4.01	7
J-404	1	1.55	1.41	0.03		2.99	4.01	0.00		4.01	7
MP511E	B4	1.27	0.91	0.76		2.93	3.97	0.10		4.07	7
MP511E	B1	1.24	1.05	0.62		2.91	3.92	0.17		4.09	7
MP511E	B2	1.23	0.81	0.90		2.94	3.88	0.17		4.06	7
MP511E	B3	1.23	0.77	0.95		2.94	3.93	0.13		4.06	7
MP27	D2-2	1.16	1.16	0.57	0.12	3.01	3.97	0.01		3.99	7
MP27	D2-1	1.15	1.18	0.54	0.13	2.99	3.98	0.03	0.01	4.01	7

A strongly altered wall-rock contained small equant *siegenite* crystals with compositional zoning. The zones show variable polishing hardness. This sample contains also *nickel-skutterudite* and *pyrite*.

Thin platy triangular *siegenite* crystals up to 0.5 mm long occurred with *millerite* in a vug. The crystals are whitish and strongly lustrous. The sample comes from the Svornost shaft, 5th level, Prokop vein.

Silver Ag

Mrňa and Pavlů (1967) [351] studied *silver* occurrences in Jáchymov. They recognized several generations of silver, showing differences in succession and paragenetic features. Primary *silver* was deposited during two stages of mineralization – the *arsenide* and *arsenic–sulphide* stage.

The oldest generation of *silver* in coarse dendritic forms consists of *silver* octahedra in uniform orientation joined in appexes. The crystal chains are connected into rectangular arrays corresponding to edges of cubes. Mrňa and Pavlů (1967) [351] described several groups based on age and morphology. Another group of Ag typology comprises anhedral *silver* in aggregates of colloform *rammelsbergite* and *nickeline*.

Silver aggregates are always rimmed by nickel arsenides, mainly *rammelsbergite,* or rarely by *nickeline* coated by *rammelsbergite.* Minor *uraninite* grains may be located along boundary of the two arsenides. Major quantities of *silver* were leached out in the course of younger mineralization stages and replaced by more complex Ag minerals [351], which form perimorphs after *silver*. However, no examples of direct replacement of dendritic *silver* by diarsenides constituting the rims were observed. *Silver* dendrites are rare-

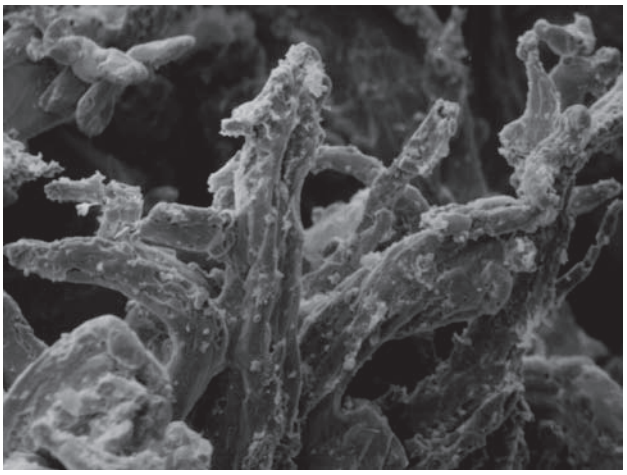

Fig. 173. VS20291. Texture of a spongy aggregate of native silver. SE image. Magnification 550×. Photo A. Gabašová.

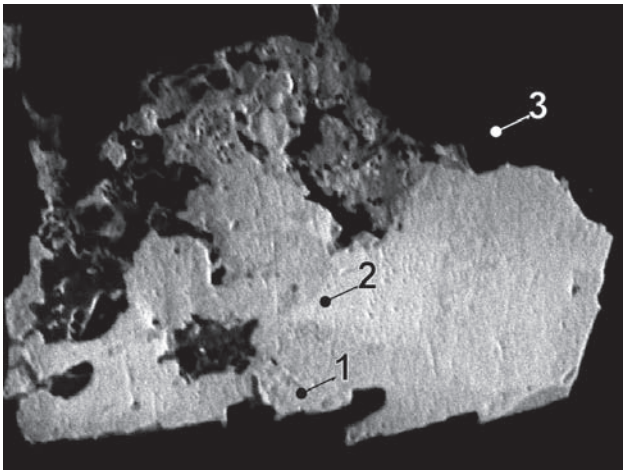

Fig. 174. J171P/B. 1 – silver, 2 – Hg-silver, 3 – dolomite. Zimní Eliáš dump. BSE image. Magnification 720×.

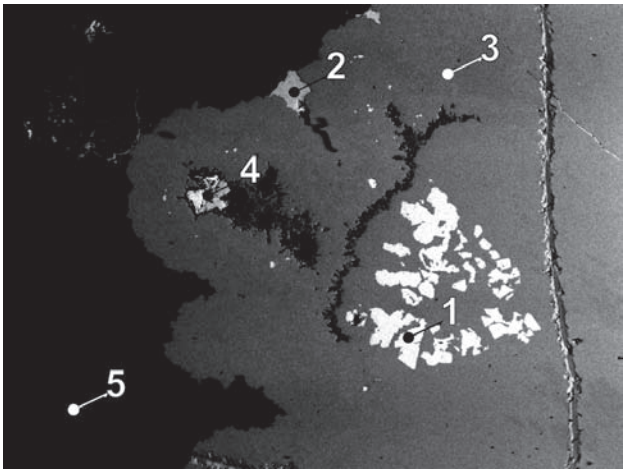

Fig. 175. MP27/A-1. 1 – silver, 2 – argentite, 3 – rammelsbergite, 4 – Hg-silver, imiterite and argentite, 5 – quartz. Eliáš mine. BSE image. Magnification 16×.

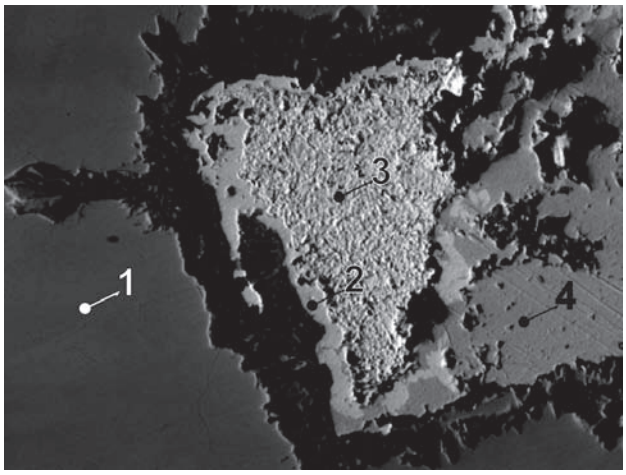

Fig. 176. MP27/A. 1 – rammelsbergite, 2 – imiterite, 3 – Hg-silver, 4 – argentite. Eliáš mine. BSE image. Magnification 1150×.

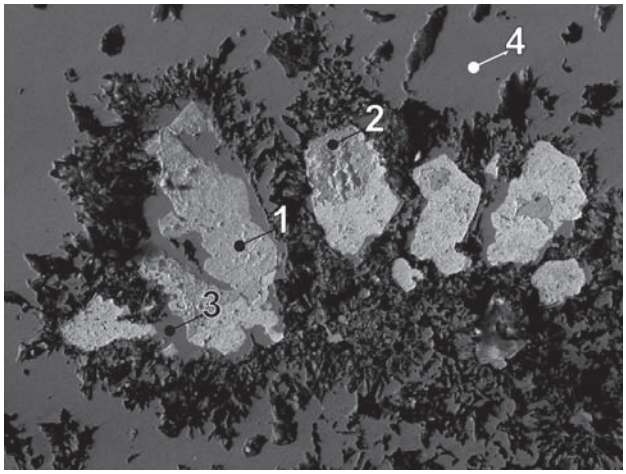

Fig. 177. MP27/A-2. 1 – silver, 2 – Hg-silver, 3 – nickeline, 4 – rammelsbergite. Eliáš mine. BSE image. Magnification 540×.

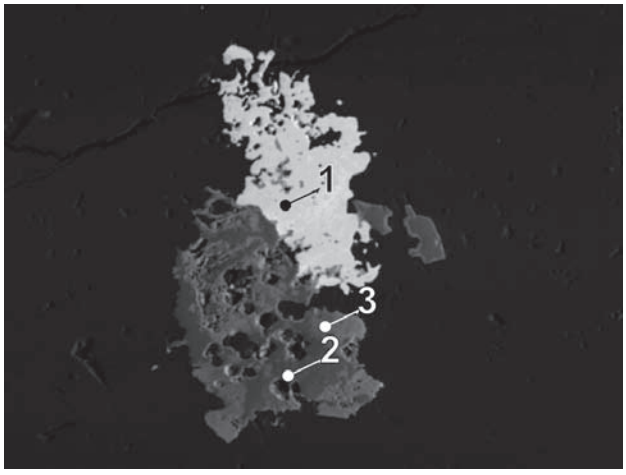

Fig. 178. MP271B/A-5. 1 – silver, 2 – marcasite, 3 – Fe-gersdorffite. Barbora shaft, 4th/5th level, vein No. 32. BSE image. Magnification 1600×.

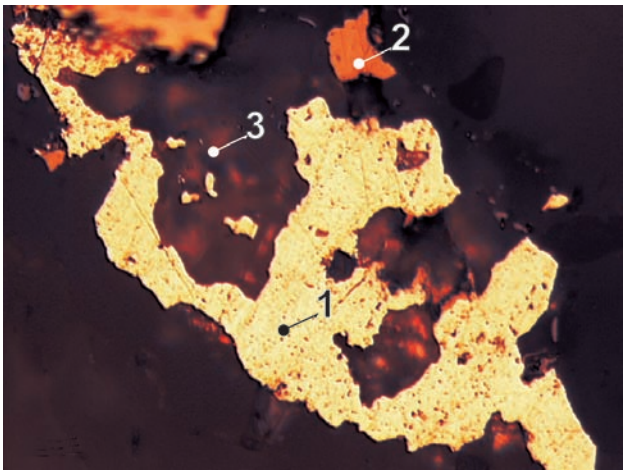

Fig. 179. MP271B. Platy aggregates of silver enriched in Hg and chalcopyrite enclosed in gangue. 1 – Hg-silver, 2 – chalcopyrite, 3 – calcite. Barbora shaft, 4th/5th level, vein No. 32. Reflected light, single polarizer. Magnification 65×.

Fig. 180. The wire silver aggregates with acanthite coatings (width of figure 4 cm). Photo J. & E. Sejkora.

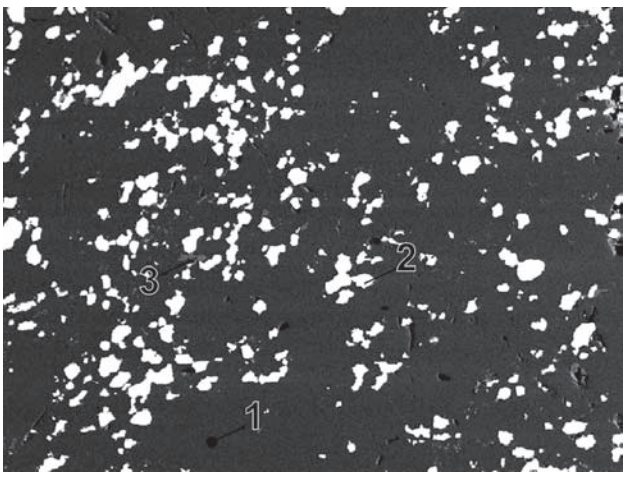

Fig. 181. The roll of silver wires in gangue cavity (width of figure 1.3 cm). Photo J. & E. Sejkora.

ly observed in their original state, with at least a part of the crystal aggregate preserved. According to Mrňa and Pavlů [383] delicate aggregates of dendritic *silver* indicate formation during tectonically quiet period with a gentle flow of fluids. Structure of arsenide rims around *silver* indicates that similar conditions prevailed during arsenide rim deposition.

Several samples from a single site represent 1 cm wide veinlet of coarse beige *dolomite* enclosing preserved skeletal *silver* crystals free of arsenide rim. The *dolomite* is also free of arsenides, sulphides or *uraninite*. It is probable that after the Ag deposition the particular domain of a vein remained isolated until the deposition of beige *dolomite*.

Zückert [423] considered dendritic *silver* as older than skeletal bismuth.

Cavities after dendritic *silver* are often partly filled by *acanthite*, *proustite*, *chalcopyrite*, younger b*ismuth*, *uraninite*, and *quartz*. Zückert [423] observed in this position also *argentopyrite*, *chalcocite*, *sphalerite*, *galena*, and *enargite.*

In arsenic-sulphide ores, *silver* occurs in lenses of *arsenic* as dendritic aggregates partly or completely replaced by *proustite*.

Silver is scattered in *arsenic* also as small anhedral and globular aggregates. In contrast to dendritic *silver*, anhedral *silver* is not significantly affected by replacement and it is not rimmed by arsenides [351].

Silver in hair-thin wires interwoven in spongy aggregates several mm across is enclosed in carbonates or along contact of *calcite* and *dolomite*. Somewhat coarser wires, up to 1 cm long and wider than 0.1 mm are rare and their occurrence in open vugs is exceptional. Wire *silver* crystallized later than the dendritic type, described above (Figs 180–181).

Silver also occurs as anhedral particles in cavities of vein filling or as small pieces of sheet *silver* in fractures of *quartz* gangue or altered wall-rock. The latter type of *silver* is probably the youngest.

In copper paragenesis with *bornite*, *tennantite*, and *chalcopyrite, silver* occurs in *quartz* gangue particularly in places where Cu-sulphides replaced *pyrite.* Here *silver* replaces or overgrows sulphide relics and fills cavities carrying rhombohedral *calcite* crystals.

According to Mrňa and Pavlů [351], genetic and succession aspects of native *silver* deposition in the form of wires, small sheets or bands are not clarified. Such *silver* occurs in numerous veins, mainly in their upper parts, but also at medium levels. According to historic reports (Vogl 1856 [59], Kraus 1916 [119]), these modes of *silver* occurrence in upper parts of veins represented important ores. *Silver* was largely freely deposited in vugs of various ore and gangue minerals or directly in crushed wall-rock.

Wire *silver* and rare sheet *silver* in the cementation zone of veins obviously represents descendent mineralization [351].

Zückert [423] interpreted the dendritic *silver* and skeletal *bismuth* as the oldest ore components in Jáchymov veins. He refused the view presented by other authors (Babánek, Becke and Štěp) on deposition of Co–Ni minerals prior to silver. He assumed that leaching of dendritic *silver* provided the source of Ag for crystallization of other Ag minerals – younger *silver*, *argentite*, *proustite*, *pyrargyrite* and others. The opposing views concerning relative age of Ag and Co–Ni minerals can be reconciled by admitting that the two lines of interpretation referred to different Ag mineralization stages. The interpretation of Zückert is clearly defined. The opposing authors apparently did not refer to the oldest dendritic *silver* but to younger *silver*, *argentite*, *proustite* and *polybasite,* which by that time represented majority of Ag in exploited ore. Zückert, and later on Geceva and Dubinkina [358], assumed that ores carrying dendritic *silver* served as the main type of Ag-rich ores which were exploited by mining. However, it is probable that dendritic *silver* never constituted important part of Ag-rich ores, due to the extensive leaching and re-deposition of this type of *silver*.

Table 121. Calculated unit-cell parameters of silver from Jáchymov for the space group $Fm\bar{3}m$.

sample	*a* (Å)
J-696	4.0910(4)

Table 122. Chemical analyses of silver.

sample	pt.		Ag	Hg	Fe	Cu	Zn	S	As	Sb	Total
						weight %					
99408	r1	wire	99.65	0.01	0.05	0.13		0.06			99.90
99408	r2	wire	99.56	0.01	0.07	0.14		0.02			99.80
99408	r3	wire	99.59	0.01	0.04	0.14		0.03			99.81
99408	r4	wire	99.47	0.01	0.12	0.17		0.07			99.84
99408	r5	wire	99.24	0.03	0.25	0.19		0.08			99.79
99408	r6	wire	99.38	0.03	0.14	0.18		0.06			99.79
99408	r7	wire	99.55	0.01	0.05	0.11		0.05			99.77
99408	r8	wire	99.63	0.03	0.09	0.04		0.04			99.83
J010P	r1	plate	98.27	0.01	0.53	0.77		0.11			99.69
J010P	r2	plate	98.22	0.06	0.42	0.89		0.22			99.81
J010P	r3	plate	98.56	0.05	0.19	0.78		0.09			99.67
J010P	r4	plate	98.35	0.02	0.29	0.74		0.41			99.81
J010P	r5	plate	98.71	0.10	0.14	0.72		0.11			99.78
J010P	r6	plate	98.06	0.16	0.23	1.25		0.05			99.75
J010P	r7	plate	97.89	0.03	0.24	1.50		0.04			99.70
J010P	r8	plate	98.23	0.08	0.25	0.88		0.14			99.58
J011P	r1	plate	98.09	0.01	0.13	1.32		0.11			99.66
J011P	r2	plate	98.25	0.02	0.29	1.08		0.12			99.76
J011P	r3	plate	98.24	0.02	0.29	1.12		0.17			99.84
J011P	r4	plate	98.56	0.09	0.25	0.66		0.19			99.75
J011P	r5	plate	98.61	0.04	0.23	0.79		0.12			99.79
J011P	r6	plate	98.98	0.01	0.17	0.64		0.06			99.86
J011P	r7	plate	98.43	0.01	0.12	1.20		0.08			99.84
J011P	r8	plate	98.24	0.04	0.19	1.22		0.06			99.75
J019P	r1	crystal	97.56	1.31	0.25	0.59		0.11			99.82
J019P	r2	crystal	97.23	1.25	0.41	0.45		0.39			99.73
J019P	r3	crystal	97.26	1.20	0.33	0.73		0.15			99.67
J019P	r4	crystal	98.39	0.31	0.27	0.35		0.35			99.67
J019P	r5	crystal	98.79	0.62	0.13	0.25		0.12			99.91
J019P	r6	crystal	99.05	0.08	0.08	0.34		0.12			99.67
J019P	r7	crystal	99.19	0.02	0.12	0.35		0.15			99.83
J019P	r8	crystal	99.01	0.01	0.19	0.32		0.14			99.67
J062P	2		97.18		0.09	1.88	0.62	0.01	0.05	0.09	99.92
J062P	2a		96.97		0.11	1.74	0.64	0.02	0.09	0.06	99.63
J062P	2b		97.22		0.16	1.97	0.59	0.05	0.14	0.14	100.27
J062P	2c		97.54		0.14	1.14	0.12	0.07	0.01	0.18	99.20
SR2712	2		72.73	24.26	0.37	0.49	0.65	0.70	0.97	0.11	100.00
SR2712	5		61.72	34.62	0.08	0.68	0.49	0.07	1.49	0.15	99.99
SR2712	6		71.24	24.21	0.45	0.65	0.79	0.81	0.63	0.91	100.00
SR2712	7		71.13	24.85	0.39	0.29	0.20	0.77	0.96	0.04	100.01
SR2712	8		68.34	26.61	0.52	0.59	0.57	0.98	0.88	0.15	100.00
SR2712	9		71.30	24.11	0.25	0.43	0.40	0.84	1.29	0.06	100.00
SR2712	10		71.58	24.80	0.47	0.32	0.41	0.79	0.49	0.12	100.01
SR2712	11		70.95	25.91	0.35	0.50	0.62	0.25	1.00	0.24	100.01

The present study confirmed the results of previous studies [358], [423] and brought some new information on distribution of mercurian *silver*. Uppermost parts of skeletal *silver* crystals, uneffected by leaching, set in beige *dolomite,* contain approximately 1 wt.% Hg. The sample comes from the Svornost shaft, Daniel level, intersection of Trojická and Geschieber veins. Dendritic *silver* rimmed by *nickeline* and *rammelsbergite* in a sample from the Eliáš mine contains a thin rim of *mercurian silver* (Fig. 179) between dendritic *silver* and *nickeline*. Another example of mercurian *silver* is in a form of 10 mm grains enclosed in dolomite gangue or intergrown with *arsenpolybasite* of a similar size. Spongy *silver* aggregates are tied to uneven *arsenpolybasite* surface.

Mercurian *silver* is evidently younger than the old, dendritic *silver*. An example of mercurian *silver* rimmed by Hg-free *silver*, enclosed in *dolomite*, indicates that the mercurian *silver* does not represent the latest *silver* generation. The sample comes from the Eliáš mine.

Skutterudite $CoAs_3$

In a detailed description of *skutterudite* from Jáchymov, Mrňa and Pavlů (1967) [351] [419] characterized three *skutterudite* types: the oldest one preceded deposition of native

Table 123. Calculated unit-cell parameters of skutterudite from Jáchymov for the space group $Im\bar{3}$.

sample	*a* (Å)
J042P	8.173(4)
J148P (J-920)	8.2189(4)
J042P	8.238(1)
J-772	8.2383(4)
J124P (J-918)	8.2387(2)
J043P	8.2401(3)
J108P (J-934)	8.2443(7)
J057P	8.2486(3)
J152P (J-919)	8.2542(3)
HK24077	8.2592(1)

metals, a younger *skutterudite* accompanied native *silver* and the youngest generation was associated with *bismuth*.

The oldest *skutterudite* forms small euhedral crystals of cube or octahedron shape up to 1 mm long. The crystals are disseminated in quartz gangue, they show compositional zoning and selective leaching. This generation is rarely preserved, its relics are associated with arsenide ores containing *bismuth*.

Skutterudite crystals accompanying *silver* are typically subhedral, up to 1.5 cm long, of pentagonal dodecahedron shape. Zoning is absent or very weak and inclusions of *rammelsbergite* and *nickeline* are common.

Table 124. Chemical analyses of skutterudite.

sample	pt.	Co	Ni	Fe	Zn	Cu	Ag	As	S	Sb	Total
						weight %					
99453	c2	11.06	8.89	1.11	0.38			77.39	1.18		100.01
99453	c3	10.09	8.80	1.83	0.25			77.67	1.35		99.99
99453	c4	12.53	7.86	1.22	0.39			75.99	2.01		100.00
99453	c5	10.17	7.73	3.32	0.30			76.99	1.50		100.01
99453	c6	10.46	8.43	2.41	0.37			76.58	1.75		100.00
99453	rc1	9.77	9.65	1.65	0.33			77.53	0.89		99.82
99453	rc2	11.15	9.22	1.24	0.32			76.79	0.95		99.67
99453	rc3	9.86	9.14	1.73	0.26			77.44	1.14		99.57
99453	rc4	12.43	7.97	1.12	0.34			75.72	2.12		99.70
J020P	r1	10.42	8.56	2.75	0.32			76.88	0.84		99.77
J020P	r2	10.60	8.05	2.56	0.25			76.88	1.38		99.72
J020P	r3	11.78	9.13	2.66	0.39			74.35	1.53		99.84
J020P	1	10.94	8.91	2.76	0.27			76.50	0.61		99.99
J020P	2	10.47	7.73	2.31	0.26			77.98	1.25		100.00
J020P	3	11.61	9.58	2.46	0.38			74.24	1.73		100.00
J020P	4	11.48	8.27	3.09	0.35			74.77	2.05		100.01
J026P	a1	10.05	8.26	2.52	0.30			77.34	1.53		100.00
J026P	a2	11.25	9.31	1.80	0.36			76.00	1.28		100.00
J026P	a3	12.23	7.70	3.22	0.32			75.55	0.98		100.00
J026P	a4	9.87	8.45	2.39	0.31			77.18	1.81		100.01
J026P	ar1	10.25	8.06	2.47	0.23			77.05	1.47		99.53
J026P	ar2	11.11	9.21	2.08	0.32			75.75	1.31		99.78
J026P	ar3	12.05	8.41	2.27	0.32			75.55	1.12		99.72
J042P	a3	15.56	3.52	1.79			0.28	76.80	3.41	0.25	101.61
J042P	a4	13.09	7.64	0.63	0.41	0.45	0.40	75.43	2.08	0.38	100.51
J042P	e2	13.29	6.47	1.10	0.34	0.47	0.42	73.94	2.91	0.62	99.56
J042P	e3	13.72	6.09	0.62	0.24	0.55		76.10	2.53	0.43	100.28
J042P	2a	12.85	6.68	0.91	0.50	0.57	0.33	75.01	3.01	0.39	100.25
J052P	4	10.28	6.67	3.42		0.34		76.82	2.17	0.09	99.79
J052P	5	11.51	6.12	2.69		0.50		76.86	2.57	0.15	100.40
J056P	1	14.01	3.97	1.61		0.06		77.56	2.25		99.46
J056P	2	12.87	6.22	0.97		0.45		77.13	2.06		99.70
J056P	3	10.30	4.54	5.34		0.48		77.73	1.53		99.92
J057P	3	11.25	6.99	2.63		0.33		75.73	2.28	0.46	99.67
J057P	6	12.44	6.98	1.11		0.42		75.06	3.22	0.49	99.72
J057P	7	11.88	7.87	0.63		0.37		75.58	2.61	0.57	99.51
J057P	8	12.08	4.84	3.26		0.20		77.30	1.54	0.45	99.67
J057P	9	11.76	8.09	0.82		0.76		75.68	2.57	0.34	100.02
J108P	1-7	13.87	2.39	3.87		0.46		77.40	2.34	0.42	100.76
J124P	1	12.05	7.23	2.08		0.08		75.90	2.44	0.02	99.81
J124P	2	10.41	6.84	3.88		0.47		77.12	1.63		100.35
J148P	1	13.34	4.09	3.41		0.36		75.27	3.88	0.02	100.38
J148P	3	14.42	3.90	2.19	0.04	0.00		75.88	3.66		100.10
J152P	1	11.25	7.90	1.83	0.03	0.08		77.49	2.46		101.04
J152P	2	11.74	7.81	1.66		0.03		76.93	2.69	0.10	100.95
J152P	3	10.04	10.14	0.61	0.04	0.02		77.32	2.33	0.05	100.55
J152P	4	10.58	8.76	1.39	0.03	0.05		77.26	2.09		100.16

Table 124. *(continued)*

sample	pt.	Co	Ni	Fe	Zn	Cu	Ag	subtotal	As	S	Sb	subtotal	Total
						number of atoms							
99453	c1	0.45	0.46	0.09	0.01			1.02	2.94	0.05		2.98	4
J152P	4	0.50	0.37	0.12	0.01			0.99	2.90	0.11		3.01	4
J026P	a4	0.47	0.44	0.09	0.01			1.00	2.90	0.10		3.00	4
99453	rc3	0.47	0.46	0.08	0.01			1.02	2.90	0.08		2.98	4
99453	c3	0.48	0.42	0.09	0.01			1.00	2.89	0.12		3.00	4
J056P	1	0.66	0.19	0.08				0.93	2.88	0.20		3.07	4
J026P	ar3	0.57	0.23	0.16		0.01		0.97	2.88	0.13		3.02	4
99453	c2	0.52	0.42	0.06	0.02			1.02	2.88	0.10		2.98	4
J020P	r1	0.49	0.22	0.27		0.02		0.99	2.88	0.13		3.01	4
J026P	a2	0.53	0.44	0.06	0.01			1.05	2.87	0.08		2.95	4
J020P	2	0.50	0.41	0.14	0.01			1.06	2.87	0.07		2.95	4
J052P	4	0.49	0.38	0.12	0.01			1.00	2.87	0.13		3.00	4
J152P	3	0.47	0.39	0.13	0.01			1.00	2.87	0.13		3.00	4
J056P	2	0.61	0.29	0.05		0.02		0.97	2.86	0.18		3.03	4
J020P	r2	0.50	0.38	0.13	0.01			1.02	2.86	0.12		2.98	4
J020P	1	0.52	0.42	0.14	0.01			1.09	2.85	0.05		2.91	4
99453	c5	0.48	0.37	0.17	0.01			1.02	2.85	0.13		2.98	4
99453	rc1	0.46	0.40	0.12	0.01			0.99	2.85	0.16		3.01	4
99453	c6	0.49	0.41	0.07				0.98	2.84	0.18		3.02	4
J056P	3	0.49	0.32	0.19		0.02		1.02	2.84	0.14		2.98	4
J108P	1-7	0.64	0.11	0.19		0.02		0.96	2.83	0.20	0.01	3.04	4
J124P	2	0.49	0.40	0.12	0.02			1.02	2.83	0.15		2.98	4
J026P	ar1	0.48	0.31	0.17		0.02		0.98	2.83	0.19		3.02	4
J026P	a1	0.47	0.47	0.03				0.97	2.83	0.20		3.03	4
J057P	3	0.53	0.44	0.09	0.02			1.07	2.82	0.11		2.93	4
J057P	8	0.57	0.40	0.11	0.01			1.10	2.81	0.10		2.91	4
J020P	4	0.53	0.29	0.13		0.02		0.97	2.81	0.22		3.02	4
99453	rc2	0.52	0.37	0.09		0.00		0.98	2.81	0.21		3.02	4
J026P	ar2	0.52	0.44	0.10	0.01			1.08	2.81	0.11		2.92	4
99453	c4	0.59	0.37	0.06	0.02			1.03	2.80	0.17		2.97	4
99453	rc4	0.58	0.36	0.16	0.01			1.11	2.80	0.09		2.89	4
J042P	e3	0.64	0.29	0.03	0.01	0.02		0.99	2.79	0.22	0.01	3.01	4
J057P	6	0.58	0.38	0.06	0.01			1.03	2.79	0.18		2.97	4
J124P	1	0.56	0.37	0.03		0.02		0.97	2.79	0.23		3.01	4
J152P	2	0.54	0.36	0.08		0.00		0.98	2.79	0.23		3.02	4
J052P	5	0.53	0.33	0.13		0.01		1.00	2.79	0.20		2.99	4
J057P	7	0.56	0.34	0.10				1.01	2.78	0.21		2.99	4
J042P	a4	0.61	0.36	0.03	0.02	0.02	0.01	1.05	2.77	0.18	0.01	2.95	4
J020P	r3	0.55	0.38	0.04		0.03		1.00	2.77	0.22		2.99	4
J042P	a3	0.71	0.16	0.09			0.01	0.96	2.75	0.29	0.01	3.04	4
J148P	3	0.66	0.18	0.11				0.95	2.74	0.31		3.05	4
J026P	a3	0.58	0.33	0.05		0.02		0.97	2.74	0.28		3.02	4
J057P	9	0.55	0.43	0.13	0.02			1.13	2.74	0.13		2.87	4
J152P	1	0.53	0.39	0.15	0.02			1.09	2.74	0.18		2.91	4
J042P	2a	0.60	0.31	0.04	0.02	0.02	0.01	1.00	2.73	0.26	0.01	3.00	4
J020P	3	0.54	0.45	0.12	0.02			1.13	2.72	0.15		2.87	4
J148P	1	0.62	0.30	0.05	0.01	0.02	0.01	1.02	2.71	0.25	0.01	2.98	4
J042P	e2	0.61	0.19	0.16		0.02		0.98	2.70	0.32		3.02	4

Zepharovich determined the density of *skutterudite* of 6.81 g/cm^3 [391].

Several types of *skutterudite* accompany *bismuth* – subhedral zoned and also free of zoning, colloform, a rod-shaped form and the youngest anhedral type [351]. Mrňa and Pavlů (1967) [351], [419] conducted their study before the introduction of electron microprobe and their work is based mainly on optical study of polished sections, etching tests and some spectral analyses. With the methods used, *nickel-skutterudite* could not be distinguished from *skutterudite* properly.

During the present study no firm evidence supporting the existence of the oldest generation of *skutterudite* has been found but its existence cannot be ruled out. In summarizing occurrences of *skutterudite* and *nickel-skutterudite* associated with *silver* and *bismuth* it appears that there is not a significant difference between the two groups. Both native metals are accompanied mainly by *nickel-skutterudite*, often with compositional zoning and leaching of some zones. On the other hand, true *skutterudite* is less common, more massive, with a weak zoning (if any) and it does not contain dendritic *silver*. In its appearance, *skutterudite* is rather similar to *nickel-skutterudite* except for features such as zoning or massive aggregates.

Skutterudite is less common than *nickel-skutterudite,* which shows sometimes greater predominance of Ni over Co. Samples of the latter type, in spite of the relation

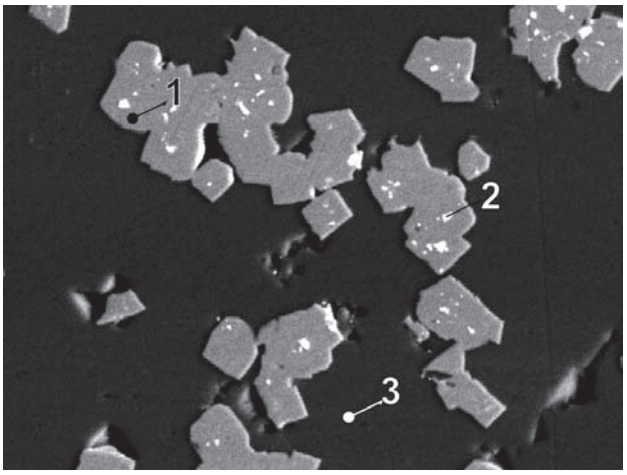

Fig. 182. J087P/E. 1 – skutterudite, 2 – bismuth, 3 – sphalerite. Adit No. 1. BSE image. Magnification 160×.

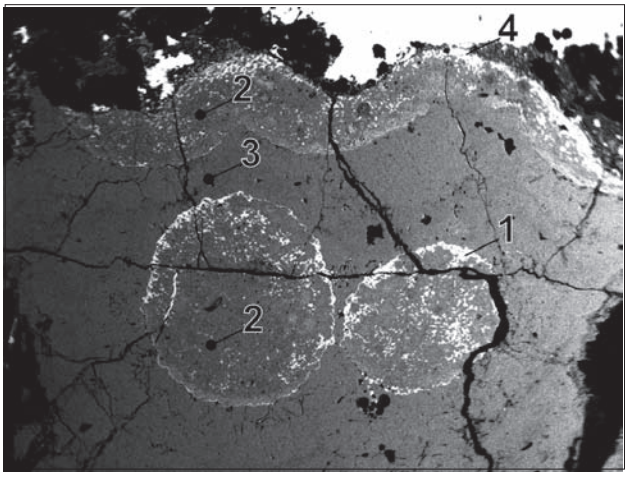

Fig. 183. MP340D/A. 1 – bismuth, 2 – Ni-rich skutterudite, 3 – Co-rich nickel-skutterudite, 4 – bismuth and rammelsbergite. Plavno, vein No. 28. BSE image. Magnification 18×.

Ni > Co, carry red-violet *köttigite-annabergite* coating, which is caused by the strong colouring properties of Co.

One *skutterudite* sample rich in Ni carried minute inclusions of skeletal *bismuth*. Oval aggregates of *Co-gersdorffite* up to 0.2 mm long were deposited on surface of this *skutterudite* from the No. 7 adit.

Smectite

Two types of *smectite* occurrence were found out. It occurred as yellow-olive filling among carbonate crystals. The sample comes from Svornost shaft, Daniel level. Light brown volcanic dyke rock with *bismuthinite* veinlets is altered to a mixture of *smectite* and *sanidine* (samples No. NM 11049, VS 4238).

Smythite $Fe_{13}S_{16}$

Smythite was found in small cavities of ferroan *dolomite* as imperfect octahedral crystals up to 1 mm long (Fig. 187). The crystals are yellow brown with a bluish

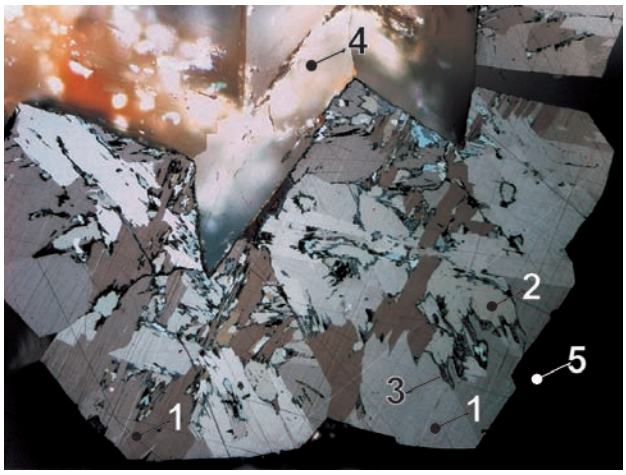

a

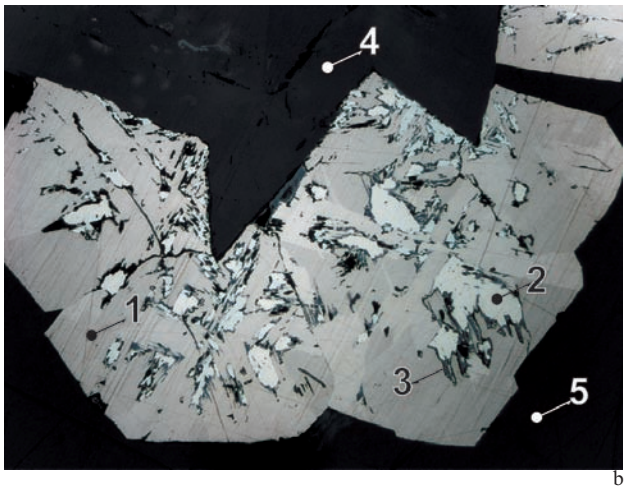

b

Fig. 184a, b. J183P. Agregates of smythite with distinctive bireflection. Strong anisotropy in bluish white and greyish brown tints emphasizes polycrystalline texture of seemingly homogeneous crystals. Svornost shaft, 2nd level, Hildebrand vein. 1 – smythite, 2 – pyrite, 3 – magnetite, 4 – ankerite, 5 – calcite. Reflected light, crossed polarizers (a) and single polarizer (b). Objective 20×.

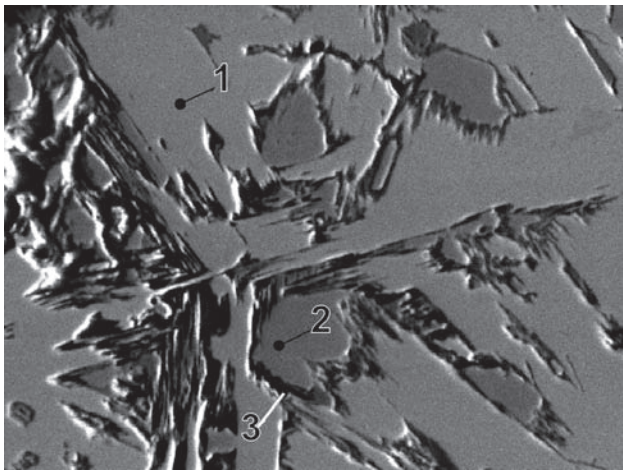

Fig. 185. J183P/1. 1 – smythite, 2 – pyrite, 3 – magnetite. Svornost shaft, 2nd level, Hildebrand vein. BSE image. Magnification 400×.

sheen and yellowish bronze brown on fracture. The mineral is strongly ferromagnetic. In polished section the mineral is ochre yellow with distinct bireflectance and a strong anisotropy. Equant crystals are composed of a number of individuals, in part of lamellar shape (Fig. 184).

X-ray powder diffraction indicates that the material is a mixture of *smythite*, *pyrite*, *marcasite* and *magnetite* but crystal morphology indicates an originally cubic mineral. Examination of crystals with four-circle goniometer shows that the apparent single crystals are composed of a number of differently orientated domains. Local electron microanalyses indicate *smythite*, with local *pyrite* inclusions rimmed by a narrow zone of *magnetite* (Figs 185 and 186). It is possible that the material represents *smythite* pseudomorphs after *pyrite*, as indicated by pyrite relics enclosed in *smythite*. The presence of *magnetite* suggests a strong oxidation prior to the *smythite* crystallization. As *smythite* is stable below 75 °C [554] its presence indicates low-temperature crystallization.

Smythite is covered by scattered rhombohedral *calcite*. The matrix of *smythite* sample consists of *Fe-dolomite* carrying spheroidal *sphalerite* covered by successive zones of *Fe-dolomite* and *pyrite*. Chemical composition of both types of *pyrite* is comparable. The sample comes from the Svornost shaft, 2nd level, Hildebrand vein.

Table 125. Calculated unit-cell parameters of smythite from Jáchymov for the space group $R\bar{3}m$.

sample	*a*	*c*
	(Å)	
J-444	3.4688(7)	34.305(7)

Table 126. Chemical analyses of smythite.

sample	pt.	Fe	Co	Ni	Cu	S	As	Total
					weight %			
J183P	Sm1	58.71		0.05	0.02	41.65	0.11	100.55
J183P	Sm2	58.16			0.00	41.61	0.06	99.83
J183P	Sm3	58.56	0.03		0.02	41.46	0.09	100.16
J183P	Sm4	57.99				41.56	0.26	99.81
J183P	Sm5	58.28				41.62	0.00	99.89
J183P	Sm6	57.95	0.09	0.02		41.28	0.16	99.50

sample	pt.	Fe	Co	Ni	subtotal	S	As	subtotal	Total
					number of atoms				
J183P	Sm1	12.96		0.01	12.97	16.01	0.02	16.03	29
J183P	Sm2	12.91			12.91	16.09	0.01	16.09	29
J183P	Sm3	12.97	0.01		12.98	16.00	0.01	16.02	29
J183P	Sm4	12.88			12.88	16.08	0.04	16.12	29
J183P	Sm5	12.92			12.92	16.08		16.08	29
J183P	Sm6	12.92	0.02		12.94	16.03	0.03	16.06	29

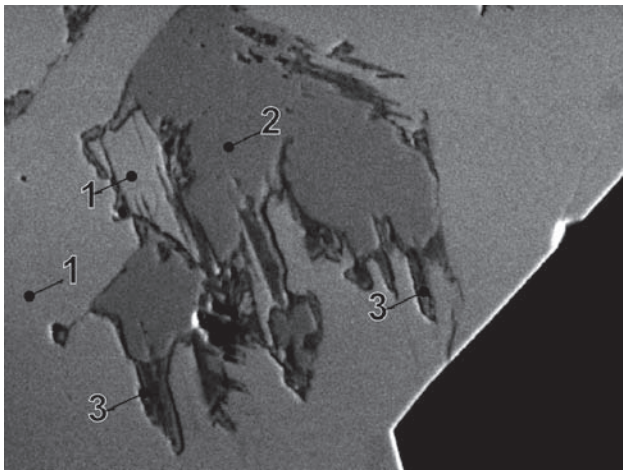

Fig. 186. J183P/3. 1 – smythite, 2 – pyrite, 3 – magnetite. Svornost shaft, 2nd level, Hildebrand vein. BSE image. Magnification 540×.

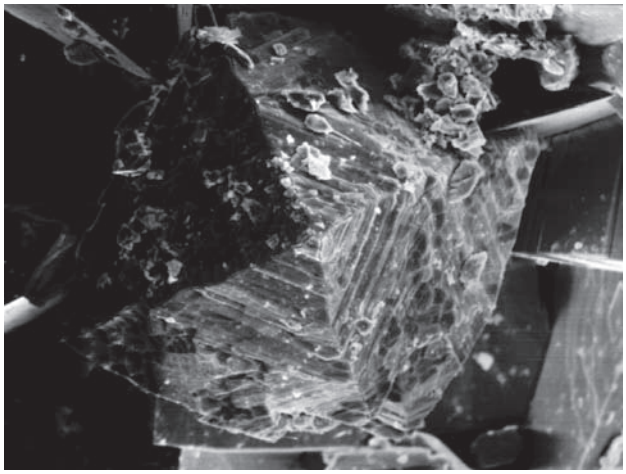

Fig. 187. J-444. Bipyramidal crystals od smythite on dolomite. Svornost schaft, 2nd level, Hildebrant vein. Magnification 245×. Photo A. Gabašová.

Sphalerite ZnS

Sphalerite rich in Fe (up to 10.72 wt.%), with somewhat increased Cd and In (up to 0.28 and 0.19 wt.%), was described by Bernardová and Poubová [372] from the No. 14 shaft, Severní Jeroným vein. It was present in a lense with *chalcopyrite* and *pyrite,* and accessory *pyrrhotite* rimmed by zones of *chlorite* and *chlorite+muscovite*. The high Fe content indicates that it belongs to the *Sn–W sulpharsenide* stage [372]. *Sphalerite* was also studied by Mrňa and Pavlů (1967) [351]. They described *sphalerite* as a fine-grained impregnation in veins or as small massive lenses. Usually it encloses *chalcopyrite* and is accompanied by other *sulphides*, mainly *galena*. Light-coloured *sphalerite* of the *sulphidic* stage prevails in veins but *sphalerite* in skarnized

Table 127. Calculated unit-cell parameters of sphalerite from Jáchymov for the space group $F\bar{4}3m$.

sample	*a* (Å)
J055P	5.4057(5)
J060P	5.418(1)
J125P	5.4174(2)

Table 128. Chemical analyses of sphalerite.

sample	pt.	Zn	Fe	Mn	Cd	Co	Ni	Cu	S	As	Total
						weight %					
99454	r10	65.20	0.50			0.15	0.45	0.48	32.38	0.52	99.68
99454	r11	64.37	0.39			0.17	0.55	0.53	32.38	1.25	99.64
99454	r12	64.78	0.47			0.41	0.59	0.61	32.57	0.26	99.69
J017P	r10	64.41	0.41			0.21	0.56	0.54	33.06	0.67	99.86
99453	r1	65.81	0.29			0.34	0.41		31.82	0.91	99.58
99453	r6	66.01	0.27			0.32	0.39		32.06	0.41	99.46
J125P	1	60.51	6.40			0.01	0.06	0.25	32.46		99.69
J125P	2	59.79	6.81			0.06	0.00	0.18	32.53		99.37
J125P	3	60.70	6.64			0.00	0.05	0.00	32.88		100.27
J060P	12	66.54	0.29			0.29	0.15	0.59	31.69	0.07	99.72
99453	r1b	64.04	1.55	0.42	0.25			0.37	32.35	0.25	99.23
J012P	rAa	63.06	2.25	0.20	0.28			0.15	32.78	0.09	98.81
J012P	rAb	63.88	2.66	0.15	0.32			0.13	32.27	0.22	99.63
J012P	rAc	63.66	2.42	0.21	0.35			0.13	32.05	0.11	98.93
J012P	rB2	63.55	3.32	0.35	0.38			0.29	32.02	0.27	100.18
J012P	rB4	63.22	2.27	1.10	0.39			0.52	32.27	0.19	99.96
J012P	rB1	62.89	2.88	0.55	0.41			0.36	33.07	0.19	100.35
J015P	Ar2	63.17	2.56	0.32	0.62			0.33	32.23	0.29	99.52
J015P	Ar1	62.76	2.40	0.41	0.98			1.11	32.05	0.27	99.98
99453	r1c	62.22	2.07	0.26	1.01			0.41	32.70	0.30	98.97
J016P	r1a	64.76	0.36	0.05	1.02			0.15	32.61	0.31	99.26
J016P	r1b	64.75	0.27	0.04	1.23			0.15	32.55	0.35	99.34
J012P	rB3	62.53	2.54	0.78	1.35			0.25	32.01	0.39	99.85
J016P	r1c	64.83	0.39	0.04	1.35			0.16	32.67	0.35	99.79

sample	pt.	Zn	Fe	Mn	Cu	subtotal	S	As	Total
					number of atoms				
99454	r10	0.98	0.01		0.01	1.00	0.99	0.01	2
99454	r11	0.97	0.01		0.01	0.99	0.99	0.02	2
99454	r12	0.97	0.01		0.01	1.00	0.99		2
J017P	r10	0.96	0.01		0.01	0.98	1.00	0.01	2
99453	r1	0.99	0.01			1.01	0.98	0.01	2
99453	r6	0.99	0.01			1.01	0.98	0.01	2
J125P	1	0.90	0.11			1.01	0.98		2
J125P	2	0.89	0.12			1.01	0.99		2
J125P	3	0.90	0.11			1.01	0.99		2
J060P	12	1.00				1.01	0.97		2
99453	r1b	0.96	0.03		0.01	1.01	0.99		2
J012P	rAa	0.95	0.04			1.00	1.00		2
J012P	rAb	0.96	0.05			1.01	0.99		2
J012P	rAc	0.96	0.04			1.01	0.99		2
J012P	rB2	0.95	0.06			1.02	0.98		2
J012P	rB4	0.94	0.04	0.02	0.01	1.02	0.98		2
J012P	rB1	0.93	0.05		0.01	1.00	1.00		2
J015P	Ar2	0.95	0.05		0.01	1.01	0.99		2
J015P	Ar1	0.94	0.04		0.02	1.02	0.98		2
99453	r1c	0.94	0.04		0.01	0.99	1.00		2
J016P	r1a	0.98	0.01			0.99	1.00		2
J016P	r1b	0.98	0.01			1.00	1.00		2
J012P	rB3	0.94	0.05			1.02	0.98		2
J016P	r1c	0.97	0.01			1.00	1.00		2

crystalline limestones in the Svornost and Plavno shafts is dark, with increased Fe and In, similar to the type in *Sn–W sulpharsenide* paragenesis [351].

Vogl [560] described small hemispheric aggregates and botryoidal stalactic specimens described as "*voltzin*" containing Zn and S as major elements. It was straw yellow, brown red or greenish white in colour, translucent, with a greasy to vitreous lustre. It had a conchoidal fracture, hardness of 3.5 and density of 3.5 to 3.8 g/cm^3 [60]. Our XRD study confirmed the presence of *sphalerite.*

The present study shows that *sphalerite* belongs to common ore minerals in the veins. It forms crystals enclosed in gangue, small crystals lining cavities, and monomineralic bands in some veins. Other sulphides – *chalcopyrite*, *pyrite* and *galena* accompany *sphalerite.* Its colour varies from brown to brown-black and to brown yellow, some crystals show darker rims. The older generation is sometimes replaced by *nickeline. Sphalerite* is deposited on *safflorite*, *rammelsbergite* and *nickeline,* which rim native *arsenic*. A sample of black sphalerite from an adit above the Unruhe adit contains 6.5 wt.% Fe.

Sphalerite sample with *nickeline* from the Svornost shaft, 8th level, Geschiebersouth vein, contains an outer *sphalerite* zone, 10 mm wide, containing minute *argentite.*

Botryoidal *sphalerite* shows colour zoning. The cores of aggregates often enclose *galena*, which also makes granular inclusions along boundaries of some zones (Fig. 189). Geceva and Dubinkina [358] first mentioned the possible deposition of this *sphalerite* from a gel as a colloform aggregate.

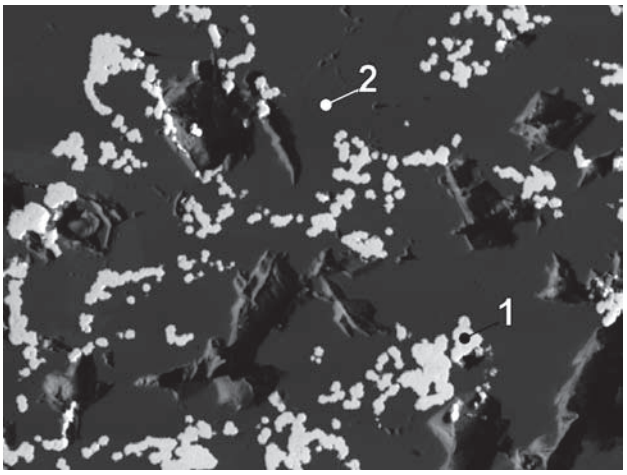

Fig. 188. J105P/F-1. 1 – sphalerite and wurtzite, 2 – dolomite. Svornost shaft, Adit level, Hildebrand vein. BSE image. Magnification 230×.

Sphalerite also replaces imperfectly *stibnite* needles in samples from Svornost shaft, Adit level, Hildebrand vein (Figs 188, 190).

Stannite Cu_2FeSnS_4

Stannite forms indvidual grains up to 0.2 mm long or aggregates, in part of myrmekitic shape, always enclosed in *chalcopyrite*. *Stannite* particles along the margin of myrmekite are coarser-grained, with an orientated pattern

Table 129. Calculated unit-cell parameters of stannite from Jáchymov for the space group $I\bar{4}2m$.

sample	*a*	*c*
	(Å)	
J109P (J-916)	5.4470(9)	10.815(2)

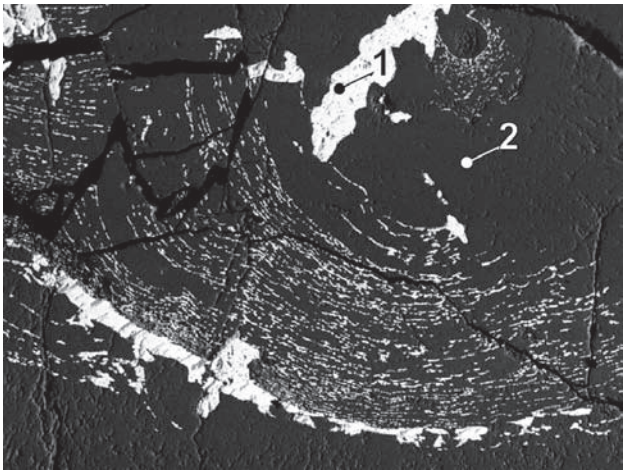

Fig. 189. J134P. 1 – galena, 2 – sphalerite. Svornost shaft, dump. BSE image. Magnification 80×.

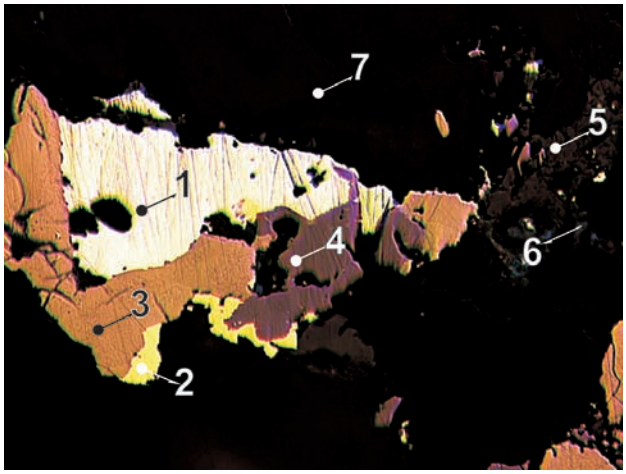

Fig. 191. J012P. Galena grain is rimmed by sphalerite and stannite, chalkopyrite rims sphalerite. In the right part of the sample is covellite after chalcopyrite and galena replaced by a secondary mineral. 1 – galena, 2 – chalcopyrite, 3 – sphalerite, 4 – stannite, 5 – Pb-secondary mineral, 6 – covellite, 7 – quartz. Small old dump near Eliáš mine. Reflected light, single polarizer. Magnification 130×.

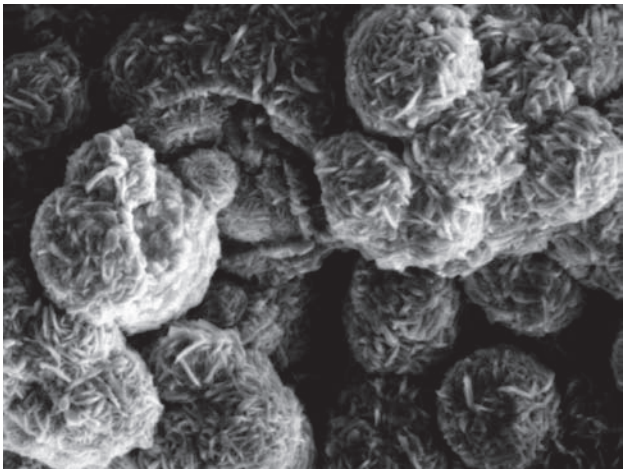

Fig. 190. J-807. Sphalerite, SE image. Magnification 900×. Photo A. Gabašová.

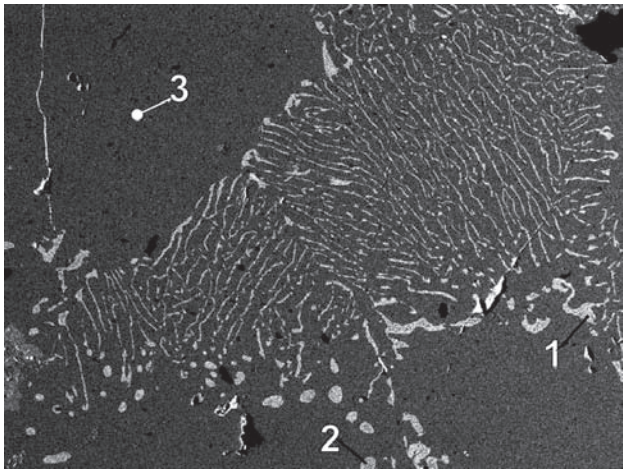

Fig. 192. J109P/3. 1 – stannite, 2 – chalcopyrite. Klement shaft. BSE image. Magnification 160×.

Table 130. Chemical analyses of stannite.

sample	pt.	Cu	Ag	Fe	Zn	Sn	S	As	Total
					weight %				
J012P	br2	28.66	0.15	8.29	5.86	26.75	29.76	0.08	99.55
J012P	br1	29.13	0.24	8.05	6.79	26.06	29.45	0.09	99.81
J012P	r3	29.23	0.65	6.66	8.65	24.64	29.65	0.11	99.59
J061P	8	28.62	0.33	9.68	3.85	27.32	29.35		99.15
J061P	9	28.74	0.41	9.47	3.77	27.64	29.22		99.25
J061P	10	28.91	0.39	9.58	3.61	27.46	29.37		99.32
J061P	11	28.47	0.29	9.61	3.59	27.71	29.41		99.08
J066P	1	31.89		6.87	6.73	25.32	28.64		99.44
J066P	2	31.23		9.39	4.15	26.15	29.04		99.97
J066P	3	31.61		8.97	4.65	25.35	29.35		99.93
J066P	4	31.40		7.95	7.50	22.44	29.14		98.43
J066P	5	32.13		9.73	4.03	25.22	29.19		100.30
J066P	21	32.12		6.81	7.65	24.69	29.05		100.33
J066P	22	32.30		8.42	4.99	25.82	28.70		100.23
J109P	1	28.28		8.61	9.69	24.90	29.12		100.61
J109P	2	30.41		7.62	8.46	24.83	29.08		100.40
J126P	1	30.67		8.77	5.33	26.61	29.17		100.55
MP544B	A	29.20		8.76	5.22	27.39	28.60		99.17

sample	pt.	Cu	Fe	Zn	subtotal	Ag	Sn	Zn	subtotal	S	As	subtotal	Total
							number of atoms						
J066P	5	2.17	0.75	0.26	1.01		0.91		0.91	3.91		3.91	8
J061P	8	1.97	0.76		0.76	0.01	1.01	0.26		4.00		4.00	8
J061P	11	1.96	0.75		0.75	0.01	1.02	0.24		4.01		4.01	8
J061P	10	1.99	0.75		0.75	0.02	1.01	0.24		4.00		4.00	8
J061P	9	1.98	0.74		0.74	0.02	1.02	0.25		3.99		3.99	8
J066P	2	2.13	0.73	0.27	1.00		0.95		0.95	3.92		3.92	8
J066P	3	2.14	0.69	0.31	1.00		0.92		0.92	3.94		3.94	8
J126P	1	2.08	0.68	0.35	1.03		0.97		0.97	3.92		3.92	8
MP544B	A	2.02	0.69	0.35	1.04		1.01		1.01	3.92		3.92	8
J109P	1	1.91	0.66	0.64	1.30		0.90		0.90	3.89		3.89	8
J066P	22	2.20	0.65	0.33	0.98		0.94		0.94	3.87		3.87	8
J012P	br2	1.96	0.64	0.37	1.01	0.01	0.98	0.02	1.00	4.03	0.01	4.03	8
J012P	br1	1.98	0.62	0.41	1.03	0.01	0.95	0.04	1.00	3.98	0.01	3.98	8
J066P	4	2.14	0.62	0.50	1.11		0.82		0.82	3.93		3.93	8
J109P	2	2.06	0.59	0.56	1.14		0.90		0.90	3.90		3.90	8
J066P	1	2.19	0.54	0.45	0.98		0.93		0.93	3.90		3.90	8
J066P	21	2.18	0.52	0.50	1.03		0.90		0.90	3.90		3.90	8
J012P	r3	1.99	0.52	0.49	1.01	0.03	0.90	0.08	1.00	4.00	0.01	4.00	8

of *chalcopyrite* and *galena* inclusions (Figs 191–192), and they are rimmed by pure *chalcopyrite*, forming structures interpreted as produced by solid-state diffusion. Minute *galena* grains occur along border of pure *chalcopyrite* and myrmekite. *Stannite* always contains low Zn. Structural features of myrmekites may indicate orientation of crystals of the original unstable phase, disintegrated to myrmekite.

The sample carrying *roquesite* contains two genetic types of *stannite* – independent grains enclosed in *chalcopyrite* and myrmekitic *stannite* exsolved in *chalcopyrite*. Composition of the two types of *stannite* is comparable – both show Fe and Zn variation up to boundary with *këesterite*. *Mawsonite* forming rims around *stannite* of the first type contains low Zn up to 2 wt.%. This also suggests that myrmekite domains represent an independent unstable phase.

Minor *stannite* occurrences were recorded in the whole ore district, with somewhat increased abundance in its northeastern part.

Stephanite Ag_5SbS_4

Mrňa and Pavlů (1967) [351] studied s*tephanite* from Jáchymov. They reported *stephanite* as nearly perfect, thin tabular or prismatic crystals up to 5 mm long. The mineral is black with a weak bluish tint and metallic lustre (Fig. 193). It is associated mainly with *proustite-pyrargyrite*, sometimes as a major component of ore. Notable occurrences are in lower levels of the Geschieber vein [351].

The present study established two types of *stephanite* occurrence in the central part

Fig. 193. Tabular crystal of stephanite (width of figure 6.7 mm). Photo J. & E. Sejkora.

Table 131. Calculated unit-cell parameters of stephanite from Jáchymov for the space group $Cmc2_1$.

sample	*a*	*b*	*c*
		(Å)	
J031P	7.8253(9)	12.451(1)	8.5391(9)
J032P	7.8164(9)	12.434(2)	8.5448(9)
[333]-NM9512	7.810(4)	12.441(5)	8.548(3)
VS20291	7.814(1)	12.431(1)	8.550(1)

Table 132. Microhardness of stephanite.

sample	mean	range	load
	[kp/mm^2]	[kp/mm^2]	[g]
[333]-NM9512	110	101–116	20

of the ore district. The first type includes granular aggregates and veinlets in fragments of vein quartz breccia cemented by *calcite*. *Stephanite* occurs with *argentite*, massive *proustite*, *marcasite* and wire *silver*. Some veins of this ore were probably up to 10 cm wide. It also forms grains with *nickel-skutterudite*, *rammelsbergite*, *argentite*, *proustite*, *chalcopyrite* and *pyrite*. Crystals up to 2 cm long of a thick columnar habit with striations on basal faces or tabular crystals showing a hypoparallel growth represent the second type of *stephanite*.

Stephanite with *proustite–pyrargyrite* and *polybasite* are deposited on red and white hornfelsic *quartz* in vugs of brecciated central part of vein. The analysed *stephanite* crystal contains a central inclusion of *arsenpolybasite*. Material of this type comes from the Svornost shaft, 8th, 10th and 12th levels, Geschieber vein.

Table 133. Chemical analyses of stephanite.

sample	pt.	Ag	Cu	Fe	Co	Ni	Zn	Pb	Bi	Sb	As	S	Total
							weight %						
[333]-NM9512		69.54						0.03	0.02	13.51	0.90	15.78	99.78
21017	1	67.91	0.28	0.81						15.10	0.28	16.33	100.71
21017	2	68.47	0.54	0.60						15.17	0.24	16.22	101.24
21018	b	68.33	0.27	0.71						15.02	0.25	16.34	100.92
21018	a	68.21	0.33	0.50						15.24	0.19	16.51	100.98
21018	c	68.59	0.53	0.57						15.28	0.19	16.11	101.27
21019	1	68.37	0.17	0.14			0.02			15.04	0.16	16.12	100.02
21019	2	68.24	0.13	0.19			0.09			15.09	0.78	16.19	100.71
21019	3	68.25	0.13	0.61			0.05			14.59	0.25	16.12	100.00
21019	5	68.26	0.16	0.16			0.08			14.97	0.06	16.28	99.97
J031P	a1	67.06	0.71	0.11	0.27	0.09				15.18	0.15	16.02	99.59
J031P	a4	66.73	1.31	0.52	0.03	0.15				15.83	0.79	16.43	101.79
J031P	5	67.85	0.39	0.10	0.10	0.54				15.52	0.23	16.06	100.79
J031P	6	67.52	0.82	0.19	0.30	0.29				15.11	0.16	15.91	100.30
J031P	11	67.17	0.78	0.03	0.10	0.23				15.43	0.13	16.01	99.88
J031P	12	66.48	0.97	0.17	0.26	0.05				15.86	0.04	15.96	99.79
J031P	13	66.43	0.90	0.65	0.06	0.09				14.63	0.41	16.36	99.53
J031P	14	65.53	0.97	0.12	0.53	0.33				14.61	0.42	16.43	98.94
J031P	15	67.23	0.13	0.35	0.17	0.06				14.67	0.81	16.63	100.05
J-702	a4	67.84	0.13	0.56		0.01	0.16			15.42	0.72	15.96	100.80
J-702	a5	67.40	0.36	0.42		0.23	0.19			15.24	0.07	16.28	100.19
J-702	1	67.41	0.63	0.48	0.34	0.18				15.05	0.29	16.23	100.61
J-702	1	67.87	1.31	0.11	0.13	0.53				14.51	0.35	16.40	101.21
J-702	2	68.42	0.09	0.30	0.38	0.11				15.11	0.15	16.55	101.11
J-702	2	66.81	1.05	0.24	0.22	0.11				14.75	0.02	16.21	99.41
J-702	3	68.00	0.26	0.36	0.21	0.10				14.59	0.90	16.39	100.81
J-702	3	68.11	1.03	0.12	0.11	0.15				14.09	0.83	16.25	100.69
J-702	4	67.29	0.10	0.57	0.12	0.10				14.98	0.77	16.89	100.82
J-702	4	68.25	0.18	0.16	0.17	0.27				14.99	0.54	16.35	100.91
J-841	4	69.90								12.06	2.03	16.44	100.43
J-841	5	68.39								12.02	2.38	16.33	99.13
J-841	6	68.25								14.34	0.74	16.53	99.86

Table 133. *(continued)*

sample	pt.	Ag	Cu	Fe	Co	Ni	Zn	subtotal	Sb	As	subtotal	S	Total
						number of atoms							
J031P	12	4.86	0.12	0.02	0.04	0.01		5.05	1.03	0.00	1.03	3.92	10
J031P	5	4.92	0.05	0.01	0.01	0.07		5.06	1.00	0.02	1.02	3.92	10
J031P	11	4.91	0.10	0.00	0.01	0.03		5.05	1.00	0.01	1.01	3.94	10
J031P	a4	4.74	0.16	0.07	0.00	0.02		5.00	1.00	0.08	1.08	3.93	10
J-702	a4	4.92	0.02	0.08		0.00	0.02	4.94	0.99	0.08	1.07	3.90	10
J-702	a5	4.89	0.04	0.06		0.03	0.02	4.93	0.98	0.01	0.99	3.97	10
21018	c	4.95	0.07	0.08				5.09	0.98	0.02	1.00	3.91	10
J031P	a1	4.91	0.09	0.02	0.04	0.01		5.06	0.98	0.02	1.00	3.94	10
21019	2	4.95	0.02	0.03			0.01	5.00	0.97	0.08	1.05	3.95	10
21019	5	4.98	0.02	0.02			0.01	5.03	0.97	0.01	0.97	4.00	10
21019	1	5.00	0.02	0.02			0.00	5.04	0.97	0.02	0.99	3.97	10
21017	1	4.90	0.03	0.11				5.04	0.97	0.03	0.99	3.96	10
21018	a	4.91	0.04	0.07				5.01	0.97	0.02	0.99	4.00	10
21017	2	4.93	0.07	0.08				5.08	0.97	0.03	0.99	3.93	10
J031P	6	4.91	0.10	0.03	0.04	0.04		5.12	0.97	0.02	0.99	3.89	10
J-702	2	4.91	0.01	0.04	0.05	0.02		4.92	0.96	0.02	0.98	4.00	10
J-702	4	4.92	0.02	0.02	0.02	0.04		5.02	0.96	0.06	1.01	3.97	10
21018	b	4.92	0.03	0.10				5.06	0.96	0.03	0.99	3.96	10
J-702	1	4.86	0.08	0.07	0.05	0.02		4.94	0.96	0.03	0.99	3.94	10
J-702	4	4.80	0.01	0.08	0.02	0.01		4.81	0.95	0.08	1.03	4.05	10
J-702	2	4.87	0.13	0.03	0.03	0.02		5.07	0.95	0.00	0.95	3.97	10
21019	3	4.97	0.02	0.09			0.01	5.08	0.94	0.03	0.97	3.95	10
J031P	15	4.85	0.02	0.05	0.02	0.01		4.94	0.94	0.08	1.02	4.04	10
J031P	13	4.81	0.11	0.09	0.01	0.01		5.03	0.94	0.04	0.98	3.99	10
J031P	14	4.76	0.12	0.02	0.07	0.04		5.01	0.94	0.04	0.98	4.01	10
J-702	3	4.89	0.03	0.05	0.03	0.01		4.92	0.93	0.09	1.02	3.97	10
J-841	6	4.96							0.92	0.08	1.00	4.04	10
J-702	1	4.85	0.16	0.02	0.02	0.07		5.11	0.92	0.04	0.95	3.94	10
J-702	3	4.90	0.13	0.02	0.01	0.02		5.08	0.90	0.09	0.99	3.94	10
[333]-NM9512		5.12						5.12	0.88	0.10	0.98	3.91	10
J-841	5	4.98							0.78	0.25	1.02	4.00	10
J-841	4	5.04							0.77	0.21	0.98	3.98	10

Experiments in the dry system Ag-Sb-S show that the mineral does not form above 197 ± 5 °C. *Stephanite* disintegrates to *argentite* and *pyrargyrite* [444]. Under natural hydrothermal conditions the temperature limit may be somewhat different but the information from experiments indicates that *stephanite* was not exposed to higher temperatures after its crystallization.

Sternbergite $AgFe_2S_3$

Haidinger [491] described *sternbergite* from Jáchymov as a new mineral. Mrňa and Pavlů [351] found out that *sternbergite* is very rare in their study material. It is associated with arsenide ores, where it takes position similar to that of *argentite* but it is somewhat more common in *arsenic–sulphide* ores in association with *proustite*. *Sternbergite* also occurs in *pyrite–marcasite* aggregates.

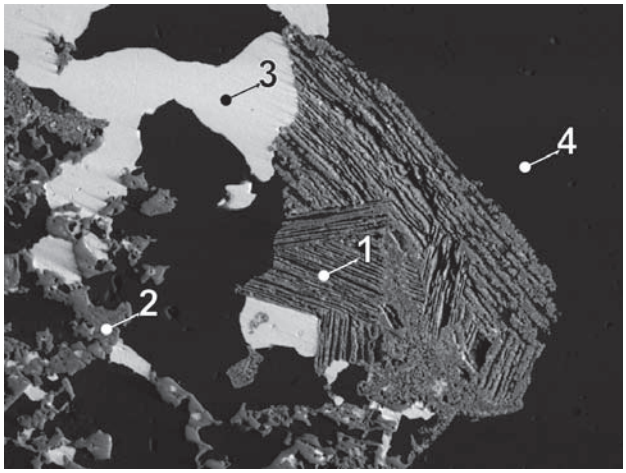

Fig. 194. MP271E/A. 1 – sternbergite, 2 – rammelsbergite, 3 – acanthite, 4 – calcite. Barbora shaft, 4th /5th level, vein No. 32. BSE image. Magnification 40×.

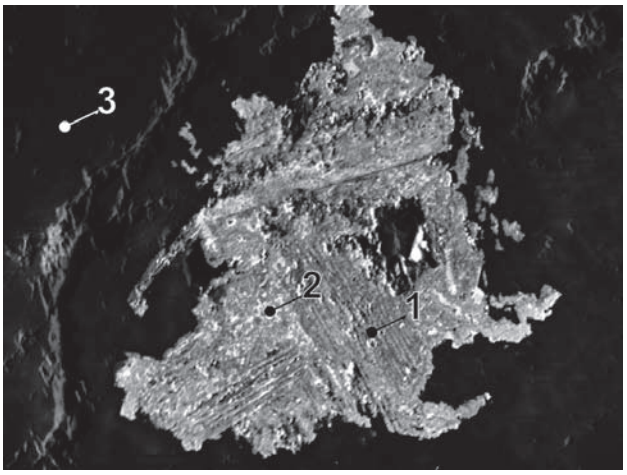

Fig. 195. MP271D. 1 – sternbergite, 2 – acanthite, 3 – calcite. Barbora shaft, 4th/5th level, vein No. 32. BSE image. Magnification 160×.

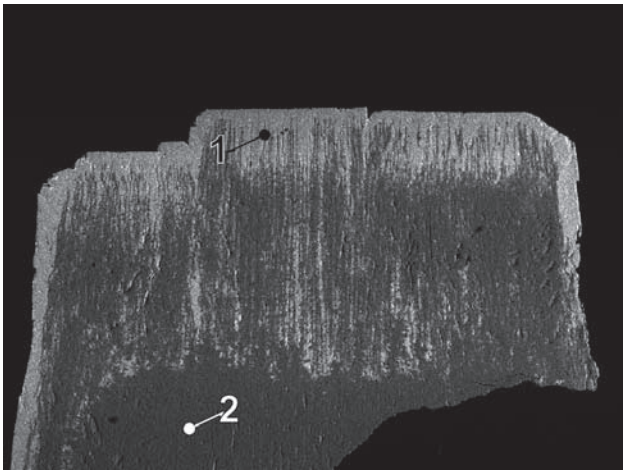

Fig. 196. VS7651/B. Section of a pseudomorph of sternbergite and pyrite (+marcasite) after an unknown mineral ("frieseite"?). 1 – sternbergite, 2 – pyrite (+marcasite). BSE image. Magnification 40×.

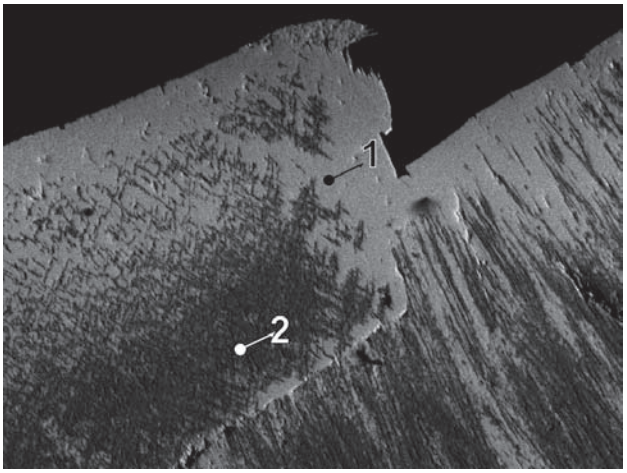

Fig. 197. VS7651/A. Detail from the section of the crystal. 1 – sternbergite, 2 – pyrite (+marcasite). BSE image. Magnification 80×.

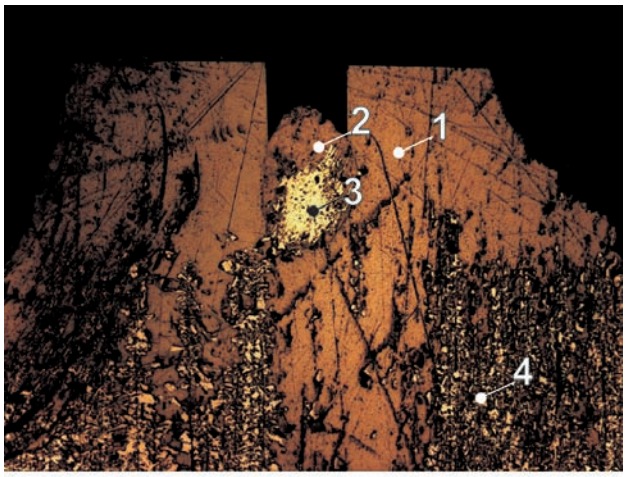

a

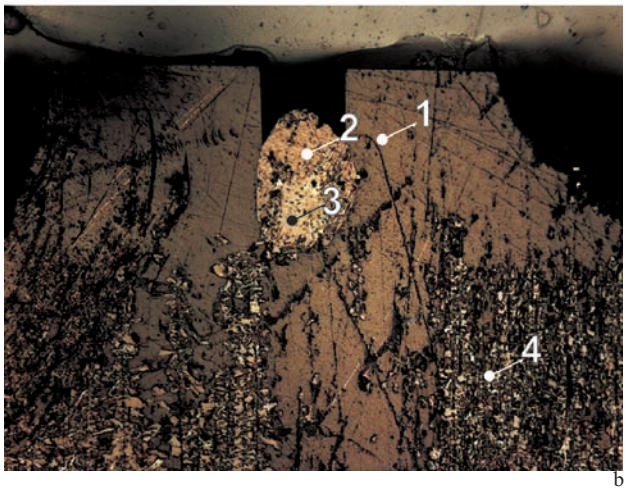

b

Fig. 198a, b. NM9519. 1 – sternbergite crystal parallel with section, 2 – sternbergite crystal perpendicular to section, 3 – marcasite, 4 – mixture of acanthite and marcasite. Reflected light, single polarizer (a), crossed polarizers (b). Magnification 50×.

Fig. 199. Group of tabular crystals of sternbergite (width of figure 1.3 cm). Photo J. & E. Sejkora.

Table 134. X-ray diffraction pattern of sternbergite (VS7651). *h*, *k*, *l* indices and intensity I_{calc} obtained from Rietveld structure refinement.

h	*k*	*l*	d	I_{calc}	I_{obs}	*h*	*k*	*l*	d	I_{calc}	I_{obs}	*h*	*k*	*l*	d	I_{calc}	I_{obs}
0	0	2	6.345	6	8	4	0	7	1.5379	3	1	0	4	8	1.1455	<1	1
2	0	0	5.810	13	20	2	0	8	1.5302	1	<1	6	0	9	1.1399	3	3
2	0	1	5.283	17	18	1	1	8	1.5292	9	4	3	3	9	1.1360	10	6
1	1	1	5.241	2	2	4	2	6	1.5193	5	2	4	4	7	1.1269	1	1
2	0	2	4.285	96	100	5	3	3	1.4971	6	4	5	3	8	1.1267	1	1
1	1	2	4.262	23	23	2	4	3	1.4904	3	1	8	2	6	1.1260	5	4
2	0	3	3.420	55	49	6	2	4	1.4790	3	1	2	4	8	1.1238	3	2
1	1	3	3.408	1	1	8	0	0	1.4526	1	1	5	5	3	1.1105	2	2
0	2	0	3.312	45	40	8	0	1	1.4431	1	1	5	1	10	1.0983	<1	1
3	1	1	3.233	74	59	4	4	0	1.4386	2	1	9	3	2	1.0978	3	4
0	0	4	3.172	100	84	7	1	4	1.4359	<1	1	4	2	10	1.0972	<1	1
3	1	2	2.958	23	30	0	2	8	1.4306	7	7	10	2	0	1.0965	1	2
0	2	2	2.936	5	5	5	3	4	1.4291	3	2	1	3	10	1.0953	<1	1
4	0	0	2.905	13	11	6	0	6	1.4283	3	2	8	4	0	1.0920	<1	1
2	2	0	2.877	19	15	2	4	4	1.4232	3	3	10	0	4	1.0912	1	2
4	0	1	2.832	3	4	8	0	2	1.4159	3	1	3	1	11	1.0905	3	7
2	0	4	2.784	2	2	4	4	2	1.4030	4	2	6	4	6	1.0816	3	7
1	1	4	2.778	93	77	5	1	7	1.3972	3	3	9	3	3	1.0778	<1	2
3	1	3	2.623	21	27	4	0	8	1.3922	3	2	4	0	11	1.0722	<1	2
2	2	2	2.620	17	21	2	2	8	1.3891	4	2	8	0	8	1.0712	1	2
4	0	3	2.395	33	21	8	0	3	1.3738	<1	1	7	3	7	1.0707	3	6
2	2	3	2.379	2	2	2	0	9	1.3702	2	3	4	4	8	1.0656	1	2
2	0	5	2.326	32	28	4	4	3	1.3620	4	6	6	0	10	1.0614	<1	<1
3	1	4	2.301	1	1	7	1	5	1.3597	3	2	3	3	10	1.0583	3	2
0	2	4	2.291	15	9	5	3	5	1.3539	8	5	5	3	9	1.0580	3	2
4	2	0	2.184	12	4	2	4	5	1.3489	4	2	0	0	12	1.0575	10	8
5	1	1	2.161	2	1	8	2	0	1.3302	2	2	2	4	9	1.0556	<1	<1
4	0	4	2.142	5	3	8	0	4	1.3207	<1	<1	2	6	3	1.0505	<1	<1
2	2	4	2.131	7	8	7	3	1	1.3197	3	3	2	0	12	1.0404	<1	<1
0	0	6	2.115	2	8	3	3	7	1.3175	3	3	10	2	4	1.0364	<1	1
5	1	2	2.073	2	2	6	2	6	1.3116	4	3	8	4	4	1.0325	<1	1
4	2	2	2.065	2	2	4	4	4	1.3102	1	<1	7	5	1	1.0320	<1	1
1	3	2	2.052	5	3	1	5	1	1.3092	2	1	11	1	2	1.0294	<1	<1
3	1	5	2.022	2	5	0	4	6	1.3038	4	2	8	2	8	1.0193	<1	3
2	0	6	1.9873	58	47	8	2	2	1.3019	2	1	4	6	2	1.0186	<1	1
5	1	3	1.9469	3	3	3	1	9	1.2992	5	4	10	0	6	1.0184	<1	1
4	2	3	1.9405	2	1	7	3	2	1.2988	2	1	7	3	8	1.0177	<1	1
6	0	0	1.9368	14	10	5	1	8	1.2852	<1	<1	11	1	3	1.0129	<1	1
1	3	3	1.9301	1	1	4	2	8	1.2834	4	2	8	0	9	1.0117	<1	1
6	0	1	1.9146	7	6	1	3	8	1.2804	8	3	6	2	10	1.0108	<1	1
4	0	5	1.9113	10	8	4	0	9	1.2684	4	4	0	2	12	1.0073	5	4
2	2	5	1.9033	2	1	1	5	3	1.2568	3	3	4	4	9	1.0070	2	1
3	3	1	1.8966	36	27	6	4	1	1.2524	2	1	7	5	3	1.0058	2	1
3	3	2	1.8361	8	3	4	4	5	1.2515	2	1	4	6	3	1.0025	<1	1
5	1	4	1.8039	3	3	3	5	1	1.2474	1	1	2	6	5	0.9973	<1	1
4	2	4	1.7989	5	5	9	1	2	1.2428	2	3	7	1	10	0.9967	<1	1
1	3	4	1.7905	34	29	2	0	10	1.2397	2	3	5	3	10	0.9944	<1	1
0	2	6	1.7825	7	6	1	1	10	1.2392	<1	1	4	0	12	0.9937	2	1
6	0	3	1.7609	8	10	6	4	2	1.2345	<1	1	2	2	12	0.9925	3	2
3	3	3	1.7469	17	17	6	0	8	1.2272	6	8	6	0	11	0.9911	2	1
2	0	7	1.7305	10	10	8	2	4	1.2268	1	1	3	3	11	0.9886	7	5
2	2	6	1.7041	26	19	7	3	4	1.2241	1	1	0	6	6	0.9786	1	2
6	2	0	1.6719	7	7	6	4	3	1.2063	2	2	10	0	7	0.9783	<1	<1
5	1	5	1.6593	7	7	7	1	7	1.2039	2	1	10	2	6	0.9735	<1	1
6	2	1	1.6575	<1	<1	3	5	3	1.2018	2	1	8	4	6	0.9703	<1	<1
0	4	0	1.6559	1	1	5	3	7	1.1999	4	2	7	3	9	0.9663	<1	1
4	2	5	1.6554	<1	1	8	0	6	1.1974	11	5	12	0	1	0.9656	<1	1
6	0	4	1.6530	6	5	2	4	7	1.1964	3	1	11	1	5	0.9649	<1	1
1	3	5	1.6489	<1	<1	4	4	6	1.1895	11	10	2	0	13	0.9626	<1	<1
3	3	4	1.6414	1	<1	3	1	10	1.1864	2	2	1	5	9	0.9621	3	4
6	2	2	1.6167	2	<1	5	1	9	1.1860	<1	1	6	6	1	0.9563	<1	<1
0	4	2	1.6022	2	1	1	3	9	1.1821	1	1	4	6	5	0.9559	<1	<1
7	1	1	1.5975	2	2	7	3	5	1.1759	2	4	8	0	10	0.9556	1	1
3	1	7	1.5936	3	4	1	5	5	1.1684	<1	1	4	2	12	0.9518	4	4
2	4	0	1.5925	7	7	10	0	0	1.1621	2	3	4	4	10	0.9516	<1	1
0	0	8	1.5862	22	22	2	2	10	1.1610	1	2	11	3	1	0.9503	<1	<1
7	1	2	1.5608	2	1	6	2	8	1.1507	3	3	12	0	3	0.9440	<1	1
5	3	2	1.5521	1	<1	5	5	1	1.1462	1	1	11	3	2	0.9424	<1	1

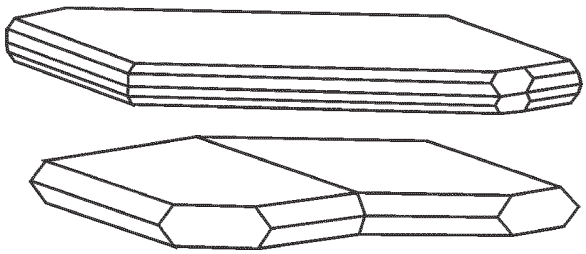

Fig. 200. Drawing of sternbergite crystal and twin by Haidinger [492].

In both types of occurrence, *sternbergite* does not usually exceed 0.01 mm in size [351].

The present study shows that *sternbergite* occurs in lamellar crystals in cavities of dolomite gangue; it may be coated by *calcite* crystals. It is intergrown in gangue along *dolomite–calcite* contact or deposited on minor fractures in gangue minerals. *Sternbergite* occurs intergrown with *proustite* as minor platy crystals coating *proustite*, together with *acanthite*, *galena*, *sphalerite,* and *pyrite.* Fresh *sternbergite* is light grey with a strong metallic lustre, but it rather quickly looses lustre and tarnishes to black. It has a perfect cleavage in one direction (Figs 194, 199). *Sternbergite* is perfectly malleable – a property, which serves for recognition of *sternbergite* from *argentopyrite*. It is a very rare mineral, which crystallized at temperatures below 150 °C.

Table 135. Calculated unit-cell parameters for the space group *Ccmb*, density and hardness of sternbergite from Jáchymov.

sample	unit-cell parameters (Å)			density (g.cm^{-3})	hardness
	a	*b*	*c*	D_m	H
VS7651	6.615(3)	11.620(5)	12.688(3)		
J-930 [485]	6.6190(4)	11.6400(8)	12.7070(10)		
[337]	6.625	11.558	12.750	4.158	
[491]				4.215	1–1.5

Table 136. Chemical analyses of sternbergite.

sample	pt.	Ag	Fe	Cu	Pb	Bi	S	As	Sb	Total
					weight %					
NM9519	1	34.91	35.55	0.07			29.85	0.13		100.50
NM9519	2	35.51	35.55	0.06			30.19			101.32
NM9519	3	34.46	35.53				30.09			100.09
NM9519	4	34.84	35.17				29.79			99.81
NM9519	5	34.82	35.08				29.81	0.14		99.84
NM9519	6	35.06	35.44				29.93	0.06		100.49
VS7651	1	34.19	35.44				30.28			99.91
VS7651	2	34.19	35.17				29.84			99.20
VS7651	3	33.49	35.10				30.38			98.96
VS7651	4	34.67	35.22				29.83			99.73
VS7651	5	34.49	34.83				29.85			99.16
VS7651	6	34.93	35.38				30.06			100.37
NM9520	0	34.89	34.66				30.45			100.00
NM9520	1	34.89	34.66				30.45			100.00
NM9520	2	35.71	34.85				30.41			100.98
NM9520	3	35.78	34.52	0.04			30.70	0.13		101.17
NM9520	4	34.70	34.89				30.25			99.84
NM4807	1	35.37	33.85	0.03			30.41	0.10		99.77
[487]		35.27	35.97				29.10			100.34
SR003	1	33.26	35.04	0.13			30.53	0.06	0.07	99.09
SR003	2	34.15	35.24	0.07			31.45	0.07	0.04	101.02
NM9514	1	34.03	36.05		0.15		30.99	0.07		101.29
NM9514	2	34.03	36.14		0.17		30.27			100.61
NM9514	3	33.89	35.51	0.07	0.20		30.72			100.39
NM9514	4	33.70	35.96		0.11		30.41			100.18
NM9514	5	33.59	35.83		0.24		30.63			100.29
NM9514	6	34.07	36.00		0.07		31.11			101.25
NM9514	7	34.16	35.27				30.29	0.07		99.79
NM9514	8	33.69	36.16			0.26	30.54			100.65
NM9514	9	34.16	35.56			0.07	30.18			99.97
NM9514	10	33.69	35.82			0.17	30.41			100.09
NM9514	11	33.77	35.92		0.17	0.03	30.66			100.55
NM9514	12	32.88	34.91	0.10			30.53			98.42
NM9514	13	33.18	35.38	0.15			31.13			99.84
NM9514	14	33.31	34.82	0.08	0.26		30.96			99.43
NM9514	15	33.56	34.80				30.97			99.33
NM9514	16	33.73	35.05		0.25		30.75			99.78
NM9514	17	33.90	34.94		0.11	0.06	30.85			99.86

Although more than fifty samples with Ag-Fe sulphides were inspected, none of them carried a joint association of the two polymorphs – *sternbergite* with *argentopyrite*.

A significant part of *sternbergite* is altered. The foliated crystals became brittle and magnetic. Polished sections show that such grains are decomposed to a fine-grained mixture of *acanthite* and remains of *sternbergite* (Figs 195, 198). Some *sternbergite* aggregates are altered to *pyrite–sternbergite* mixture. Alteration aggregates show indications of *sternbergite* perfect cleavage. This alteration is similar to that observed with *argentopyrite.*

Experiments at dry synthesis of *sternbergite* and *argentopyrite* were unsuccessful. *Sternbergite* on heating above 175 °C disintegrates to a mixture of strongly magnetic monoclinic *pyrrhotite+argentite+pyrite*. During prolonged quenching, *pyrrhotite* and *argentite* react to *pyrite* and *silver*. *Argentopyrite* decomposed at lower temperature (150 °C), suggesting that it is a lower-temperature polymorph [445].

The fact that *sternbergite* was unaltered in majority of studied samples indicates that it has a larger stability field than *argen-*

Table 136. *(continued)*

sample	pt.	Ag	Cu	Fe	S	As	Total
				number of atoms			
NM9519	1	1.03		2.02	2.95	0.01	6
NM9519	2	1.04		2.00	2.96		6
NM9519	3	1.01		2.02	2.97		6
NM9519	4	1.03		2.01	2.96		6
NM9519	5	1.03		2.00	2.96	0.01	6
NM9519	6	1.03		2.01	2.96		6
VS7651	1	1.00		2.01	2.99		6
VS7651	2	1.01		2.01	2.97		6
VS7651	3	0.99		2.00	3.01		6
VS7651	4	1.02		2.01	2.97		6
VS7651	5	1.02		2.00	2.98		6
VS7651	6	1.03		2.01	2.97		6
NM9520	0	1.02		1.97	3.01		6
NM9520	1	1.02		1.97	3.01		6
NM9520	2	1.04		1.97	2.99		6
NM9520	3	1.04		1.94	3.01	0.01	6
NM9520	4	1.02		1.98	3.00		6
NM4807	1	1.04		1.93	3.02		6
SR003	1	0.98	0.01	1.99	3.02		6
SR003	2	1.00	0.01	2.00	2.98	0.01	6
NM9514	1	0.98		2.01	3.01		6
NM9514	2	0.99		2.04	2.97		6
NM9514	3	0.99		2.00	3.01		6
NM9514	4	0.98		2.03	2.99		6
NM9514	5	0.98		2.02	3.00		6
NM9514	6	0.98		2.00	3.01		6
NM9514	7	1.00		2.00	2.99		6
NM9514	8	0.98		2.03	2.99		6
NM9514	9	1.00		2.02	2.98		6
NM9514	10	0.98		2.02	2.99		6
NM9514	11	0.98		2.02	3.00		6
NM9514	12	0.97	0.01	1.99	3.03		6
NM9514	13	0.96	0.01	1.99	3.04		6
NM9514	14	0.97		1.97	3.05		6
NM9514	15	0.98		1.97	3.05		6
NM9514	16	0.99		1.98	3.03		6
NM9514	17	0.99		1.97	3.03		6

The samples SR003/1,2 represent anhedral sternbergite grains in proustite; analysed in 1986 (O. Navrátil, L. Megerská).

topyrite. Altered *sternbergite* crystals show magnetism of variable intensity. The mechanism of *sternbergite* disintegration is probably similar to that of *argentopyrite*.

Unit-cell parameters and powder diffraction patterns are presented in Table 134 and Table 135.

Stibarsen SbAs

Small grains up to 5 μm in small cavities of *arsenic* were identified in a sample from the Svornost shaft, Adit level, Hildebrand vein. *Stibarsen* occurred also as angular grains along contact of *marcasite* rim around *bismuth* in the second sample from the Svornost shaft, Geschieber vein (Fig. 201).

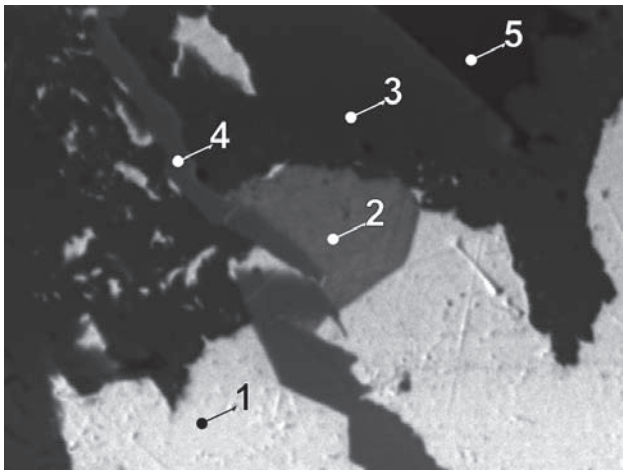

Fig. 201. G115A/F1. 1 – bismuth, 2 – stibarsen, 3 – marcasite, 4 – gersdorffite, 5 – carbonate. Svornost shaft, Geschieber vein. BSE image. Magnification 540×.

Stibnite Sb_2S_3

Stibnite from Jáchymov was described by Zückert [423]. Mrňa and Pavlů [351] reported an isolated find of *stibnite* with *pyrite* and *pyrargyrite* from the Svornost shaft, Adit

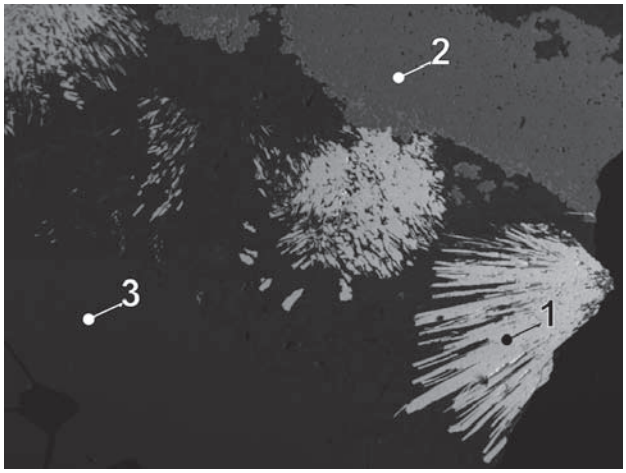

Fig. 202. J099P/B-1. 1 – stibnite, 2 – pyrite, 3 – calcite. Svornost shaft, Adit level, Hildebrand vein. BSE image. Magnification 16×.

Table 137. Chemical analyses of stibarsen.

sample	pt.	Sb	As	Bi	S	Ag	Fe	Cu	Total	Sb	As	Bi	Fe	Total
					weight %					number of atoms				
G115A	F-1	59.73	34.72	4.44	0.06		1.16		100.10	0.98	0.93	0.04	0.04	2
G115A	F-3	59.67	35.38	4.48	0.01		0.43		99.97	0.99	0.95	0.04	0.02	2
J105P	A1-1	60.70	36.36	3.44		0.09	0.08		100.67	0.99	0.97	0.03		2
G115A	F-2	59.97	34.98	4.47			0.32	0.04	99.78	1.00	0.95	0.04	0.01	2
G115A	F-4	59.77	34.99	4.69	0.02		0.20		99.66	1.00	0.95	0.05	0.01	2
J105P	A1-2	60.77	35.59	3.14			0.13	0.03	99.67	1.01	0.96	0.03		2

Table 138. Chemical analyses of stibnite.

sample	pt.	Sb	S	Fe	As	Total	Sb	S	Total
		weight %					number of atoms		
J105P	A	72.16	27.26	0.04	0.05	99.52	2.05	2.94	5
J099P	1	72.53	27.08		0.20	99.81	2.06	2.93	5

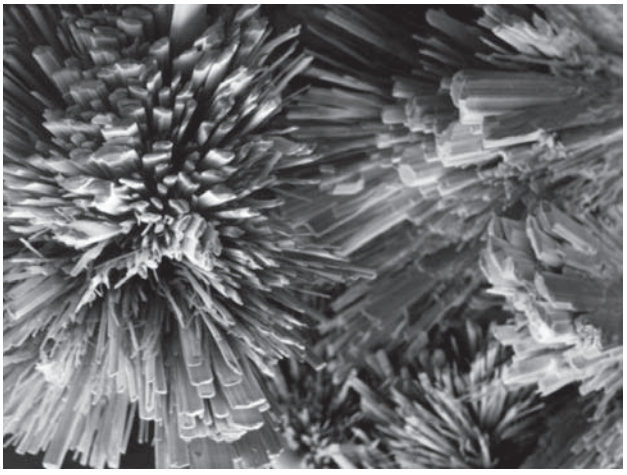

Fig. 203. Aggregates of stibnite crystals. Svornost shaft, Adit level, Hildebrand vein. SE image. Magnification 55×. Photo A. Gabašová.

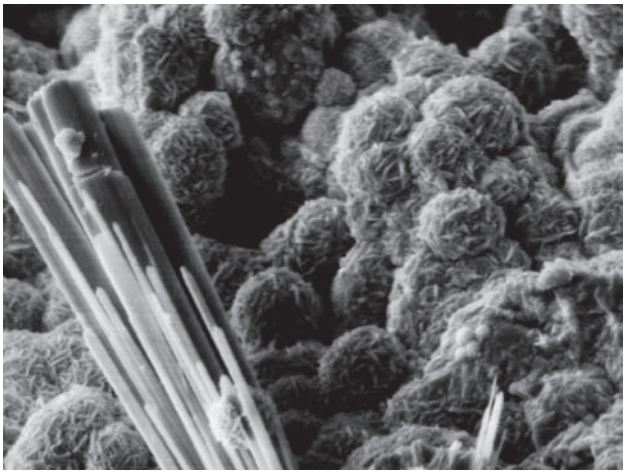

Fig. 204. Stibnite crystals on pyrite. Svornost shaft, Adit level, Hildebrand vein. SE image. Magnification 670×. Photo A. Gabašová.

level, Hildebrand vein. Zepharovich [391] mentioned *stibnite* from the Geister vein. *Stibnite* is usually listed as a rare mineral in Jáchymov. Wherever a closer location is given it refers always to the Hildebrand vein.

Stibnite forms acicular perfect crystals to 3 mm long, deposited on botryoidal *pyrite* and protruding into transparent *calcite* (Figs 202–204). Pink gangue *dolomite* is older than *pyrite* and *stibnite*. Radiating *stibnite* aggregates are sometimes replaced by aggregates of small, brown yellow *sphalerite* spheres (Figs 188, 190). *Pyrargyrite* described from this find [351] is in fact *miargyrite*. The studied sample, with the paragenesis *miargyrite–antimony–dyscrasite–stibnite–arsenic* comes from the Svornost shaft, Adit level, Hildebrand vein.

Stromeyerite AgCuS

It was identified as aggregates of lustrous black crystals in aggregates up to 0.5 mm long (Fig. 205), deposited on *chalcopyrite* coating minor vugs in *quartz–pyrite–chalcopyrite–bornite* vein. *Stromeyerite* also occurs in anhe-

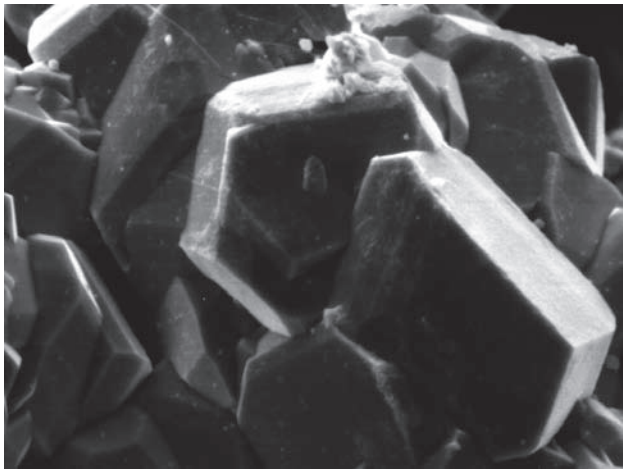

Fig. 205. J-716. Stromeyerite crystals in a cavity in chalcopyrite. Svornost shaft, Daniel level, Trojická or Geschieber vein. SE image. Magnification 1220×. Photo A. Gabašová.

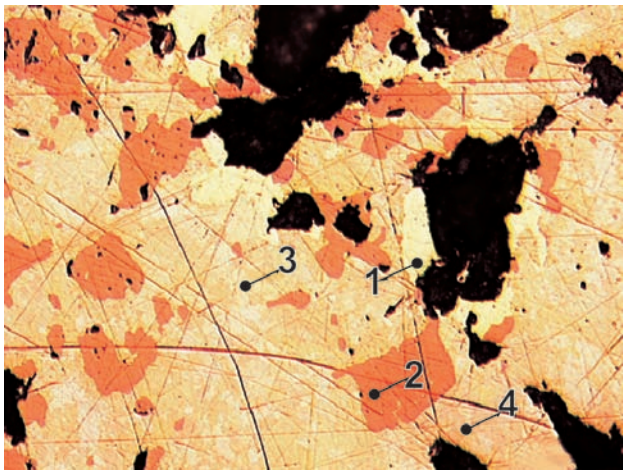

Fig. 206. J058P. Aggregates of young native silver at margins of myrmekitic aggregates of stromeyerite and tetrahedrite. Irregular aggregates and grains of bornite are also at the margins. 1 – silver, 2 – bornite, 3 – stromeyerite, 4 – tetrahedrite. Svornost shaft, Daniel level, intersection of Trojická and Geschieber veins. Reflected light, single polarizer. Magnification 130×.

Table 139. Calculated unit-cell parameters of stromeyerite from Jáchymov for the space group *Cmcm*.

sample	*a*	*b*	*c*
		(Å)	
J058P	4.0638(6)	6.6267(8)	7.975(1)

Table 140. Chemical analyses of stromeyerite.

sample	pt.	Cu	Ag	Fe	Co	Ni	S	Sb	As	Total	Cu	Ag	Fe	S	Total
		weight %									number of atoms				
J058P	3	30.93	50.92	0.40	0.34	0.12	15.43	0.62	0.24	99.00	1.00	0.97	0.02	0.99	3
J058P	4	31.41	50.86	0.54	0.40	0.11	15.58	0.67	0.33	99.90	1.00	0.96	0.02	0.99	3
J058P	8	31.77	50.92	0.29	0.18	0.17	15.36	0.55	0.36	99.60	1.02	0.96	0.01	0.98	3
J003P	1	31.43	52.67				15.17			99.27	1.02	1.01		0.97	3

dral grains up to 100 mm long in the vein material. It is accompanied by intergrown aggregate of *bornite*, *chalcopyrite*, *tennantite* and *covelite,* with individual *bornite* grains rimmed by myrmekitic intergrowth of *stromeyerite* and probable *tennantite* (Fig. 206).

The studied sample comes from the Svornost shaft, Daniel level, intersection of Trojická vein with Geschieber vein.

Synchysite-(Ce) $Ca(Ce,La)(CO_3)_2F$

Synchysite-(Ce) was identified by its chemical composition: Ca, O, Ce, Nd, Gd, La, Y, F, and C. It forms subhedral to euhedral lath-shaped crystals up to 100 μm long. This very rare mineral is enclosed in *dolomite* of a *dolomite–calcite* vein carrying *arsenic*, *galena* and *Cu-löllingite* (Fig. 207). The sample comes from the Barbora shaft.

Synchysite-(Ce) in anhedral to subhedral 30 μm grains enclosed with *monazite-(Ce)* in *chlorite* was identified in altered wall-rock carrying also minor *gold*. The sample is again from the Barbora shaft, between 7th and 8th level, probably near 1S vein.

Tennantite $Cu_{12}As_4S_{13}$

Vogl (1856) [59] reported massive *tennantite* occurrence with *skutterudite*, *galena*, *bismuth* and other minerals from Geister vein, Barbora adit. Sandberger (1885) mentioned *tennantite* in the succession of Jáchymov minerals.

According to Bernard [493] *tennantite* forms aggregates with *chalcopyrite* in a veinlet in white *calcite*. A sample from the Bratrství shaft, from the easternmost part of the district, contained also Ag, Bi, Cd, and Zn (spectral analysis) [493].

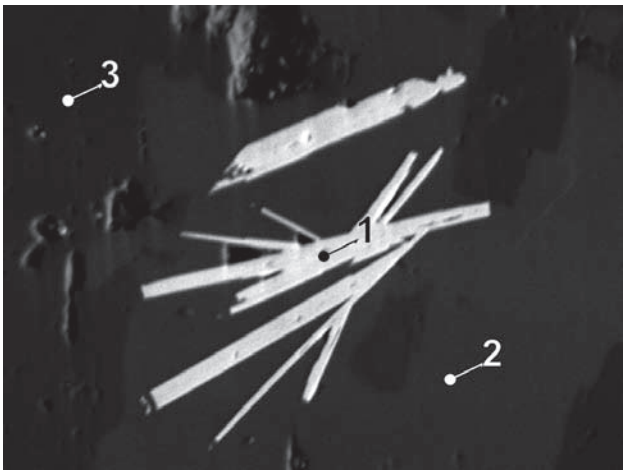

Fig. 207. MP420A/D-5. 1 – synchysite-(Ce), 2 – calcite, 3 – dolomite. Barbora shaft. BSE image. Magnification 400×.

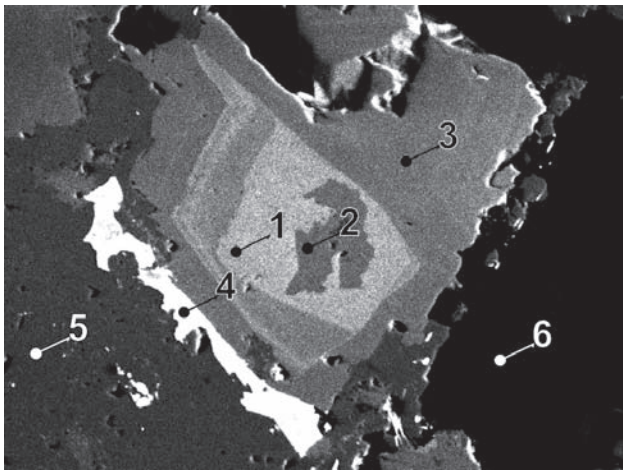

Fig. 208. J066P/11. 1 – Bi-tennantite, 2 – tennantite, 3 – Zn-tennantite, 4 – galena, 5 – chalcopyrite, 6 – dolomite. Giftkies adit. BSE image. Magnification 270×.

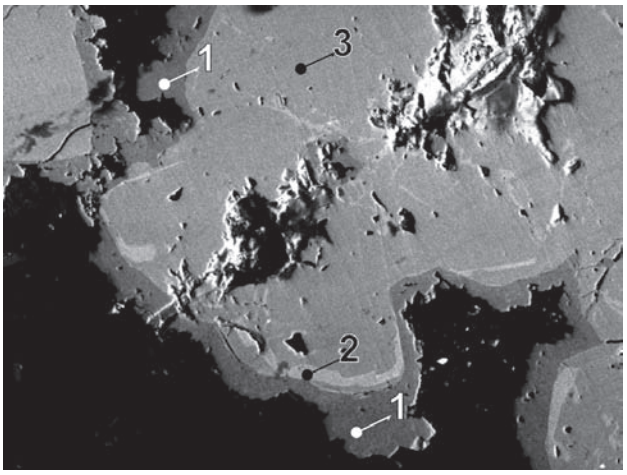

Fig. 209. MP389L. 1 – chalcopyrite, 2 – Sb-tennantite, 3 – tennantite. Rovnost I shaft. BSE image. Magnification 80×.

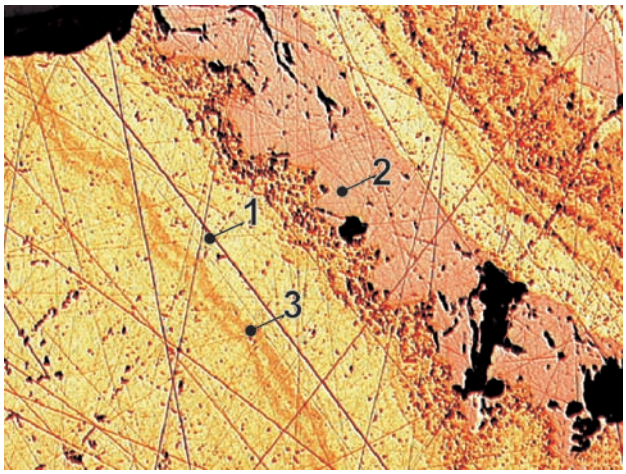

Fig. 211. J046P. Texture of repeated zones of botryoidal chalcopyrite and tennantite. Zones of chalcopyrite enriched in As may represent a submicroscopic intergrowths of chalcopyrite and tennantite. 1 – chalcopyrite, 2 – tennantite, 3 – As-chalcopyrite. Svornost shaft, 5th level, Prokop vein. Reflected light, single polarizer. Magnification 130×.

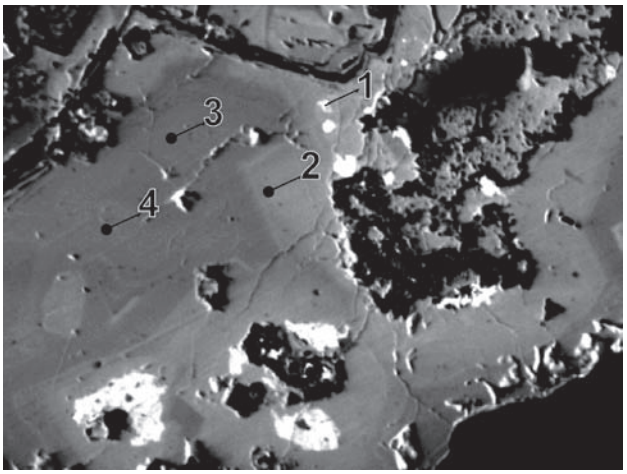

Fig. 210. J082P. 1 – bismuth, 2 – Bi-tennantite, 3 – tennantite, 4 – Sb-tennantite. BSE image. Magnification 200×.

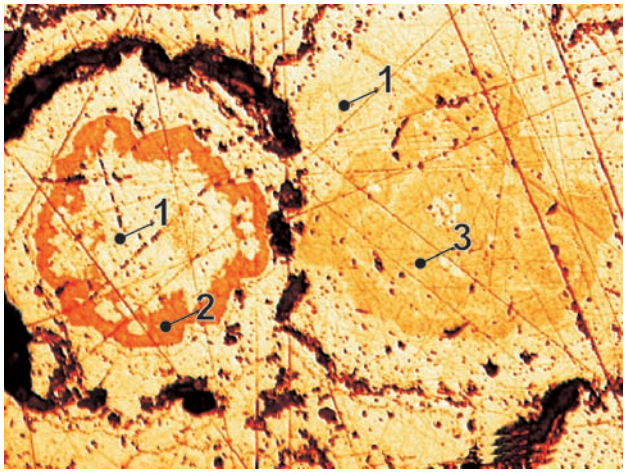

Fig. 212. J046P. 1 – chalcopyrite, 2 – tennantite, 3 – As-chalcopyrite. Svornost shaft, 5th level, Prokop vein. Reflected light, single polarizer. Magnification 260×.

Mrňa and Pavlů [351] presented data on *tennantite.* They noted massive, nearly monomineralic occurrences of *tennantite* with minor sulphides of polymetallic ores, mainly *chalcopyrite* [351].

In the present study, *tennantite* was typically observed as anhedral grains or aggregates in gangue or in other sulphides. It is often rimmed by *chalcopyrite*, which replaces *tennantite*. It was also identified in several separated zones in botryoidal *chalcopyrite* (Figs 211 and 212). This type of *tennantite* evolved from a colloform material, as noted by Geceva and Dubinkina [358]. *Tennantite* contains up to 10 wt.% Ag and shows zoned distribution of Sb and Ag or Sb, Pb and Bi. Central parts of aggregates contain lower amounts of minor elements. Zoning in Bi and Pb content was also recorded. Variation in Bi content in *tennantite* around *bismuth* inclusion suggests a possible solid-state diffusion of Bi (Fig. 210). In domains free of *bismuth* inclusions, representing probable growth zoning, the highest Bi concentration is 10 wt.% (Fig. 208). One example of *greenockite* inclusion in *tennantite* occurred.

Compositional variation in the series *tetrahedrite–tennatite* in connection with thermodynamic properties was discussed in several papers [426], [450], [451], [402], [405], [406], [407].

Tennantite is a quite common mineral in the district, usually accompanied by *chalcopyrite* and *pyrite,* less frequently by *sphalerite*, *galena,* and *löllingite*. It overgows *rammelsbergite*, *sphalerite* or *nickeline*.

Table 141. Calculated unit-cell parameters of tennantite from Jáchymov for the space group $I\bar{4}3m$.

sample	*a* (Å)
[493]	10.225(12)
J059P	10.1952(4)

Table 142. Chemical analyses of tennantite.

sample	pt.	Cu	Ag	Bi	Fe	Zn	Hg	Co	Ni	As	Sb	S	Total
							weight %						
J010P	r4	43.87	0.49		3.37	4.16				19.87	0.20	28.42	100.38
J010P	r5	42.57	0.46		3.26	4.61				20.51	0.09	28.32	99.82
J010P	r5a	42.77	0.47		3.28	4.75				20.62	0.01	28.23	100.13
J010P	4	42.91	0.59		3.35	4.75	0.22			19.80	0.25	28.14	100.01
J010P	5b	41.99	0.99		3.75	4.48	0.07			19.96	0.60	28.16	100.00
J010P	5	42.17	0.56		3.51	4.69	0.24			20.41	0.08	28.32	99.98
J010P	5a	42.13	0.57		3.48	4.83	0.12			20.50		28.37	100.00
J014P	A2	42.33	0.61		3.56	4.81	0.19			19.84	0.22	28.44	100.00
J014P	A/3	42.37	0.49		3.57	4.61	0.32			20.33	0.12	28.21	100.02
J014P	Ar3	43.47	0.45		3.29	4.51				20.53	0.11	28.33	100.69
J014P	Ar2	43.29	0.49		3.52	4.51				19.94	0.09	28.56	100.40
J014P	Ar1	42.59	0.56		2.71	5.62				19.73	0.01	28.12	99.34
J014P	A1	42.89	0.58		2.51	5.71	0.22			19.93		28.16	100.00
J022P	Ar2	42.01	0.89		3.19	4.67				19.83	0.39	28.21	99.19
J022P	A2	42.19	1.01		3.21	4.76	0.37			19.75	0.38	28.33	100.00
J022P	A1	42.21	0.45		3.67	4.55	0.41			19.52	0.35	28.74	99.90
J022P	Ar1	43.31	0.41		3.57	4.42				19.72	0.34	28.45	100.22
J022P	A3	42.40	0.64		3.50	4.39	0.27			20.12	0.24	28.44	100.00
J022P	Ar3	42.23	0.55		3.41	4.28				20.25	0.22	28.31	99.25
J022P	Ar4	42.26	0.45		3.59	4.63				19.83	0.21	28.45	99.42
J022P	A4	42.46	0.54		3.71	4.78	0.35			19.63	0.20	28.33	100.00
J023P	r	43.68	0.51		4.35	3.56				19.68	0.19	28.45	100.42
J023P	1	42.91	0.53		4.21	3.76	0.48			19.37	0.20	28.54	100.00
J046P	6	42.18	0.37		5.79	1.07		0.17	0.09	20.63	0.66	27.47	98.43
J046P	9	42.62	0.31		4.95	2.90			0.24	19.10	2.14	27.76	100.02
J046P	10	42.15	0.50		6.58	0.88		0.20	0.11	20.08	0.55	27.81	98.86
J046P	11	43.12	0.50		7.22	0.19		0.23	0.35	19.86	0.38	27.54	99.39
J046P	12	43.19	0.35		4.60	2.48		0.11		19.05	1.20	27.61	98.59
J058P	15	43.24	0.76		6.39	0.96			0.18	20.10	0.64	27.82	100.09
J058P	16	42.43	0.55		6.95	0.65		0.12	0.18	19.35	1.40	27.78	99.41
J058P	17	42.60	0.72		6.82	0.50		0.11	0.06	18.68	2.51	27.64	99.64
J059P	1	43.26	0.50		6.24	0.88		0.10		20.16	0.31	27.95	99.40
J059P	2	44.07	0.37		6.12	1.06		0.10	0.14	19.49	0.98	27.83	100.16
J059P	6	44.09	0.39		5.66	0.96			0.07	19.44	0.83	27.86	99.30
J059P	7	44.16	0.19		5.62	1.37			0.16	20.09	0.91	27.93	100.43
J059P	8	43.83	0.47		7.43	0.21		0.14	0.21	19.25	0.37	28.30	100.21
J059P	10	43.01	0.23		5.16	1.47		0.13	0.11	20.11	0.62	27.97	98.81
J059P	11	44.21	0.66		6.31	0.79		0.18	0.27	19.18	0.39	28.09	100.08
J062P	1b	42.59	1.29		6.01	0.86				20.24	0.61	28.69	100.29
J062P	1a	42.67	1.34		7.13	0.87				20.34	0.57	28.72	101.64
J062P	1c	42.91	1.57		5.87	1.26				20.67	0.43	28.64	101.35
J062P	1	42.82	1.40		5.99	1.95				20.30	0.41	28.74	101.61
J065P	4	39.76			2.13	5.56				11.04	17.49	23.92	99.89
J065P	5	40.88	0.13		6.69					18.13	7.95	26.64	100.41
J066P	1	40.04		9.70	3.13	4.30				14.08	0.36	27.20	98.80
J066P	2	42.17		0.32	5.26	2.44				20.81	0.25	28.88	100.14
J066P	3	41.68		0.10	1.86	6.61				20.03	0.33	27.53	98.14
J066P	4	41.36		0.29	1.10	7.79				19.90	1.26	28.48	100.17
J066P	5	39.69		10.05	3.22	4.32				15.03	0.43	25.60	98.34
J066P	6	40.39		9.78	4.50	2.37				15.62	0.26	26.10	99.03
J066P	7	42.93		0.70	5.29	1.74				20.50	0.13	27.58	98.86

Table 142. *(continued)*

sample	pt.	Cu	Ag	Fe	Zn	Hg	Co	Ni	subtotal	As	Sb	Bi	S	subtotal	Total
							number of atoms								
J010P	r4	10.15	0.07	0.89	0.94				12.04	3.90	0.02		13.03	16.96	29
J010P	r5	9.91	0.06	0.86	1.04				11.88	4.05	0.01		13.06	17.12	29
J010P	r5a	9.94	0.06	0.87	1.07				11.94	4.06	0.00		13.00	17.06	29
J010P	4	10.00	0.08	0.89	1.08	0.02			12.06	3.91	0.03		13.00	16.94	29
J010P	5b	9.80	0.14	1.00	1.02	0.01			11.95	3.95	0.07		13.02	17.05	29
J010P	5	9.81	0.08	0.93	1.06	0.02			11.90	4.03	0.01		13.06	17.10	29
J010P	5a	9.79	0.08	0.92	1.09	0.01			11.89	4.04	0.00		13.07	17.11	29
J014P	A2	9.84	0.08	0.94	1.09	0.01			11.96	3.91	0.03		13.10	17.04	29
J014P	Ar3	10.05	0.06	0.87	1.01					4.02	0.01		12.98	17.01	29
J014P	Ar2	10.00	0.07	0.93	1.01				12.01	3.91	0.01		13.08	16.99	29
J014P	A/3	9.87	0.07	0.95	1.04	0.02			11.95	4.02	0.01		13.02	17.05	29
J014P	Ar1	9.97	0.08	0.72	1.28				12.04	3.92	0.00		13.04	16.96	29
J014P	A1	10.00	0.08	0.67	1.29	0.02			12.05	3.94	0.00		13.01	16.95	29
J022P	Ar2	9.85	0.12	0.85	1.06				11.89	3.95	0.05		13.11	17.11	29
J022P	A2	9.85	0.14	0.85	1.08	0.03			11.94	3.91	0.05		13.10	17.06	29
J022P	Ar1	10.03	0.06	0.94	1.00				12.02	3.87	0.04		13.06	16.98	29
J022P	A1	9.80	0.06	0.97	1.03	0.03			11.89	3.84	0.04		13.22	17.11	29
J022P	Ar4	9.85	0.06	0.95	1.05				11.91	3.92	0.03		13.14	17.09	29
J022P	Ar3	9.88	0.08	0.91	0.97				11.83	4.02	0.03		13.12	17.17	29
J022P	A3	9.86	0.09	0.93	0.99	0.02			11.89	3.97	0.03		13.11	17.11	29
J022P	A4	9.88	0.07	0.98	1.08	0.03			12.04	3.87	0.02		13.06	16.96	29
J023P	r	10.09	0.07	1.14	0.80				12.10	3.86	0.02		13.02	16.90	29
J023P	1	9.96	0.07	1.11	0.85	0.04			12.03	3.81	0.02		13.13	16.97	29
J046P	6	9.98	0.05	1.56	0.25		0.04	0.02	11.90	4.14	0.08		12.88	17.10	29
J046P	9	9.98	0.04	1.32	0.66			0.06	12.06	3.79	0.26		12.88	16.94	29
J046P	10	9.89	0.07	1.76	0.20		0.05	0.03	12.00	4.00	0.07		12.94	17.00	29
J046P	11	10.08	0.07	1.92	0.04		0.06	0.09	12.26	3.94	0.05		12.76	16.74	29
J046P	12	10.21	0.05	1.24	0.57		0.03		12.09	3.82	0.15		12.94	16.91	29
J058P	15	10.06	0.10	1.69	0.22			0.05	12.12	3.97	0.08		12.83	16.88	29
J058P	16	9.94	0.08	1.85	0.15		0.03	0.05	12.09	3.84	0.17		12.90	16.91	29
J058P	17	10.01	0.10	1.82	0.11		0.03	0.02	12.09	3.72	0.31		12.88	16.91	29
J059P	1	10.10	0.07	1.66	0.20		0.03		12.05	3.99	0.04		12.93	16.96	29
J059P	2	10.25	0.05	1.62	0.24		0.03	0.04	12.22	3.84	0.12		12.82	16.79	29
J059P	6	10.32	0.05	1.51	0.22			0.02	12.12	3.86	0.10		12.92	16.88	29
J059P	7	10.24	0.03	1.48	0.31			0.04	12.10	3.95	0.11		12.84	16.90	29
J059P	8	10.11	0.06	1.95	0.05		0.04	0.05	12.26	3.77	0.05		12.94	16.75	29
J059P	10	10.10	0.03	1.38	0.34		0.03	0.03	11.90	4.00	0.08		13.02	17.10	29
J059P	11	10.24	0.09	1.66	0.18		0.05	0.07	12.29	3.77	0.05		12.90	16.71	29
J062P	1b	9.85	0.18	1.58	0.19				11.80	3.97	0.07		13.15	17.20	29
J062P	1a	9.75	0.18	1.85	0.19				11.98	3.94	0.07		13.01	17.02	29
J062P	1	9.80	0.19	1.56	0.43				11.98	3.94	0.05		13.03	17.02	29
J062P	1c	9.86	0.21	1.53	0.28				11.88	4.03	0.05		13.04	17.12	29
J065P	4	10.16		0.62	1.38				12.16	2.39	2.33		12.12	16.84	29
J065P	5	9.81	0.02	1.83					11.65	3.69	1.00		12.67	17.35	29
J066P	1	9.94		0.88	1.04				11.87	2.97	0.05	0.73	13.39	17.13	29
J066P	2	9.73		1.38	0.55				11.66	4.07	0.03	0.02	13.21	17.34	29
J066P	3	9.66		0.29	1.76				11.71	3.92	0.16	0.02	13.19	17.29	29
J066P	4	10.11		1.28	0.58				11.97	3.32	0.03	0.74	12.94	17.03	29
J066P	5	9.91		0.50	1.53				11.94	4.04	0.04	0.01	12.97	17.06	29
J066P	6	10.07		0.93	1.07				12.06	3.23	0.06	0.78	12.87	16.94	29
J066P	7	10.12		1.42	0.40				11.94	4.10	0.02	0.05	12.89	17.06	29

Tetrahedrite $Cu_{12}Sb_4S_{13}$

According to Vogl [59], minerals of the *tetrahedrite* group are rare in Jáchymov veins. Babánek [364] reported *terahedrite* from Hildebrand vein, Svornost shaft, in a zone of white *quartz* with *bornite*, *nickeline*, *chalcocite,* and *silver*.

Scharizer [535] considered *tetrahedrite* from Jáchymov as a new mineral named "*falkenhaynit*". Kutina [366] revised the type specimen of "*falkenhaynit*" from Fiedler vein, deposited in the National Museum, Prague, No. 4854. The mineral with density of 4.83 g/cm^3 and unit-cell parameter a = 10.357 Å was shown to be identical with *tetrahedrite*.

During the present study, *tetrahedrite* was found only in several cases. In a sample from the Giftkies adit, it fills a thin fracture in milky white vein *quartz* enclosing minute *tennantite*, *bornite*, *chalcocite,* and *chalcopyrite,* suggesting that *tetrahedrite* is younger than the associated sulphides. A second sample is massive *tetrahedrite* with *quartz* and *ankerite*, described originally as "*falkenhaynit*" (see above). The third sample from the

Fig. 213. Well-formed tetrahedrite crystals on calcite (width of figure 1.1 cm). Photo J. & E. Sejkora.

Table 143. Calculated unit-cell parameters of tetrahedrite from Jáchymov for the space group $I\bar{4}3m$ [443].

sample	*a* (Å)
NM4854 (J-844)	10.3332(3)

Table 144. Chemical analyses of tetrahedrite.

sample	pt.	Cu	Ag	Fe	Zn	Co	Ni	Sb	As	S	Total
						weight %					
J065P	1	38.49		1.50	5.88			20.19	8.38	25.30	99.74
J065P	2	38.02	0.10	1.31	6.23			19.16	9.27	25.45	99.54
J065P	3	38.13	0.03	1.70	5.91			19.65	9.14	25.16	99.72
J173P	A1	38.63	0.66	4.74	1.69			22.00	7.53	25.49	100.73
J173P	A2	37.73	0.85	4.62	1.53			22.31	7.64	25.11	99.78
J173P	A3	38.20	0.47	4.30	1.94			22.57	7.13	24.86	99.46
J173P	A4	37.48	0.59	4.29	2.13			26.44	3.61	24.44	98.98
J173P	A5	37.27	0.81	4.44	1.77			24.90	5.10	24.62	98.92
J058P	13	38.23	0.65	1.28	7.09	0.25	0.13	22.63	3.73	25.46	99.45
J058P	14	38.92	0.48	1.57	6.46	0.09	0.09	20.03	6.69	25.88	100.21

sample	pt.	Cu	Ag	Fe	Zn	Co	Ni	subtotal	Sb	As	S	subtotal	Total
							number of atoms						
J065P	1	9.82		0.44	1.46			11.71	2.69	1.81	12.79	17.29	29
J065P	2	9.68	0.02	0.38	1.54			11.61	2.55	2.00	12.84	17.39	29
J065P	3	9.73		0.49	1.46			11.69	2.62	1.98	12.72	17.31	29
J173P	A1	9.79	0.10	1.37	0.42			11.67	2.91	1.62	12.80	17.33	29
J173P	A2	9.69	0.13	1.35	0.38			11.56	2.99	1.67	12.79	17.44	29
J173P	A3	9.86	0.07	1.26	0.49			11.68	3.04	1.56	12.72	17.32	29
J173P	A4	9.87	0.09	1.29	0.54			11.80	3.64	0.81	12.76	17.20	29
J173P	A5	9.77	0.13	1.32	0.45			11.67	3.41	1.13	12.79	17.33	29
J058P	13	9.83	0.10	0.37	1.77	0.07	0.04	12.18	3.04	0.81	12.97	16.82	29
J058P	14	9.82	0.07	0.45	1.59	0.02	0.03	11.98	2.64	1.43	12.95	17.02	29

Vladimír shaft, M-2 vein, contains several *tetrahedrite* grains enclosed in *bornite* veinlet. Other well-formed *tetrahedrite* crystals come from collection of National Museum, Prague (Fig. 213).

Tetrahedrite is rare in Jáchymov though local *tennantites* contain a common admixture of Sb.

Topaz $Al_2SiO_4(F,OH)_2$

Coarse-grained parts of greisen carry euhedral *topaz* crystals, usually transparent and colourless, but fine blue crystals also occur. This type of greisen comes from the Rovnost I shaft, probably 8th level. Inconspicuous *topaz* was identified in muscovite mica schist with *arsenopyrite* and zoned W-rich *rutile* from the Nikolaj shaft, 1st level, cross cut to the Rovnost I shaft.

Table 145. Calculated unit-cell parameters of topas from Jáchymov for the space group *Pbnm*.

sample	*a*	*b*	*c*
		(Å)	
J-912	4.6501(8)	8.830(1)	8.413(1)

Uraninite $(U^{4+}_{1-x-y-z}U^{6+}_{x}REE^{3+}_{y}M^{2+}_{z}\square_{v})O_{2+x-0.5y-z-2v}$

Mrňa and Pavlů [351] characterized *uraninite* as the main mineral of *carbonate-uraninite* mineralization stage. It forms massive botryoidal aggregates or thin veinlets bordering wall-rocks, while central parts of veins are filled with *dolomite* pigmented by Fe oxides (Figs 214–215). Less common gangue mineral with *uraninite* is *quartz*. *Uraninite* is present nearly in all N-S veins and exceptionally it may occur in some parts of the E-W veins (see the section *Genetic and paragenetic relations of the vein system*).

Janeczek [150] characterized *uraninite* from Jáchymov as very heterogeneous. This is shown by variation in chemical analyses, particularly in Pb, Zr and Y contents. The increased Si contents, interpreted in [150] by entry of Si into interlayer positions along [111], could be alternatively interpreted by a heterogeneous admixture of amorphous gels $SiO_2 \cdot nH_2O$. The latter interpretation would correspond to geochemi-

cal conditions of formation, low totals of analyses indicating increased H_2O content confirmed by IR analysis [150], as well as the heterogeneous composition of *uraninite*. *Uraninite* often contains increased amounts of rare earth elements [351]. Breithaupt [556] determined density of Jáchymov *uraninite* of 6.609 g/cm^3.

The position of *uraninite* in succession is not uniform. Owing to tendency to migrate, some *uraninite* was remobilized from sites of primary deposition in the course of younger mineralization processes. This results in several generations of *uraninite,* which can be identified by associations of accompanying minerals. A small quantity of uranium was mobilized during the *arsenide* stage, resulting in deposition of tiny *uraninite* spherolites along internal contours of arsenide lenses. The spherolites are sometimes sitting directly on *silver* or *bismuth* and they often follow growth zones in arsenide aggregates or contacts of arsenides with gangue minerals.

Uraninite lenses tend to form "ore columns" in favourable parts of veins.

During the present research, attention was paid mainly to a younger generation of *uraninite* in association with arsenides and to the few examples of association with copper-dominated sulphides.

Uraninite occurs in carbonate gangue, hosting later crystallized skeletal Ni-arsenides, mainly *rammelsbergite*.

Table 146. Calculated unit-cell parameters and density of uraninite from Jáchymov.

sample	unit-cell parameter (Å)	density (g.cm^{-3})	
	a	D_m	D_X
[339]	5.47		
[150]	5.385		
[453]		6.53	9.94
[468]		9.22–9.28	

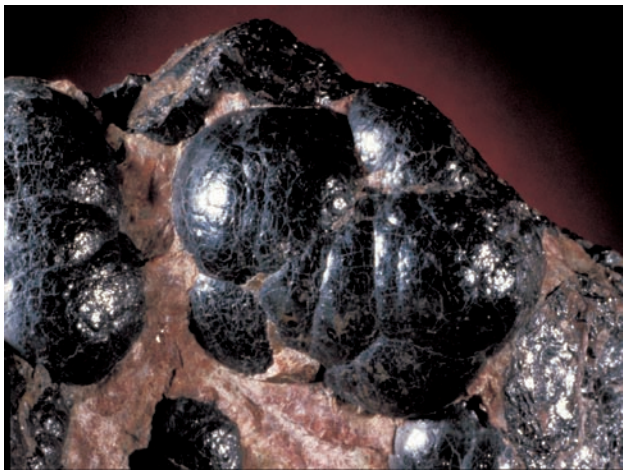

Fig. 214. Black uraninite aggregates in gangue (width of figure 6 cm). Photo J. & E. Sejkora.

Fig. 215. Uraninite vein. Magnification 1.5×. Photo J. Hloušek.

Table 147. Chemical analyses of uraninite.

sample		pt.	UO_2	ZrO_2	TiO_2	FeO	PbO	Y_2O_3	Ce_2O_3	SiO_2	P_2O_5	Bi_2O_3	BaO	CaO	Total
									weight %						
SR004	rim	1	76.36	0.09	0.23	0.61	2.73	0.67		2.31	0.45	0.11	0.43	1.24	85.23
SR004	rim	2	79.84	0.15	0.19	0.54	1.43	0.42		2.06	0.39	0.09	0.37	1.31	86.79
SR004	center	3	81.66	0.40	0.25	0.61	1.85	0.57		1.37	0.32	0.14	0.20	1.54	88.91
SR004	center	4	83.12	–	0.07	0.43	2.36	0.49		1.12	0.17	0.09	0.12	1.43	89.40
[150]		1	78.18	0.08		0.78	1.77	0.58	0.49	1.77	0.25			4.46	88.36
[150]		2	81.54	0.02			1.93	0.70	0.54	1.23	0.14			5.30	91.90*

* sample contains also: (wt.%): La_2O_3 (0.07), Gd_2O_3 (0.10), Tb_2O_3 (0.34)

sample		pt.	U^{4+}	Ca^{2+}	Ba^{2+}	Fe^{2+}	Pb^{2+}	Zr^{4+}	Ti^{4+}	Y^{3+}	Ce^{3}	Si^{4+}	P^{5+}	subtotal	O
									number of atoms						
SR004	rim	1	0.79	0.06	0.01	0.02	0.03		0.01	0.02		0.11	0.02	1.07	2
SR004	rim	2	0.81	0.06	0.01	0.02	0.02		0.01	0.01		0.09	0.02	1.05	2
SR004	center	3	0.83	0.08		0.02	0.02	0.01	0.01	0.01		0.06	0.01	1.05	2
SR004	center	4	0.87	0.07		0.02	0.03			0.01		0.05	0.01	1.06	2
[150]		1	0.76	0.21		0.03	0.02			0.01	0.01	0.08	0.01	1.13	2
[150]		2	0.78	0.25			0.02			0.02	0.01	0.05	0.01	1.14	2

samples SR002/1-4 represents *arsenide* stage, Bratrství mine (analyst O. Navrátil, 1987).

Radiating *rammelsbergite* aggregates often rim *uraninite* of the second generation. *Rammelsbergite* also penetrates *uraninite* along contraction fractures up to central parts of spheroidal aggregates. In these cases *uraninite* is affected by a weak coffinitization. In some instances, *uraninite* is partly replaced apart from arsenides also by sulphides such as *galena*, *sphalerite,* and *chalcopyrite*.

Special interest represent *uraninites* associated with *quartz* or *chalcedony* and in exceptional cases also with V-rich minerals, e.g., *roscoelite* and V-rich mica. *Uraninite* spherolites show radial fractures, which provided access for silica-rich solutions. This resulted in extensive coffinitization of *uraninite* up to predominance of *coffinite* over *uraninite*. In such cases contraction fractures carry *bornite* aggregates and rare *chalcopyrite*, *pyrite, covellite* or rare examples of minor sheet *silver.*

In a rare example of great interest is *uraninite* containing clusters of flaky *roscoelite* with a decreased V content (V_2O_3 as low as 9 wt.%) at contact with *uraninite*. Notable is the presence of Y-rich phosphate, possibly corresponding to *xenotime-(Y)*.

Rare *uraninite* was recorded in greisen as 15 μm sphere enclosed in *zircon*, or a grain 50 μm long, enclosed in *annite*. This sample comes from the Rovnost I shaft, probably 8th level.

According to older analyses [354], Jáchymov *uraninite* is free of Se but contains some Tl. Vanadium contents in uranium ores were 0.2 wt.%. Wöhler in [336] assumed that the source of vanadium was in red carbonates accompanying *uraninite*, but Patera [336] found no traces of vanadium in carbonates of various colours. Molybdenum, for long time unknown in Jáchymov, was determined in various products in the process of the manufacture of yellow uranium colours [336]. A black mineral intergrown with pyrite and named "*pateraite*" [209] was considered as carrying Mo. The mineral was discredited but respective samples do contain some Mo [475].

Uraninite aggregates show mostly colloform structure with typical pattern of radiating and tangential fractures, suggesting fractures in a drying gel. Ore and gangue minerals of nearly all the younger mineralization stages, including a younger *uraninite*, occur as filling of the fractures. *Uraninite* is often accompanied by *pyrite*.

Vaesite NiS_2

Disulphides of Fe and Ni are closely intergrown in some samples, suggesting the possibility that crystals with predominance of *pyrite* component may contain growth zones with variable Ni content (Figs 139, 216).

Table 148. Calculated unit-cell parameters of vaesite from Jáchymov for the space group $Pa\bar{3}$.

sample	*a* (Å)
J-790	5.6808(1)
J-236	5.638(1)

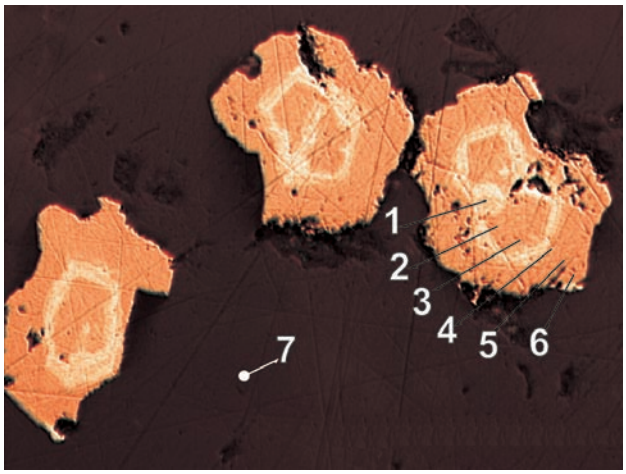

Fig. 216. MP295. Zoned and corroded crystals of pyrite-vaesite with internal zones of chalcopyrite. Zones with varying Fe and Ni content cannot be visually distiguished. 1 – chalcopyrite, 2 – Ni-pyrite, 3 – vaesite-(22%Fe), 4 – vaesite-(19%Fe), 5 – vaesite-(11%Fe), 6 – vaesite-(7%Fe), 7 – dolomite. Eva shaft, 3rd level, vein No. 2. Reflected light, single polarizer. Magnification 325×.

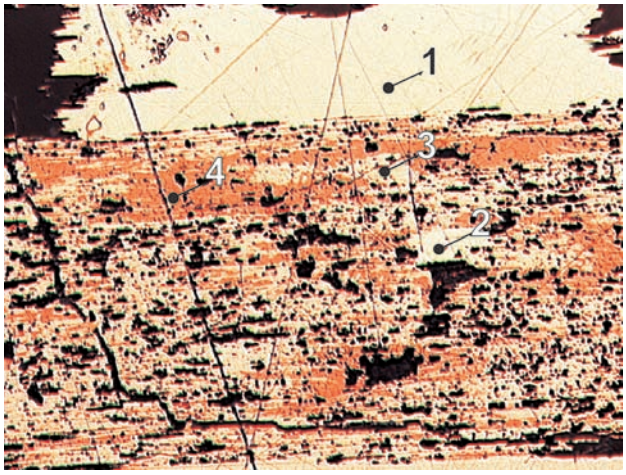

Fig. 217. MP430. Partly disintegrated nickel-skutterudite is replaced along growth zones by rammelsbergite and vaesite, showing variable composition and optical properties. 1 – nickel-skutterudite, 2 – rammelsbergite, 3 – S-rammelsbergite, 4 – vaesite. Barbora shaft, 5th level, vein No. 32. Reflected light, single polarizer. Magnification 260×.

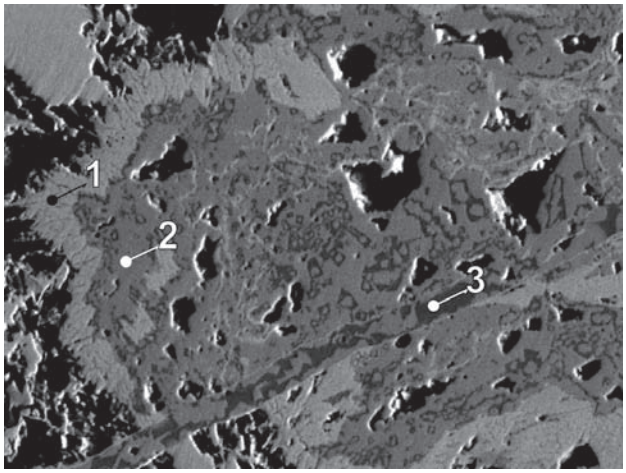

Fig. 218. MP175B/d. 1 – nickeline, 2 – gersdorffite, 3 – vaesite. Eva shaft, 3rd level, vein No. 25. BSE image. Magnification 270×.

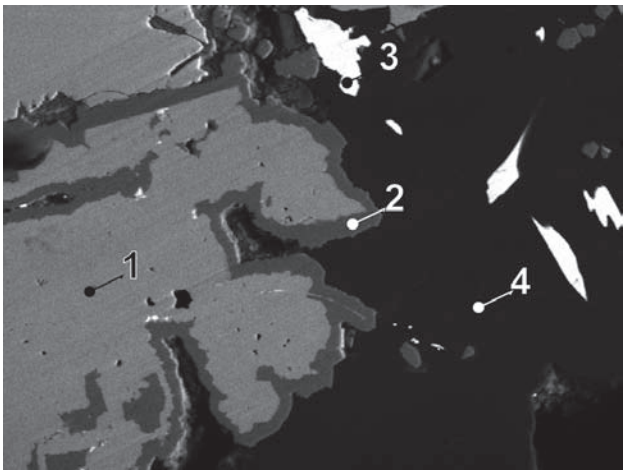

Fig. 219. MP296/B. 1 – rammelsbergite, 2 – vaesite-pyrite, 3 – bismuthinite, 4 – dolomite. Bratrství shaft, 5th level, Františka vein. BSE image. Magnification 400×.

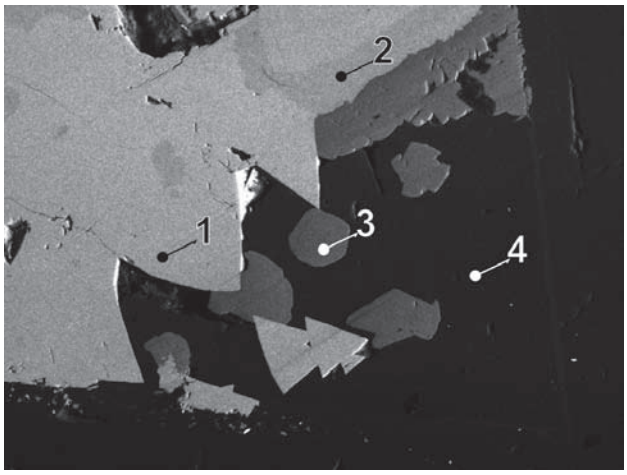

Fig. 220. MP296/E. 1 – nickel-skutterudite, 2 – rammelsbergite, 3 – vaesite-pyrite, 4 – dolomite. Bratrství shaft, 5th level, Františka vein. BSE image. Magnification 130×.

Table 149. Chemical analyses of vaesite.

sample	pt.	Ni	Fe	Co	Cu	Zn	Sb	S	As	Total
					weight %					
MP175B	D1	40.62	4.48	0.16	0.23			44.99	9.72	100.19
MP175B	D2	40.27	5.53	0.21	0.00			43.84	10.06	99.93
J017P	ar2	38.01	8.11	0.12	0.63	0.55		45.54	7.02	99.98
J017P	ar1	37.66	9.03	0.35	0.79	0.51		46.51	5.51	100.36
J017P	r9	37.55	8.62	0.56	0.63	0.50		47.05	4.97	99.88
MP295	6	35.46	5.75	5.18	1.35		1.30	47.81	3.68	100.53
MP295	5	34.17	10.72	1.74	0.88		0.99	49.59	1.67	99.76
MP430	8	33.05	6.34	7.21	0.47		0.33	46.86	5.34	99.60
MP430	7	32.01	8.73	6.28	1.10		0.37	45.95	5.17	99.61
MP430	9	31.20	6.89	8.70	0.54		0.56	46.56	5.82	100.27
J017P	ar4	30.93	13.32	0.52	0.55	0.51		45.59	8.05	99.47
J017P	r11	30.24	20.05	0.55	0.61	0.44		46.04	2.13	100.06
MP295	4	27.15	19.16	1.49	0.61		1.07	49.67	1.80	100.95
J017P	ar3	26.00	17.65	0.79	0.71	0.60		46.25	7.13	99.13
MP296	B1	21.47	19.14	5.75	0.09			48.53	5.37	100.36
MP296	B1a	20.78	19.28	5.57	0.16			48.16	5.08	99.04

sample	pt.	Ni	Fe	Co	Cu	subtotal	S	As	subtotal	Total
						number of atoms				
MP175B	D1	0.90	0.10			1.00	1.82	0.17	1.99	3
MP175B	D2	0.90	0.13			1.03	1.79	0.18	1.97	3
J017P	ar2	0.84	0.19		0.01	1.05	1.83	0.12	1.95	3
J017P	ar1	0.82	0.21	0.01	0.02	1.06	1.85	0.09	1.94	3
J017P	r9	0.82	0.20	0.01	0.01	1.05	1.87	0.09	1.96	3
MP295	6	0.77	0.13	0.11	0.03	1.03	1.89	0.06	1.95	3
MP295	5	0.73	0.24	0.04	0.02	1.02	1.94	0.03	1.97	3
MP430	8	0.72	0.15	0.16	0.01	1.03	1.87	0.09	1.96	3
MP430	7	0.70	0.20	0.14	0.02	1.06	1.85	0.09	1.93	3
MP430	9	0.68	0.16	0.19	0.01	1.04	1.86	0.10	1.96	3
J017P	ar4	0.68	0.31	0.01	0.01	1.02	1.84	0.14	1.98	3
J017P	r11	0.65	0.46	0.01	0.01	1.14	1.82	0.04	1.86	3
MP295	4	0.57	0.43	0.03	0.01	1.04	1.92	0.03	1.95	3
J017P	ar3	0.57	0.41	0.02	0.01	1.02	1.86	0.12	1.98	3
MP296	B1	0.46	0.43	0.12		1.01	1.90	0.09	1.99	3
MP296	B1a	0.45	0.44	0.12		1.01	1.90	0.09	1.99	3

Vaesite occurs as brownish yellow, zoned rims up to 30 μm wide on *rammelsbergite* and *nickel-skutterudite* (Fig. 219), and as spheroidal forms in small cavities and along crystal edges of *nickel-skutterudite* (Fig. 220). Chemical compositions are near the *pyrite-vaesite* boundary, with *pyrite* dominant in cores of spheres and a prevalence of *vaesite* in outer rims. This material comes from the Bratrství shaft, 5th level, Františka vein and a similar material comes from the Nikolaj shaft, 1st level, vein No. 25.

Vaesite was also identified in a thin veinlet in nickeline composed of *nickeline*, *gersdorffite*, and *vaesite* in a sample from the Eva shaft, 3rd level, vein No. 25 (Fig. 218).

Violarite $FeNi_2S_4$

Violarite is a rare mineral, with pink yellow or pink colour in polished section (Fig. 221). Sample from the Svornost shaft contains 50 μm grain of *violarite* enclosed in *argentite*, surrounded by *nickel-skutterudite*. It is interesting that this *violarite* contains no Co. The sample comes from the Svornost shaft, 8th level, Geschieber vein, the southern section.

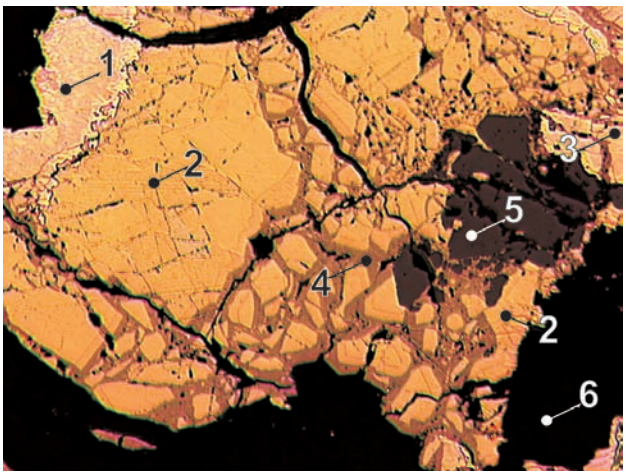

Fig. 221. J017P. Nickeline veinlet enclosing sphalerite is partly replaced by pyrite and rammelsbergite. Violarite forms corrosive zones around fractured nickeline in proximity of carbonate. 1 – As-pyrite, 2 – nickeline, 3 – rammelsbergite, 4 – violarite, 5 – sphalerite, 6 – carbonate. Bratrství shaft. Reflected light, single polarizer. Magnification 160×.

Table 150. Chemical analyses of violarite.

sample	pt.	Ni	Fe	Co	Cu	S	Sb	As	Total
					weight %				
J114P	F1	43.12	13.78	0.08	0.00	42.48	0.12		99.59
J114P	F2	42.56	14.68	0.07	0.21	43.11	0.00		100.63
J114P	F3	44.52	12.90	0.05	0.00	42.94	0.49		100.90
MP72	F	33.65	21.48	2.08	0.27	42.75	0.07	0.37	100.66

sample	pt.	Ni	Fe	Co	subtotal	S	Total
					number of atoms		
J114P	F1	2.23	0.75		2.98	4.02	7
J114P	F2	2.17	0.79		2.96	4.03	7
J114P	F3	2.28	0.69		2.97	4.02	7
MP72	F	1.72	1.15	0.11	2.98	3.99	7

Another *violarite* occurrence from the Eliáš mine, 2A vein, represents 50 μm grains on *sphalerite* or among *millerite* crystals. This *violarite* contains 2 wt.% Co.

Wittichenite Cu_3BiS_3

Wittichenite forms an intermediate zone around *sphalerite* "eyes" (up to 50 μm in size), carrying *greenockite* grains. The internal zone consists of *galena*, while the outer zone is *bismuthinite* (Fig. 79). In some places

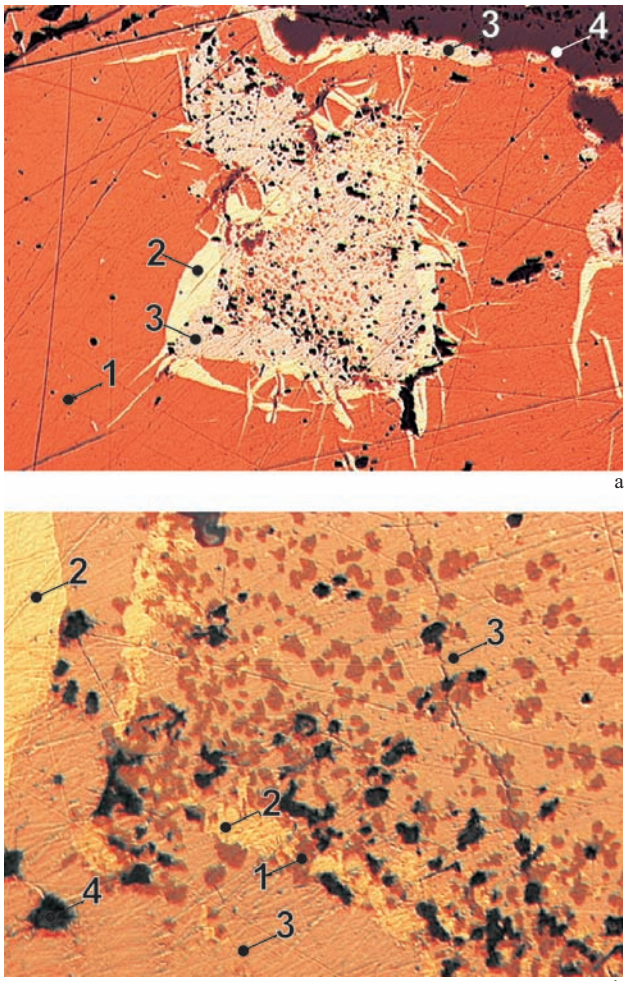

Fig. 222. Wittichenite forms exsolutions in bornite or discontinuous rims on bornite. Wittichenite is partly intergrown with chalcopyrite and partly bound by lenticular chalcopyrite domains. Oval grains of bornite also occur inside wittichenite grains. MP112. Eliáš mine, 180m level, vein A. 1 – bornite, 2 – chalcopyrite, 3 – wittichenite, 4 – quartz. Magnification a) 130×, b) 325×.

wittichenite replaced lobate *bismuth*. The sample comes from the Barbora shaft, 5th level, No. 32 vein.

It also forms 10 μm wide rims of *sphalerite* aggregates, which are younger than adjacent *Co-nickel-skutterudite* in a sample from the Eva shaft, 3rd level, No. 25 vein (Fig. 223). In another sample from the same shaft, 5th level, No. 32 vein, *wittichenite* forms 5 μm wide cir-

cular zone in *chalcopyrite* "eye" (Fig. 67). The central part of the concentric aggregate consists of *millerite* and *fletcherite* occurs next to the *millerite-chalcopyrite* interface. A round *wittichenite* grain 30 μm across is enclosed in *chalcopyrite* in brecciated vein with *quartz*, *chalcopyrite* and *bornite* from the shaft Vladimír, M-5 vein (Fig. 222).

In a sample from the Giftkies adit, w*ittichenite* forms exsolved, suboval particles up to 3 μm scattered in *chalcopyrite*, intergrown with *stannite*, *sphalerite*, *galena*, and *bornite*. It was also identified as two 5 μm grains intergrown with 30 μm long *greenockite* grain in milky *quartz* from the Giftkies adit.

These observations indicate the presence of two generations of *wittichenite.* Association with *stannite* is characteristic of the older generation and with *nickel-skutterudite* is characteristic of the younger one.

Xanthoconite Ag_3AsS_3

Babánek [364] described black tabular crystals of *xanthoconite* deposited on *proustite.* The crystals are partly

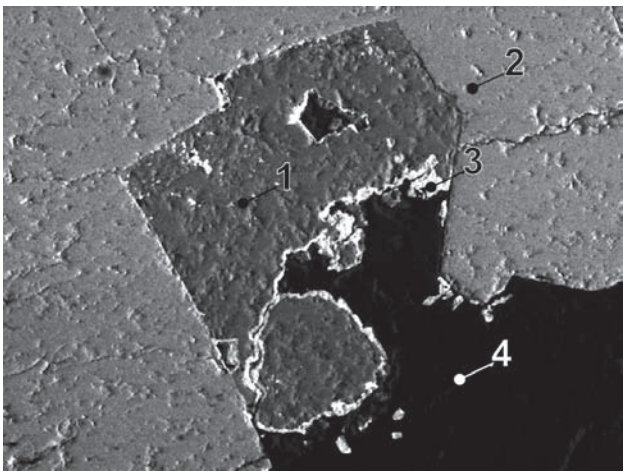

Fig. 223. MP175A/1. 1 – sphalerite, 2 – nickel-skutterudite, 3 – wittichenite, 4 – quartz. Eva shaft, 3rd level, vein No. 25. BSE image. Magnification 160×.

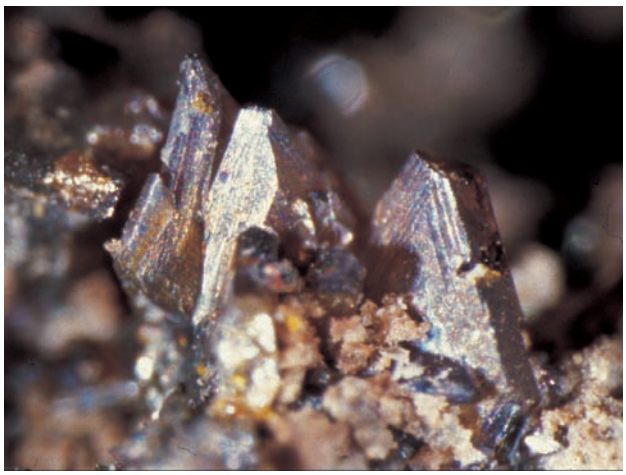

Fig. 224. Yellow-brown xanthoconite crystals (width of figure 1.9 mm). Photo J. & E. Sejkora.

Table 151. Chemical analyses of wittichenite.

sample	pt.	Cu	Ag	Sb	Fe	Bi	Pb	S	Total
					weight %				
MP112	1	37.32	0.20	0.21	0.36	41.93		19.64	99.66
MP112	2	37.52	0.52	0.49	0.13	41.77		19.30	99.73
MP112	3	38.14	0.19	0.28	0.46	41.50		19.40	99.97
MP112	6	38.30	0.94	0.65	0.31	41.13		19.43	100.76
MP112	7	38.42	0.66	0.47	0.12	41.46		19.55	100.68
MP112	1	37.82	0.64	0.39	0.25	41.97		19.17	100.24
MP112	1a	37.85	0.49	0.19	0.39	41.66		19.38	99.96
MP112	1b	37.67	0.37	0.34	0.42	41.97		19.27	100.04
MP230	2	36.49	0.11		2.01	41.22	0.20	19.06	99.08
MP175A	1	35.49	0.70			40.20	0.32	19.78	96.50

sample	pt.	Cu	Ag	Fe	subtotal	Bi	Pb	Sb	subtotal	S	Total
						number of atoms					
MP112	1	2.91	0.01	0.03	2.96	1.00		0.01	1.01	3.04	7
MP112	2	2.95	0.02	0.01	2.98	1.00		0.02	1.02	3.00	7
MP112	3	2.97	0.01	0.04	3.02	0.98		0.01	0.99	2.99	7
MP112	6	2.96	0.04	0.03	3.03	0.97		0.03	0.99	2.98	7
MP112	7	2.97	0.03	0.01	3.01	0.98		0.02	0.99	3.00	7
MP112	1	2.96	0.03	0.02	3.01	1.00		0.02	1.02	2.97	7
MP112	1a	2.95	0.02	0.04	3.01	0.99		0.01	1.00	3.00	7
MP112	1b	2.95	0.02	0.04	3.00	1.00		0.01	1.01	2.99	7
MP230	2	2.86	0.01	0.18	3.05	0.98			0.99	2.96	7
MP175A	1	2.84	0.03		2.87	0.98	0.01		0.99	3.14	7

Fig. 225. Orange xanthoconite crystals (width of figure 3.2 cm). Photo J. & E. Sejkora.

Table 153. Chemical analyses of xanthoconite.

sample	pt.	Ag	Cu	Fe	Sb	As	S	Total
				weight %				
SR005	1	65.39	0.11	0.08	0.23	14.93	19.48	100.22
SR005	2	65.63	0.07	0.08	0.17	14.90	19.26	100.11
SR005	3	65.72	0.14	0.05	0.13	14.80	19.30	100.14
SR005	4	64.90	0.18	0.10	0.06	15.34	19.57	100.15

sample	pt.	Ag	Cu	Fe	Sb	As	S	Total
				number of atoms				
SR005	1	2.99	0.01	0.01	0.01	0.98	3.00	7
SR005	2	3.02	0.01	0.01	0.01	0.99	2.98	7
SR005	3	3.02	0.01	0.00	0.01	0.98	2.98	7
SR005	4	2.96	0.01	0.01		1.01	3.01	7

The sample SR005 represents a crystal grown on dolomite from Jáchymov collected in 1974 and analysed in 1981 (L. Megerská).

Table 152. Calculated unit-cell parameters of xanthoconite from Jáchymov for the space group *C*2/*c* and density.

sample	unit-cell parameters (Å, °)				density (g.cm^{-3})	
	a	*b*	*c*	β	D_m	D_x
MP531	12.08(1)	6.314(1)	17.110(3)	110.90(4)		
[334]	12.00(1)	6.26(1)	17.08(1)	110.0(3)		
[338]	12.02	6.272	17.09	110.35	5.54	5.53

translucent in golden yellow to orange colours. Some old-time descriptions of *xanthoconite* (*rittingerite)* exist [338], [369], [371], [388], [557].

Xanthoconite was identified in *calcite* veinlet with a vug. Cleavable, yellow orange grains to 1 mm long are enclosed in *calcite*. The vug in *calcite* carries *xanthoconite* crystals of the same colour, up to 1 mm long, with adamantine lustre (Figs 224 and 225). Typical are yellow brown internal reflections in polished section; microhardness VHN_{20} = 123(107-131) kp/mm^2 [500].

Xanthoconite in Jáchymov occurs in the succession: *dolomite*–Ni,Co-arsenides–*proustite–xanthoconite*.

The mineral was rarely found as small isolated crystals up to 2 mm long, deposited in cavities after dendritic silver in arsenic. This *xanthoconite* is dark red with an orange tint, which make it difficult to recognize from *proustite*, associated in crystals of a similar size. This sample comes from the Svornost shaft, 5th level, Geschieber vein.

Xenotime-(Y) (Y,U,Ca)PO$_4$

Xenotime-(Y) was identified in rock and in the vein material. One 10 μm grain was enclosed with *zircon* in zoned W-rich *rutile* in *quartz* in mineralized micaceous gneiss from the Giftkies adit.

Table 154. Chemical analyses of xenotime-(Y).

sample	pt.	SiO_2	Y_2O_3	P_2O_5	UO_3	CaO	As_2O_5	Total
				weight %				
J059P	1	3.16	19.00	19.30	42.12	5.45	6.96	95.99
J059P	1a	3.25	18.79	19.11	42.07	5.32	6.75	95.29
J059P	1b	2.59	18.83	19.51	41.25	5.68	6.22	94.08

sample	pt.	Y	U	Ca	subtotal	P	As	Si	subtotal	O
					number of atoms					
J059P	1	0.39	0.34	0.22	0.96	0.63	0.14	0.12	0.89	4
J059P	1a	0.39	0.34	0.22	0.95	0.63	0.14	0.13	0.90	4
J059P	1b	0.39	0.34	0.24	0.98	0.65	0.13	0.10	0.88	4

Table 155. Calculated unit-cell parameters of xenotime-(Y) from Jáchymov for the space group $I4_1/amd$.

sample	*a*	*c*
	(Å)	
J-912	6.9081(8)	6.045(2)

Xenotime-(Y) in radiating prismatic crystals up to 5 mm long was identified in brownish red hornfelsic *quartz* from the Geister and Schweizer veins. *Xenotime-(Y)* has the same colour as quartz gangue which makes the mineral very inconspicuous.

Zavaritskite BiOF

The mineral constitutes replacement rims up to 50 μm wide around bismuth. The porous aggregates with *zavaritskite* deposited on fluorite are violet black. The sample comes from the Schönerz adit (Fig. 226).

Table 157. Chemical analyses of an unknown phase BiSb.

sample	pt.	Fe	Cu	As	Sb	Bi	Total
				weight %			
J105P	a1	0.10	0.07	1.60	36.22	61.15	99.13
J105P	a2	0.00	0.16	1.32	37.75	60.75	99.98

sample	pt.	As	Sb	Bi	Total
		number of atoms			
J105P	a1	0.03	0.48	0.48	1
J105P	a2	0.03	0.50	0.47	1

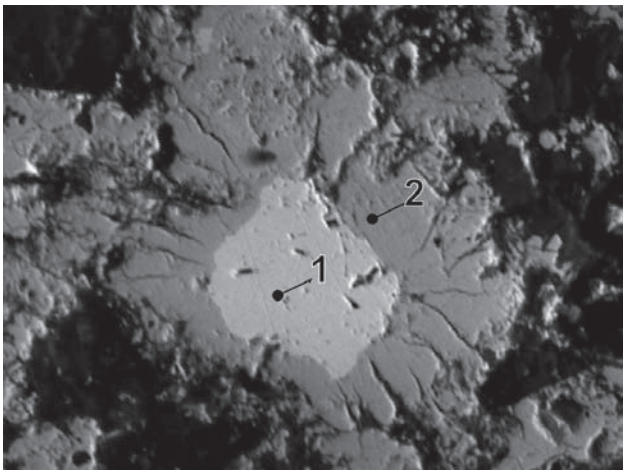

Fig. 226. J101P. 1 – bismuth, 2 – zavaritskite. Schönerz adit. BSE image. Magnification 320×.

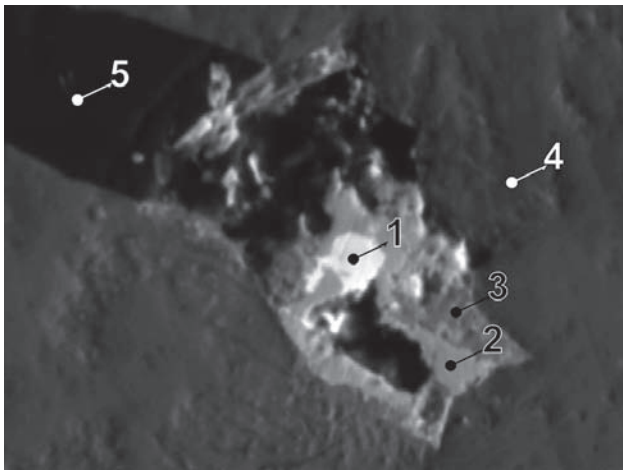

Fig. 227. J105P/A-1. 1 – BiSb, 2 – stibarsen, 3 – Sb-Bi-arsenic, 4 – arsenic, 5 – calcite. Svornost shaft, Adit level, Hildebrand vein. BSE image. Magnification 1300×.

Table 156. Calculated unit-cell parameters of zavaritskite from Jáchymov for the space group *Pcab*.

sample	*a*	*c*
	(Å)	
J101P (J-917)	3.7549(3)	6.2393(8)

IMPERFECTLY IDENTIFIED MINERAL PHASES

BiSb

It forms 7 μm rounded grain surrounded by *stibarsen* and an As(Sb,Bi) alloy (see *arsenic* and *stibarsen* analyses) in a small cavity of older *arsenic*. *Calcite* fills the remaining space of the cavity. The sample carrying the paragenesis *arsenic–miargyrite–antimony–stibnite* comes from the Svornost shaft, Adit level, Hildebrand vein. Chemical analyses are in Table 157.

$(Ag,Cu,Fe)_2BiS_3$

It was identified in a sample from Giftkies adit. It forms up to 10 μm grains in an assemblage with *arsenopyrite*, *chalcopyrite*, *pyrite*, *stannite*, *matildite*, *aikinite*, and *cassiterite*. Chemical analyses are in Table 158.

Cu_3AsS_3

It forms up to 15 μm rounded grains intergrown with *tennantite* occurring in an assemblage with *stromeyerite, tennantite, pyrite, chalcopyrite* and *tennantite*, *As-chalcopyrite, chalcopyrite*, respectively. It was identified in a sample from Trojická vein and Prokop vein, Svornost shaft. Chemical analyses are in Table 159.

Ni_2As_3

It was identified in a sample from adit No. 1 of Bratrství shaft associated with *rammelsbergite* in grey rims of *nickeline* aggregate. The width of rims is about 1 mm. Chemical analyses are in Table 160.

Table 158. Chemical analyses of an unknown phase $(Ag,Cu,Fe)_2BiS_3$.

sample	pt.	Ag	Cu	Fe	Co	Bi	S	Sb	As	Total
					weight %					
J061P	2	18.35	8.29	7.63	0.14	43.66	21.25	0.46	0.18	99.96
J061P	3	20.47	7.91	7.20	0.15	42.43	21.68	0.28	0.19	100.31
J061P	4	13.63	10.67	9.48	0.16	42.99	21.54	0.37	0.11	98.95

sample	pt.	Ag	Cu	Fe	Co	subtotal	Bi	S	Sb	As	subtotal	Total
						number of atoms						
J061P	2	0.77	0.59	0.62	0.01	2.00	0.95	3.02	0.02	0.01	3.05	6
J061P	3	0.86	0.56	0.58	0.01	2.01	0.92	3.05	0.01	0.01	3.07	6
J061P	4	0.56	0.75	0.76	0.01	2.08	0.92	2.99	0.01	0.01	3.01	6

Table 159. Chemical analyses of an unknown phase Cu_3AsS_3.

sample	pt.	Cu	Fe	Ag	Co	Ni	Zn	As	Sb	S	Total
						weight %					
J059P	9	49.12	2.52	0.35	0.25	0.27	0.17	19.88	0.43	25.98	98.97
J058P	5	48.55	2.33	1.25	0.15	0.15		20.97	0.87	25.95	100.22
J058P	9	49.08	2.56	1.35	0.11	0.14		19.85	0.23	26.79	100.11
J058P	10	49.56	2.59	0.51	0.13	0.16		20.27	0.25	26.45	99.92

sample	pt.	Cu	Ag	Fe	Co	Ni	Zn	subtotal	As	Sb	S	subtotal	Total
							number of atoms						
J059P	9	2.83	0.01	0.17	0.02	0.02	0.01	3.05	0.97	0.01	2.97	3.95	7
J058P	5	2.79	0.04	0.15	0.01	0.01		3.00	1.02	0.03	2.95	4.00	7
J058P	9	2.79	0.05	0.17	0.01	0.01		3.02	0.96	0.01	3.02	3.98	7
J058P	10	2.82	0.02	0.17	0.01	0.01		3.03	0.98	0.01	2.99	3.97	7

Table 160. Chemical analyses of an unknown phase Ni_2As_3.

sample	pt.	As	S	Sb	Fe	Co	Ni	Cu	Total
					weight %				
J017P	r1	63.97	0.39	0.50	0.57	0.35	33.32	0.53	99.63
J017P	r2	65.51	0.12	0.11	0.71	0.14	32.98	0.03	99.60
J017P	r3	64.11	0.35	0.54	0.87	0.12	33.35	0.20	99.54

sample	pt.	Ni	Fe	Co	Cu	subtotal	As	S	Sb	subtotal	Total
						number of atoms					
J017P	r1	1.94	0.04	0.02	0.03	2.03	2.92	0.04	0.01	2.98	5
J017P	r2	1.93	0.04	0.01	0.00	1.98	3.00	0.01	0.00	3.02	5
J017P	r3	1.95	0.05	0.01	0.01	2.02	2.93	0.04	0.02	2.98	5

ERRONEOUSLY QUOTED MINERALS, IMPERFECTLY IDENTIFIED MINERALS

Argentopentlandite

Nickel and Nichols [519] mentioned Jáchymov and the Siberian deposits Oktyabr and Talnakh near Norilsk as the type localities of *argentopentlandite*. However, the original source [442] does not mention Jáchymov. The reference to Jáchymov is obviously based on error.

Bi-telluride

The mineral occurs as round grains up to 7 μm long, intimately intergrown with *bismuth* and sometimes also with *aurostibite*. The small grain size prevented reliable EMP analysis of pure phase. Variable Bi/Te ratio (up to 5:1) does not allow a clear identification. The mineral is free of S and the associated *bismuth* does not show replacement by *bismuthinite*.

The mode of formation of this unique local paragenesis is not clarified. Some role of *amphibolite* rock is possible.

Boulangerite

Zückert [423] identified *boulangerite* in polished sections but gave no details. Geceva and Dubinkina [358] did not mention this mineral and *boulangerite* was not observed during the present study. Mrňa et al. [408] mentioned the presence of this mineral in *calcite* gangue. Vogl [59] reported a presence of "Zundererz", a name used for *jamesonite* or *boulangerite*.

Breithauptite

Breithauptite was mentioned from Jáchymov without further information [118]. It forms sporadic rims along fractures in zoned *skutterudite* from the Svornost shaft [141]. Pavlů listed *breithauptite* with *gersdorffite* and *glaucodot* as minerals formed by alteration of arsenides.

Cobaltite

The presence of *cobaltite* in Jáchymov is reported in several older textbook sources [118] but no detailed description or identification has been published. Ježek [189] noted that *cobaltite* occurrence was questionable. Some crystallized specimens in museums, labelled as *cobaltite* from Jáchymov, were subsequently identified as *skutterudite* or *nickel-skutterudite.* Cubic crystal morphology and variable Co contents prompted some mineralogist to designate the samples as *cobaltite*.

Bouška a Netolický [518] described *cobaltite* as inclusions in sphalerite and in association with *chalcopyrite* in *quartz* in samples from the Adam shaft.

"Frieseite"

Vrba [532] studied several samples from the Hildebrand and Geister veins with *sternbergite* and *argentopyrite.* Two samples representing the two veins contained a mineral similar to *sternbergite* but showing different crystal morphology. Vrba introduced the name "*frieseite"* for this new mineral. It formed thick tabular crystals elongated on *b* axis (Figs 228, 229, 231, and 232). The samples contained yellow grey, slightly weathered *marcasite* with drusy surface, covered by pseudomorphs after *pyrrhotite* or *sternbergite,* accompanied by *dolomite* and minor

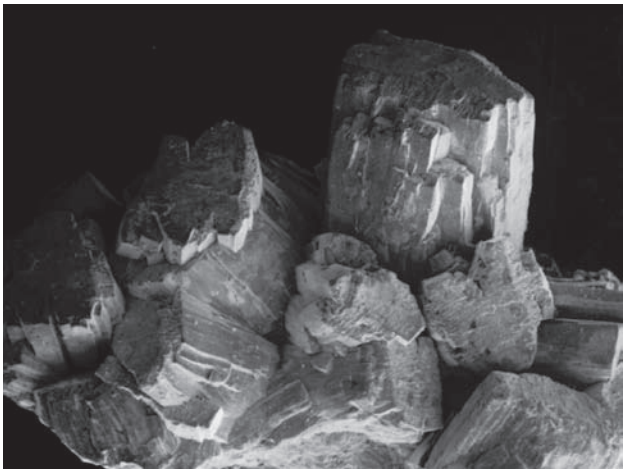

Fig. 228. VS7651. Crystals of "frieseite". XRD analysis confirmed that the mineral is a mixture of sternbergite, pyrite and marcasite. Magnification 30×. Photo A. Gabašová.

Fig. 229. VS7651. Detail of "frieseite" crystals. Magnification 170×. Photo A. Gabašová.

Fig. 230. NM 4807. "Frieseite" crystal parallel with section. Reflected light, single polarizer. Magnification 200×.

Fig. 231. NM 4807. "Frieseite" crystal parallel with section. Reflected light, crossed polarizers. Magnification 200×.

Fig. 232. NM 4807. Aggregate of tabular crystals of "frieseite" from Jáchymov. Magnification 20×. Photo A. Gabašová.

Fig. 233. NM 4807. Tabular crystals of "frieseite" (width of figure 0.5 cm) from Jáchymov. Photo A. Gabašová.

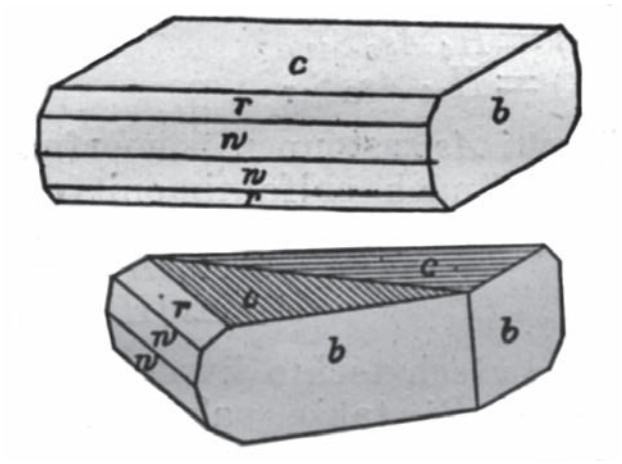

Fig. 234. Thick tabular singlecrystal of "frieseite" from Jáchymov and a twin by Vrba [362]. Crystal forms: c(001), b(010), w(301), r(102).

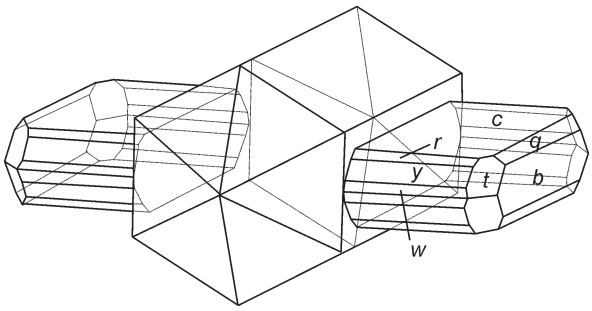

Fig. 235. Orientated intergrowth of a thick tabular crystal of "frieseite" and argentopyrite, by Vrba [362]. Crystal forms: c(001), b(010), q(043), r(102), y(101), w(301), t(131).

proustite. Up to 6 mm high and 6 mm wide short prismatic crystals of an Ag-Fe sulphide were deposited on this matrix. The crystals had altered central parts suggesting analogy with *argentopyrite* description by Tschermak [469]. Among the partly altered *argentopyrite* crystals, there were rectangular "*frieseite*" crystals up to 6 mm long, so closely intergrown with *argentopyrite* that often only a single face protruded to surface.

"*Frieseite*" has a lower lustre compared to *sternbergite,* dark bronze to brown black colour. It is very soft, cleavage flakes along basal plane are malleable. It is sometimes accompanied by *xanthoconite*. Density representing average of three measurements is 4.217 g/cm^3 (4.212–4.220) at 17 °C, hardness 2 [4 on (010) faces], thin flakes are semi-translucent dark green grey (Vrba 1878 [532]).

Small samples prepared by Vrba and analysed by Preiss (1875) gave 37.3 and 37.4 wt.% Fe, 27.6 and 29.1 wt.% Ag and 33.0 and 33.9 wt.% S (Vrba 1879 [531]).

In 1880, Vrba obtained several samples with "*frieseite*" crystals in orientated intergrowth with *argentopyrite.* The alongation axis of *argentopyrite* prisms was parallel with *a* axis of "*frieseite*" with the result that half of *argentopyrite* crystal is above the tabular "*frieseite*" and the lower half below "*frieseite*". This suggests that either the two minerals crystallized contemporaneously or during alternating episodes. Vrba pointed to the close chemical relations of "*frieseite*" to *argentopyrite* and *sternbergite* and suggested some similarity to *pyrite* and *marcasite* dimorphism. (Vrba 1881, [533]).

Babánek described "*frieseite*" as small prisms with strongly striated faces from the Svornost shaft, Hildebrand vein. The crystals occurred on rhombohedral *dolomite* crystals and small *proustite* crystals were deposited on "*frieseite*" [364].

The present XRD study of crystals corresponding in morphology to "*frieseite*" pictures shows they are composed of *sternbergite*, *pyrite* and *marcasite.* Electron mi-

croprobe and ore microscopy show that the outer zones are composed of an Ag–Fe sulphide with no detectable cleavage (Figs 230–231). The central lower part of the crystal was *pyrite* and/or *marcasite*. The remaining parts of the crystals represent a very fine lamellar intergrowth of all above named phases. The type of alteration products is similar to those resulting from decomposition of *argentopyrite.* However, inversion of *argentopyrite* to *sternbergite* was never observed. It is important to note that at the time of "*frieseite*" study, exact chemical composition of *argentopyrite* and *sternbergite* was unknown and "*frieseite*" was distinguished from the two minerals of similar composition on the basis of morphological crystallography.

The available information indicates that "*frieseite*" crystallized as an unknown high-temperature Ag–Fe–S phase (above 190 °C) with composition very similar to *argentopyrite* and *sternbergite* but probably with a distinct structure. The situation may be possibly similar to *argentopyrite* story: the status of *argentopyrite* as a distinct mineral species was long time doubted and its true chemical composition was unknown even longer. A slim chance remains that in future a relict, unaltered "*frieseite*" crystal will be found and will allow a definitive solution of the "*frieseite*" problem. The rarity of "*frieseite*" suggests the chances are not very good.

The report on the phase $Ag_2Fe_5S_8$, not studied in detail (Kühn [534]), indicates likely existence of additional phases in the Ag–Fe–S system. Kühn did not use correction procedures for processing of results. During this study, identical material was analysed with microprobe and a phase $AgFe_2S_3$ was detected only. The grains had not a cleavage, therefore, it was probably *argentopyrite*. Another Ag–Fe–S phase, $AgFe_8S_{11,}$ is referenced by Ixer et al. [559] from an Ag–Ni–Co mineral association at Tynebottom mine, Garrigill, England.

Gladite

Geceva and Dubinkina [358] reported g*ladite* from Jáchymov, with reference to identification by another person. A presence of this mineral was not confirmed in the present study.

Heteromorphite

Geceva and Dubinkina [358] reported the mineral in cavities of *galena* and *sphalerite* in ore samples. The cavities carried fibres of native *silver*, *marcasite* and *argentite*. *Heteromorphite* was not confirmed by the present work.

Maucherite $Ni_{11}As_8$

Mrňa and Pavlů described *maucherite* from Jáchymov in the following way (Mrňa-written communication): it is a rather rare product of nickel arsenides affected by cataclastic deformation. It replaced *nickeline* and sometimes *nickel-skutterudite* along fractures. In polished sections, parquet-pattern twinning is typical, with prevailing orientation of one set of lamellae perpendicular to fracture in arsenide. *Maucherite* aggregates along fractures in *nickeline* are 1 mm wide in maximum. Also, Mrňa and Pavlů [419] reported frequent replacement of *nickeline* from the Eva shaft by *maucherite*. It was identified in the vein No. 39 (Eva shaft) and No. 32 (Barbora shaft) in association with *nickeline*.

No *maucherite* was identified during the present study, including some original samples. Alteration of *nickeline* may possibly result in formation of a rare phase NAP (*nickeline* alteration product), described by Karup-Møller and Makovicky [354] in an old sample from an unspecified locality in Germany. The phase NAP evolves by partial alteration of *nickeline* along fractures as lamellae 2×20 μm in parallel orientation. Border between NAP

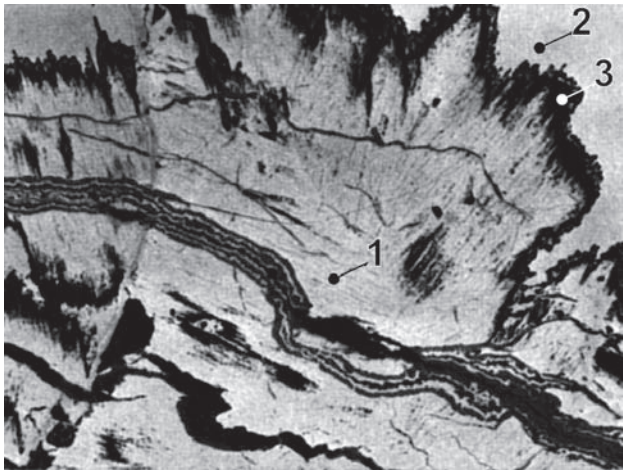

Fig. 236. Topotactic replacement of nickeline along small fissures by orientated intergrowths of rammelsbergite (NAP), from [354]. 1 – NAP, 2 – nickeline, 3 – Ni-arsenete? Germany. Reflected light, single polarizer. Magnification 120×.

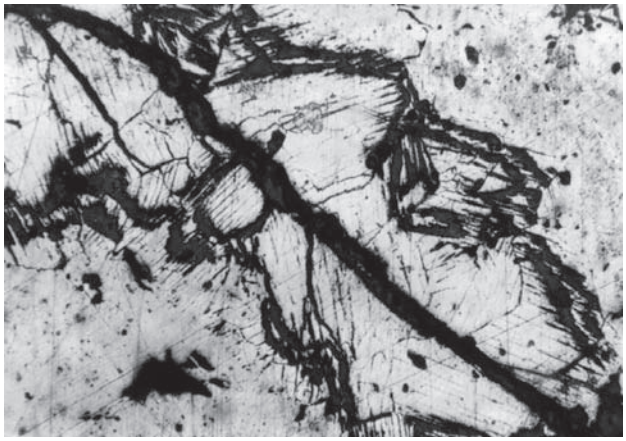
Fig. 237. Interpretation of Mrňa and Pavlů [383] – maucherite rims a fissure in nickeline, arsenide mineralization stage. Eva shaft, vein No. 39. Magnification 80×.

and *nickeline* is formed by a Ni–As phase, probably arsenate. NAP is white in reflected light and similar to *rammelsbergite.* Polarization colours are similar to those of *rammelsbergite* but less vivid. EMP spot analyses are similar to *rammelsbergite* with 3–5 wt.% S, they show a small (As+S) surplus with ratio Me/(As+S) = 0.53–0.57; (Fe+Co) = 2–3 wt.%. XRD study identified *nickeline* with some diffuse reflections of *rammelsbergite.* Single-crystal study [354] found out three different orientated intergrowths of *rammelsbergite* and *nickeline*.

Tetradymite

Tetradymite was allegedly found in 1855 in the Barbora adit and a sample was deposited in the Krantz's collection [118]. According to information from Krantz heirs, the collection was sold in several parts. This makes the verification of *teradymite* occurrence impossible.

Wurtzite ZnS

Zückert [423] identified *wurtzite* in polished sections but gave no further details. In a similar way, *wurtzite* appears in the list of identified minerals by Geceva and Dubinkina [358].

In the present study, *wurtzite* was inconclusively indicated as a minor component in a mixture with *sphalerite*. The presence of *wurtzite* cannot be ruled out and these samples will require a further crystallographic research. *Sphalerite* with possible *wurtzite* forms light yellow spheroidal aggregates grouped in chains. The aggregates replace radiating *stibnite* crystals with some *antimony* relics enclosed in pink *dolomite* with the assemblage: *arsenic*, *miargyrite*, *stibnite*, *dyscrasite*, *stibarsen,* and *pyrite*. The sample with probable *wurtzite* comes from the Svornost shaft, Adit level, Hildebrand vein (Figs 188, 190).

Primární minerály jáchymovského rudního revíru

117 primárních minerálů je popsáno v této práci z jáchymovského rudního revíru, z čehož okolo 60 jich bylo známo již před touto studií. U jednotlivých minerálů jsou uvedena všechna data nově získaná i přejatá. Pro argentopyrit, sternbergit a neobvyklý (Co,Fe)-rammelsbergit jsou i nová a úplná rtg prášková data. V závěrečné kapitole jsou popisy neznámých minerálních fází, chybně a nedostatečně určených minerálů. Počet všech hodnověrně popsaných minerálů z jáchymovského rudního revíru tak nyní dosáhl čísla 384.